

Characterisation of the ADAMTS family in *Xenopus* development

Ines Desanlis

Thesis submitted for the degree of Doctor of
Philosophy

University of East Anglia
School of Biological Sciences
Norwich, United Kingdom

August 2017

Word count: 40,361

© This copy of the thesis has been supplied on condition that anyone who consults it is understood to recognize that its copyright rests with the author and that use of any information derived there from must be in accordance with current UK Copyright Law. In addition, any quotation or extract must include full attribution

Abstract

Extracellular matrix (ECM) remodeling by metalloproteinases is crucial during development. The ADAMTS (A Disintegrin and Metalloproteinase with Thrombospondin type I motifs) enzymes are secreted, multi-domain matrix-associated zinc metalloendopeptidases that have diverse roles in tissue morphogenesis and patho-physiological remodeling. The human family includes 19 members. In this study *Xenopus* was used as an *in vivo* model for studying the function of ADAMTSs during development. 19 members of the ADAMTS family were identified in *Xenopus*. A phylogenetic study and synteny analysis revealed strong conservation of the ADAMTS family, provided a view of the evolutionary history and contributed to a better annotation of the *Xenopus* genomes.

The expression of the *ADAMTS* family was studied from early stages to tadpole stages of *Xenopus* with a focus on *ADAMTS9* showing expression in neural crest (NC) derivative tissues and in the pronephros. *ADAMTS9* function was investigated in these structures. *ADAMTS9* knock-down does not affect NC migration but causes a phenotype in the pronephros defined by a delay of development from early tailbud stage of pronephric nephrostomes, tubules and duct. Versican, a matrix component substrate of *ADAMTS9*, is expressed in the pronephros at tailbud stage but not at tadpole stage suggesting a transient role during development. The lack of its degradation by *ADAMTS9* could be the cause of the delay of pronephros development.

The expression of the *ADAMTS* family as well as other metalloproteinases, ECM components and tissue inhibitor of metalloproteinases was studied in the skin, the brain and the heart undergoing remodeling during *Xenopus laevis* metamorphosis, as well as in the heart after ventricular resection to look at regeneration during *Xenopus laevis* metamorphosis. The results showed specific gene regulation depending on the stage of development and in response to heart injury revealing an important role for the ECM and its remodeling during these processes.

Table of contents

Abstract	ii
Table of contents	iii
List of figures	vii
List of tables	x
Abbreviations	xi
Acknowledgements	xiv
Chapter I: Introduction	1
1.1 <i>Xenopus</i> as an animal model	2
1.1.1 Life cycle and advantages.....	2
1.1.2 Animal model to study ECM remodeling during organogenesis .	3
1.1.3 Animal model to study ECM remodeling during metamorphosis	4
1.1.4 Animal model to study ECM remodeling during regeneration.....	6
1.2 ECM in development	7
1.2.1 Collagen	8
1.2.2 Fibronectin	10
1.2.3 Proteoglycans	10
1.2.3.1 Hyalactans	11
1.2.3.2 Syndecans	13
1.2.4 Matricellular proteins	14
1.3 Metalloproteinases	15
1.3.1 Matrix Metalloproteinases (MMP)	16
1.3.2 ADAM	19
1.3.3 ADAMTSL	21
1.3.4 ADAMTS	21
1.3.4.1 Evolutionary history.....	21
1.3.4.2 Molecular structure	24
1.3.4.2.1 Pro-domain	24
1.3.4.2.2 Catalytic domain	26
1.3.4.2.3 Ancillary domain.....	26
1.3.4.3 Post-translational modifications	27
1.3.4.4 Functions in development	27
1.3.4.4.1 Aggrecanase/Hyalactanase family.....	27
1.3.4.4.2 Procollagen N-propeptidase family	29
1.3.4.4.3 von-Willebrand Factor family	29
1.3.4.4.4 COMP proteinases family	30
1.3.4.4.5 “orphan” family	30
1.3.4.5 Different mode of actions	30
1.3.4.6 Functions in cancer and diseases.....	31
1.3.5 TIMP.....	31
1.4 Aims of the project	32
Chapter II: Materials and Methods	35
2.1 Data source of ADAMTS gene sequences	36

2.2	Alignment and phylogenetic analysis	36
2.3	Obtaining <i>Xenopus laevis</i> and <i>Xenopus tropicalis</i> embryos ..	36
2.4	Fixing and storage of <i>Xenopus</i> embryos	37
2.5	Skin and brain dissection from stage 57 to stage 66	37
2.6	RNA extraction	37
2.6.1	For <i>Xenopus</i> embryos from unfertilised egg to stage 45	37
2.6.2	For <i>Xenopus</i> embryos from stage 57 to stage 66	38
2.7	DNase treatment	38
2.8	cDNA synthesis	39
2.8.1	For <i>Xenopus</i> embryos from unfertilised egg to stage 45	39
2.8.2	For <i>Xenopus</i> embryos from stage 57 to stage 66	39
2.9	Pre-amplification of cDNA	39
2.10	Polymerase Chain Reaction (PCR)	39
2.11	Quantitative PCR	40
2.11.1	96 well plate	40
2.11.2	384 well plate	40
2.12	Microfluidics	40
2.12.1	Primers validation.....	40
2.12.2	Reaction	41
2.13	Statistical analysis	42
2.14	Cloning into pGEM®-T Easy Vector	42
2.15	Gateway cloning	43
2.16	Transformation	44
2.17	Mini and Midi Extraction of Plasmid DNA	45
2.18	Probe synthesis	45
2.18.1	Template	45
2.18.1.1	Linearized plasmid	45
2.18.1.2	PCR product	46
2.18.2	Reaction	46
2.19	Capped RNA synthesis	47
2.20	Microinjection, morpholinos and mRNA used, GFP detection	48
2.21	Wholemout <i>in situ</i> hybridization	48
2.22	Wholemout antibody staining	49
2.23	Cryosectioning	50
2.24	Western-blot	50
2.24.1	Protein extraction	50
2.24.2	Sample preparation	51
2.24.3	Protein electrophoresis.....	51
 Chapter III: Evolutionary history of the ADAMTS family in		
2.25	<i>Xenopus laevis</i> and <i>Xenopus tropicalis</i>	55
3.1	Introduction	56
3.2	Results	58
3.2.1	Gene identification in <i>Xenopus laevis</i> and <i>Xenopus tropicalis</i> ..	58
3.2.2	Phylogenetic study of <i>Xenopus laevis</i> and <i>Xenopus tropicalis</i> ADAMTS.....	58

3.2.3 Synteny analysis of <i>ADAMTS</i> genes between <i>Xenopus laevis</i> subgenomes L and S and <i>Xenopus tropicalis</i>	61
3.2.4 Conservation of the <i>Xenopus ADAMTS</i> genes between <i>Xenopus laevis</i> subgenomes L and S	65
3.3 Discussion	66
Chapter IV: Characterisation of the ADAMTS family in <i>Xenopus</i> during organogenesis	69
4.1 Introduction	70
4.1.1 ECM remodeling during neural crest cell migration in <i>Xenopus</i>	70
4.1.2 Remodeling during pronephros development in <i>Xenopus</i>	71
4.2 Results	74
4.2.1 ADAMTSs expression and function in <i>Xenopus tropicalis</i>	74
4.2.1.1 Expression profiles of the <i>ADAMTS</i> family in <i>Xenopus tropicalis</i>	74
4.2.1.2 Expression pattern of <i>ADAMTS9</i> in <i>Xenopus tropicalis</i>	74
4.2.1.3 <i>ADAMTS9</i> knockdown in <i>Xenopus tropicalis</i>	76
4.2.2 ADAMTSs expression and function in <i>Xenopus laevis</i>	79
4.2.2.1 Expression profile of the hyaluronanases family in <i>Xenopus laevis</i>	79
4.2.2.2 Expression pattern of <i>ADAMTS9</i> in <i>Xenopus laevis</i>	82
4.2.2.3 <i>ADAMTS9</i> knockdown in <i>Xenopus laevis</i>	87
4.2.2.4 <i>ADAMTS9</i> knockdown in neural crest of <i>Xenopus laevis</i>	92
4.2.2.5 <i>ADAMTS9</i> knockdown in the pronephros of <i>Xenopus laevis</i>	94
4.2.2.5.1 Protocol of injection and analysis	94
4.2.2.5.2 Early markers, <i>wt1</i> and <i>pax8</i>	95
4.2.2.5.3 Late tailbud markers, <i>atp1b1</i> , <i>Xlim1</i> and <i>pax2</i>	98
4.2.2.5.4 Late markers, <i>4a6</i>	101
4.2.2.6 Morpholinos efficiency	103
4.3 Discussion	105
4.3.1 ADAMTSs expression in <i>Xenopus</i>	105
4.3.2 Functional study of <i>ADAMTS9</i> in <i>Xenopus tropicalis</i> and in <i>Xenopus laevis</i>	108
4.3.2.1 <i>ADAMTS9</i> knockdown in <i>Xenopus tropicalis</i> and in <i>Xenopus laevis</i> embryos	108
4.3.2.2 <i>ADAMTS9</i> knockdown in neural crest of <i>Xenopus laevis</i>	108
4.3.2.3 <i>ADAMTS9</i> knockdown in the pronephros of <i>Xenopus laevis</i>	110
4.3.2.4 Morpholinos efficiency	113
Chapter V: Characterisation of the ADAMTS family, metalloproteinases and extracellular components in <i>Xenopus laevis</i> during metamorphosis and heart regeneration	115
5.1 Introduction	116
5.1.1 Brain remodeling during <i>Xenopus laevis</i> metamorphosis	117
5.1.2 Skin remodeling during <i>Xenopus laevis</i> metamorphosis	118
5.1.3 Heart remodeling during <i>Xenopus laevis</i> metamorphosis	119
5.1.4 Heart regeneration during <i>Xenopus laevis</i> metamorphosis	120
5.2 Results	121

5.2.1 ADAMTSs, versican, aggrecan and TIMPs expression in the skin and the brain during <i>Xenopus laevis</i> metamorphosis.....	121
5.2.2 Gene expression in the heart undergoing remodeling and in the heart after ventricular resection during <i>Xenopus laevis</i> metamorphosis.....	124
5.2.2.1 Gene expression in the heart undergoing remodeling during <i>Xenopus laevis</i> metamorphosis	126
5.2.2.2 Gene expression in the heart after ventricular resection during <i>Xenopus laevis</i> metamorphosis	132
5.3 Discussion.....	137
5.3.1 ADAMTSs, versican, aggrecan and TIMPs expression in the skin and the brain during <i>Xenopus laevis</i> metamorphosis.....	137
5.3.1.1 Brain remodeling during <i>Xenopus laevis</i> metamorphosis	137
5.3.1.2 Skin remodeling during <i>Xenopus laevis</i> metamorphosis	139
5.3.2 Gene expression in the heart undergoing remodeling and in the heart after ventricular resection during <i>Xenopus laevis</i> metamorphosis.....	140
5.3.2.1 Heart remodeling during <i>Xenopus laevis</i> metamorphosis ...	140
5.3.2.2 Heart regeneration during <i>Xenopus laevis</i> metamorphosis .	142
Chapter VI: Discussion	148
6.1 The ADAMTS family in <i>Xenopus</i> genome.....	149
6.2 ADAMTS9 in the pronephros	150
6.3 ECM and metalloproteinases in post embryonic development.....	153
6.4 ECM and metalloproteinases in heart regeneration	155
References	159
Appendices	179
8.1 Appendix 1: Primers used in this study.....	180
8.2 Appendix 2: Melt curve of primers used for the microfluidic	184
8.3 Appendix 3: Graphs of gene expression and regulation in the heart during <i>Xenopus laevis</i> metamorphosis	188
8.4 Appendix 4: Graphs of gene expression and regulation in the heart after ventricular resection during <i>Xenopus laevis</i> metamorphosis.....	192

List of figures:

Chapter I: Introduction.....	1
Figure 1-1: <i>Xenopus</i> life cycle.	2
Figure 1-2: Schematic representation of plasma level of thyroid hormones during <i>Xenopus laevis</i> metamorphosis.....	5
Figure 1-3: Schematic representations of two types of collagens.....	9
Figure 1-4: Hyalactan/lectican family.....	13
Figure 1-5: Basic domain organisation of ADAMTS, ADAM and MMP proteins.....	16
Figure 1-6: Basic domain organisation of MMP proteins.....	18
Figure 1-7: Basic domain organisation of ADAM proteins..	20
Figure 1-8: Basic domain organisation of ADAMTS-like proteins....	21
Figure 1-9: Schematic representation of the evolutionary history of the ADAMTS family.....	23
Figure 1-10: Molecular structure of the 19 members of the ADAMTS family.....	25
Figure 1-11: Aims of the project.	34
Chapter II: Materials and Methods.....	35
Figure 2-1: 96.96 Dynamic Array™ integrated fluidic circuits (IFCs) chip used to perform the microfluidic experiment.	42
Figure 2-2: Transfer sandwich containing the electrophoresis gel, the PVDF membrane, filter papers and foam pads (sponge).	53
Chapter III: Evolutionary history of the ADAMTS family in <i>Xenopus laevis</i> and <i>Xenopus tropicalis</i>	55
Figure 3-1: Phylogenetic tree illustrating the evolutionary history of <i>Xenopus laevis</i> and <i>Xenopus tropicalis</i>	57
Figure 3-2: Evolutionary relationships of the ADAMTS protein.	60
Figure 3-3: Phylogeny of ADAMTS in both <i>X. laevis</i> subgenomes L and S and <i>X. tropicalis</i>	61
Figure 3-4: Synteny of single copy ADAMTS genes in subgenomes S and L of <i>Xenopus laevis</i> and <i>Xenopus tropicalis</i>	63
Figure 3-5: Synteny of <i>X. laevis</i> ADAMTS genes with similar organisation in subgenome L and <i>X. tropicalis</i> genome but different to <i>X. laevis</i> subgenome S.....	64
Figure 3-6: Synteny of <i>X. laevis</i> ADAMTS genes in subgenomes L and S with similar chromosomal organisation as <i>X. tropicalis</i> ADAMTS genes.	64
Figure 3-7: Synteny of <i>X. laevis</i> ADAMTS genes in subgenomes L and S and with different chromosomal position compare to <i>X. tropicalis</i> ADAMTS genes..	65
Figure 3-8: <i>Xenopus laevis</i> ADAMTS9L and ADAMTS9S structure..	66
Chapter IV: Characterisation of the ADAMTS family in <i>Xenopus</i> during organogenesis	69
Figure 4-1: <i>Xenopus</i> neural crest cells migration pathways.	71
Figure 4-2: Pronephros development in <i>Xenopus</i>	72
Figure 4-3: Expression of the ADAMTS genes family during <i>Xenopus tropicalis</i>	

development.....	75
.....	75
Figure 4-4 The expression pattern of ADAMTS9 in <i>Xenopus tropicalis</i> embryos.	77
Figure 4-5: The phenotype obtained after ADAMTS9 knockdown in <i>Xenopus tropicalis</i>	78
Figure 4-6: Expression profiles of the hyaluronanases family and VCAN during <i>Xenopus laevis</i> development..	81
Figure 4-7: The expression pattern of ADAMTS1 in <i>Xenopus laevis</i>	82
Figure 4-8: The expression pattern of ADAMTS9 in <i>Xenopus laevis</i> embryos.	84
Figure 4-9: The expression pattern of ADAMTS9 in the pancreas of <i>Xenopus laevis</i> tadpoles.	85
Figure 4-10: Sectioned <i>Xenopus laevis</i> embryos after WISH for ADAMTS9.....	86
Figure 4-11: Expression of ADAMTS9L and ADAMTS9S during <i>Xenopus laevis</i> development.....	88
Figure 4-12: The phenotype obtained after ADAMTS9 knockdown in <i>Xenopus laevis</i>	90
Figure 4-13: The expression pattern of VCAN in <i>Xenopus laevis</i> embryos.	91
Figure 4-14: Knockdown of ADAMTS9 in neural crest of <i>Xenopus laevis</i>	93
Figure 4-15: Loss of function experiment for ADAMTS9 during pronephros development in <i>Xenopus laevis</i>	94
Figure 4-16: Wholemout <i>in situ</i> hybridisation for <i>wt1</i> in <i>Xenopus laevis</i> injected embryos with both ADAMTS9L and ADAMTS9S morpholinos..	96
Figure 4-17: Wholemout <i>in situ</i> hybridisation for <i>pax8</i> in <i>Xenopus laevis</i> injected embryos with both ADAMTS9L and ADAMTS9S morpholinos.	97
Figure 4-18: Wholemout <i>in situ</i> for <i>atp1b1</i> , <i>Xlim1</i> and <i>pax2</i> in <i>Xenopus laevis</i> injected embryos with both ADAMTS9L and ADAMTS9S morpholinos.....	100
Figure 4-19: Wholemout immuno staining with 4a6 antibody on injected <i>Xenopus laevis</i> embryos with ADAMTS9S, ADAMTS9L and control morpholinos.	102
Figure 4-20: Western blot for ADAMTS9S-HA and ADAMTS9L-HA.	104
.....	104
Figure 4-21: Hyaluronanases family expression profile by RT-qPCR in <i>Xenopus laevis</i> and by RNA-seq in <i>Xenopus tropicalis</i>	106
Figure 4-22: The expression pattern of VCAN in <i>Xenopus laevis</i> embryos..	111
Chapter V: Characterisation of the ADAMTS family, metalloproteinases and extracellular components in <i>Xenopus laevis</i> during metamorphosis and heart regeneration	115
Figure 5-1: Gene expression of the ADAMTS family, versican (VCAN), aggrecan (ACAN) and TIMP1, TIMP2 and TIMP3 evaluated	

by RT-qPCR on brain and skin tissues from <i>Xenopus laevis</i> tadpole and juvenile during metamorphosis.	123
Figure 5-2: Schematic of the different experimental conditions used to look at gene expression in the heart during <i>Xenopus laevis</i> metamorphosis.	124
Figure 5-3: Heat-map of gene expression in the heart during <i>Xenopus laevis</i> metamorphosis.	127
Figure 5-4: Different profile of gene expression in the heart during <i>Xenopus laevis</i> metamorphosis.	130
Figure 5-5: Different gene expression profiles in the heart after ventricular resection during <i>Xenopus laevis</i> metamorphosis.....	135
Figure 5-6: Model of regulation of the cardiac regeneration process by the uPA/tPa/plasmin pathways and the inhibitor PAI1.....	143
Appendices	179
Appendix 8-1: Sequences and terms of use of each primer set for RT-qPCR and microfluidic in <i>Xenopus laevis</i>	180
Appendix 8-2: Sequences and terms of use of each primer set for RT-PCR in <i>Xenopus tropicalis</i>	182
Appendix 8-3: Sequences and terms of use of M13 primer set for PCR on plasmids.....	182
Appendix 8-4: Sequences and terms of use of each primer set to make <i>Xenopus laevis</i> probes.....	183
Appendix 8-5: Sequences and terms of use of each primer set to make <i>Xenopus tropicalis</i> probes.....	183
Appendix 8-6: Melt curve of primers used for RT-qPCR and microfluidic experiments in <i>Xenopus laevis</i>	184
Appendix 8-7: Melt curve of primers used for RT-qPCR and microfluidic experiments in <i>Xenopus laevis</i>	185
Appendix 8-8: Melt curve of primers used for RT-qPCR and microfluidic experiments in <i>Xenopus laevis</i>	186
Appendix 8-9: Efficiency of the genes analysed in heart development and regeneration during <i>Xenopus laevis</i> metamorphosis.	187
Appendix 8-10: Genes up regulated in the heart during <i>Xenopus laevis</i> metamorphosis.	188
Appendix 8-11: Genes down regulated in the heart during <i>Xenopus laevis</i> metamorphosis..	189
Appendix 8-12: Genes up regulated in the <i>Xenopus laevis</i> heart at metamorphic climax.	190
Appendix 8-13: Genes down regulated in the <i>Xenopus laevis</i> heart at metamorphic climax..	191
Appendix 8-14: Genes showing no change of expression in the heart during <i>Xenopus laevis</i> metamorphosis.	191
Appendix 8-15: Different profile of gene expression in the heart after ventricular resection during <i>Xenopus laevis</i> metamorphosis.....	192

List of tables:

Chapter I: Introduction.....	1
Table 1-1: Different sub-families of collagens with their different members.	9
Table 1-2: Sub-families of the main members of MMP family.....	17
Table 1-3: Specific action of each TIMP on the inhibition of metalloproteinases and the binding to pro-MMPs.....	32
Chapter II: Materials and Methods	35
Table 2-1: Terms of use of the plasmids used to make probes.....	46
Table 2-2: Terms of use of the plasmids used to make capped RNA.	47
Table 2-3: Sequences of the morpholinos used in this study.	48
Table 2-5: Composition of the stacking gel.....	52
Table 2-6: Composition of the resolving gel.	53
Table 2-7:Composition of the running buffer at 10X..	53
Table 2-9:Term of use of the antibodies used for western-blot in <i>Xenopus</i>.....	54
Chapter III: Evolutionary history of the ADAMTS family in <i>Xenopus laevis</i> and <i>Xenopus tropicalis</i>	55
Table 3-1: Chromosomal location of ADAMTS genes in <i>Xenopus laevis</i> and <i>Xenopus tropicalis</i>.....	59
Table 3-2: Percentage similarity between homoeologous <i>X. laevis</i> ADAMTS genes on the two subgenomes L and S.	66
Chapter V: Characterisation of the ADAMTS family, metalloproteinases and extracellular components in <i>Xenopus laevis</i> during metamorphosis and heart regeneration	115
Table 5-1: List of genes analysed in heart development and regeneration during <i>Xenopus laevis</i> metamorphosis.	125
Table 5-2: Summary table of the different gene expression profiles in the heart during <i>Xenopus laevis</i> metamorphosis.....	131
Table 5-3: Summary table of the different gene expression profiles in the heart after ventricular resection during <i>Xenopus laevis</i> metamorphosis.	136
Table 5-4: List of genes analysed in heart development during <i>Xenopus laevis</i> metamorphosis in embryos treated with T3.....	147

Abbreviations

ADAM: A disintegrin and metalloproteinases

ADAMTS: A disintegrin and metalloproteinase with thrombospondin type-1 motifs

BLAST: Basic local alignment search tool

BMP: Bone morphogenetic proteins

BSA: Bovine serum albumin

Cas9: CRISPR associated protein 9

CKD: Chronic kidney disease

CNS: Central nervous system

COMP: Cartilage oligomeric protein

CRISPR: Clustered regularly interspaced short palindromic repeats

CRP: Complement regulatory protein

CS: Chondroitin sulfate

CSPG: Chondroitin sulphate proteoglycan

Ct: Threshold cycle

CUB: Complement C1r/C1s, Uegf {epidermal growth factor-related sea urchin protein}, BMP-1

DNA: Deoxyribonucleic acid

Dpa: Day post amputation

DS: Dermatan sulfate

ECM: Extracellular matrix

EDTA: Ethylenediaminetetraacetic acid

EGF: Epidermal growth factor

EMT: Epithelium-to-mesenchyme transition

FACIT: Fibril-associated collagens with interrupted triple helices

FC: Fold change

FN: Fibronectin

G: Globular domain

GAG: Glycosaminoglycan

GBM: Glomerular basement membrane

GF: Growth factor

GFP: Green fluorescent protein

GFR: Growth factor receptor
GON: Gonadal
GPI: Glycosylphosphatidylinositol
HA: Hyaluronan
HCG: Human chorionic gonadotrophin
HS: Heparan sulfate
HSPG: Heparan sulfate proteoglycans
Ig: Immunoglobulin-like domain
KS: Keratan sulfate
LP: Link proteins
Ma: Million years ago
MAB: Maleic acid buffer
MACIT: Membrane-associated collagens with interrupted triple helices
MEGA: Molecular evolutionary genetics analysis
MMP: Matrix metalloproteinases
MMR: Marc's modified ringer's
NC: Non collagenous
NCAM: Neural cell adhesion molecule
NCBI: National center for biotechnology information
NCC: Neural crest cells
NF: Nieuwkoop & Faber
OA: Osteoarthritis
PAI-1: Plasminogen activator inhibitor-1
PBS: Phosphate buffer saline
PCR: Polymerase chain reaction
PG: Proteoglycan
PMSG: Pregnant mare serum gonadotrophin
PPC: Pro-protein convertases
PTR: Proteoglycan tandem repeats
RIP: Regulated intramembrane proteolysis
RNA: Ribonucleic acid
RT: Reverse Transcriptase
RXR: *9-cis* retinoic acid receptor
SSC: Sodium chloride and sodium citrate

T3: 3,5,3' -triiodothyronine
T4: Thyroxine
TBE: Tris-borate-EDTA
TBS: Tris-buffered saline
TE: Transposable element
TH receptor: TR
TH: Thyroid hormone
TIMP: Tissue inhibitors of metalloproteinases
TN: Tenascin
Tpa: Tissue plasminogen activator
TPP: Thrombotic thrombocytopenic purpura
TRE: TH response element
TSP: Thrombospondin
TSR: Thrombospondin type 1 Sequence Repeat
UCSC: University of California Santa Cruz
UPAR: Urokinase plasminogen activator receptor
VEGF: Vascular endothelial growth factor
VEGFR: Vascular endothelial growth factor receptor
VWF: Von-Willebrand Factor
VWFCP: Von Willebrand factor-cleaving protease
WMS: Weill–Marchesani syndrome
Wt1: Wilms' tumor suppressor

Acknowledgements

Grant Wheeler, thank you for giving me the freedom to try all experiments I wanted and for just saying 'c'est la vie' when it did not work.

Dylan Edwards, thank you for your knowledge and your encouragements.

Marta Marin-Barba, we started this PhD together in this foreign country, thank you for all your help and for being my translator for the first six months, at least.

Danielle Blackwell, thank you for being my friend and my housemate and for sharing some house wine when our PhDs were too much.

Nicole Ward, thank you for telling all your funny Nicole stories and for being my ginger friend.

Katy Saide, thank you for all your eye rolls and your sarcastic comments.

Vicky Hatch, thank you for teaching me all the frog techniques and for bringing fun in the lab.

Angels Ruyra-Ripoll, Camille Viaut, Geoff Mok and James McColl.

Thanks Angels for being my 'mum' for a year, thanks Camille for your help in the lab, thanks Geoff for being a fun officemate and thanks James for reading my thesis and correcting the English.

DevCom fellows and PIs, thank you to people from this amazing fellowship, which allowed me to travel and meet brilliant people from around the world.

Laurent Coen and his team, thank you for our collaboration.

Louis Theret, Nicolas Arnaud, thank you for being an everyday French support during these four years, we did our PhDs together in three different cities. Thank you for coming to England. Thank you to Louis for your support during the writing.

Papa, Thibaut and Pascal, thank you for your support, your Skype calls allowing me to speak French and your visits to England.

Maman, thank you for reminding me I was just doing a PhD, not a real job, when I was complaining too much about the amount of work and for coming to visit me.

Chapter I: Introduction

This study looks at the role of the extracellular matrix (ECM) and its remodeling by metalloproteinases during organogenesis using *Xenopus laevis* and *tropicalis* as a model organism.

1.1 *Xenopus* as an animal model

1.1.1 Life cycle and advantages

Xenopus laevis and *Xenopus tropicalis* are two species of African clawed frog commonly used as vertebrate animal models for studying early and late development (Heasman, 2006) (Blitz et al., 2006). The *Xenopus* life cycle is separated into key developmental stages according to the (Nieuwkoop and Faber, 1994) fate map as a standard of *Xenopus* stages. *Xenopus laevis* develops into a frog in twelve months when incubated at 25°C, incubating at 12-25°C slows-down their development so that precise control over staging can be established. Below 12°C embryos do not develop (figure 1-1).

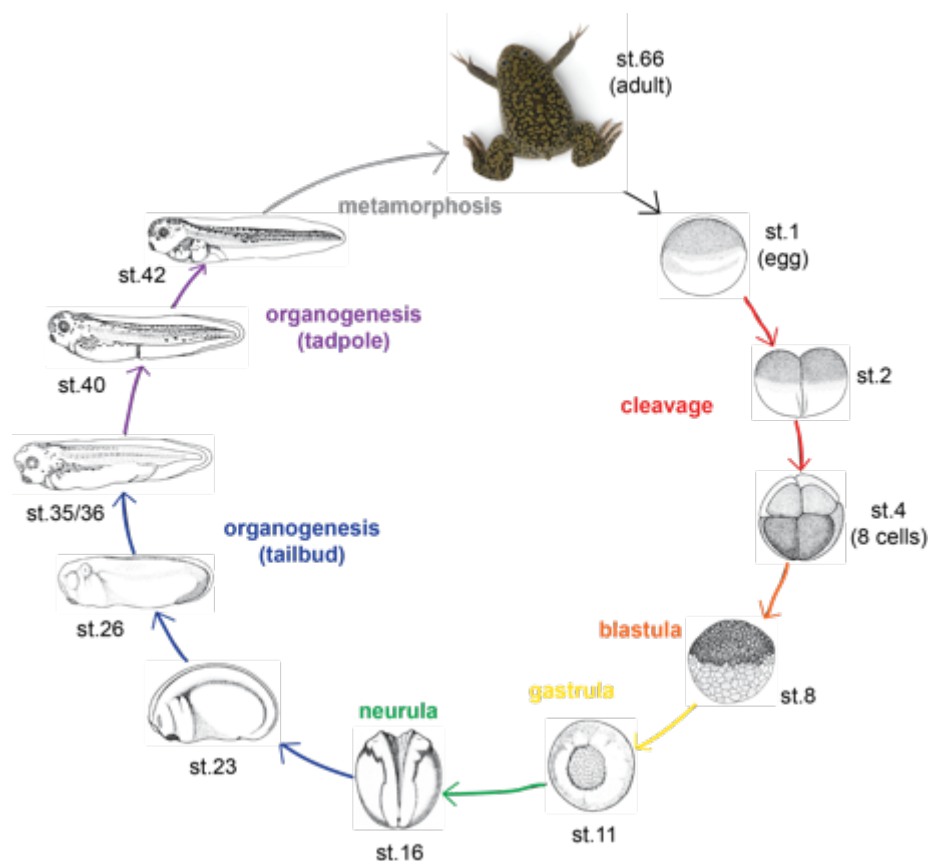


Figure 1-1: *Xenopus* life cycle. Key developmental steps are indicated by different colors. Cleavage, stage 1 to stage 4 (red). Blastula, stage 4 to stage 9 (orange). Gastrula, stage 9 to stage 12 (yellow). Neurula, stage 11 to stage 20 (green). Organogenesis, including tailbud stages, stage 20 to stage 35/36 (blue). Finally tadpole stages from stage 35/36 to stage 57 (purple) and metamorphosis from stage 57 to adult (grey). The developmental stage representations are from (Nieuwkoop and Faber, 1994).

Large numbers of synchronous embryos can be generated *ex utero*. *Xenopus laevis* eggs are large (1.2-1.4mm in diameter) allowing easy manipulation. The embryos are extremely robust to microinjection and surgical manipulation, allowing specific ablation and transplantation experiments (Harland and Grainger, 2011). *Xenopus tropicalis* embryos are more commonly used today for genetic studies as they have a well-sequenced diploid genome unlike the *Xenopus laevis* allo-tetraploid genome (Session et al., 2016). Gain of function experiments can be realised by injection of mRNA of the gene of interest and loss of function experiments can be carried out by injection of small antisense oligonucleotides (around 20 nucleotides) called morpholinos. In addition genetic engineering techniques such as CRISPR/Cas9 are also possible. Well characterised cell-fate maps allow blastomere-specific microinjection to target specific tissues and organs (Harland and Grainger, 2011), (Guo et al., 2014) (Dale and Slack, 1987).

1.1.2 Animal model to study ECM remodeling during organogenesis

The development and the morphology of most organs are conserved between *Xenopus* and mammals, which makes it a good model to study developmental processes giving rise to functional organs. The focus of the present study was the matrix remodeling during neural crest cell migration and pronephros development.

Neural crest (NC) are a transient embryonic cell population found exclusively in vertebrates that differentiate into many different cell types including enteric ganglia, neuroendocrine cells, glial cells, neurons, melanophores, craniofacial cartilage, skeletal bones and connective tissue (Le Douarin and Dupin, 2003) (Crane and Trainor, 2006). Cell-ECM interaction modulation and ECM remodeling are necessary to allow NC migration. The NC are restricted to very precise routes by the presence of negative and positive signals at the borders of each route (Szabo et al., 2016).

The mammalian kidney is a complex structure when compared to the *Xenopus* embryonic kidney, which has a simpler structure with conserved organisation that makes it a robust model to study kidney organogenesis and disease. The embryonic structure called the pronephros, consisting of a single nephron, is conserved in vertebrates. In *Xenopus* this embryonic kidney is

found on each side of the tadpole and is functional, regulating salt balance and filtering fluids, although in mammals the pronephros is not functional. The pronephros is then replaced by the mesonephros at metamorphosis and becomes the adult kidney in *Xenopus* whereas the metanephric kidney replaces the mesonephros in mammals (Krneta-Stankic et al., 2017). ECM remodeling plays an important role in kidney organogenesis and ECM composition depends on the location in the kidney such as the glomular and tubular basement membranes and the interstitial ECM. Regulated degradation of the kidney ECM by metalloproteinases is an important process (Genovese et al., 2014).

1.1.3 Animal model to study ECM remodeling during metamorphosis

Xenopus laevis, a fully aquatic tadpole moving by undulatory movements, metamorphoses into a tetrapod semiaquatic adult frog leading to drastic changes in most of the organs. *Xenopus* is an anuran amphibian meaning that it loses the tail at metamorphosis. This complex process is regulated by a peak of thyroid hormone (TH) at the metamorphic climax, between seven and eight weeks of development (stage 59 to 66) (Brown and Cai, 2007). Metamorphosis is divided into three periods: pre-metamorphosis (no secretion of TH), pro-metamorphosis (low level of secreted TH and first metamorphic changes) and metamorphic climax (peak of TH, remodelling of the tadpole) (figure 1-2) (Brown and Cai, 2007). The thyroid axis is conserved between mammals and *Xenopus laevis*. Thyroxine (T₄) is produced by the thyroid gland (located between the eyes) and it is converted by deiodinase activity in peripheral tissues to the active hormone 3,5,3'-triiodothyronine (T₃). T₃ binds to the nuclear TH receptor (TR), a heterodimer with 9-*cis* retinoic acid receptor (RXR), and acts as a transcription factor to regulate gene expression with TH response elements (TREs) in their promoter. Two types of TR are found in *Xenopus laevis*, TR α and TR β . TR α is expressed during pre-metamorphosis when the level of plasmatic T₃ is low whereas TR β is expressed during climax when TH concentration increases (Ishizuya-Oka, 2011).

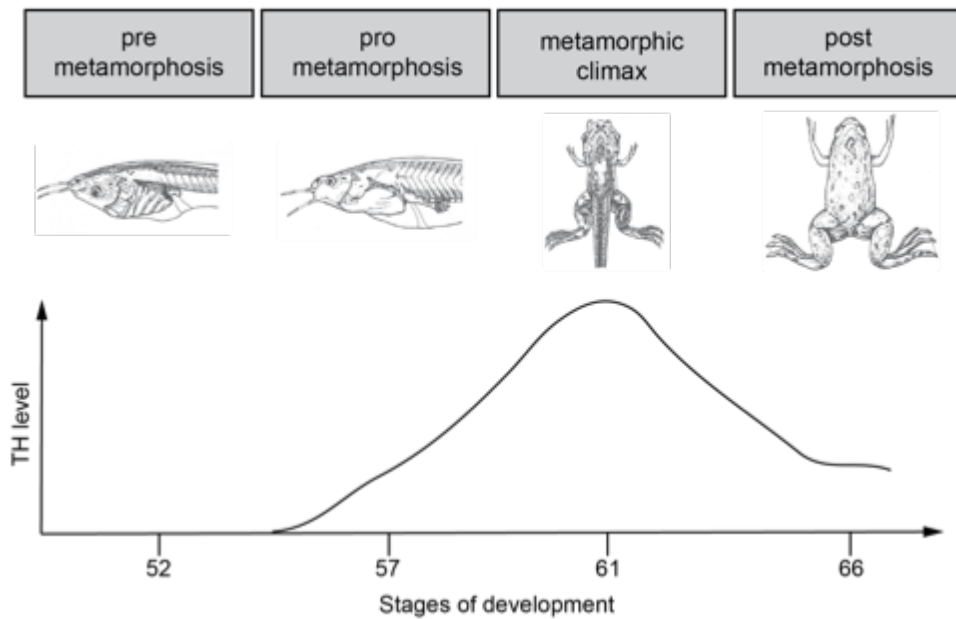


Figure 1-2: Schematic representation of plasma level of thyroid hormones during *Xenopus laevis* metamorphosis. Different metamorphosis periods are indicated in the grey boxes, schematic representation of a *Xenopus* during these periods is shown below. The diagram shows the level of plasmatic thyroid hormone on the vertical axis in function of different *Xenopus* stages indicated on the horizontal axis. The developmental stage representations are from (Nieuwkoop and Faber, 1994).

The peak of TH at metamorphic climax is similar to that at birth for humans and so it is comparable to post embryonic development in mammals. The dependence of metamorphosis on the thyroid hormone regulation is a good model for perinatal development in humans. A lack of thyroid hormone during human perinatal development can lead to cretinism. Although perinatal and post-embryonic organ remodelling in mammals is not under the control of TH the processes are similar and studying *Xenopus* can help us to understand the mechanisms (Brown and Cai, 2007; Buchholz, 2015).

Matrix remodeling in skin and brain during metamorphosis was the focus of the present study. Embryonic and adult *Xenopus laevis* skin structures remodeling are similar to the mammalian foetal skin called 'periderm' and vertebrate adult skin (Brown and Cai, 2007). Cell-cell, cell-ECM interactions and ECM remodeling are important to regulate apoptosis of embryonic cells and differentiation and proliferation of adult cells in the skin remodeling during metamorphosis (Suzuki et al., 2009). Although the central nervous system (CNS) circuits are simpler in *Xenopus* than in mammals the basic organisation is conserved making *Xenopus* an easier model for studying brain development and neurodevelopmental disorders. The CNS is remodeled during

metamorphosis (Lee-Liu et al., 2016) (Pratt and Khakhalin, 2013). ECM composition and its remodeling is important for CNS development such as tenascin-C that regulates neural stem cells maintenance in the sub-ventricular zone stem cell niche by modulation of FGF2 and BMP4 signaling (Garcion et al., 2004) and MMP2 that plays a role in the guidance of the retinal ganglion cell axons by potential cleavage of guidance molecules or ECM components modulating signaling pathways (Hehr et al., 2005).

1.1.4 Animal model to study ECM remodeling during regeneration

Xenopus tadpole has the ability to regenerate the lens, tail and limb. This capacity diminishes during development and is completely lost past metamorphosis. The stage-dependant capacity for regeneration is comparable to that of in mammals (Beck et al., 2009).

Heart development is a highly regulated process conserved in vertebrates involving cell specification and differentiation along with remodeling of the cardiac tissue. Compared to mammals and birds that have a four-chambered heart with two atria and two ventricles, amphibians have a three-chambered heart with a single ventricle similar to the mammalian left ventricle. Fish have a two-chambered heart. Although the adult heart in vertebrates have a different final morphology the early-embryonic events are highly conserved (Hempel and Kühn, 2016). ECM remodeling is an important process for heart development.

The focus of the present study was heart regeneration before, during and after metamorphosis. The heart of adult mammals has limited regenerative capacity and cardiovascular disease remains one of the biggest health risks worldwide (World Health Organisation, The top 10 causes of death, 2017). An infarcted adult heart cannot regenerate the loss of cardiomyocytes and replaces damaged tissue with a fibrotic scar due to the accumulation of collagen leading to a loss of contractile capacity of the heart. Cardiac regeneration therapies are very exciting future therapy possibilities. The adult human heart cannot regenerate whereas heart regeneration does occur in neonatal mammals, some fish and amphibians after injury. Understanding the process of regeneration in these species could help improve cell-based therapies and re-activation of regenerative processes in the human adult after myocardial infarction

(Kochegarov and Lemanski, 2016). Cardiomyocyte proliferation, activation of epicardial tissue and neo-vascularization are key processes for heart regeneration. Amphibians are excellent models to study heart regeneration as they metamorphose from an aquatic tadpole to a tetrapod terrestrial or semiaquatic adult frog, comparable to post embryonic development in mammals. These transitions lead to adaptation of the cardiovascular system and are associated with the decrease of cardiac regeneration. Although little is known about heart regeneration in *Xenopus*, studies on limb, retina and nerve tissue show that they have the ability to regenerate only at tadpole stages (Vivien et al., 2016). It has been shown that the *Xenopus laevis* adult heart cannot regenerate after ventricle resection (Marshall et al., 2017) but *Xenopus laevis* tadpoles at pro-metamorphosis stage have the ability to regenerate their heart after amputation (unpublished data by Dr. Laurent Coen). It will be interesting to look at the difference in gene expression that leads to this loss of cardiac regeneration after metamorphosis.

1.2 ECM in development

The extracellular matrix is present in all tissues and organs providing a physical scaffold and regulating cellular processes such as migration, differentiation, survival and morphogenesis. ECM regulates these processes by direct interaction with cells, via specific surface receptors, by regulating the availability of growth factors, via binding with ECM components, and so intracellular signalling pathways. The ECM is formed of a well-organised three-dimensional network of macromolecules that can vary during development and between tissues. The pericellular and the interstitial matrices are the two distinct types of ECM different in their composition, structure and localisation. The pericellular matrices are close to the cells, for example basement membrane located at the interface between parenchyma and connective tissue, whereas the interstitial matrices surround cells. The major matrix components are collagens, fibronectin (FN), laminins, glycoproteins, proteoglycans (PGs), and glycosaminoglycans (GAGs) (Theocharis et al., 2016).

Specific matrix components, described below, and their function during morphogenesis in *Xenopus* were investigated in the present study.

1.2.1 Collagen

Collagen is the most abundant component of the interstitial and pericellular ECM and is mainly secreted by fibroblasts. The collagen superfamily in vertebrates is composed of twenty-eight different collagen types that are formed by at least forty-six distinct polypeptide chains (α chains). Vertebrate collagens are given a Roman numeral, from I to XXVIII. Collagens are triple α chain helix proteins with non-triple helical domains at their N- and C-termini called 'non collagenous' (NC) domains and numbered from the C-terminus (NC1, NC2, etc.). Collagen type I represents the basic organisation, composed of triple helix without imperfections (without interruption in the helix) and without NC domains assembling into fibrils providing structural scaffolds in a large number of tissues. α chains can assemble into homo- and heterotrimeric helices. For example type I collagen is formed of two identical α chains 1 and a different third α chain 2 whereas collagen II is formed of three identical α chains. The nomenclature of these proteins is $[\alpha 1(I)]_2\alpha 2(I)$ for collagen I and $[\alpha 1(II)]_3$ for collagen II. Members of the superfamily of collagens can be divided into seven sub-families based on their structures and functions. They are fibrillar and network-forming collagens, FACITs (fibril-associated collagens with interrupted triple helices), MACITs (membrane-associated collagens with interrupted triple helices), anchoring fibrils, beaded-filament-forming collagens, and MULTIPLEXIN (multiple triple-helix domains and interruptions) / endostatin-producing collagens (table 1-1 and figure 1-3). Collagen can bind to different cell surface receptors such as integrins that are cell-surface heterodimeric (formed of two subunits α and β) receptors that link the ECM with the intracellular cytoskeleton. Collagen scaffolds provide a structural support for the tissues and regulate intra-cellular signaling affecting various cellular functions including cell migration, adhesion, angiogenesis, tissue development, and repair (Theocharis et al., 2016).

Regulation of *col1a1* expression in *Xenopus laevis* heart during metamorphosis and after ventricular resection was investigated in the present study. Homozygous mutation is lethal in mice due to aortic rupture at 14 days of gestation indicating that *col1a1* is not essential for early development but for late morphogenesis as a structural support for blood vessels (Lohler et al.,

1984). Mutations of col1a1 making it resistant to the cleavage by MMP1 and MMP13 in the helical domain of the collagen α 1(I) chain lead to a delay of wound healing showing the important role of the rapid col1a1 cleavage in wound repair (Beare et al., 2003). Col1a1 is conserved in *Xenopus* (Aldea et al., 2013).

Table 1-1: Different sub-families of collagens with their different members.

Sub-family of collagens	Members
fibrillar	I / II / III / V / XI / XXIV / XXVII
network-forming	IV / VIII / X
FACITs	IX / XII / XIV / XVI / XIX / XX / XXI / XXII
MACITs	XIII / XVII / XXIII / XXV
anchoring fibrils	VII
beaded-filament-forming	VI / XXVI / XXVIII
MULTIPLEXIN	XV / XVII

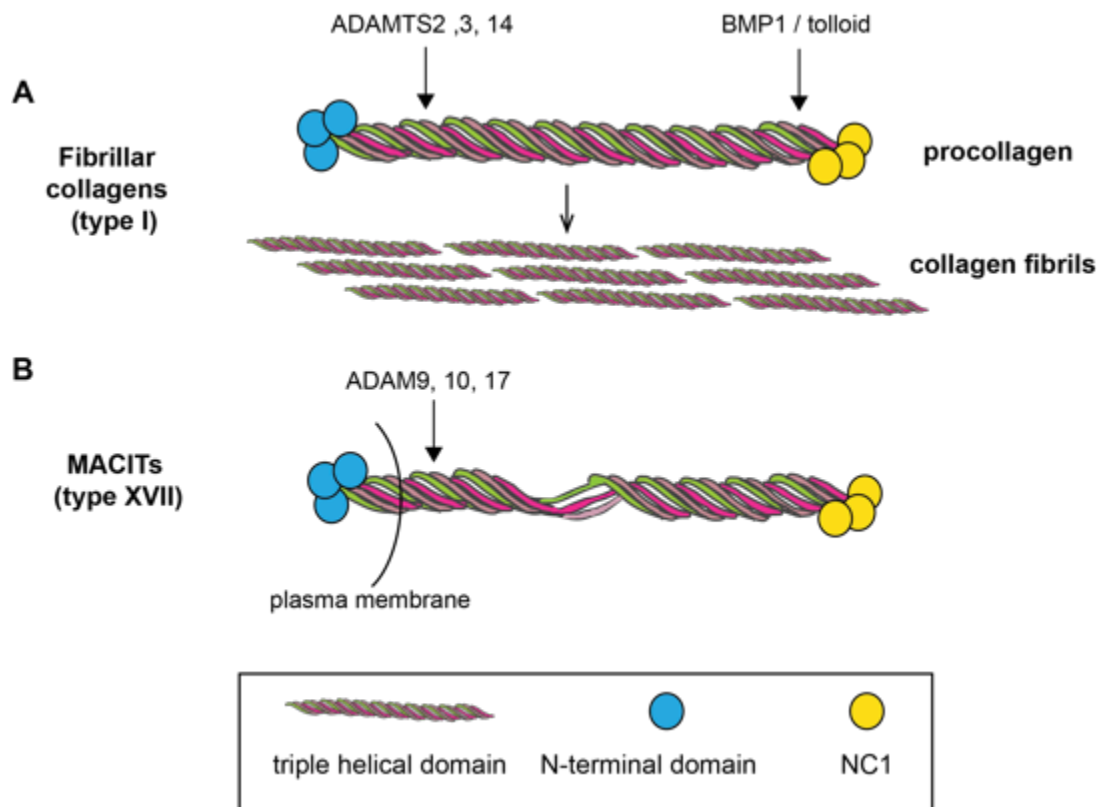


Figure 1-3: Schematic representations of two types of collagens. (A) Type I collagen belongs to the fibrillar collagens sub-family and represent the typical collagen structure. It is synthesised as procollagen protein with N-terminal and C-terminal NC proteins that are cleaved by procollagen N-propeptidases (such as ADAMTS2, 3 and 14) and by procollagen C-propeptidases (such as BMP1 and tolloid). The mature type I collagen is composed of a triple helix without interruption and can form collagen fibrillin stabilised by non-reducible covalent crosslinks necessary for mechanical properties of collagen-containing tissues. (B) Type XVII collagen belong to the MACITs sub-family composed of transmembrane collagens that can act as cell surface receptors and after cleavage of the ectodomain by proteases such as ADAMs (ADAM9, 10 and 17) in a

process called 'ectodomain shedding' they act as soluble collagens in the ECM Theocharis et al. (2016).

1.2.2 Fibronectin

Fibronectin (FN) mostly exists as a dimer composed of two nearly identical subunits linked covalently near their C-termini by a pair of disulfide bonds. Each monomer consists of three types of repeating units (FN repeats): type I, type II and type III. Variants of FN can be found due to alternative splicing of a single pre-mRNA from a single gene. FN can be soluble in the plasma, synthesized by hepatocytes, and less soluble cellular FN synthesized by many cell types including fibroblasts, endothelial cells, chondrocytes, synovial cells and myocytes. The cellular FN sub-families are composed of different isoforms due to cell-type-specific and species-specific splicing patterns. FN can bind to cell surface receptors, such as integrins and syndecan, and to ECM components, such as collagen, heparan sulfate (HS) proteoglycans and fibrin. Several distinct structural and functional domains of FN protein mediate these interactions. FN binds more effectively to denatured collagen/gelatin (after proteolytic cleavage) than to native collagen. Insoluble FN fibrils assemble into the ECM during a highly regulated process called FN fibrillogenesis or FN matrix assembly. FN matrix is essential during embryonic development and is a dynamic matrix during formation, remodeling, or repair of tissues (Theocharis et al. (2016).

Mutant mice for fibronectin die before birth at ED10 due to cardiovascular and vascular defects (George et al., 1993). It has recently been shown that after ventricular resection, adult *Xenopus laevis* heart do not regenerate but present a fibrotic scar composed of fibronectin (Marshall et al., 2017). In the present study the regulation of fibronectin expression was assessed in *Xenopus laevis* heart after ventricular resection during metamorphosis in order to identify difference of regulation between heart with the capacity of regeneration (tadpole) and heart unable to regenerate (adult).

1.2.3 Proteoglycans

Proteoglycan can be classified into four different families, intracellular, cell surface, pericellular-basement membrane, and extracellular defining in function of their localisation and their structures (Theocharis et al., 2016).

1.2.3.1 Hyallectans

The hyallectan/lectican family of chondroitin sulfate proteoglycans is named after their ability to bind to hyaluronan (HA) and lectin. The family comprises aggrecan, versican, neurocan and brevican, which belong to the extracellular family of proteoglycans. They are composed of a core glycoprotein and side chains of glycosaminoglycan (GAG) attached by a covalent bond to serine residues (Brunet et al., 2012). GAGs are long highly negatively charged heteropolysaccharides that comprise different types such as chondroitin sulfate (CS), dermatan sulfate (DS), heparan sulfate, keratan sulfate (KS) and hyaluronan (Stanton et al., 2011). The core protein is composed of an N-terminal globular (G) 1 domain comprising an immunoglobulin-like domain (Ig) and two proteoglycan tandem repeats (PTR) domains binding to hyaluronan, variable sizes and properties GAG-attachment regions and a C-terminal G3 domain comprising a variable number of epidermal growth factor (EGF) like domains, a lectin-like domain, and a complement regulatory protein (CRP) like domain (Avram et al., 2014).

Aggrecan (encoded by the *ACAN* gene) is the major proteoglycan in articular cartilage. Its core protein is formed of an N-terminal G1 domain, G2 domain comprising two PTRs. Keratan sulfate can bind between those two domains, it also has GAG-attachment regions, where KS and chondroitin sulfate can bind, and a C-terminal G3 domain (figure 1-4). The G3 domain interacts with ECM components such as fibulin, fibrillin and tenascin. The two PTR of the G2 domain do not interact with HA. G1 domain binds to HA and cartilage link proteins (LP) stabilize this interaction. The complex aggrecan/HA are negatively charged, which makes them highly hydrated, which in turn creates a loose ECM that confers viscoelasticity to the cartilage. Degradation of aggrecan in articular cartilage is a major factor of osteoarthritis (OA) (Roughley and Mort, 2014).

The versican (encoded by the *VCAN* gene) core protein is formed of an N-terminal G1 domain, central GAG-attachment regions (GAG α and GAG β) where CS can bind and a C-terminal G3 domain comprising two EGF-like domains. Versican can be found in five isoforms (V0, V1, V2, V3 and V4), that differ by their GAG-attachment regions; V0 has both GAG α and GAG β containing up to

23 CS chains, V1 has just GAG β and up to 15 CS chains binding, V2 only has GAG α and up to 8 CS chains, V3 does not have any GAG-attachment regions and V4 has a truncated GAG β domain with 5 predicted CS chains (figure 1-4) (Nandadasa et al., 2014). The G3 domain can bind to ECM components such as fibrillin, fibulins, fibronectin, tenascins, cellular receptors such as integrin β 1 and EGF receptors via its EGF-like repeat to regulate cell proliferation. CS chains can bind to the cell surface glycoprotein CD44. Versican G1 domain can bind to hyaluronan via two link modules (Wu et al., 2005). These complexes form macro-aggregates that regulate viscoelasticity and hydration of the skin, HA and CS chains are negatively charged and attract water. Versican-HA complexes create a loose hydrated matrix. Hyaluronan cell surface receptor CD44 mediates cell interaction with the versican-HA complexes (Smith and Melrose, 2015). V0 and V1 are expressed in the heart and limb during development, vascular smooth muscle cells, fibroblasts, whereas versican V2 and V3 are mostly expressed in the nervous system (Nandadasa et al., 2014). Homozygous mutant mice for versican (called hdf (heart defect) mice) die before birth between ED10.5 and 11 with severe heart development defects (Yamamura et al., 1997). Versican is an important matrix component during development creating a loose hydrated ECM permissive for morphogenesis and remodeling. It has been shown to play a role in neural crest migration by defining migratory routes providing confinement to allow directional migration (Szabo et al., 2016).

Brevican and neurocan (encoded by *BCAN* and *NCAN* genes respectively) are specifically expressed in the central nervous system. They have an N-terminal G1 domain, GAG-attachment regions, where chondroitin sulfate can bind, and a C-terminal G3 domain comprising two EGF-like domains in neurocan (figure 1-4). An isoform of brevican can have the C-terminal G3 domain replaced by a glycosylphosphatidylinositol (GPI)-anchor. Neurocan is able to bind matrix components such as HA, tenascin and neural cell adhesion molecule (NCAM). Brevican can bind to tenascin. *NCAN* mutation is associated with psychiatric disorders such as bipolar disorder and schizophrenia (Avram et al., 2014) (Bandtlow and Zimmermann, 2000).

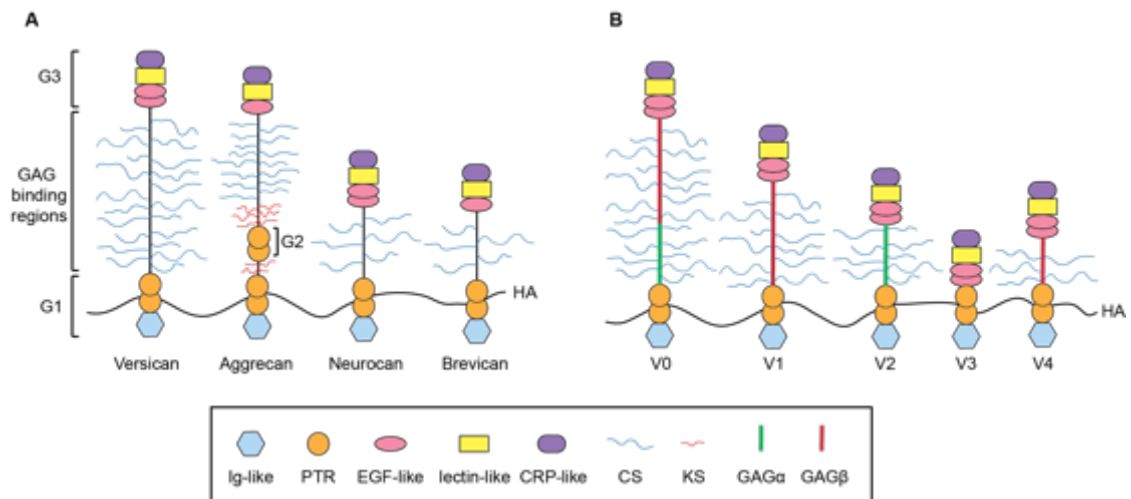


Figure 1-4: Hyalactan/lectican family. (A) The four members of the family all have an N-terminal G1 domain containing an Ig-like domain and PTR domains that can bind to hyaluronan (HA), central GAG binding regions where keratan sulfate (KS) and chondroitin sulfate (CS) can bind by covalent bonds, and a C-terminal G3 domain containing one or two EFG-like domains, a lectin-like domain and a CRP-like domain. Only aggrecan has a G2 domain separated from the G1 domain by a GAG binding region where KS can bind. (B) The five versican isoforms all have the same G1 and G3 domain but their GAG attachment regions, GAG α and GAG β , differ. V0 have GAG α and GAG β , V1 has only GAG β , V2 has only GAG α , V3 does not have any GAG and V4 has a truncated GAG β .

1.2.3.2 Syndecans

Syndecans are a family of four type I transmembrane heparan sulfate proteoglycans (HSPGs), syndecan-1 to -4. Three distinct domains constitute their core protein, a short cytoplasmic domain containing various binding motifs, a single transmembrane domain and an ectodomain domain where several glycosaminoglycans chains are attached to specific serine residues. The extracellular part of syndecans varies between syndecan family members, in contrast to the transmembrane and cytoplasmic domains, which are highly conserved. Various GAGs can bind covalently to the ectodomain, HS, CS or DS are attached to syndecan-1 and -3 but only HS is attached to syndecan-2 and -4. The transmembrane domain is necessary for the dimerisation of syndecans into homodimers. Their cytoplasmic domain is composed of two conserved regions (C1 and C2) separated by a variable region (V) that can interact with several intracellular kinases and the actin cytoskeleton, promoting various cell functions. Ectodomains of syndecans mediate several cell-cell and cell-matrix interactions via the GAG chains. Syndecans can bind to FN, collagen, thrombospondin (TSP) and tenascin-C (TN-C). Syndecans are cellular

receptors for growth factors (GFs) and can act as co-receptors with growth factor receptors (GFRs) and with integrins regulating downstream signalling. Proteases can cleave syndecans in the process of ectodomain shedding (Theocharis et al., 2016).

Knockout for syndecans do not give rise to severe developmental phenotype however it causes defects under pathological conditions such as wound healing and cardiac fibrosis. Knockout mice for syndecan 4 present a defect in heart function and an increase of mortality due to cardiac rupture after myocardial infarction (MI). In the absence of syndecan 4 the number of fibroblasts and myofibroblasts was reduced as a result of a decrease in migration due to a dysregulation of the fibronectin-induced signaling leading to an impaired granulation tissue formation. In addition a reduced angiogenesis is observed in this mice following MI as a result of an impaired bFGF-induced signaling because syndecan 4 acts as a coreceptor for bFGF (Matsui et al., 2011). Similar phenotype is observed in mice when shed form of syndecan 4 is overexpressed showing that it acts as an inhibitor of the endogenous syndecan 4 signaling (Matsui et al., 2011). In the present study the expression of syndecans was measured in *Xenopus laevis* heart during metamorphosis and after ventricular resection. Syndecans are conserved in *Xenopus* and syndecan 4 has been shown to be essential for convergent extension movements during early development by regulation of the non-canonical Wnt pathways through activation of syndecan4 by fibronectin and Frizzled7 by Wnt ligands (Munoz et al., 2006).

1.2.4 Matricellular proteins

Matricellular proteins are in the ECM, interact with cells to modulate cellular functions but do not contribute to the structure of the ECM. The matricellular family contains a large number of members such as thrombospondin (TSP), tenascins (TN), cartilage oligomeric protein (COMP, or TSP-5) and fibulins. All matricellular proteins can directly or indirectly regulate cellular function by interaction with cellular receptors, ECM macromolecules, growth factors, and proteases. They can be localised at the plasma membrane, intracellularly, in body fluids as soluble proteins, or in the ECM. They can be cleaved by proteases generating protein fragments. They are incorporated into

the ECM of remodeling tissues during development, wound healing, and in response to injury and stress, especially in fibrotic ECM (Theocharis et al., 2016). Tenascin-C is expressed in the cardiac regenerative matrix after ventricle amputation in newt and regulates the proliferation of cardiomyocytes by increasing their cell cycle re-entry (Mercer et al., 2013). In the present study the expression of tenascin-C was investigated in *Xenopus laevis* tadpoles, juveniles and adults hearts after ventricular resection to look at its regulation during cardiac regeneration.

1.3 Metalloproteinases

Proteolysis of the ECM is a highly regulated important process in development, morphogenesis, tissue remodeling and repair and its dysregulation can cause many diseases. Proteases are highly conserved from archaea to bacteria and from plant to animals. The repertoire of proteases produced by cells, comprise of at least 569 human proteases or protease-like proteins and homologs and 156 human protease inhibitors, is known as the “degradome” (Quesada et al., 2009).

The A Disintegrin and Metalloproteinase with Thrombospondin type-1 motifs (ADAMTS) family will be the main focus of the present study, as well as A Disintegrin And Metalloproteinases (ADAM) and Matrix Metalloproteinases (MMP) involved in ECM remodeling. They belong to the metzincin family so-called for the conserved Met residue at the active site and a zinc-binding motif (HEXXHXXGXXH) in the active site of the protease domain necessary for the enzymatic reaction (figure 1-5) (Huxley-Jones et al., 2007). The metalloproteinases belong to the MA (M from metallo, A as a classifier) clan. In this clan MMPs belong to the M10A family, and ADAMs and ADAMTs to the M12B family in the MEROPS database of proteolytic enzymes (Rawlings et al., 2008).

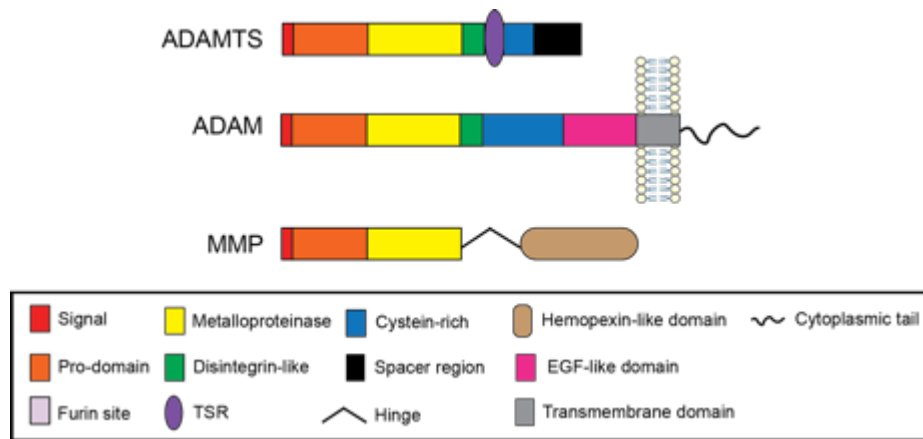


Figure 1-5: Basic domain organisation of ADAMTS, ADAM and MMP proteins. Names of the different domains are indicated in the key below the diagrams.

1.3.1 Matrix Metalloproteinases (MMP)

The MMPs are one of the major families of proteinases that can degrade all major ECM components, adhesion molecules, growth factors, cytokines, chemokines and receptors leading to tissue remodeling and regulation of cell behaviour. MMPs are essential for embryogenesis, bone growth, angiogenesis, wound healing and tissue regeneration. They are expressed mostly in fibroblasts and are also found in neutrophils, monocytes, macrophages and endothelial cells. Fragments generated after MMP cleavage can regulate cellular activities by interacting with specific receptor; they are called matrikines. The first MMP was identified in 1962, in frog by an *in vitro* experiment looking at the resorption of the tail during metamorphosis (Gross and Lapiere, 1962). They named it collagenase-1, now referred to as MMP-1. 24 members have been identified in vertebrates comprising MMP-1 to MMP-28 without MMP-4, MMP-5, MMP-6 and MMP-22 that were identified by different research teams at the same time (Loffek et al., 2011) (Jablonska-Trypuc et al., 2016). They are divided into six sub-families, based on their molecular structure and substrate preference, collagenases, gelatinases, stromelysins, matrilysins, membrane-type and others (table 1-2) (Loffek et al., 2011) (Jablonska-Trypuc et al., 2016).

MMP-7 and -26 represent the basic molecular organization of an MMP. The basic MMP structure consists of a signal peptide, a propeptide and a metalloproteinase domain containing the zinc-binding consensus sequence HEXGHXXGXXHD common to all metalloproteinases. Generally, a hemopexin-like domain is linked to the metalloproteinase domain by a linker or hinge

domain (figure 1-6). The addition of these two domains is found in MMP-1, -3, -8, -10, -11, -12, -13, -18, -19, -20, -21, -27 and -28. MMP-2 and MMP-9 have a fibronectin-like domain between the pro-domain and the metalloproteinase domain. Transmembrane MMPs (MMP-14, -15, -16 and -24) have a transmembrane domain and a short cytoplasmic domain. MMP-17 and -25 have a GPI anchor domain. MMP-23 has a unique organisation containing an N-terminal transmembrane domain, a pro-domain, a metalloproteinase domain, a cysteine-rich domain and an immunoglobulin domain (Loffek et al., 2011) (Jablonska-Trypuc et al., 2016).

Table 1-2: Sub-families of the main members of MMP family.

Sub-family	Sub-family name	General name
Collagenases	Collagenase-1	MMP-1
	Collagenase-2	MMP-8
	Collagenase-3	MMP-13
Gelatinases	Gelatinase A	MMP-2
	Gelatinase B	MMP-9
Stromelysins	Stromelysin-1	MMP-3
	Stromelysin-2	MMP-10
	Stromelysin-3	MMP-11
Matrilysins	Matrilysin	MMP-7
	Metalloelastase	MMP-12
	Matrilysin-2	MMP-26
Membrane-type	MT1-MMP	MMP-14
	MT2-MMP	MMP-15
	MT3-MMP	MMP-16
	MT4-MMP	MMP-17
	MT5-MMP	MMP-24
	MT6-MMP	MMP-25

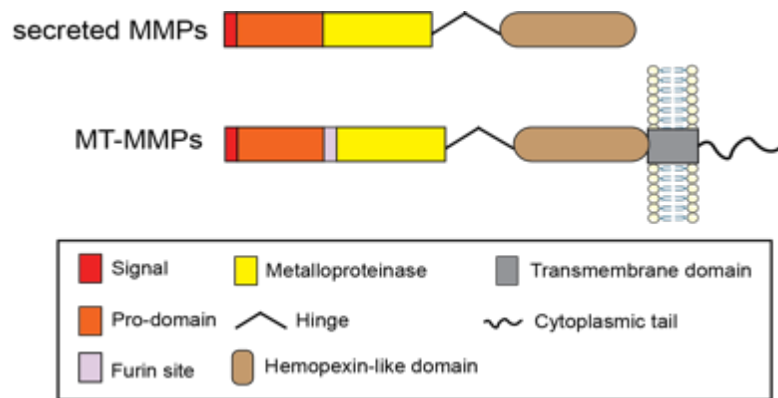


Figure 1-6: Basic domain organisation of MMP proteins. Names of the different domains are indicated in the key below the diagrams. Some MMPs do not have the hinge and hemopexin-like domain and some other have additional domains.

MMPs are initially synthesised as inactive pro-forms called zymogens, their pro-domain is cleaved by an endoproteinase for activation. The latency of the enzyme is maintained by the “cysteine switch” motif that interacts with the catalytic zinc ion and prevents binding and cleavage of the substrate. Some MMPs, including the membrane-type MMPs, as well as MMP-11, -23 and -28 have a conserved furin cleavage site (RX(R/K)R) before their metalloproteinase domain and thus can be activated in the trans-Golgi and act as active proteases on the cell surface or secreted in the ECM. The other MMPs are secreted as zymogens and must be activated by cleavage of their pro-domain by proteases including some MMPs such as MMP-1, -2, -8 and -9 as well as membrane-type MMPs. Tissue inhibitors of metalloproteinases (TIMPs) can inhibit the active forms of MMPs and the process of activation or conversion of the pro-MMPs into MMPs (Loffek et al., 2011) (Jablonska-Trypuc et al., 2016).

Mice knocked-out for single MMPs in general do not show severe phenotypes however combined knock-out mice for several MMPs present more severe phenotypes, such as MMP-2/MMP-14 knock-out die after birth due to respiratory failure and vascular defects, suggesting functional redundancy of MMPs (Oh et al., 2004). Over expression of both MMP-2 and MMP-14 in *Xenopus laevis* lead to developmental defects and embryonic death (Hasebe et al., 2007a). Mutated mice for MMP9 show a defect in wound healing and regeneration of the corneal epithelium due to dysregulation of the level of the cytokine IL-1 α and the accumulation of fibrin (Mohan et al., 2002). MMP1 has been shown to be necessary for keratinocytes migration on type I collagen

toward the wound healing site by cleavage of type I collagen creating a loose matrix and reducing the association of $\alpha 2\beta 1$ integrin with native collagen allowing cell migration. The association of $\alpha 2\beta 1$ integrin with native collagen, in the frontobasal end of the cells, regulates this process by activating MMP1 expression (Pilcher et al., 1997). MMP2 and MMP9 can activate TGF- β signaling by cleavage of the latent TGF- β . MMP9 is associated to the cell surface hyaluronan receptor CD44 and cleave latent TGF- β at the cell surface (Yu and Stamenkovic, 2000). In the present study the regulation of expression of the several MMPs was investigated in *Xenopus laevis* heart during metamorphosis and after ventricular resection.

1.3.2 ADAM

A Disintegrin And Metalloproteinases (ADAMs) are type-I transmembrane and soluble glycoproteins that have diverse functions in cell adhesion, migration, proteolysis and signaling. Forty ADAM genes have been identified in mammalian genomes so far. 22 ADAMs are expressed in human but only 12 (ADAM8, 9, 10, 12, 15, 17, 19, 20, 21, 28, 30 and 33) are active proteinases containing the consensus sequence (HEXGHXXGXXHD) common to zinc-binding metalloproteases, eight are inactive missing the consensus sequence in their metalloproteinase domain (ADAM2, 7, 11, 18, 22, 23, 29 and 32) and two are described as pseudogenes (ADAM5P and 6). Some ADAMs (ADAM9, 12 and 28) have splicing variants that are expressed as soluble active proteinases without the transmembrane and cytoplasmic regions (Edwards et al., 2008). ADAMs are composed of a N-terminal signal peptide, a pro-domain, a metalloproteinase domain, a disintegrin domain, a cysteine-rich domain, an EGF-like domain (except for ADAM10 and 17), a transmembrane domain and a cytoplasmic domain (figure 1-7). The EGF-like domain can bind cell surface proteoglycans. The cytosolic tail is the most variable region between members and has been shown to regulate ADAMs proteolytic activity, intracellular transport, localisation and cell signaling (Weber and Saftig, 2012).

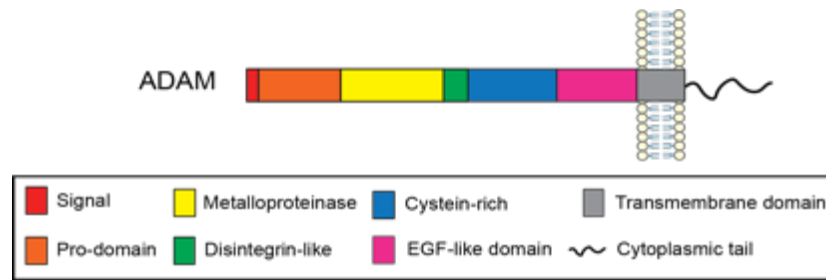


Figure 1-7: Basic domain organisation of ADAM proteins. ADAMS 10 and 17 do not have an EGF-like domain and soluble ADAMs do not have a transmembrane and a cytoplasmic domain. The cytosolic tail is the most variable region between members. Names of the different domains are indicated in the key below the diagrams.

ADAMs are widely expressed and play fundamental roles during developmental processes. The best-characterised function of the transmembrane ADAMs is their involvement in ectodomain shedding, which is the cleavage of type I and type II transmembrane proteins and GPI-anchored proteins close to the cell surface. This process has been shown to regulate signaling pathways in the host cells or in neighbouring cells by down-regulation of cell surface receptors or by increasing the liberation of soluble ligands. ADAM19 knockout mice show heart development defects due to the lack of ectodomain shedding of ErbB ligands, such as Neuregulin necessary for ErbB signaling essential for heart development (Kurohara et al., 2004). Knockout for ADAM9 leads to a faster re-epithelialization during wound repair as a result of the lack of collagen XVII ectodomain shedding that acts as an inhibitor of keratinocyte motility (Mauch et al., 2010). In addition, ectodomain shedding can generate cleaved intracellular domains that translocate to the nucleus and regulate gene transcription. This process is called “regulated intramembrane proteolysis” (RIP). ADAM10 knockout mice die at E9.5 due to multiple malformation such as delay of heart development similar to the phenotype obtain in Notch1 knockout mice (Hartmann et al., 2002). ADAM10 has been shown to be essential for extracellular cleavage of Notch removing the extracellular domain allowing a second cleavage by γ -secretase releasing the intracellular domain that enters the nucleus (van Tetering et al., 2009). The function of inactive ADAMs is still unclear but they can act as adhesion molecules (Weber and Saftig, 2012). ADAMs play key roles in development and morphogenesis. The ADAM family has been shown to be conserved in *Xenopus* with the exception of ADAM7 and ADAM8 (Wei et al., 2010). In the present study their expression was assessed in *Xenopus laevis* heart and after

ventricular resection during metamorphosis.

1.3.3 ADAMTSL

ADAMTS-like is a family of 7 members, ADAMTSL1 to 6 and papilin. They are secreted protein without a proteinase domain so they do not have proteolytic activity (figure 1-8). The C-terminal region is the most variable between members with additional Thrombospondin type 1 Sequence Repeat (TSR) domain and specific domains such as Immunoglobulin domain and PLAC domain (Dancevic et al., 2013). Little is known about this family. In human, *ADAMTSL2* mutations cause geleophysic dysplasia, an inherited condition that affects many parts of the body and is characterized by abnormalities involving the bones, joints, heart, and skin, and *ADAMTSL4* mutations cause ectopia lentis, an inherited connective tissue disorder characterised by lens dislocation of the eye, which can cause serious vision problems. ADAMTSL4 and 6 promote the formation of microfibril network *in vitro* (Dubail and Apte, 2015).

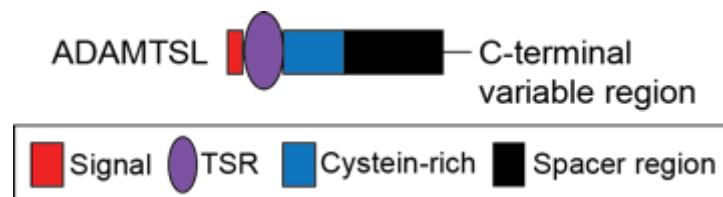


Figure 1-8: Basic domain organisation of ADAMTS-like proteins. ADAMTS-like proteins do not have a proteinase domain but only an ancillary domain with a C-terminal variable region between the 7 members of the family. Names of the different domains are indicated in the key below the diagrams.

1.3.4 ADAMTS

The ADAMTSs are extracellular, secreted enzymes that have diverse functions in development and disease. 19 members are present in mammalian genomes. The first ADAMTS gene, *ADAMTS1*, was identified in 1997 as a gene associated with inflammation (Kuno et al., 1997). The characterisation of the ADAMTS family in *Xenopus laevis* and *Xenopus tropicalis* was the focus of the present study.

1.3.4.1 Evolutionary history

The evolutionary history of the 19 mammalian *ADAMTS* genes has been marked by duplication and retrotransposition events giving rise to different subfamilies, in association with the organism's complexity, creating neofunctionalization. Comparisons of protostomes (such as insects and

nematodes) and deuterostomes (chordates and vertebrates) genomes show that an ancestral *ADAMTS* gene duplicated prior to their divergence, around 650 million years ago (Ma). This is the origin of the distinction between the aggrecanases (*ADAMTS*1, 4, 5, 8, 15, 9 and 20) and the other subfamilies of *ADAMTS* (figure 1-9 and 1-10). *ADAMTS-A* and *CG4096* represent these two distinct evolutionary branches in *Drosophila melanogaster* (figure 1-9) (Ismat et al., 2013). But the nematode *Caenorhabditis elegans* only has one gene, *Gon-1*. This is similar to the aggrecanases subfamily, more specifically to *ADAMTS*9 and 20, suggesting a loss of the founder gene of the other *ADAMTS* subfamilies (figure 1-9) (Nicholson et al., 2005). In chordates duplication and retrotransposition events occurred generating new clades of *ADAMTS*. In the ascidian *Ciona intestinalis*, four genes are duplicated from the ancestral gene represented by *CG4096* in *D. melanogaster*, they are *Ciona ADAMTS7*, *Ciona ADAMTS6*, *Ciona ADAMTS18* and *Ciona ADAMTS3*. Retrotranspositions of the ancestral gene of the other branch, represented by *CG6107* in *D. melanogaster* and *Gon-1* in *C. elegans*, gives rise to *Ciona ADAMTS9* and *Ciona ADAMTS15* (figure 1-9). In mammals, the expansion of the *ADAMTS* family occurred by two whole genome duplication events. This suggests that *Ciona ADAMTS7* is the ancestral gene of vertebrate *ADAMTS7* and *ADAMTS12*, *Ciona ADAMTS6* for vertebrate *ADAMTS6* and *ADAMTS10*, *Ciona ADAMTS18* for vertebrate *ADAMTS16* and *ADAMTS18*, *Ciona ADAMTS3* for vertebrate *ADAMTS2*, *ADAMTS3* and *ADAMTS14*, *Ciona ADAMTS9* for vertebrate *ADAMTS9* and *ADAMTS20* and *Ciona ADAMTS15* for vertebrate *ADAMTS1*, *ADAMTS4*, *ADAMTS5*, *ADAMTS8* and *ADAMTS15* by gain of new introns (figure 1-9). No ancestral genes are present in *C. intestinalis* for the vertebrate *ADAMTS13* and the pair *ADAMTS17/19*, suggesting that they were derived from duplication during evolution from chordate ancestors (figure 1-9) (Huxley-Jones et al., 2005).

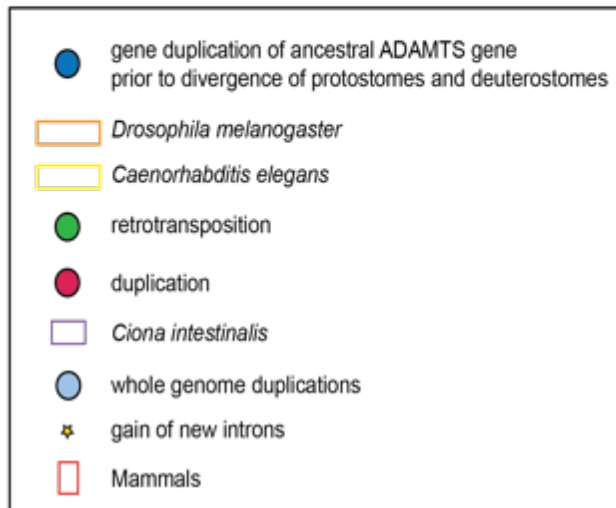
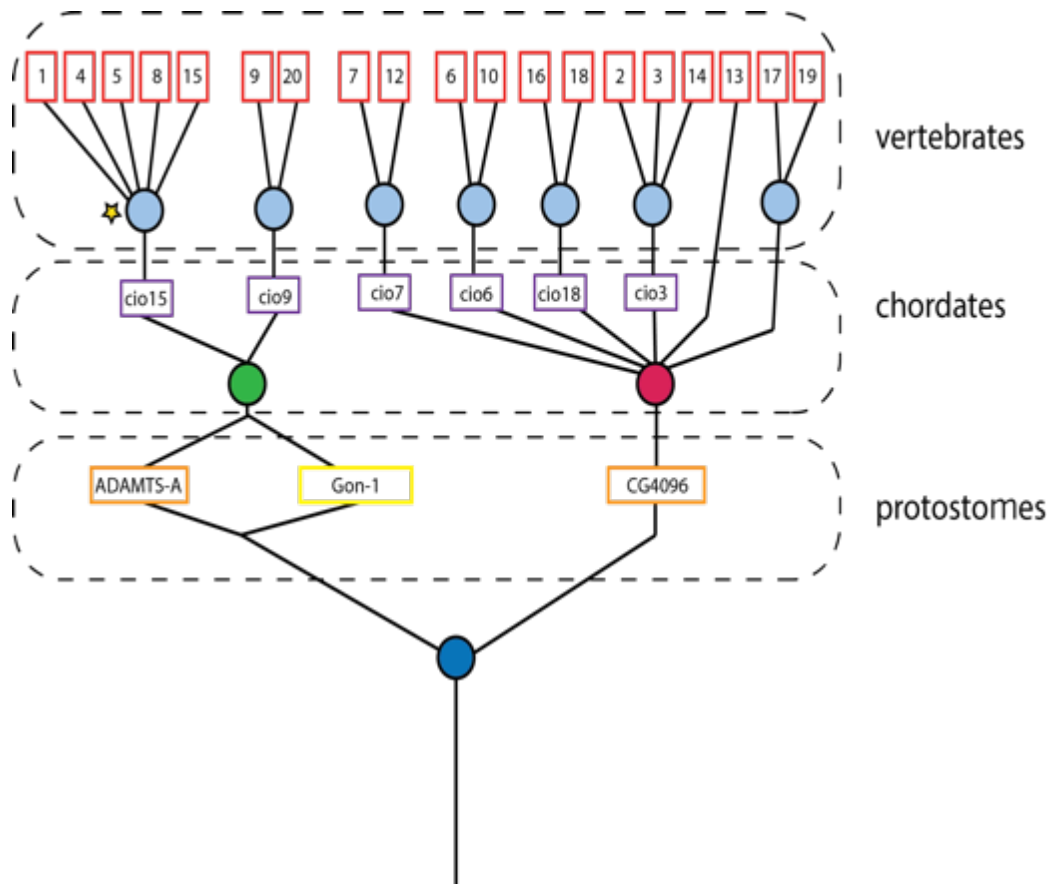


Figure 1-9: Schematic representation of the evolutionary history of the ADAMTS family. A duplication event of an ancestral gene prior to divergence between protostomes and deuterostomes lead to two branches of ADAMTS genes. Other duplications and retrotranspositions events increased the diversity of ADAMTS subfamily in chordates. The 19 ADAMTS present in vertebrates derive from duplication and gain of intron of chordate ancestral genes. The figure is not to scale for evolutionary distance. Names of the genes are indicated in the boxes corresponding to the specie such as cio15 for *Ciona ADAMTS15*, 1 for mammals *ADAMTS1*.

1.3.4.2 Molecular structure

All ADAMTS proteins have the same basic domain organisation defined by a proteinase domain and an ancillary domain. The proteinase domain comprises an amino (N)-terminal signal peptide, a pro-domain and a catalytic domain containing the metalloproteinase domain and the disintegrin-like domain. The basic ancillary domain has a central Thrombospondin type 1 Sequence Repeat (TSR), a cysteine-rich domain and a spacer region. ADAMTS4 is the only member of the family to have this basic structure (figure 1-10). The carboxy (C)-terminal region of the ancillary domain is the most variable between the ADAMTSs. The differences in domain organisation and function define eight sub-groups of ADAMTSs: the hyaluronanases/aggrecanases (ADAMTS1, 4, 5, 8, 9, 15 and 20), the pro-collagen N-propeptidases (ADAMTS2, 3 and 14), the von-Willebrand Factor (vWF) cleaving protease (ADAMTS13), the Cartilage Oligomeric Matrix Protein (COMP) proteinases (ADAMTS7 and 12) and the “orphan” (ADAMTS6, 10, 16, 18,17 and 19) (figure 1-9) (Kelwick et al., 2015a).

1.3.4.2.1 Pro-domain

The ADAMTS pro-domain is composed of 220 to 300 amino acids except for ADAMTS13 that has a short 70 amino acid pro-domain. All ADAMTSs contain at least one site capable of being cleaved by furin-like pro-protein convertases (PPC). PPC enzymes can act extracellularly, intracellularly or on the cell surface. These different locations of action can regulate some ADAMTS activity. Pro-ADAMTS4 and 1 are cleaved intracellularly, in the trans-Golgi network, by PPC enzymes and are secreted in the mature form (Wang et al., 2004) (Rodriguez-Manzaneque et al., 2000). Pro-ADAMTS 5 is cleaved extracellularly whereas pro-ADAMTS 9 is cleaved on the cell surface via formation of a complex with the cellular chaperone heat shock protein gp96/GRP94 (Longpre et al., 2009) (Koo and Apte, 2010). The pro-domain can have different roles in the regulation of ADAMTSs activities. Some ADAMTSs do not have to lose their pro-domain to be active. For example, it has been shown that the efficiency of ADAMTS9 for cleaving versican is reduced without its pro-domain (Koo et al., 2007). ADAMTS13 and 7 have a catalytic activity with their pro-domain (Majerus et al., 2003) (Somerville et al., 2004).

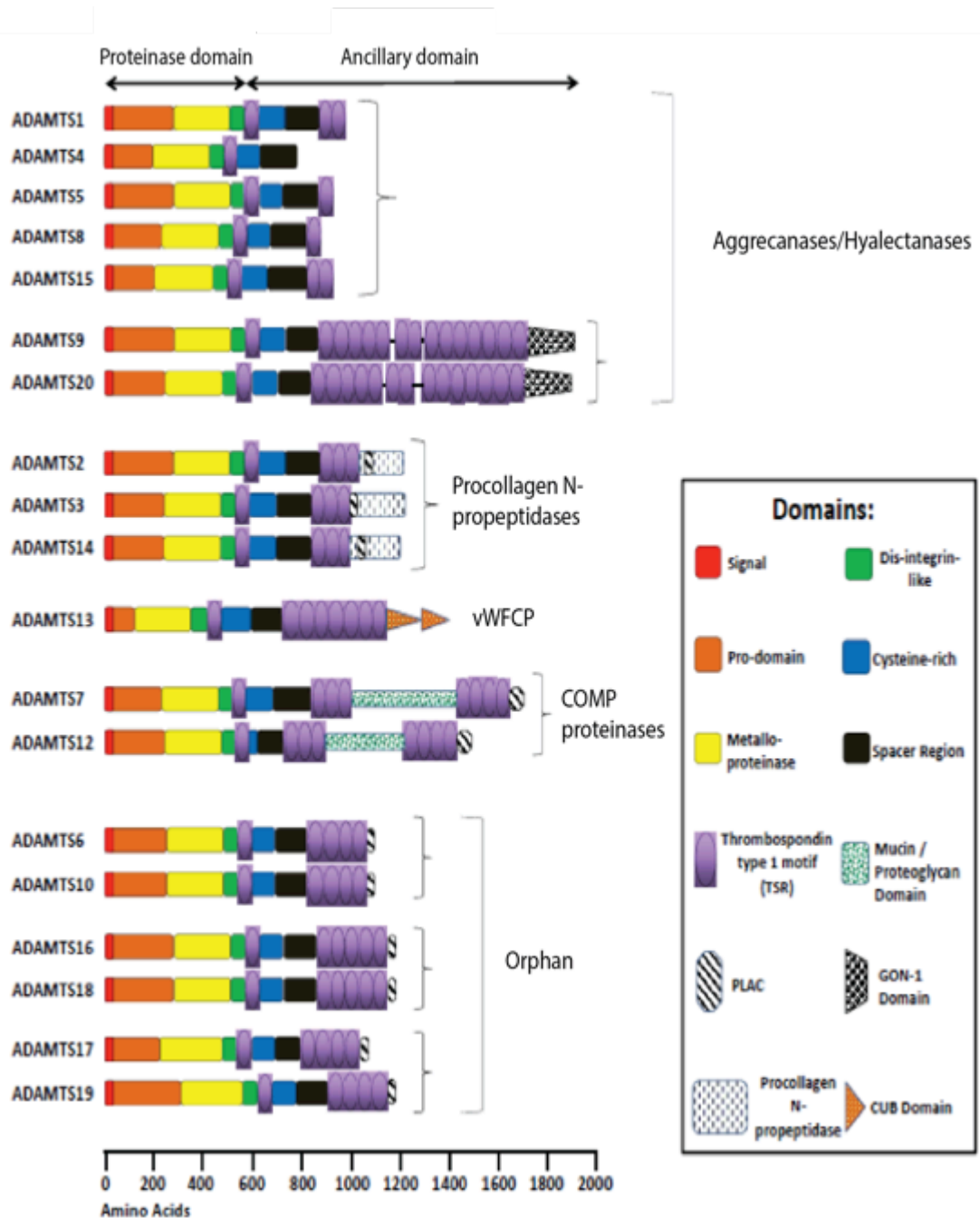


Figure 1-10: Molecular structure of the 19 members of the ADAMTS family. ADAMTS4 is the only member with the ‘basic’ organisation common to all members composed of a proteinase domain containing an amino (N)-terminal signal peptide, a pro-domain and a metalloproteinase domain and a disintegrin-like domain. The basic ancillary domain has a central TSR, a cysteine-rich domain and a spacer region. The carboxy (C)-terminal region of the ancillary domain is the most variable between the ADAMTSs containing one to fourteen additional TSR motifs and specific domains defining different sub-groups. Names of the different domains are indicated in the key below the diagrams. The different ADAMTS representations are drawn to scale of their amino acids indicated on the axis below. Adapted from (Kelwick et al., 2015a).

1.3.4.2.2 Catalytic domain

This domain is composed of the metalloproteinase and disintegrin-like domains. The metalloproteinase domain is composed of 227 to 247 amino acids and contains the zinc-binding motif HEXXHXBG(/N/S)BXHD. It forms an active site cleft where substrates can bind, common configuration to the metzincin family (Gomis-Ruth, 2009). The substrate specificity of this domain defines the different sub-groups of the ADAMTS family. The disintegrin-like modules of the ADAMTSs are approximately 65 amino acids and are highly conserved between all members. The disintegrin-like domains do not interact with integrins. ADAMTS1, 4 and 5 disintegrin-like domain is a cysteine-rich region located close to the active site cleft and has a possible regulatory role or function on the substrate preference (Gerhardt et al., 2007) (Mosyak et al., 2008). ADAMTS 4 and 5 have two alternative conformations states ('open' and 'closed') for their active site depending on additional Ca²⁺ ion binding that can possibly be used as a regulation of their catalytic activity through the binding to other proteins (Mosyak et al., 2008).

1.3.4.2.3 Ancillary domain

The ancillary domain can interact with ECM components and can regulate ADAMTSs activity and their binding to their specific substrates. This domain contains up to 15 TSR domains, composed of around 50 amino acids, including a central common at all ADAMTSs. These domains are similar to the type I repeats of thrombospondins 1 and 2. The central TSR is followed by a cysteine-rich domain composed of around 100 amino acids in all ADAMTSs except ADAMTS12 that has a smaller cysteine-rich domain, and a spacer domain composed of 103 to 160 amino acids. The C-terminal region of the ancillary domain is the most variable between ADAMTSs, except in ADAMTS4 the spacer domain is followed by additional TSR domains and specific domains defining the different sub-groups. The ADAMTS9, 20 pair contains 14 additional TSRs and a gonadal (GON) domain in C-terminal. ADAMTS13 has two CUB (complement C1r/C1s, Uegf (epidermal growth factor-related sea urchin protein), BMP-1 (bone morphogenetic protein-1)) domains in addition to 7 additional TSRs. Several ADAMTSs (ADAMTS2, 3, 6, 7, 10, 12, 14, 16, 17, 18 and 19) contain a PLAC (protease and lacunin) domain. In the pro-collagen N-

propeptidases (ADAMTS2, 3 and 14) sub-group the PLAC domain is embedded within a region unique to these enzymes, while in all others the PLAC modules mark the C-terminus of the proteins. In ADAMTS7 and 12, a mucin/proteoglycan domain is interposed between the 7 additional TSRs, precisely between TSR4 and TSR5 (figure 1-9) (Kelwick et al., 2015a).

1.3.4.3 Post-translational modifications

ADAMTSs are subject to post-translational modifications that can affect their association with the cell surface or the ECM, as well as their activation and their catalytic functions. Their pro-domain is N-glycosylated, except for ADAMTS4 and for ADAMTS9 this modification is necessary for its secretion. TSR domains can be modified by C-mannosylation of tryptophans residues and O-fucosylation of Ser/Thr residues in the TSRs. ADAMTS7 mucin domain is modified by addition of CS chains (Somerville et al., 2004) (Kelwick et al., 2015a). Proteolysis of the ancillary domain has been shown for a number of ADAMTSs such as ADAMTS4 (Kashiwagi et al., 2004).

1.3.4.4 Functions in development

ADAMTSs are large, highly post-translationally modified by glycosylation and proteolysis of the ancillary domain, have a low secretion level by cells and have catalytic activity depending on the recognition of their specific substrate, such as the interaction of ADAMTS5 ancillary domain with CS chains of versican (Foulcer et al., 2014). These features make them difficult to study *in vitro*. Mouse genetics have provided a useful tool for characterising the function of these proteinases in development *in vivo*. Identification of a mutation responsible for a phenotype (forward genetic), creation of a mutation and analysis of the phenotype (reverse genetic), have both been used (Dubail and Apte, 2015).

1.3.4.4.1 Aggrecanase/Hyalactanase family

The largest subgroup of the ADAMTS family is the aggrecanases/hyalactanases comprising ADAMTS1, 4, 5, 8, 9, 15 and 20. These enzymes are so-called because they are able to cleave members of the hyalactan (also known as lectican) family of hyaluronan-binding chondroitin sulphate proteoglycan (CSPG) extracellular proteins, which include aggrecan,

versican, brevican and neurocan (Stanton et al., 2011). Antibodies against a neo-epitope generated after the cleavage of these substrates by these ADAMTSs and 'cleavage-resistant' substrates have been used *in vitro* and *in vivo* to characterise the mode of action of the hyalactanases. These different techniques have identified that all hyalactanases, except ADAMTS20, can cleave aggrecan, the cleavage of versican has been shown to be processed by ADAMTS1, 4, 5, 9 and 20. Neurocan and brevican can be cleaved by ADAMTS1, 4 and 5 (Stanton et al., 2011). The cleavage of versican at the Glutamic acid (GLU) 441- Alanine (ALA) 442 position in the GAG β domain generates a fragment containing the G1 domain and exposing the neo-epitope DPEAAE at the C-terminal position. This shorter versican fragment is called 'versikine'. These smaller fragments of proteoglycans generated after proteolysis by the hyalactanases can have a biological function different from the intact form such as promoting apoptosis during interdigital web regression by decreasing the threshold of BMP required to induce apoptosis (McCulloch et al., 2009b).

Hyalactanases play diverse roles during development. ADAMTS1 cleaves the surrounding versican-rich matrix during ovulation, which allows release of the oocyte and its maturation within the oocyte-cumulus complex (Brown et al., 2010). Mutated mice for ADAMTS1 and 4 show perinatal renal development failure. ADAMTS1 and 4 have redundancy functions in this process as the renal phenotype observed in ADAMTS4 mutants can be compensated when ADAMTS1 is not mutated but ADAMTS4 cannot rescue the ADAMTS1 renal phenotype in ADAMTS1 mutated mice. When ADAMTS1 and 4 are both mutated the phenotype is more severe. The mode of action of these proteases in renal development remains unclear but it is independent of versican and aggrecan proteolysis as the quantity of cleaved forms of these proteoglycans is unchanged in the mice mutants (Boerboom et al., 2011). A mature matrix containing collagen, proteoglycan and elastin replaces the initially immature versican-rich ECM during heart morphogenesis (Stankunas et al., 2008). ADAMTS5 and 9 are essential for heart development by cleaving versican (Dupuis et al., 2011) (Kern et al., 2010). ADAMTS5 is required for maintaining the correct architecture of the skin (Hattori et al., 2011). ADAMTS4 has been shown to have a role in brain development and brain pathologies (Hisanaga et

al., 2012). *ADAMTS9*^{-/-} mice die before gastrulation although a conditional mouse allele has been generated. It has been shown that *ADAMTS9*, 20 and 5 have non-redundant and cooperative roles in interdigital web regression by degrading versican (Dubail et al., 2014) (McCulloch et al., 2009b). *ADAMTS20* mutant mice (belted) have a distinctive coat with a white belt in the lumbar region suggesting the role of *ADAMTS20* in the development of skin pigmentation (Rao et al., 2003). This phenotype is stronger when they are also heterozygous for an *Adamts9* null allele suggesting cooperation between *ADAMTS9* and 20 for melanoblast survival (Silver et al., 2008) (Rao et al., 2003). The double mutated mice (*ADAMTS9*^{+/-}; *bt/bt*) have a cleft palate associated with decreased versican cleavage and reduced cell proliferation in the palatal shelves showing that versican proteolysis is necessary for cell proliferation in the fusing palate (Enomoto et al., 2010).

1.3.4.4.2 Procollagen N-propeptidase family

Another group of ADAMTSs (*ADAMTS 2, 3 and 14*) are pro-collagen N-propeptidases that are essential for the maturation of triple helical collagen fibrils. *ADAMTS2* is a procollagen N-proteinase necessary for the maturation of the collagen by cleaving the propeptide of the α chains. Mature α chains assemble to form collagen fibrils. *ADAMTS2* is expressed in type I collagen-rich tissues such as the collagen lamella in the skin. The mutation of *ADAMTS2* in human and mouse leads to skin fragility due to collagen fibril anomalies causing Ehlers–Danlos syndrome type VIIc (or dermatosparaxis type). The aminoprocollagen, chain of collagen with a propeptide at the N-terminal position due to the lack of cleavage by *ADAMTS2*, accumulates and does not assemble correctly creating a structure with poor mechanical properties leading to skin fragility (Bekhouche and Colige, 2015).

1.3.4.4.3 von-Willebrand Factor family

ADAMTS13 is the von-Willebrand Factor (vWF)-cleaving protease that processes large multimeric vWF precursor proteins, which generate vWF of optimal size for blood coagulation. *ADAMTS13* mutations or inhibition by autoantibodies cause hereditary or acquired thrombotic thrombocytopenic purpura (TTP) leading to vWF platelet aggregation and abnormal coagulation in targeted organs such as kidney, heart and brain (Zheng et al., 2001).

1.3.4.4.4 COMP proteinases family

ADAMTS7 and 12 cleave cartilage oligomeric matrix protein (COMP). ADAMTS7 and 12 have not been shown to play important roles during development. No phenotype has been reported for knock-out mice for *ADAMTS7* (Dubail and Apte, 2015).

1.3.4.4.5 “orphan” family

The remaining sub-group of ADAMTSs do not have an identified substrate and are called “orphan”. It includes three sets of pairs based on their domain organizations; ADAMTS 6 and 10; ADAMTS 16 and 18; ADAMTS 17 and 19. *ADAMTS10* and *ADAMTS17* mutations in human cause Weill–Marchesani Syndrome (WMS), a disorder leading to eye and skeletal abnormalities. This syndrome is also due to a mutation in fibrillin-1 (WMS2), an ECM molecule that assembles and form microfibrils structures. ADAMTS10 and ADAMTS17 play a critical role in crystalline lens zonules and connective tissue formation (Morales et al., 2009). ADAMTS6 and ADAMTS10 play opposite roles in heparan sulphate-rich cellular interfaces such as focal adhesions and epithelial cell-cell junctions *in vitro*. ADAMTS6 disrupt these structures by affecting microfibril deposition by its metalloproteinase activity whereas ADAMTS10 down regulates ADAMTS6 and is required for the integrity of these structures. ADAMTS10 function appears to be independent of its protease activity (Cain et al., 2016). *ADAMTS8* knock-out mice show developmental defects in the lungs, eye and females are infertile (Ataca et al., 2016). ADAMTS10 is implicated in the sperm–oocyte interactions through sperm adhesion to the zona pellucida (Dun et al., 2012).

1.3.4.5 Different mode of actions

Little is known about the non-catalytic mode of action of ADAMTSs. It has been shown that ADAMTS1 can bind to vascular endothelial growth factor (VEGF) and block the activation of VEGF signalling pathway via VEGF receptor 2 (VEGFR2) (Dancevic et al., 2013). In *Xenopus* ADAMTS1 has been shown to negatively regulate FGF independently to its catalytic activity (Suga et al., 2006). ADAMTS15 reduces breast cancer cell migration, which is independent of its protease activity and is dependant on the number of cell surface syndecan-4 (Kelwick et al., 2015b).

1.3.4.6 Functions in cancer and diseases

ADAMTSs are not only important during development but have been shown to play roles in angiogenesis (Rodriguez-Manzanque et al., 2015), in a number of cancers (Cal and Lopez-Otin, 2015), in diseases such as arthritis (Kelwick et al., 2015a) and in central nervous system disorders (Gottschall and Howell, 2015).

1.3.5 TIMP

Tissue inhibitors of metalloproteinases (TIMPs) are secreted inhibitors of active metalloproteinases. There are four TIMPs, TIMP1, 2, 3 and 4 in mammals. TIMP2 and 4 are similar whereas TIMP1 is the most unique member. They all use a similar mode of inhibition, they comprise two domains, a small carboxy-terminal domain and a larger amino-terminal domain. The N-terminal specifically folds within itself and is responsible for wedging into the active site of metalloproteinases, above the catalytic Zn^{2+} necessary for catalytic activity, which thus inhibits these proteins. The C-terminal domain is responsible for the binding of TIMPs to metalloproteinases. In contrast to plasma α 2-macroglobulin, which traps proteases and leads them to be cleared by endocytosis, TIMPs bind specifically to an active metalloproteinase in their catalytic domain and inhibit their protease activity. TIMPs can also bind to the zymogen forms of MMPs, interacting with their C-terminal domain, which does not bind to the catalytic site. The N-terminus is still free to bind to other metalloproteinases to inhibit them. TIMP2, through its C-terminal domain, forms a complex with MMP14 and pro-MMP2, which activates pro-MMP2 at the cell surface. TIMP4 can form a similar complex with MMP14 and pro-MMP2 but does not lead to the activation of pro-MMP2. All TIMPs are secreted, with only TIMP3 incorporated into the ECM, TIMP2 is ubiquitous and constitutively expressed whereas TIMP1 and TIMP3 are expressed in many tissues specifically. TIMPs inhibit all MMPs but are ADAMs and ADAMTs specific (table 1-3) (Jackson et al., 2017).

Table 1-3: Specific action of each TIMP on the inhibition of metalloproteinases and the binding to pro-MMPs.

TIMPs	Pro-MMPs	Metalloproteinases inhibited		
		MMPs	ADAMs	ADAMTs
TIMP1	9	All	10	
TIMP2	2	All	10, 12	
TIMP3	9, 2	All	10, 12, 17, 28, 33	1, 2, 4, 5
TIMP4	2	Most	10, 17, 28, 33	

Mouse knock-out studies have shown that TIMP1 is important for the development of reproductive organs and the heart, TIMP2 plays a role in muscular and central nervous system development and TIMP3 is the main regulator of ECM degradation by metalloproteinases leading to regulation of structural and cellular aspects of tissue architecture (Brew and Nagase, 2010).

1.4 Aims of the project

Extracellular matrix remodeling by metalloproteinases is a highly regulated key process during development and disruption of this process can be lethal or cause severe developmental defects. The aim of this study is to understand the role of ADAMTs in organogenesis during *Xenopus* development from egg to tadpole and during metamorphosis.

The identification of the *ADAMTS* gene family in *Xenopus laevis* and *Xenopus tropicalis* and its evolutionary history analysis will be the first steps of this study.

Spatio-temporal expression of *ADAMTS*s will be assessed during *Xenopus* development from egg to tadpole stages. The function of ADAMTS9 will be investigated in *Xenopus* during organogenesis, specifically in neural crest and pronephros using loss of function experiments (figure 1-11).

The expression of the *ADAMTS* gene family as well as *ADAMs*, *MMPs*, *TIMPs* and ECM components will be measured in the skin, the brain and the heart during *Xenopus laevis* metamorphosis. Finally, their regulation during cardiac regeneration will be analysed in *Xenopus laevis* hearts after ventricular resection at different stages of metamorphosis (figure 1-11).



organogenesis

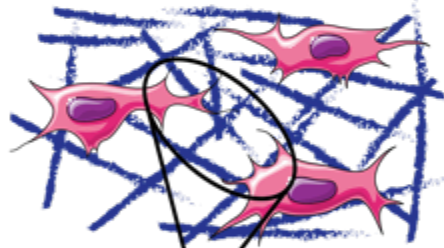
metamorphosis

neural crest cells
pronephros

skin
brain
heart
heart regeneration



Pericellular matrices



Interstitial matrices

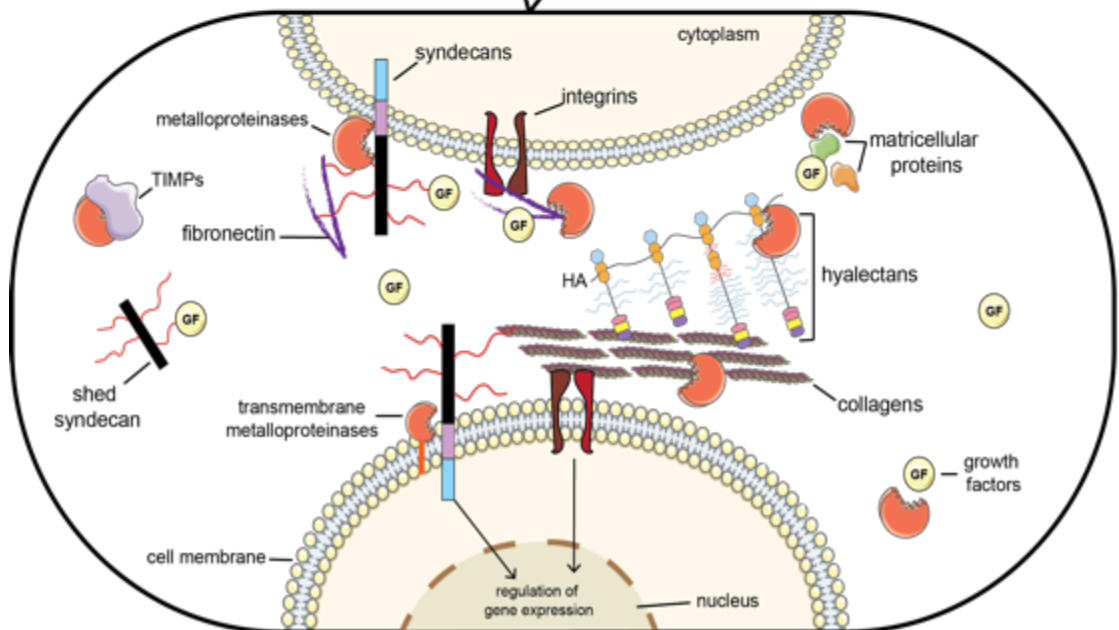


Figure 1-11: Aims of the project. *Xenopus* is used as model organism to investigate organogenesis during tailbud and tadpole stages (from stage 25 to stage 40), specifically neural crest cell migration and pronephros development, and at organogenesis during metamorphosis, specifically skin, brain and heart. Heart regeneration before, during and after metamorphosis is used as a model to determine regenerative capacity. The aims of the project are to look at the role of ECM remodeling during these different developmental processes. There are two types of ECM, the interstitial and pericellular matrices. For example basement membrane is a type of pericellular matrix and is found between epithelial cells and connective tissue mostly composed of collagen. The schematic representation of the interstitial matrix represents the main components presented in this study. It is composed of collagen fibrils, secreted proteoglycans such as hyalectans, hyaluronan (HA) and matricellular proteins that interact with each other to create a dynamic three-dimensional network. Cell-ECM interactions are mediated by cell surface receptors, such as integrins and cell surface proteoglycans such as syndecan, which activate signaling pathways and regulate cellular functions. ECM regulates the availability of growth factors (GF) that are sequestered by binding to ECM components such as proteoglycans. Metalloproteinases such as MMPs, ADAMs and ADAMTSs cleave ECM components leading to tissue remodeling and dysregulation of their proteolytic activities causes diseases. TIMPs regulate the metalloproteinases activity.

Chapter II: Materials and Methods

2.1 Data source of ADAMTS gene sequences

The *ADAMTS* genes reported by (Brocker et al., 2009) were retrieved from Genbank (<http://www.ncbi.nlm.nih.gov>). With these genes as queries, the Basic Local Alignment Search Tool (BLAST) program was used to search in National Center for Biotechnology Information (NCBI) and in The UniProt Knowledgebase (UniProtKB) against *M.musculus* and *H.sapiens* genome assemblies.

Orthologs of known human ADAMTS genes in *Xenopus* were identified by using BLAT sequence-based searches of the *Xenopus* genomes hosted at The Francis Crick Institute (UCSC Genome Bioinformatics Site). The version xenTro9.0 assembly was used for *Xenopus tropicalis* and xenLae9.1 assembly was used for *Xenopus laevis*. Nucleotide sequences were translated to a protein sequence using ExpASy - Translate tool.

2.2 Alignment and phylogenetic analysis

Multiple sequence alignments were constructed with Clustal Omega. Phylogenetic trees were constructed using the amino acid residues of the full-length genes. Trees were generated using MEGA (Molecular Evolutionary Genetics Analysis) version 6 software (Tamura et al., 2013). Synteny analyses were carried out using UCSC Genome Browser.

2.3 Obtaining *Xenopus laevis* and *Xenopus tropicalis* embryos

Embryos were obtained by *in vitro* fertilisation. This process required a series of procedures, priming and inducing females, priming the male for *Xenopus tropicalis*, male testes dissection, and then manual massage of the abdomen to collect eggs.

The priming technique was performed 5-10 days before eggs required with 100 units of Pregnant Mare Serum Gonadotrophin (PMSG) into the dorsal lymph sac on one side. To induce ovulation 14-16 hours before the eggs were required primed females were injected with 500 units of human chorionic gonadotrophin (hCG, Chorulon®) into the dorsal lymph sac on each side. Frogs were stored at 18°C for 14-16 hours prior to egg collection. To obtain eggs, the abdomen of the frog was manually squeezed over a clean petri dish. Testes were isolated from a male frog euthanized with 0.5g tricaine methane sulphonate (MS-222) dissolved in 300ml distilled H₂O for 1 hour at 4°C. Testes

were then stored in testes buffer composed of 80% Foetal Bovine Serum (FBS) and 20% 1x Marc's Modified Ringers (MMR: 100mM NaCl, 2mM KCl, 1mM MgCl₂, 2mM CaCl₂, 5mM HEPES, pH 7.5) at 4°C. The testes solution containing a small piece of male testes crushed with 1ml of 1xMMR was distributed over the collected eggs and left for 5 minutes at 18°C. 0.1xMMR (10mM NaCl, 0.2mM KCl, 0.1mM MgCl₂, 0.2mM CaCl₂, 0.5mM HEPES, pH 7.5) was then added to cover the eggs for a period of 20 minutes at 18°C. Once fertilised, eggs needed the jelly coat removed to allow experimental manipulation. The eggs were gently swirled in 2% cysteine pH 8.0 dissolved in 1xMMR until de-jellying was complete. Eggs were then immediately washed several times in 1xMMR then 0.1xMMR to remove trace amounts of cysteine. Embryos could then be left to develop in 0.1xMMR with Bovine Serum Albumin (BSA) at 18°C or 23°C depending on the purpose of the experiment and the stage of development desired.

2.4 Fixing and storage of *Xenopus* embryos

The required stage of development was according to (Nieuwkoop and Faber, 1994) (www.xenbase.org). Once embryos reached their desired stage they were fixed using MEMFA: 3.7% formaldehyde, 1xMEM salts (0.1M MOPS, 2mM EGTA, 1mM MgSO₄, pH7.4) made up with distilled H₂O. They were then dehydrated in 100% methanol and left at -20°C for storage.

2.5 Skin and brain dissection from stage 57 to stage 66

Tadpoles at the right stage according to (Nieuwkoop and Faber, 1994) were anesthetized in 0.01% tricaine methane sulphonate (MS-222) and placed on ice under sterile conditions in order to remove the skin from the head and the trunk and the brain. The skin was peeled away and transferred to a sterile tube on dry ice. The whole brain was dissected as described in (Hamodi and Pratt, 2015), transferred to a sterile tube on dry ice. Samples were kept at -80°C.

2.6 RNA extraction

2.6.1 For *Xenopus* embryos from unfertilised egg to stage 45

10 embryos were placed in a 1.5ml microcentrifuge tube and all fluid was removed. Embryos were then flash frozen in liquid nitrogen for 15 minutes. At

this step frozen dry embryos could be stored at -80°C . Samples were kept on ice and all reagents had to be cold. 1ml (1 volume) of TRIzol® was added to dry embryos. All animal tissue was broken by vortexing until solution was homogenised. Then 500 μl (half volume of TRIzol) of Chloroform was added and after centrifugation at 4°C proteins/lipids, DNA and RNA were separated. The aqueous upper phase containing RNA was put into a new 1.5ml microcentrifuge tube. To precipitate RNA 500 μl (half volume of TRIzol volume) of isopropanol, 50 μl of 5M NaCl and 2 μl of glycogen were added. After centrifugation at 4°C the supernatant was removed and replaced by 70% ethanol prepared in RNase free to wash RNA. After centrifugation at 4°C the ethanol was removed and the pellet was dissolved in 45 μl of RNase free H_2O . At this step RNA could be stored at -80°C .

2.6.2 For *Xenopus* embryos from stage 57 to stage 66

Tissue of interest was dissected and RNA was extracted using RNeasy Plus Mini Handbook kit (Qiagen) according to manufacturer's instructions. TissueLyser II (Qiagen) was used to disrupt and homogenise the tissue and an additional step using QIAshredder (Qiagen) was added to the protocol before the removal of the genomic DNA. RNA was quantified using Qubit (Invitrogen) according to manufacturer's instructions. the RNA was then quantified and quality controlled using Qubit (Thermo Fisher Scientific) and 2100 Bioanalyzer (Agilent Technologies) respectively. Samples with RNA integrity (RIN) of ≥ 7 were used for cDNA synthesis.

2.7 DNase treatment

10x DNase buffer (to a final concentration of 1x) and 1 μl of DNase I (Roche) were added to each RNA sample. Samples were then incubated at 37°C for 30 minutes to remove residual genomic DNA. To this, 50 μl of RNase free H_2O was added. Sample final volume was 100 μl . To extract RNA 100 μl (1 volume) of acidic phenol/chloroform was then added. After centrifugation at 4°C the aqueous upper phase was put into a new 1.5ml microcentrifuge tube. To precipitate RNA 70 μl of isopropanol, 7 μl of 5M NaCl and 1 μl of glycogen were added. This was centrifuged at 4°C . Then the supernatant was removed and replaced by 70% ethanol prepared RNase free to wash RNA. After centrifugation at 4°C the ethanol was removed and the pellet was resuspended

in 20µl of RNase free H₂O. The concentration was determined by spectrophotometry (Nanodrop) and sample was stored at -80°C.

2.8 cDNA synthesis

2.8.1 For *Xenopus* embryos from unfertilised egg to stage 45

To denature RNA structure, 1µg of RNA, 1µl of oligo-dT made up to 11µl with RNase free H₂O were left at 70°C for 10 minutes. Then to synthesise cDNA, 4µl of 5x First Stand Buffer (Promega), 0.5µl RNase inhibitor (Promega), 2.5µl of 10mM dNTPs, 0.5µl of Reverse Transcriptase (Promega) and 1µl Superscript II (Invitrogen) were added and left for 1hour at 42°C. cDNA was diluted 1:20 with RNase free H₂O to give a final concentration of 10ng/ml.

2.8.2 For *Xenopus* embryos from stage 57 to stage 66

125ng/µl of RNA was added to the 5x Reverse Transcription Master Mix (Fluidigm) in a final volume of 5µl. The reaction was performed using a thermocycler. Samples were incubated 5 minutes at 25°C, 30 minutes at 42°C and 5 minutes at 85°C. cDNA prepared using the Reverse Transcription Master Mix is suitable for preamplification using the Fluidigm PreAmp Master Mix.

2.9 Pre-amplification of cDNA

1.25µl of cDNA prepared with the Fluidigm Master Mix was added to a mix containing primers for genes of interest at a final concentration of 50nM and 1x of the 5x Preamp Master Mix (Fluidigm). The reaction was performed using a thermocycler. Samples were incubated 2 minutes at 95°C, 15 seconds at 95°C and 4 minutes at 60°C for 18 cycles.

2.10 Polymerase Chain Reaction (PCR)

The amplification of templates was performed using a thermocycler. Total PCR reaction was 25µl containing 10-50ng of template cDNA or small amount of bacterial colony, 0.2µM of each forward and reverse primer (see table 1), 1x of BioMix™ (2x reaction mix containing ultra-stable *Taq* DNA polymerase, Biorline). An initial denaturation step of 95°C for 3 minutes was followed by a denaturation of 1 minute at 95°C. The annealing step was carried out at an annealing temperature calculated by subtracting 5°C from the primer melting temperature, for 1 minute. This was followed by 1 minute of extension step at 72°C (according to the expected size of the PCR product, 30s/500bp) (see

appendix 1). 25-35 cycles (depending on the level of expression of the gene of interest) of denaturation, annealing and extension were carried out. Amplified products were fractionated in 1% (w/v) agarose Tris/Borate/EDTA (TBE 1x: 45mM Tris-Borate, 1mM EDTA, pH8.0) gel electrophoresis with 0.0001% (v/v) of 10mg/ml ethidium bromide and visualised under UV light using a UV trans-illuminator (BIO-RAD).

2.11 Quantitative PCR

2.11.1 96 well plate

The reaction was performed in MicroAmp optical 96 well plate (Applied Biosystems). The final volume was 15µl containing 5µl of cDNA (diluted at the optimised concentration for the experiment), 10µM of each primer (forward and reverse), 7.5µl of 2x SYBR® Green PCR Master Mix (Applied Biosystems) and 1.7µl of RNase free water. A 7500 real-time PCR instrument (Applied Biosystems) was used under the following conditions: 50°C for 2 minutes, 95°C for 10 minutes, 95°C for 15 seconds cycles 40 times and 60°C for 1 minute.

2.11.2 384 well plate

The reaction was performed in a final volume of 6µl (1µl of pre-amplification product diluted at 1/20, 6µM of each primer, 3µl of 2x SYBR® Green PCR Master Mix (Applied Biosystems) and 1,70µl of RNase free water) using a QuantStudio 6 Flex system (Applied Biosystems) under the following conditions: 50°C for 2 minutes, 95°C for 10 minutes, 95°C for 15 seconds cycles 40 times and 60°C for 1 minute.

2.12 Microfluidics

2.12.1 Primers validation

To do the microfluidic experiments all primers had to be validated with a good specificity showed by the melt curve and a good efficiency calculated using the slope of the standard curve established with five duplicates of 10-fold serial dilutions of cDNA template known to express the gene of interest (appendix 1 and 2). The formulas to established the percentage of efficiency were $E = 10^{(-1/\text{slope})}$ with E being the amplification efficiency and slope being the one obtained with the standard curve, then E was converted to percentage by $E = 100 * (1 - 10^{(-1/\text{slope})})$. The cDNA was synthesised from 250ng/µl mix of

RNA from stage 42, juvenile brain and skin *Xenopus laevis* using the 5x Reverse Transcription Master Mix (Fluidigm) (see section 2.7.2). The cDNA was then pre-amplified with a mix of all primers used for the microfluidic experiment at 50nM final concentration using the 5x Preamp Master Mix (Fluidigm) (see section 2.8) and diluted at 1/20. The quantitative PCR was performed in 384 well plates (see section 2.10.2). Only the primers with efficiency between 90 and 116% and a melt curve showing one specific amplification peak at the right melting temperature and none in the negative controls (No Template Control (NTC) and a negative control of cDNA synthesis reaction made without adding the Reverse Transcriptase enzyme (RT-)) were selected. For some of the primers amplification peaks were found in the negative controls but not at low melting temperatures due to the creation of primer dimers. To calculate the efficiency from the standard curve some points were removed due to bad amplification or bad duplicate.

2.12.2 Reaction

The microfluidic experiment was performed at the microfluidic platform at l'Ecole Normale Supérieure in Paris. The reaction was performed on a 9,216 reaction chambers chip containing 96 different sets of primers and 96 different samples (96.96 Dynamic Array™ integrated fluidic circuits (IFCs) (Fluidigm)) (figure 2-1). The 96 samples inlets contained diluted at 1/20 cDNA made with 10ng of RNA (prepared by Dr. Laurent Coen laboratory) using the 5x Reverse Transcription Master Mix (Fluidigm) (see section 2.7.2). The 96 primers inlets contained 10µM of each set of primers. The chip was then placed into the IFC Controller HX (Fluidigm) to prime the control line fluid into the chip according to manufacturers instructions. The samples and the primers were loaded into the inlets on the chip and loading reagent, containing components necessary for quantitative PCR reaction and EvaGreen® dye (Fluidigm), was added to each inlets. The chip was then placed into the IFC Controller HX (Fluidigm) where the air pressure forces samples and assays into the middle of the chip where they mix according to manufacturers instructions. Each sample was mixed with each set of primers at a final concentration of 0.04µM in 6nl final volume. After that the chip was placed into the BioMark™ HD System (Fluidigm) to perform real-

time quantitative PCR gene expression. Results were analysed using the Real-Time PCR Analysis v4.1.3 software (Fluidigm).

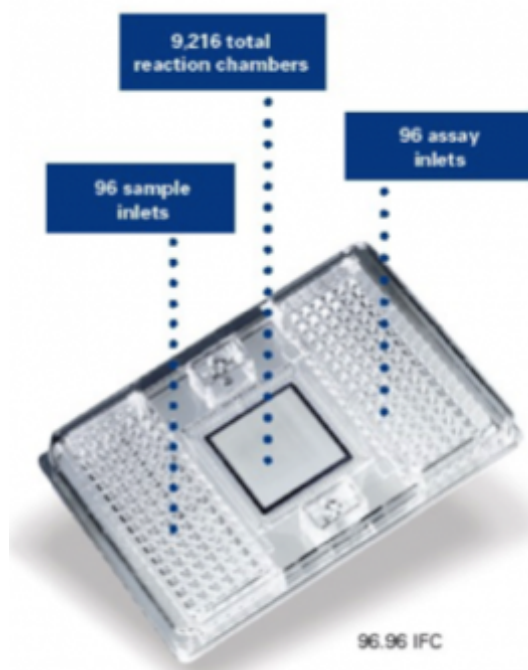


Figure 2-1: 96.96 Dynamic Array™ integrated fluidic circuits (IFCs) chip used to perform the microfluidic experiment.

2.13 Statistical analysis

All statistical tests were carried out using Graph Pad Prism 6 software. Suitable statistical tests were chosen for each data set to suit the type of data analysed. Tests used include D'Agostino-Pearson omnibus normality test, Ordinary one-way ANOVA test, Kruskal Wallis test, unpaired Welch's *t*-test and Mann–Whitney *U* test.

2.14 Cloning into pGEM®-T Easy Vector

The pGEM®-T Easy (Promega) was a linearized vectors with a single 3'-terminal thymidine at both ends. The T-overhangs at the insertion site greatly improved the efficiency of ligation of PCR products by preventing recircularization of the vector. Taq DNA polymerase (Bioline) left 'A' overhang so there was no need to add A residues at the 3' and 5' ends of the PCR products. PCR products were purified using the QIAquick PCR Purification Kit (QIAGEN) according to manufacturers instructions. The concentration was determined by spectrophotometry (Nanodrop). Ligation reactions were carried out according to the ratio of vector and insert.

This ratio was calculated as follows;

$$\frac{([\text{ng of vector}] \times [\text{kb size of insert}])}{[\text{kb size of vector}]} \times \text{molar ratio} \frac{[\text{insert}]}{[\text{vector}]} = \text{ng of insert}$$

Ligation reactions were carried out according to two conditions of ratio 3:1 and 1:1. The reaction mixture was as follows; 10-100ng of PCR products, 0.5µl of pGEM®-T Easy Vector, 5µl of 2x ligase buffer (Promega), 1µl of Ligase T4 DNA (3U/µl, Promega) made up to 10µl with RNase free H₂O. The reaction was then incubated for 2-3 hours at room temperature. Ligation reaction was then transformed into competent bacteria by the method outlined in section 2.10.

2.15 Gateway cloning

The first step of a gateway cloning was to clone the gene of interest into an entry vector. The one used was pENTR™/D-TOPO® (life technologies). The gene of interest was obtained by PCR. To enable directional cloning, the forward PCR primer had to contain the sequence, CACC, at the 5' end. The 4 nucleotides, CACC, will pair with the overhang sequence, GTGG, in pENTR™/D-TOPO®. The reverse PCR primer did not have to be complementary to the overhang sequence GTGG at the 5' end at 1 base pair mismatch. The PCR product had to be blunt-end. Total PCR reaction was 25µl containing 0.5µl of cDNA (cDNA synthesis reaction mixture as a source of template, the volume should not exceed 10% of the final PCR reaction volume), 0.5µM of each forward and reverse primer (see appendix 1), 1x of 5x Phusion HF Buffer, 0.02 U/µl of Phusion DNA Polymerase (2 U/µl stock solution) and 200 µM each dNTPs. An initial denaturation step of 98°C for 30 seconds was followed by a denaturation of 10 seconds at 98°C. The annealing step was carried out at an annealing temperature calculated by subtracting 5°C from the primer melting temperature (see appendix 1), for 45 seconds. This was followed by 1 minute of extension step at 72°C (according to the expected size of the PCR product, 15–30 s/kb, see table 1). 25-35 cycles (specific for each primer set, see table 1) of denaturation, annealing and extension were carried out. Amplified products were fractionated in 1% (w/v) agarose Tris/Borate/EDTA (TBE 1x: 45nM Tris-Borate, 1mM EDTA, pH8.0) gel electrophoresis with 0.0001% (v/v) of 10mg/ml ethidium bromide and visualised under UV light using

a UV trans-illuminator (BIO-RAD). PCR products were purified using the QIAquick PCR Purification Kit (QIAGEN) according to manufacturer's instructions. The concentration was determined by spectrophotometry (Nanodrop). The TOPO[®] Cloning reaction was then set up with a 0.5:1 to 2:1 molar ratio of PCR product: TOPO[®] vector. For chemical transformation, 1 to 5ng of PCR product of 1kb or 5 to 10ng of PCR product of 2kb were added to 1μl of salt solution and 1μl of TOPO[®] vector. The mixture was incubate for 5 minutes at room temperature. DH5 alpha competent E.coli bacteria were transformed with the plasmid. A positive colony containing the gene of interest into the TOPO[®] vector was identified by colony PCR with specific primers used to amplify the gene of interest. After mini-prep, the sequence of the gene of interest was confirmed by sequencing with M13 forward and reverse primers (Sanger Sequencing Service, Source BioScience). The LR reaction mixture was composed of 50 to 150ng of entry clone (TOPO[®] vector containing the gene of interest), 150ng of destination vector (adapted pCS2+ plasmid with a HA tag at the C-terminal position, contain the ccdB lethal gene which is disrupted after LR reaction, this plasmid was from Jim Smith lab). The final volume was 8 μl completed with TE buffer pH8 (10mM Tris and 1mM EDTA). 2 μl of LR Clonase[™] II enzyme mix (Invitrogen) was added to the mixture and incubated at 25° C for 1 hour. To terminate the reaction, 1 μl of the Proteinase K solution (Invitrogen) was added and the samples were incubated at 37° C for 10 minutes. DH5 alpha competent E.coli bacteria were transformed with the plasmid. A positive colony containing the gene of interest into the TOPO[®] vector was identified by colony PCR with specific primers used to amplify the gene of interest. After mini-prep, the sequence of the gene of interest was confirmed by sequencing with SP6 and T7 primers (Sanger Sequencing Service, Source BioScience).

2.16 Transformation

100μl of DH5 alpha competent E.coli bacteria were added to 5μl of plasmid DNA and left on ice for 30 minutes. These were heat shocked at 42°C for 90 seconds to open cells and then returned to ice for a further incubation of 5 minutes. 300μl of Lysogeny broth (LB: 5g tryptone, 2.5g yeast extract, 5g NaCl, pH7 made up to 500ml with distilled H₂O) media was added and cells were left

for 1 hour at 37°C with continuous shaking (200rpm) to allow growth. 100µl of culture was then plated on pre-warmed (37°C) LB and agar plates with the appropriate antibiotics. These were incubated overnight at 37°C.

2.17 Mini and Midi Extraction of Plasmid DNA

Single colonies of bacteria were used to inoculate either 10ml or 50ml LB/antibiotic liquid media, for mini and midi preparation, respectively. The cultures were grown at 37°C overnight with continuous shaking (200rpm). The DNA plasmid was isolated using the Plasmid Mini Kit (reSource) and NucleoBond® Xtra Midi Kit (MACHEREY-NAGEL) according to manufacturers instructions.

2.18 Probe synthesis

2.18.1 Template

2.18.1.1 Linearized plasmid

Plasmids containing gene of interest were first linearised by restriction enzyme digestion using an appropriate restriction enzyme site to give antisense and sense RNA probes (see table 2-1). 2-10µg of plasmid was added to 2µl of the appropriate enzyme, 5µl of the optimal buffer for the enzyme and then made up to 50µl with RNase free water. This was left at 37°C for a minimum of 2 hours or a maximum of overnight. The cut plasmid could be visualised on an agarose gel. To precipitate DNA 1/10 NaOH pH5.2, 250µl ethanol 100%, and 1µl of glycogen were added and incubated overnight at -20°C. After centrifugation, the supernate was removed and replaced by 70% ethanol to wash DNA. After centrifugation the ethanol was removed and the pellet was resuspended in 20µl of RNase free H₂O. The concentration was determined by spectrophotometry (Nanodrop).

Table 2-1: Terms of use of the plasmids used to make probes.

plasmid	antisense linearisation	antisense polymerase	source
XADAMTS-1	Sall	T7	EST Image Clone 4408215
xWt1-pGEM7-s52S0304	Sac1	T7	European Xenopus Resource Centre
Pax8 9pBS.KLPax8.1	EcoRI	T7	European Xenopus Resource Centre
Xlim1 pBSKS	XhoI	T7	European Xenopus Resource Centre
Pax2	EcoRI	T3	European Xenopus Resource Centre
Atp1b1a (5570138)	Sall or SmaI or EcoRI	T7	European Xenopus Resource Centre

2.18.1.2 PCR product

The gene of interest was cloned into pGEM®-T Easy vector and used as a template for a PCR reaction using M13 forward and reverse primers at a concentration of 0.1µM (appendix 1). The Mini or Midi preparation of the plasmid was diluted ten times and 1µl was used for the PCR reaction, 1x of BioMix™ (2x reaction mix containing ultra-stable *Taq* DNA polymerase, Bionline) was added for a total volume of 10µl. A thermocycler was used to perform the reaction under the following conditions; an initial denaturation step of 95°C for 3 minutes was followed by a denaturation of 1 minute at 95°C. The annealing step was carried out at an annealing temperature of 55°C for 1 minute. This was followed by 1 minute of extension step at 72°C. 25 cycles denaturation, annealing and extension were carried out. Amplified products were fractionated in 1% (w/v) agarose Tris/Borate/EDTA (TBE 1x: 45mM Tris-Borate, 1mM EDTA, pH8.0) gel electrophoresis with 0.0001% (v/v) of 10mg/ml ethidium bromide and visualised under UV light using a UV trans-illuminator (BIO-RAD).

2.18.2 Reaction

Probe was synthesised with a promoter specific RNA polymerase (see table 2), the following reaction conditions were used; 1µl linearised plasmid or PCR template, 2µl dithiothreitol (DTT, Promega), 1µl Digoxigenin (DIG) labeled UTPs (Roche), 1µl RNase inhibitor (Promega), 2µl (40U) RNA polymerase (Promega, see table 2), 4µl 5x transcription buffer (Promega) made to a final volume of

20µl with RNase free H₂O. The reaction was incubated at 37°C for 3 hours. Any remaining DNA template was removed by adding 1µl of DNase I (Roche) and incubating for 30 minutes at 37°C. 30µl of RNase free H₂O were then added to purify the probe using G50 column probe purification (GE Healthcare) according to manufacturers protocol. Probe quality and transcription efficiency was checked by agarose TBE gel electrophoresis. They were then diluted at 1/200 to be used for *in situ* hybridisation.

2.19 Capped RNA synthesis

Plasmids containing gene of interest were first linearised by restriction enzyme digestion using an appropriate restriction enzyme site (see table 2-2). 2-10µg of plasmid was added to 2µl of the appropriate enzyme, 5µl of the optimal buffer for the enzyme and then made up to 50µl with RNase free water. This was left at 37°C for a minimum of 2 hours or a maximum of overnight. The cut plasmid could be visualised on an agarose gel and purified using a Qiagen PCR purification kit according to kit instructions. The concentration was determined by spectrophotometry (Nanodrop). For capped RNA synthesis 0.1 to 1µg of linearised plasmid, 1X of 2X NTP/CAP (Ambion), 1X of 10X Reaction Buffer (Ambion), 2µl of Enzyme Mix (SP6, T7, or T3, Ambion or Promega) and made up to 20µl with RNase free H₂O. This was left for 2 hours at 37°C. 1µl of TURBO™ DNase (2 U/µL) was added for 15 minutes at 37°C. The RNA was precipitated by adding 30 µl of RNase free H₂O and 30 µl of lithium chloride precipitation solution (Ambion). This was left at -20° C for minimum 30 minutes and maximum overnight. The sample was then centrifuged at 4° C for 15 min at maximum speed to pellet the RNA. The supernatant was removed and the pellet washed with 1ml of 70% ethanol. After centrifugation at 4°C the ethanol was removed and the pellet was dissolved in 20µl of RNase free H₂O. At this step RNA could be stored at -80°C.

Table 2-2: Terms of use of the plasmids used to make capped RNA.

plasmid	linearisation	polymerase
pCS2-adamts9S-HA	Apal (Promega)	sp6
pCS2-adamts9L-HA	Apal (Promega)	sp6

2.20 Microinjection, morpholinos and mRNA used, GFP detection

Embryos undergoing microinjection were placed in 3% Ficoll (6g Ficoll PM400, 60ml 1xMMR, 140ml distilled H₂O). Targeted injections were performed at one cell stage, two-cell stage or at 8-cell stage into the V2 blastomere (according to (Nieuwkoop and Faber, 1994)) using a 10nl calibrated needle. Oxygen free nitrogen was used with a Harvard apparatus injector (Medical Systems Research products). The injector was set up at $P_{out} = 90$, $P_{balance} = 0.6$ and $P_{inject} = 16$. 2hours after injection the Ficoll was removed from the embryos and replaced with 0.1xMMR and left to develop at 18°C or 23°C depending on the purpose of the experiment. Antisense morpholino oligonucleotides (MOs) used were designed and synthesised by Gene Tools (table 2-3). Morpholino were stored at room temperature. They were stocked at -20°C when combined with GFP capped RNA for lineage tracing. They were then heated at 65°C before use for 5 minutes. The optimal concentration of morpholino for injection was defined by doing dose-response experiment. Morpholinos were coinjected with 300pg of GFP capped RNA as a control of injection and good location of the injection.

Table 2-3: Sequences of the morpholinos used in this study.

Morpholino name	Target sequence
Standard control (cMO)	5'-CCTCTTACCTCAGTTACAATTTATA-3'
ADAMTS9 (tropicalis)	5'-GAGGCAAGATGCATGTTTGTCCCCT-3'
ADAMTS9-L (laevis)	5'-TTCATGTTTGTCCGCAGGAAGCCCC-3'
ADAMTS9-S (laevis)	5'-TCCTCGTCCTTTGAAGTGCATGTC-3'

2.21 Wholemout *in situ* hybridization

Embryos were re-hydrated after fixation in 100%, 75%, 50% methanol, 25% methanol/1x phosphate buffer saline (PBS 10x: 2.5g NaH₂PO₄.H₂O, 11.94g NaHPO₄.H₂O, 102.2g NaCl, 400ml distilled H₂O, pH 7.4 and total volume of 1L) with 0.1% Tween 20 (PBST). Embryos were bleached to effectively observe *in situ* staining. For this embryos were incubated in a solution of 1.5ml 30% H₂O₂, 2.5ml formamide, 1.25ml 20x Sodium Chloride and sodium Citrate (SSC 20x: 175.3g NaCl, 88.2g Sodium citrate, pH7 and total volume of 1L with distilled H₂O) for 2 hours on a light box. Then embryos were washed in PBST and incubated in hybridisation buffer (50% formamide, 5xSSC, 1mg/ml Torula RNA,

100µg/ml heparin, 1x Denharts solution, 0.1% Tween 20, 0.1% CHAPS, 10mM EDTA) at 65°C for 2-6 hours. After that the embryos were incubated into fresh hybridisation buffer and the appropriate probe overnight at 65°C. Probe was replaced by 2xSSC and then by 0.2xSSC all at 65°C. The embryos were washed in 1xMaleic acid buffer (MAB: 100mM Maleic acid, 150mM NaCl, pH7.5) with 0.1% Tween 20 (MABT) and blocked in a 1xMABT and 2% Boehringer Mannheim Blocking (BMB) solution for 1 hour at room temperature. BMB solution was then replaced by anti-digoxigenin (1:2000), 2% BMB, 20% Goat serum and 1x MABT solution and embryos were incubated overnight at 4°C. The antibody solution was removed and embryos were washed five times with MABT at room temperature. They were kept overnight at 4°C in the final wash. The colour reaction was performed after washing the embryos in alkaline phosphate buffer (100mM Tris pH9.5, 50mM MgCl₂, 1mM NaCl, 0.1% Tween 20, 2mM levamisol) at room temperature. Detection of the probe was performed by using nitro-blue tetrazolium chloride (NBT: 75mg/ml in 70% dimethylformamide) at 4.5µl/ml and 5-bromo-4-chloro-3'-indolyphosphate p-toluidine salt (BCIP: 50mg/ml in 100% dimethylformamide) at 3.5µl/ml in alkaline phosphate buffer. Embryos were then put in 5xTris-buffered saline (TBS 10x: 40g NaCl, 1g KCl, 125ml Tris pH7.5 and total volume of 500ml) with 5% Tween 20 to remove background and photographed.

2.22 Wholemout antibody staining

Embryos were re-hydrated after fixation in 100%, 75%, 50% methanol, 25% methanol/1x PBS. Embryos were bleached to effectively observe the staining (see section 2.20). The bleaching solution was removed and the embryos were washed three times with PBT (PBS, 2mg/ml BSA, 0.1% Triton X-100) for 5 minutes. They were then incubated with fresh PBT for 2 hours at 4°C. PBT was then removed, replaced with primary antibodies diluted in PBT (see table 2-4) and incubated overnight at 4°C. The primary antibody was then removed and replaced by PBT for 1 hour at 4°C. This step was repeated four times. Embryos were then incubated with secondary antibody diluted in PBT (see table 2-4) overnight at 4°C. The secondary antibody was then removed and replaced by PBT for 1 hour at 4°C. This step was repeated three times. Embryos were then washed with alkaline phosphate buffer (see section 2.20) for 1 hour at room

temperature. The colour reaction was performed using NBT/BCIP (see section 2.20) or Fast Red (Sigma). One Fast Red TR/Naphthol AS-MX Phosphate (4-Chloro-2-methylbenzenediazonium/3-Hydroxy-2-naphthoic acid 2,4-dimethylanilide phosphate) tablet and one Tris buffer tablet were dissolved in 10 ml of distilled water providing 10ml of ready-to-use substrate. When the colour reaction was completed the substrate was removed and replaced by PBS to stop the reaction. Embryos were then fixed with MEMFA for 1 hour at 4°C. They could be stored in methanol at -20°C or in MEMFA if stained with fast red, alcohol soluble substrate.

Table 2-4: Term of use of the antibodies used for wholemount antibody staining in *Xenopus*.

antibody	dilution	source
3G8	1/10	European Xenopus Resource Centre
4A6	1/10	European Xenopus Resource Centre
Anti-Mouse IgG-Alkaline Phosphatase	1/500	Sigma

2.23 Cryosectioning

Embryos were re-hydrated after fixation in 100%, 75%, 50% methanol, 25% methanol/1xPBST, PBST and incubated in 30% sucrose solution overnight at 4°C. Embryos were then transferred to cryomolds filled with optimal cutting temperature compound (OCT) and left at room temperature. When embryos were at the bottom of cryomolds filled they could be positioned appropriately for sectioning. Embryos were then incubated 20 minutes in isopentane inside dry ice and left at -20°C.

Embryos were sectioned using the LEICA CM 1950 Cryostat and sections were placed on 5% TESPA slides overnight at 4°C. Slides were washed in PBST and covered with a coverslip using mounting media. Images were taken using a Zeiss Axioplan 2ie microscope with colour camera (HRc).

2.24 Western-blot

2.24.1 Protein extraction

Ten embryos were collected at stage 8 and solubilised in 50µl NP40 (150mM NaCl, 1% NP-40, 50mM pH8.0, one proteinase inhibitors cocktail tablet

(Roche)) lysis buffer, at this step embryos can be stored at -20°C. To extract the proteins 500µl of Freon (1,1,2, trichlorotrifluoroethane 99.9%) were added to the embryos in NP40 buffer, vortexed, left on ice for 5 minutes and centrifuged at maximum speed for 15 minutes at 4°C. The top phase was then transferred to a new clean tube and stored at -20°C.

2.24.2 Sample preparation

To quantify the amount of proteins in the samples the BSA quantification method was used with a stock solution at 4mg/ml. This stock solution was diluted with the NP40 lysis buffer at nine different concentrations of 0, 0.1, 0.2, 0.4, 0.8, 1.2, 1.6, 2 and 4µg/µl to establish the standard curve. In a 96 well plate, 5µl of each dilution point (in triplicate) and 5µl of sample was used. To these was added 25µl of mix A, composed of 1ml of Reagent A and 20µl of Reagent S (from *DC*TM Protein Assay (BIO-RAD)), and 200µl of Reagent B (from *DC*TM Protein Assay (BIO-RAD)). The absorbance (λ) was read in the VersaMaxTM ELISA Microplate Reader (Molecular Devices) at 750nm and the concentration of proteins was calculated from the standard curve using the $y=A+Bx$ where y is the absorbance, x the concentration in µg/µl and A and B specific parameters to each standard curve. The samples were then diluted to have the right amount of proteins to load on a gel, corresponding to 20µg for this study, an equal volume of 2X Laemmli sample buffer (65.8 mM Tris-HCl, pH 6.8 26.3% (w/v) glycerol, 2.1% SDS and 0.01% bromophenol blue (BIO-RAD)) completed with 5% of 2-mercaptoethanol was the added and the samples were incubated at 95°C for 5 minutes.

2.24.3 Protein electrophoresis

The protein electrophoresis was realised using the Mini-PROTEAN® Tetra Handcast Systems (BIO-RAD). The electrophoresis gel was composed of two different gels called the stacking gel (table 2-5), to concentrate all the proteins in one band, and the resolving gel (table 2-6) to separate the proteins based on their molecular weight. The gels were placed in the tank filled with 1X running buffer (table 2-7) and when the samples were loaded the migration was carried out using an electrophoresis power supply (BIO-RAD) at 100 volts for 2 hours. To transfer the proteins from the gel to a polyvinylidene difluoride (PVDF) membrane they were placed between pieces of Whatman filter papers and

foam pads (BIO-RAD) (figure 2-2). Before to be used the PVDF membrane had to be incubated in 100% methanol. The assembly of this sandwich was done in the 1X transfer buffer composed of 70% of water, 20% of methanol and 10% of transfer buffer 1X (table 2-8) kept at 4°C and placed in a cassette. The electroblotting was carried out using a Mini Trans-Blot® Cell (BIO-RAD) and an electrophoresis power supply (BIO-RAD) at 115 volts for 75 minutes. When the transfer finished, the membrane was washed in 1X TBS 0.1% Tween 20 (TBST) (TBS 10X: 24.23g Tris Base, 80.06g NaCl) for 5 minutes and then stained with Ponceau solution (0.5% Ponceau S (w/v) and 1% acetic acid) to colour the proteins and validate the transfer. The membrane was then washed with water and blocked in 5% milk solution diluted in 1X TBST for two hours at room temperature. The membrane was incubated overnight at 4°C with the primary antibody (table 2-9) diluted in 5% milk solution in 1X TBST. After being washed with 5% milk solution in 1X TBST the membrane was incubated with the secondary antibody (table 2-9) for two hours at room temperature. The membrane was then washed in 1X TBST and incubated with the ECL solution, composed of equals volume of detection reagent 1 and detection reagent 2 (Pierce™ ECL Plus Western Blotting Substrate, Thermo scientific), for 5 minutes in the dark. This solution is a chemiluminescent substrate for the detection of horseradish peroxidase (HRP) on immunoblots, the chemiluminescent signal was detected using the Image Analyzer LAS-3000 (Fujifilm Life Science).

Table 2-5: Composition of the stacking gel. APS and TEMED were added last and water was added to complete the final volume needed. TEMED: Tetramethylethylenediamine, SDS: Sodium dodecyl sulfate, APS: Ammonium persulfate.

Components	Initial concentration	Final concentration
Acrylamide/bis	30%	5%
Tris HCl pH= 6,8	1,5M	126mM
SDS	10%	0,1%
APS	10%	0,1%
TEMED		0,1%

Table 2-6: Composition of the resolving gel. APS and TEMED were added last and water was added to complete the final volume needed. TEMED: Tetramethylethylenediamine, SDS: Sodium dodecyl sulfate, APS: Ammonium persulfate.

Components	Initial concentration	Final concentration
Acrilamide/bis	30%	10%
Tris HCl pH= 8,8	1,5M	375mM
SDS	10%	0,1%
APS	10%	0,1%
TEMED		0,1%

Table 2-7:Composition of the running buffer at 10X. Water was added to complete the final volume. SDS: Sodium dodecyl sulfate.

Components	Final concentration
Tris base	30g/l
Glycine	144g/l
10% SDS	1%
pH=8.3	

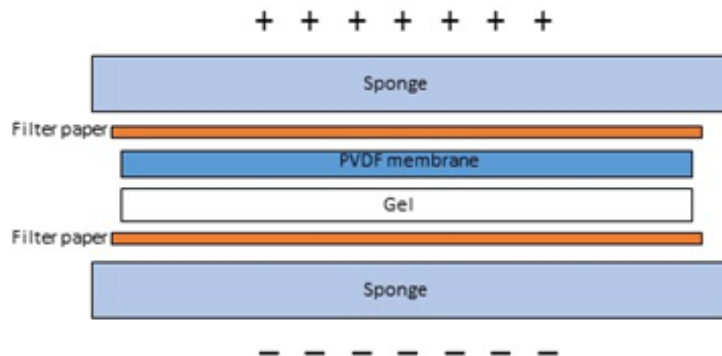


Figure 2-2:Transfer sandwich containing the electrophoresis gel, the PVDF membrane, filter papers and foam pads (sponge).

Table 2-8:Composition of the running buffer at 10X. Water was added to complete the final volume.

Components	Final concentration
Tris base	30g/l
Glycine	144g/l
pH=8.3	

Table 2-9: Term of use of the antibodies used for western-blot in *Xenopus*.

antibody	dilution	source
anti-HA Rat monoclonal 3F10	1/250	Roche #11867423001
anti-HSC70 (B-6) Mouse monoclonal	1/2500	Santa Cruz sc-7298
HRP-conjugated polyclonal goat anti-mouse immunoglobulins	1/1000	Dako Cytomation P0447
anti-Rat IgG (whole molecule)-Peroxidase Goat polyclonal	1/10000	Sigma A5795

Chapter III: Evolutionary history of the ADAMTS family in *Xenopus laevis* and *Xenopus tropicalis*

3.1 Introduction

Before this project started very little was known about the ADAMTS family in *Xenopus*. The 19 ADAMTS genes were identified in *Xenopus tropicalis* (Suga et al., 2006). During this project a new version of the *X. laevis* version 9.1 was published in open access (Session et al., 2016). The *X. laevis* genome is composed of two homoeologous subgenomes called L and S for long and short, respectively (Session et al., 2016). The subgenome S is shorter due to more deletions than L. They have similar chromosomes sizes to the *X. tropicalis* genome, suggesting they have ancestral chromosome organisation. In *X. laevis* eight out of the nine pairs of homoeologous (one copy on each set of chromosomes pairs different of homologous that defines copies on the same pair of chromosomes) have an orthologous chromosome in *X. tropicalis* and the ninth pair is the result of a fusion of chromosomes 9 and 10 found in *X. tropicalis*. No inter-chromosomal rearrangements are observed in these two amphibian species (Session et al., 2016).

X. laevis and *X. tropicalis* diverged from each other around 48 million years ago (Ma) before the divergence of the two diploid species that gave rise to the *X. laevis* subgenomes L and S, which occurred around 34 Ma. Analysis of transposable elements (TE) or 'jumping genes' specific for each subgenomes provided an evolutionary view of the two diploid ancestral species. These two species are still unknown. Specific TEs on each subgenome were active until 18 Ma suggesting that the allotetraploidization happened around 17 Ma (Session et al., 2016) (figure 3-1). *X. laevis* and *X. tropicalis* ADAMTSs will be compared to ADAMTSs in *Drosophila melanogaster*, *Caenorhabditis elegans*, *Ciona intestinalis*, *Mus Musculus* and *Homo sapiens* by phylogenetic study to determine the evolutionary history and which *X. laevis* ADAMTS homoeologous are closely related to *X. tropicalis*.

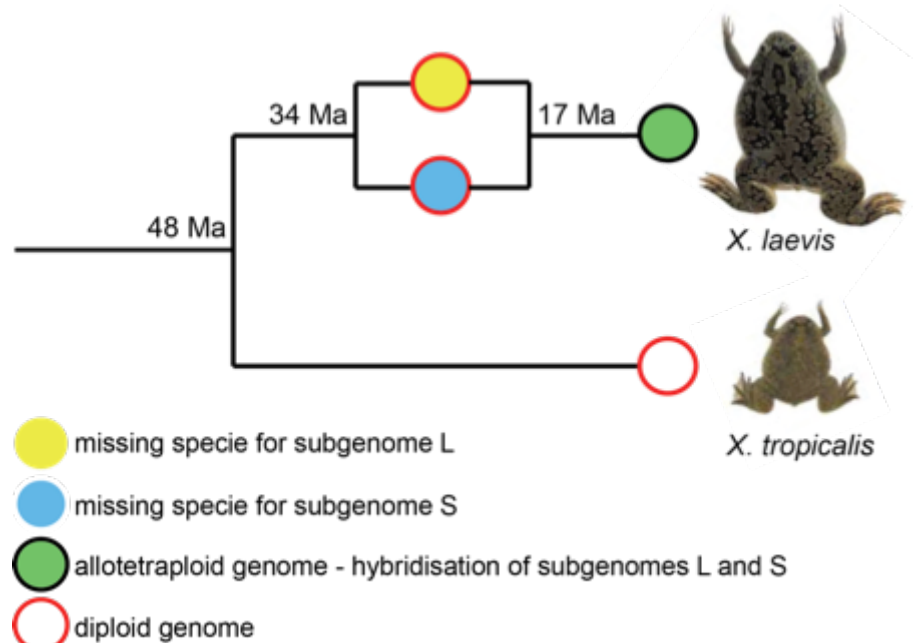


Figure 3-1: Phylogenetic tree illustrating the evolutionary history of *Xenopus laevis* and *Xenopus tropicalis*. Divergence between the allotetraploid *X. laevis* ($2n=36$) and the diploid *X. tropicalis* ($2n=20$) occurred at 48 millions years ago (Ma), divergence between the two ancestral diploid species of subgenome L and S happened at 34 Ma and the hybridisation of these two subgenomes in *X. laevis* was 17 Ma.

Comparisons between gene positions provide an overview of the possible deletions and intra-chromosomal rearrangements. These events occur more in the S subgenome. Around 50% of proteins coding genes are present in two copies in *X. laevis* (Session et al., 2016). The loss of one copy is likely to happen if their function is redundant and if there is no mutations leading to a new function. Mutations can give rise to new (neofunctionalisation) or different (subfunctionalisation) functions of one of the copies depending on where and when the gene expression is necessary but mutations lead mostly to a loss of function of one of the copies. Duplicated genes can be maintained due to gene dosage (Otto, 2007). It has been shown that the evolution of keratin gene family in *X. laevis* is marked by subfunctionalisation and loss of homoeologous on the subgenomes L and S. This could be due to their different level of expression required during development in a stage and tissue dependant manner to adapt to environmental changes (Suzuki et al., 2016).

In this chapter the evolutionary history of the ADAMTS family will be assessed in *Xenopus laevis*. The 19 *Xenopus tropicalis* ADAMTS followed the same evolutionary history as the mammalian 19 ADAMTS from protostomes ancestral genes (Kelwick et al., 2015a). The synteny, the conservation of the

chromosomal position, will be assessed for the *ADAMTS* genes present in *X. laevis* subgenomes and *X. tropicalis*. A comparison between the two *X. laevis* *ADAMTS* copies, on the L and S chromosomes, and the *X. tropicalis* copy will show the conservation of the chromosomal organisation between these two species.

3.2 Results

3.2.1 Gene identification in *Xenopus laevis* and *Xenopus tropicalis*

Protein sequences of the 19 human and mouse *ADAMTS*s were used as a reference to identify the *ADAMTS* genes in *X. laevis* (version 9.1 from 2015) and *X. tropicalis* (version 9.0 from 2015) using the UCSC Genome Browser. Genes with the highest percentage of similarity were selected. *ADAMTS8* is not annotated in the *X. laevis* genome but its chromosomal position was identified using human *ADAMTS8* as reference. All 19 *ADAMTS* genes are present in both *X. tropicalis* and *X. laevis* genomes including seven singletons. *ADAMTS7*, *ADAMTS8*, *ADAMTS12*, *ADAMTS13*, *ADAMTS16*, *ADAMTS19* and *ADAMTS20* have only one copy in the *X. laevis* genome located on the L chromosome. The chromosomal position of *ADAMTS* genes is conserved between *X. tropicalis* and *X. laevis*. *X. tropicalis* *ADAMTS3* and *ADAMTS13* are located on scaffold due to a lack of chromosomal position in the genome assembly (table 3-1).

3.2.2 Phylogenetic study of *Xenopus laevis* and *Xenopus tropicalis* *ADAMTS*

ADAMTS evolutionary history from protostomes to vertebrates is marked by duplication and retrotransposition events leading to the 19 members found in mammals. The degree of conservation of the protein *ADAMTS* family between mammals (*Homo sapiens* and *Mus musculus*) and amphibians (*Xenopus laevis* and *Xenopus tropicalis*) was assessed by phylogenetic study using the Neighbor-Joining method (figure 3-2).

Table 3-1: Chromosomal location of ADAMTS genes in *Xenopus laevis* and *Xenopus tropicalis*. Chromosome number followed by an L for the longer and an S for the shorter indicate *X. laevis* gene location on the two subgenomes. Scaffold number is indicated for the genes without a chromosomal location.

genes	<i>X.tropicalis</i> (v9.0)	<i>X.laevis</i> (v9.1)	
	chromosome	number of copy	chromosome
<i>ADAMTS1</i>	2	2	2S & L
<i>ADAMTS2</i>	3	2	3S & L
<i>ADAMTS3</i>	scaffold_51	2	1S & L
<i>ADAMTS4</i>	8	2	8S & L
<i>ADAMTS5</i>	2	2	2S & L
<i>ADAMTS6</i>	1	2	scaffold53 & 1L
<i>ADAMTS7</i>	3	1	3L
<i>ADAMTS8</i>	7	1	7L
<i>ADAMTS9</i>	4	2	4S & L
<i>ADAMTS10</i>	1	2	1S & L
<i>ADAMTS12</i>	1	1	1L
<i>ADAMTS13</i>	scaffold_620	1	8L
<i>ADAMTS14</i>	7	2	7S & L
<i>ADAMTS15</i>	7	2	7S & L
<i>ADAMTS16</i>	6	1	6L
<i>ADAMTS17</i>	3	2	3S & L
<i>ADAMTS18</i>	4	2	4S & L
<i>ADAMTS19</i>	1	1	1L
<i>ADAMTS20</i>	3	1	3L

Each *X. laevis* and *X. tropicalis* ADAMTS form a cluster on the same branch of the phylogenetic tree as the ADAMTS orthologous in *H. sapiens* and *M. musculus* (figure 3-2). They are all on the same evolutionary branch rooted by an ancestral gene of protostome (*Drosophila melanogaster* and *Caenorhabditis elegans*) and chordates (*Ciona intestinalis*) except for ADAMTS17, 19 and 13 which do not have an ancestral gene in *C. intestinalis* (figure 3-2).

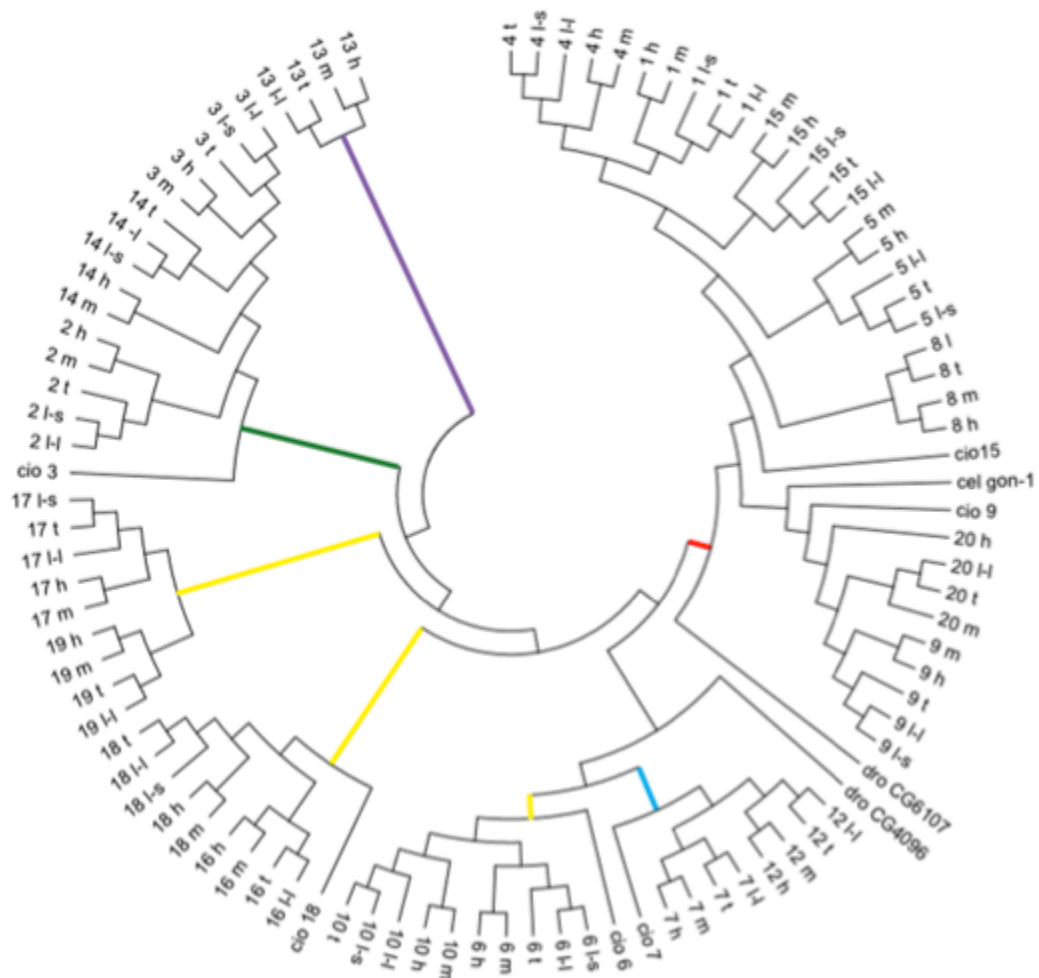


Figure 3-2: Evolutionary relationships of the ADAMTS protein. The phylogenetic tree was inferred using the Neighbor-Joining method. The different clades of ADAMTS are shown with a coloured line, purple for the vWFCP, green for the procollagen N-propeptidase, yellow for the orphan, blue for COMP proteinases and red for aggrecanases. The vertebrate ADAMTS genes are indicated by a number followed by a single letter code indicating the species: for example, ADAMTS1 t represents 1 from *Xenopus tropicalis*; 2 l represents ADAMTS2 from *Xenopus laevis*; 15 h is ADAMTS15 from *Homo sapiens*; 8 m is ADAMTS8 from *Mus musculus*. For *Drosophila melanogaster* (dro), *Caenorhabditis elegans* (cel) and *Ciona intestinalis* (cio), the annotation is the specie followed by the gene number; for example, cio 6 is ADAMTS6 from *C. elegans*. Adapted from (Kelwick et al., 2015a).

The relation between homoeologous ADAMTS in *X. laevis* subgenome L and S and orthologous ADAMTS in *X. tropicalis* analysed by the phylogenetic study using protein sequences, as previously described, was looked in more details in order to establish which ones were more conserved between these two species. Homoeologous *X. laevis* ADAMTS2, 3, 4, 6, 9 and 14 are highly conserved when compared with their orthologous in *X. tropicalis*. Whereas other *X. laevis* ADAMTSs have one of their copies on a subgenome more similar to *X.*

tropicalis than to their other copy. *X. laevis* ADAMTS1 L, 15 L and 18 L are more related to their orthologous in *X. tropicalis* than their homoeologous on subgenome S. Whereas *X. laevis* ADAMTS5 S, 10 S and 17 S are more close to *X. tropicalis* than their other copy on subgenome L (figure 3-3).

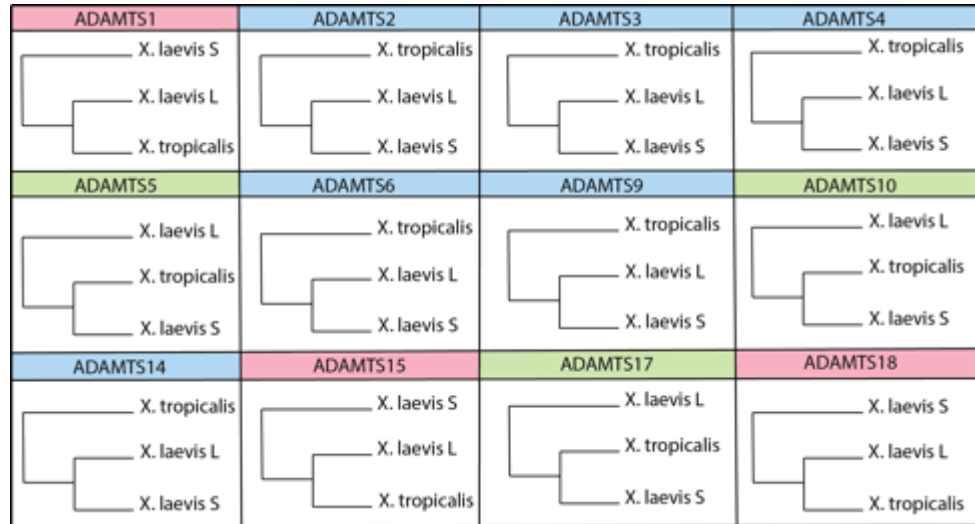


Figure 3-3: Phylogeny of ADAMTS in both *X. laevis* subgenomes L and S and *X. tropicalis*. Coloured boxes show the different relationship between orthologous ADAMTS, pink for ADAMTS more conserved between *X. laevis* L and *X. tropicalis*, blue for ADAMTS more conserved between both *X. laevis* L and S and green for ADAMTS more conserved between *X. laevis* S and *X. tropicalis*.

3.2.3 Synteny analysis of ADAMTS genes between *Xenopus laevis* subgenomes L and S and *Xenopus tropicalis*

It has been shown that more gene deletions occurred on the subgenome S than on the subgenome L, explaining the shorter size of the S subgenome compare to L and the *X. tropicalis* genome (Session et al., 2016). Synteny analysis was used to look at these events in the ADAMTS gene family. Locations and orientations of neighbour genes to one of the seven singleton ADAMTS genes in subgenome S were compared to their positions on the same chromosome in subgenome L and in *X. tropicalis*.

In order to carry out the synteny analysis, genes close to the gene of interest were selected. Due to the lack of annotation and/or assembly of scaffolds into chromosomes in the *X. laevis* (v9.1) and *X. tropicalis* (v9.0) genomes, neighbour genes were selected based on the criteria that they had to be annotated on the three genomes, even though they might not be the closest gene to the ADAMTS gene of interest.

A comparison of chromosomal location between the two *X. laevis* subgenomes L and S revealed that *ADAMTS19* is the only gene deleted on the S chromosome whereas their neighbour genes were present on both L and S chromosomes in the same location and orientation (figure 3-4F). Intra-chromosomal arrangements were observed between the homoeologous subgenomes for the chromosomes 3, 6 and 7. Conserved genes on L and S around *ADAMTS7*, *ADAMTS8*, *ADAMTS16* and *ADAMTS20* have their position and/or their orientation inverted on the S chromosome compared to the L chromosome (figure 3-4A, B, E, G). Loss of one copy is observed for several closely located genes including *ADAMTS* genes such as *ADAMTS7*, *ADAMTS8*, *ADAMTS12*, *ADAMTS13*, *ADAMTS16* and *ADAMTS20* (figure 3-4A, B, C, D, E and G). The chromosomal organisation on the *Xenopus tropicalis* genome shows more similarities to the subgenome L (figure 3-4C, E, F and G). As the assembly of the *X. tropicalis* is not yet complete, some genes are found on scaffolds and not yet allocated to a chromosome (figure 3-4D).

X. laevis subgenome L and *X. tropicalis* genomes have been shown to be more similar than with the *X. laevis* subgenome S. The synteny studies of the three copies of *ADAMTS* genes on these genomes show that six out of twelve; *ADAMTS1*, *ADAMTS2*, *ADAMTS3*, *ADAMTS9*, *ADAMTS10* and *ADAMTS17*, have their chromosomal organisation conserved between *X. tropicalis* and *X. laevis* subgenome L but not with subgenome S (figure 3-5). Intra-chromosomal rearrangement (figure 3-5A, B and C) or loss of genes (figure 3-5D, E and F) are observed in the subgenomes S around these genes.

Conservation of the synteny between the two *X. laevis* subgenomes and *X. tropicalis* genomes is observed for *ADAMTS14* and *ADAMTS18* (figure 3-6) whereas it is not conserved for *ADAMTS4*, *ADAMTS6* and *ADAMTS15* (figure 3-7).

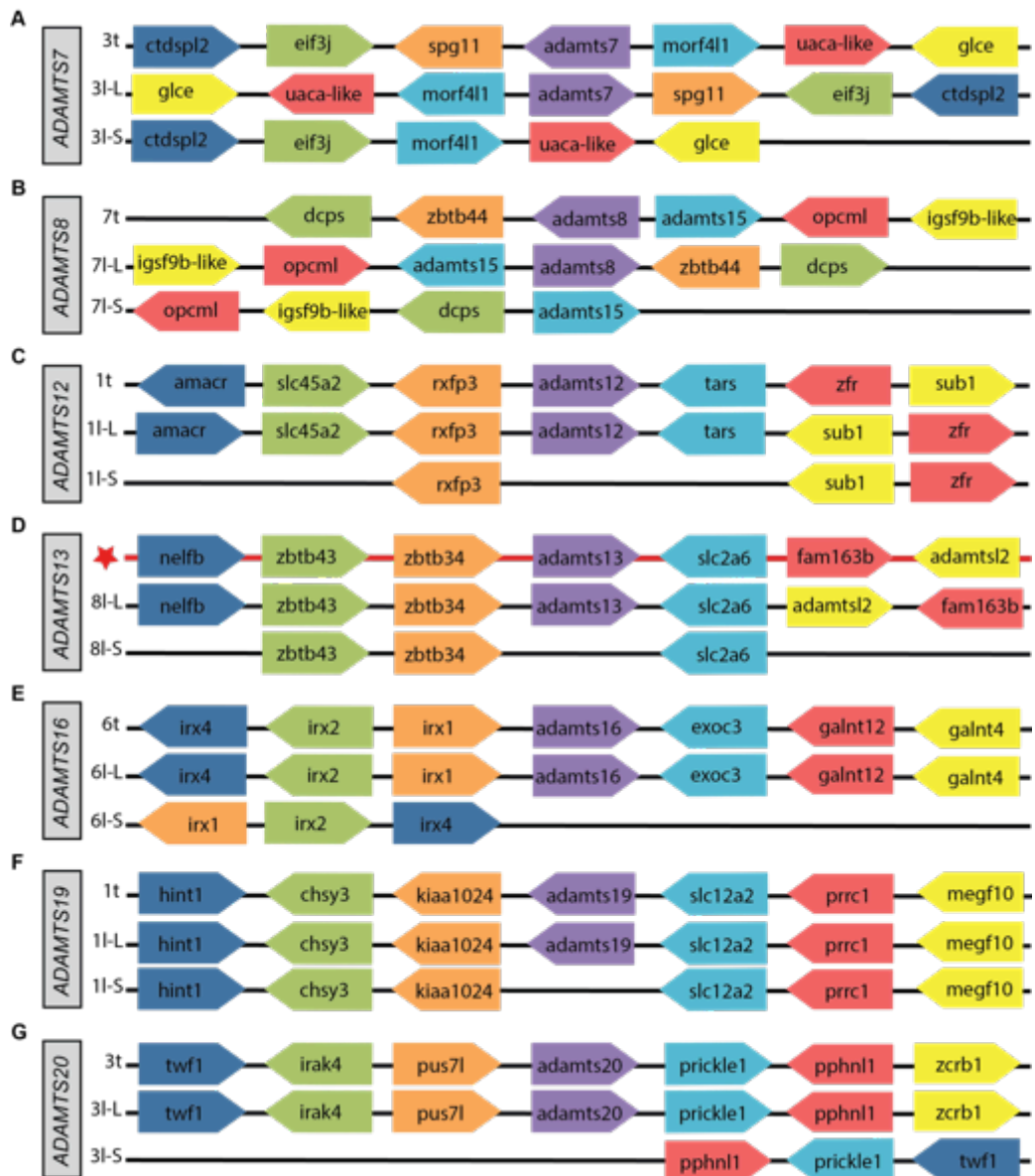


Figure 3-4: Synteny of single copy ADAMTS genes in subgenomes S and L of *Xenopus laevis* and *Xenopus tropicalis*. Chromosome number is indicated on the left followed by an l with L and S for the longer and shorter *X. laevis* subgenomes, respectively, and a t for *X. tropicalis*. The red star (D) indicates the location of scaffolds; *nelfb* on scaffold75; *zbtb43* on scaffold363; *zbtb34* on scaffold92; *ADAMTS13* on scaffold620; *slc2a6* on scaffold285; *fam163b* and *ADAMTSL2* on scaffold 353. The arrows show the orientation of the genes syntenic to (A) *ADAMTS7*; (B) *ADAMTS8*; (C) *ADAMTS12*; (D) *ADAMTS13*; (E) *ADAMTS16*; (F) *ADAMTS19*; (G) *ADAMTS20*.

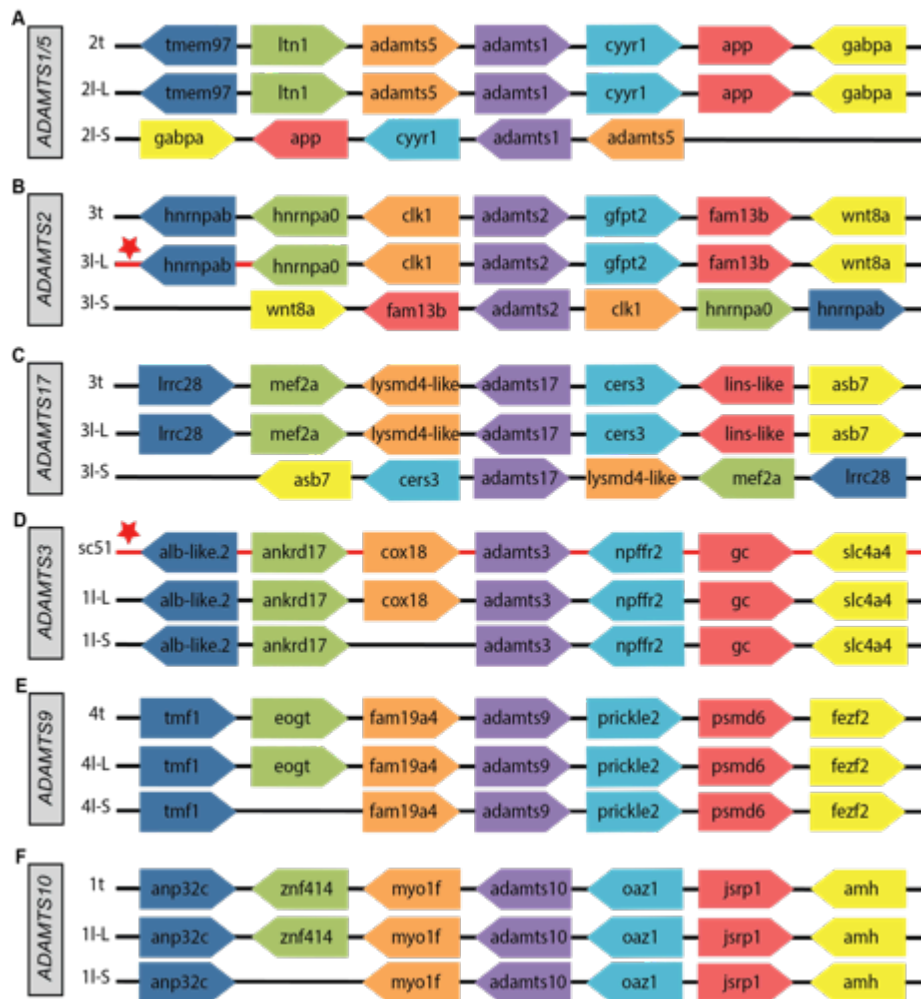


Figure 3-5: Synteny of *X. laevis* ADAMTS genes with similar organisation in subgenome L and *X. tropicalis* genome but different to *X. laevis* subgenome S. Chromosome number is indicated on the left followed by an I with L and S for the longer and shorter *X. laevis* subgenomes, respectively, and a t for *X. tropicalis*. The red stars and lines represent the location of a scaffold, scaffold89 (B) and scaffold 51 (D). The arrows show the orientation of the genes syntenic to (A) ADAMTS1/5; (B) ADAMTS2; (C) ADAMTS17; (D) ADAMTS3; (E) ADAMTS9 and (F) ADAMTS10.

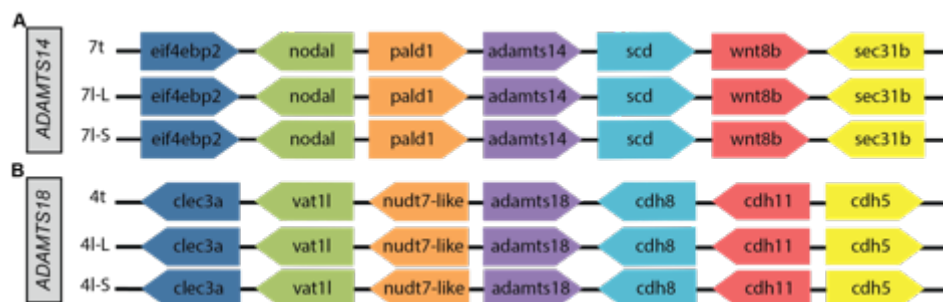


Figure 3-6: Synteny of *X. laevis* ADAMTS genes in subgenomes L and S with similar chromosomal organisation as *X. tropicalis* ADAMTS genes. Chromosome number is indicated on the left followed by an I with L and S for the longer and shorter *X. laevis* subgenomes, respectively, and a t for *X. tropicalis*. The arrows show the orientation of the genes syntenic to (A) ADAMTS14 and (B) ADAMTS18.

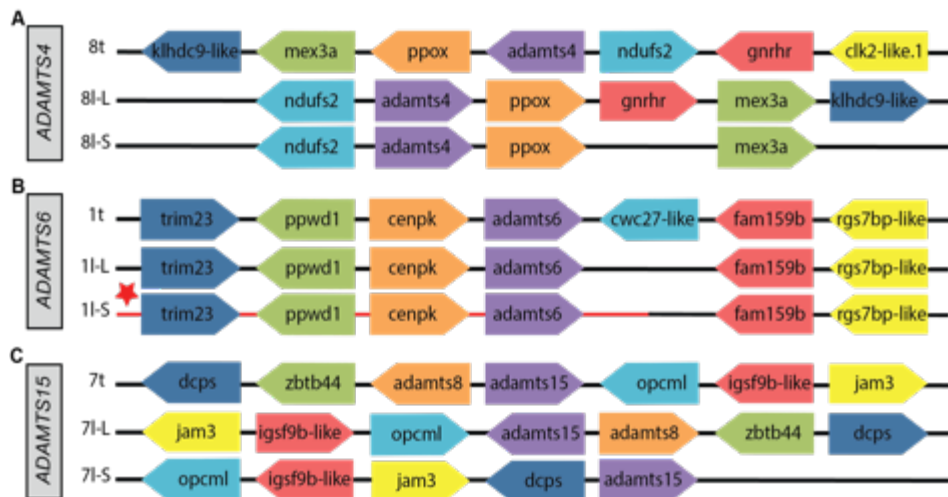


Figure 3-7: Synteny of *X. laevis* ADAMTS genes in subgenomes L and S and with different chromosomal position compare to *X. tropicalis* ADAMTS genes. Chromosome number is indicated on the left followed by an l with L and S for the longer and shorter *X. laevis* subgenomes, respectively, and a t for *X. tropicalis*. The red star and line represent the location of scaffold 53 (B). The arrows show the orientation of the genes syntenic to (A) ADAMTS4, (B) ADAMTS6 and (C) ADAMTS15.

3.2.4 Conservation of the *Xenopus* ADAMTS genes between *Xenopus laevis* subgenomes L and S

Mutations within copies of the same gene can occur in polyploid cells creating loss or new/different functions (Otto, 2007). The percentage of similarities between the two copies on the L and S *X. laevis* subgenomes of ADAMTS genes is around 95%. The lowest percentage of similarity is ADAMTS2 and the highest is ADAMTS6 (table 3-2).

The comparison by alignment of ADAMTS amino acid sequences showed that most of the differences were located at the C and N-terminal of the protein and not in the different domains. This suggests that the structure of the protein might be conserved between the L and S subgenomes as well as the function. During this analysis a missing domain for the ADAMTS9 coded by the subgenome L copy (figure 3-8) were observed. However this missing domain was due to a lack of genome sequencing in the subgenome L leading to a wrong protein sequence. Sequencing of the missing area by PCR would allow completing the ADAMTS9 gene sequence on the subgenome L.

Table 3-2: Percentage similarity between homoeologous *X. laevis* ADAMTS genes on the two subgenomes L and S.

genes	% of similarity between subgenomes L and S
ADAMTS1	95.15
ADAMTS2	86.32
ADAMTS3	94.57
ADAMTS4	92.92
ADAMTS5	96.70
ADAMTS6	98.12
ADAMTS9	92.74
ADAMTS10	95.13
ADAMTS14	94.97
ADAMTS15	94.9
ADAMTS17	95.58
ADAMTS18	93.16

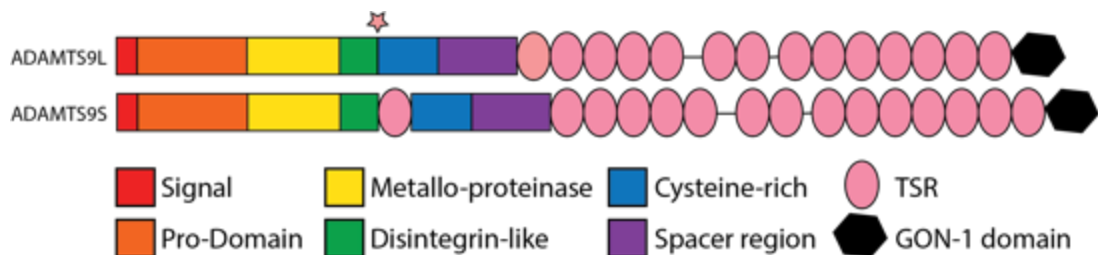


Figure 3-8: *Xenopus laevis* ADAMTS9L and ADAMTS9S structure. The name of the protein is on the left followed by an L for the subgenome L copy and a S for the subgenome S copy. The pink star indicates the missing Thrombospondin type 1 motif (TSR) in ADAMTS9L.

3.3 Discussion

The aim of this chapter was to identify the *Xenopus ADAMTS* genes, assess their degree of conservation to mammalian *ADAMTS* genes and their place in evolutionary history from protostomes to the 19 *ADAMTS* genes in mammals, analyse their chromosomal organisation on the *X. laevis* subgenomes L and S and the *X.tropicalis* genome.

19 *ADAMTS* genes are found in the *Xenopus laevis* subgenome L and *Xenopus tropicalis*, the same as in mammals, whereas only twelve are present in the subgenome S due to a loss of copy for seven *ADAMTS*s (*ADAMTS7*, *ADAMTS8*, *ADAMTS12*, *ADAMTS13*, *ADAMTS16*, *ADAMTS19* and

ADAMTS20). Loss of these copies can be explained by neofunctionalization and/or regulation of the level of expression. *X. tropicalis* and *X. laevis* *ADAMTS* chromosomal position is conserved, thus confirming the absence of inter-chromosomal rearrangements. It is known that 92% of the genes are conserved between *X. tropicalis* and the subgenome L of *X. laevis* when only 68% are conserved between *X. tropicalis* and the subgenome S of *X. laevis* (Session et al., 2016). The *Xenopus ADAMTS* gene family have the following proportions: 100% are present in *X. tropicalis* and *X. laevis* subgenome L but only 63% are present in *X. laevis* subgenome S.

First phylogenetic analysis showed that the evolutionary history of the 19 *ADAMTS* proteins present in *X. tropicalis* is similar to the 19 mammalian *ADAMTS* (Kelwick et al., 2015a). The new version of the annotated *X. laevis*, released in 2015, allowed me to look at the conservation of *ADAMTS* in *X. laevis* compare to *ADAMTS*s in *Drosophila melanogaster*, *Caenorhabditis elegans*, *Ciona intestinalis*, *Xenopus tropicalis*, *Mus Musculus* and *Homo sapiens*. It showed that they are strongly conserved suggesting that they followed the same evolutionary history starting with a duplication of an ancestral gene prior the divergence of protostomes and deuterostomes around 650 Ma. Duplications and retrotransposition events lead to the 19 *ADAMTS* genes found in mammals and in *X. laevis* and *X. tropicalis*. These data suggest that the study of the function of *ADAMTS* in *Xenopus* could provide valuable information in relation to their function in humans.

Homoeologous *X. laevis* *ADAMTS* proteins are more closely related to each other than to orthologous *X. tropicalis* *ADAMTS* proteins. For some cases one of the *X. laevis* copy on the L or S subgenomes is more closely related to *X. tropicalis* suggesting that a homoeologous gene is more related to an ancestral gene (figure 3-3). A similar phylogenetic analysis could be done using the *ADAMTS* genes sequences to confirm the relation between homoeologous and orthologous observed at the protein level. It has been shown that homoeologous pairs can have different expression levels and profiles. Such as one *X. laevis* copy can show an expression profile more similar to *X. tropicalis* copy than to the other *X. laevis* copy. The keratin gene family shows these different expression profiles between homoeologous due to neofunctionalisation to adapt to environmental changes (Suzuki et al., 2016). Whereas (Watanabe et

al., 2016) found that for most families of transcription factors, such as homeobox genes family, *sox* and *pax* gene families, homoelogenous have the same level and profile of expression suggesting that they are conserved due to the need of high expression of these genes.

The synteny of the *ADAMTS* gene family is more conserved between *X. tropicalis* and *X. laevis* subgenome L than with the subgenome S, indicating the ancestral synteny is the one found on these two genomes. Intra-chromosomal rearrangements occurred creating inverted chromosomal organisation on a group of genes or on an individual gene, between the three chromosomes. Some of the genes used in this study are located on scaffolds but with the same synteny found on annotated chromosomes. These data can help improve the genome assembly by allocating scaffolds into the correct chromosome (Watanabe et al., 2016).

ADAMTS gene copies on *X. laevis* subgenome L and S are not identical. This suggests that mutations occurred before and/or after the hybridisation of the two different subgenomes. It could lead to loss of function, neofunctionalisation or subfunctionalisation in function of the gene dosage (Watanabe et al., 2016) or on the specific need at specific time and place during development (Suzuki et al., 2016). It is not known if these differences disrupt the structure and/or the function of the *ADAMTS* proteins.

In order to investigate the role of the *ADAMTS*s in more detail, their expression profiles during development have to be defined, which will be describe in the next two chapters along with functional studies on one of the *ADAMTS*s, *ADAMTS9*.

**Chapter IV: Characterisation of the ADAMTS family
in *Xenopus* during organogenesis**

4.1 Introduction

4.1.1 ECM remodeling during neural crest cell migration in *Xenopus*

In this chapter the expression profiles of the ADAMTS family will be looked at in early development and the function of ADAMTS9 will be investigated in neural crest (NC) and in kidney development.

Neural crest (NC) development starts with a complex interplay of signals between the neural and non-neural ectoderm during gastrulation leading to the formation of a broad progenitor domain named the “neural plate border”. Transcription factors named “neural plate border specifiers” activate NC-specific markers in a subset of neural plate border cells at the end of gastrulation. The epithelium-to-mesenchyme transition (EMT), which is characterising by the loss of tight and adherent junctions, modifications of the apical-basal cell polarity and rearrangements of the cytoskeleton, is then activated and initiates NC migration during neurulation. The NC emerge along the anterior-posterior axis of the embryo, posterior to the mid-diencephalon and during organogenesis NC migrate along defined routes, proliferate, and populate their target tissues and organs where they differentiate (Pegoraro and Monsoro-Burq, 2013) (Thiery et al., 2009) (Theveneau and Mayor, 2012). The NC migrate in four main streams in a solitary or collective way. The enteric NC migrate into the gut, the cardiac NC migrate to the heart loops, the cephalic NC migrate anteriorly (through the branchial arches) into the head and the trunk NC migrate down the trunk of the embryo. Trunk NC pass in-between the neural tube and the somites and some NC migrate straight up where they will give rise to mesenchymal and pigment cells in the dorsal fin (figure 4-1) (Theveneau and Mayor, 2013).

In vivo and *in vitro* studies show that versican is a nonpermissive matrix for NC migration leading them along the correct migratory direction by creating restrictive boundaries. Confinement is essential for collective NC migration (Szabo et al., 2016). ADAMs play a role in NC migration (Alfandari et al., 2001). ADAM9, 13 and 19 have been shown to play a role in NC migration. ADAM9 and 13 can cleave cadherin-11, which stimulates NC migration (McCusker et al., 2009). The cleavage of ADAM13 releases a cytoplasmic domain that translocates to the nucleus and activates gene transcription promoting NC migration (Cousin et al., 2011). Loss of function experiments for ADAM9 lead to

a reduction of NC markers and NC migration (Neuner et al., 2009). The membrane-bound MMP14 is expressed in cephalic and trunk migrating NC and may play a role in the remodeling of the ECM (Harrison et al., 2004) (Tomlinson et al., 2009).

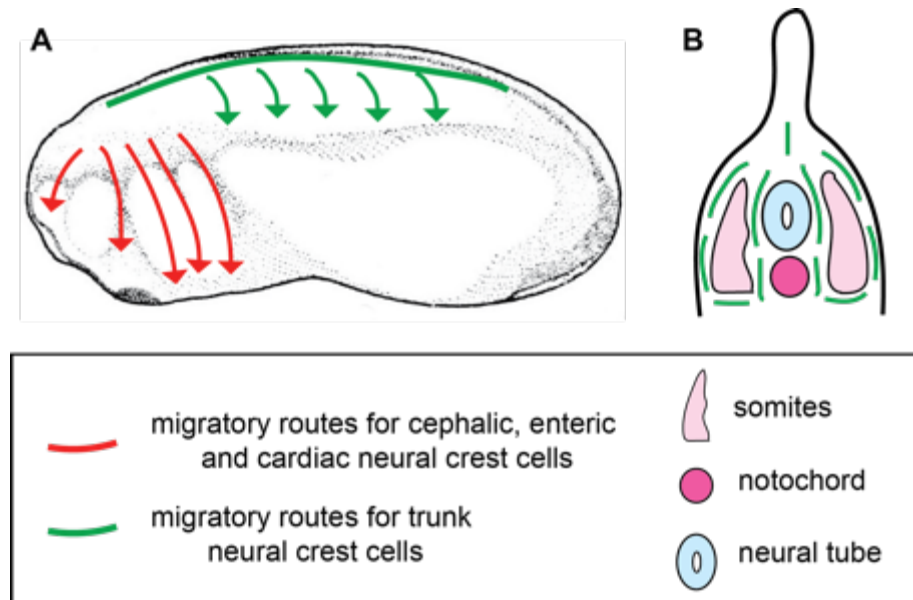


Figure 4-1: *Xenopus* neural crest cells migration pathways. Migratory routes for the cephalic, enteric and cardiac NC are indicated in red and routes for the trunk NC is indicated in green. (A) Migratory NCC in a stage 24 embryo, (B) transversal section of a *Xenopus* embryo stage 23 showing the migrating trunk NC between the neural tube and the somites and straight up to the dorsal fin. The developmental stage representations are from (Nieuwkoop and Faber, 1994).

4.1.2 Remodeling during pronephros development in *Xenopus*

In *Xenopus* kidney development starts at late gastrulation (stage 12.5) when renal precursor cell lineage is specified. In early neurula embryos the kidney fields are formed in the intermediate mesoderm. At tailbud stage the specified intermediate mesoderm condenses to form the pronephric primordium that by a medio-lateral patterning, regulated by notch signaling, gives rise to tubules, nephrostomes and glomus. The glomus is the equivalent of the mammalian glomerulus but directly filters into the coelomic cavity that surrounds embryonic organs and not into the Bowman's capsule. Major morphological changes occur at tadpole stage (stage 36) characterised by cell movements. Distal cells of the tubule move in the proximal direction leading to the curvature of the tubule that becomes the intermediate tubule. At the same time the

diameter of the proximal tubule decreases and convergent extension movements lead to its elongation. At stage 38 the tubule of the pronephros forms a stereotypic S-shape loop segmented along its proximal-distal axis, in proximal, intermediate and distal tubule, and urine flow starts (Lienkamp, 2016) (figure 4-2A). The *Xenopus* pronephros is structurally and functionally similar to the mammalian nephron. The pronephros is composed of three domains: the glomus, where the blood is filtrated into the coelomic cavity; the tubule where selective re-absorption and secretion takes place, and the duct that transports waste to the cloaca. Nephrostomes are thin ciliated funnels that transfer the fluids from the coelom to the tubule (figure 4-2B). At metamorphosis the pronephros is replaced by the mesonephros with a more complex structure; the adult kidney (Lienkamp, 2016).

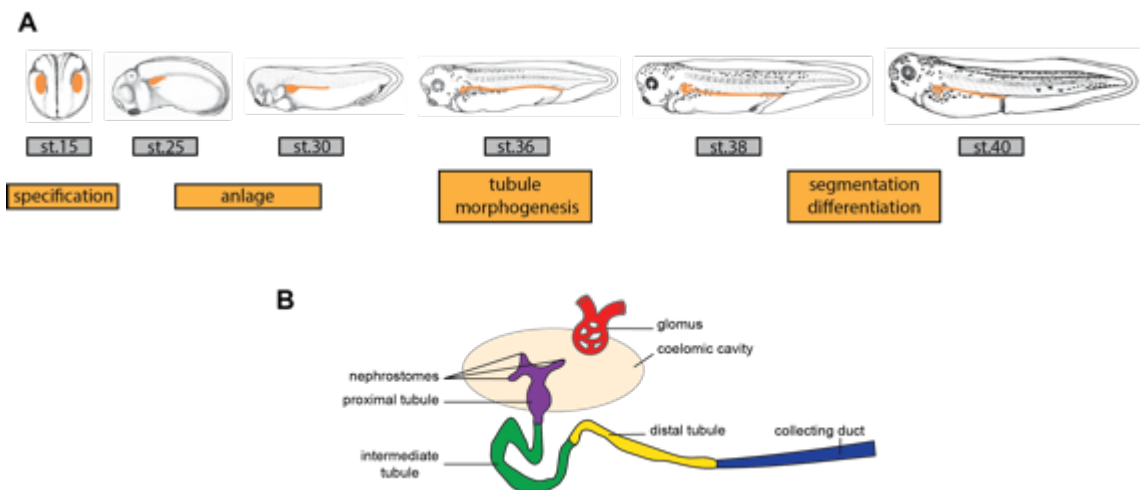


Figure 4-2: Pronephros development in *Xenopus*. (A) Localisation of the pronephros at different stages of development indicated in the grey box corresponding to different steps of the pronephros organogenesis indicated in the orange box. (B) Morphology of the pronephros at tadpole stage (stage 38). The developmental stage representations are from (Nieuwkoop and Faber, 1994).

The globular basement membrane (GBM) is the thickest basement membrane in the kidney and is composed of laminin, type IV collagen and heparan sulfate proteoglycans. The main function of this pericellular ECM is to act as a filter between the vascular system and the urinary space. This is dependant upon the charge of the basement membrane, which is negatively charged due to the presence of GAGs chains linked to the heparan sulfate proteoglycans. Mutations in these components lead to kidney diseases in human and mouse. The interstitial ECM in the kidney is mostly composed of

different types of collagens, fibronectin, thrombospondin, proteoglycans such as versican and hyaluronan. In renal fibrosis the scar tissue is caused by the accumulation of ECM components in the interstitial ECM due to decreased degradation and elevated synthesis making them good markers of renal fibrosis. Dysregulation of the interstitial ECM components are seen in most kidney diseases. Interstitial renal ECM has different functions such as hydration, force-resistance and as a growth factor reservoir. *ADAM19* mRNA is expressed in human kidney in distal tubules but not in proximal tubules or glomerulus, whereas in renal disease it is expressed in proximal tubules and the glomerulus and it is up regulated in distal tubules. These profiles of expression suggest a role for *ADAM19* in kidney development and in renal diseases (Melenhorst et al., 2006). A similar observation has been reported for *ADAM* family member *ADAM17* found weakly expressed in human proximal tubules, peritubular capillaries, glomerular endothelium and parietal epithelium. *ADAM17* was up regulated after interstitial fibrosis and tubular atrophy and found expressed in the mesangium suggesting a role in kidney disease fibrosis (Mulder et al., 2012). MMP-1, -2, -3, -9, -13, -14, -24, -25, -27 and -28 are expressed in the kidney and have been shown to be involved in ECM remodeling, degradation of basement membrane, angiogenesis, cell migration and cell apoptosis. They are implicated in renal diseases such as fibrosis, especially MMP-2, -7 and -9. TIMP1, 2 and 3 are expressed in the kidney and TIMP1 and 2 are increased in renal diseases (Genovese et al., 2014).

Little is known about the role of the ADAMTS family in the neural crest migration and in the pronephros development. The ECM remodeling is important for these two developmental processes. The ADAMTSs function in neural crest cells and pronephros development using *Xenopus* as an animal model will be investigated in this chapter.

4.2 Results

4.2.1 ADAMTSs expression and function in *Xenopus tropicalis*

4.2.1.1 Expression profiles of the ADAMTS family in *Xenopus tropicalis*

To look at the expression profiles of the ADAMTS family in *Xenopus tropicalis* during development the RNA of different all embryos (n=10) at key stages of development such as unfertilised egg, blastula (stage 9), neurula (stage 15), organogenesis at early tailbud (stage 22), tailbud (stage 27) and late tailbud (stage 33), and organogenesis at tadpole (stages 40, 42 and 45) was extracted (figure 4-3). cDNA synthesis was then carried out and the expression profiles established by RT-PCR. The same number of PCR cycles (35 cycles) was used for all ADAMTSs genes; p300 was used as a loading control and H₂O as a negative control. The signal intensity was different for the members of the ADAMTS family. ADAMTS1, ADAMTS6 and ADAMTS10 were the most strongly expressed whereas ADAMTS2 and ADAMTS13 (figure 4-3). The maternal expression was measured at the unfertilised egg stage as the embryonic transcription only begins the mid blastula transition (stage 8). Only ADAMTS17, ADAMTS6, ADAMTS7, ADAMTS2, ADAMTS3, ADAMTS5 and ADAMTS1 had a maternal expression (figure 4-3). The expression of the ADAMTSs is dynamic across *Xenopus tropicalis* developmental stages (figure 4-3).

4.2.1.2 Expression pattern of ADAMTS9 in *Xenopus tropicalis*

PCR only gives temporal expression. Wholemount *in situ* hybridisation (WISH) provides spatial as well as temporal information. *In situ* probes were generated for a number of ADAMTSs.

WISH were carried out, with probes generated from PCR products, for all the ADAMTSs in *Xenopus tropicalis* but with the exception of ADAMTS9 (figure 4-4), they did not show any specific signals.

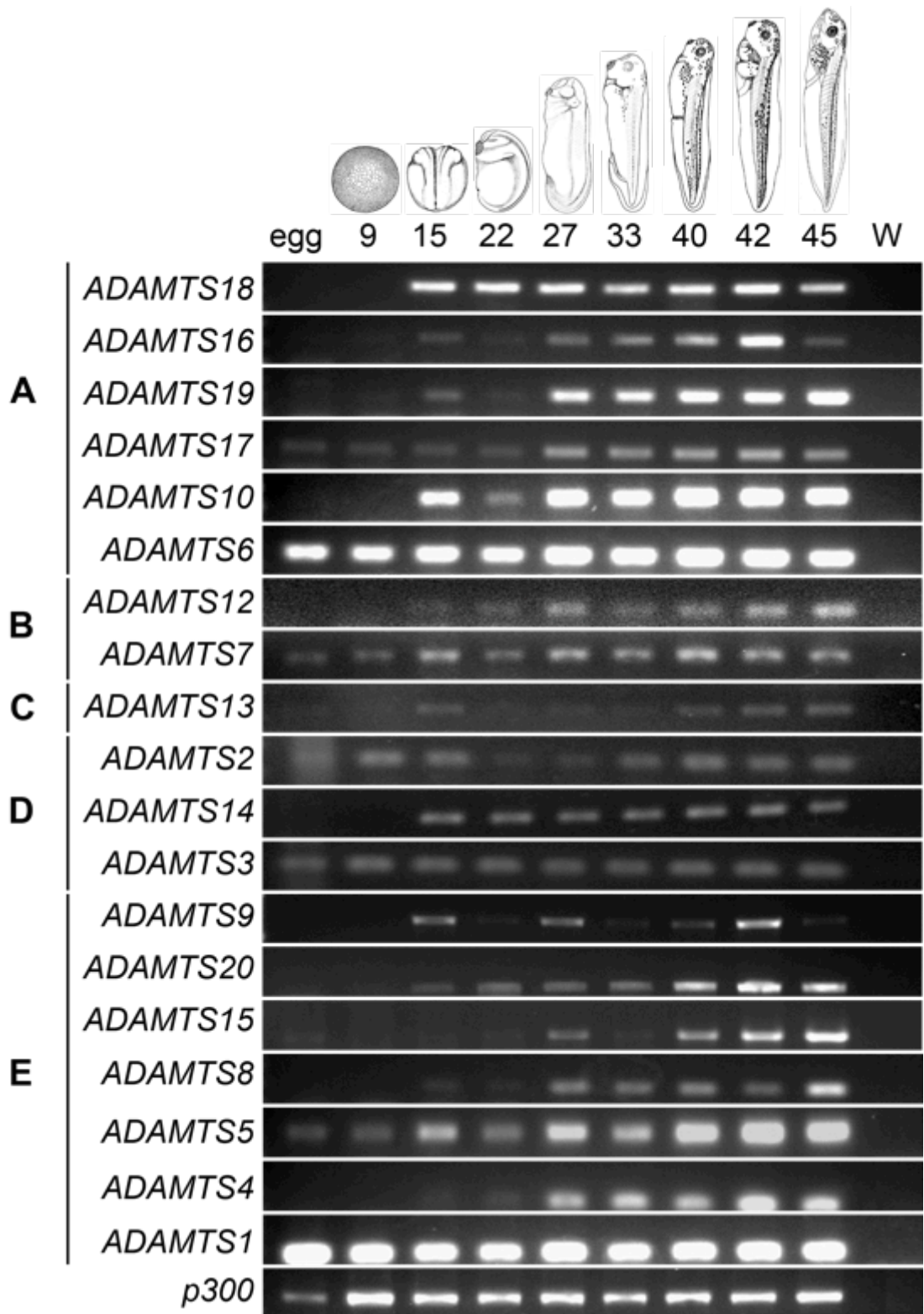


Figure 4-3: Expression of the ADAMTS genes family during *Xenopus tropicalis* development. Analysis by RT-PCR of mRNA from egg to stage 45. *Xenopus* stages are indicated at the top according to (Nieuwkoop and Faber, 1994) (NF) and gene names are indicated on the left. W: water (H₂O), is a negative control and p300 is a loading control. ADAMTS genes are organised by clade as follow, (A) orphan, (B) COMP proteinases, (C) vWFCP, (D) Procollagen N-propeptidase and (E) Hyalactanases.

WISH for *ADAMTS9* did not show any specific signal in early stages before tailbud stages in *X.tropicalis* which confirm RT-PCR results showing that *ADAMTS9* was not expressed before neurula and early tailbud stages (figure 4-3). At early tailbud stages (stages 24) *ADAMTS9* expression was mostly found in the developing eye and in the cloaca (figure 4-4A). At tailbud stages (stages 27), the expression was observed in the eye, in the midbrain hindbrain boundary, in the pronephros and in the pronephric duct and in the cloaca (figure 4-4B). At stage 33 the *ADAMTS9* expression was found in numbers of developing organs and structures such as the pronephros, the pronephric duct, the olfactory placode, the optic cup, the otic vesicle, the branchial arches and the cloaca (figure 4-4C). At tadpole stages (stages 41) the eye structure was more defined and the *ADAMTS9* expression was specific to the lens and the retinal pigment epithelium, the expression was also found in the pancreas and in the fin (figure 4-4D).

4.2.1.3 ADAMTS9 knockdown in *Xenopus tropicalis*

To study the function of *ADAMTS9* in *Xenopus tropicalis* development, a morpholino was designed to block the translation of the *ADAMTS9* protein. *ADAMTS9* morpholino was injected into both cells of a two-cell stage embryo at varying concentrations (30 and 60ng) to determine a concentration, which would give a consistent phenotype. At the same time a control morpholino (morpholino that targeted a human beta-globin intron mutation that causes beta-thalassemia and is known to not cause phenotypes in *Xenopus*) was injected in the same way at the highest concentration of *ADAMTS9* morpholino (60ng) (figure 4-5). This morpholino was used as a negative control to assess the specificity of the observed phenotypes to *ADAMTS9* morpholinos.

This experiment showed that the injection of 30ng and 60ng of *ADAMTS9* morpholino did not appear to have an effect on *Xenopus tropicalis* development. Injected embryos with 30ng and 60ng of *ADAMTS9* morpholino appeared wild type, as demonstrated in the two group images (figure 4-5A and B) compared to the injected embryos with the control morpholino, as demonstrated in the group image (figure 4-5C).

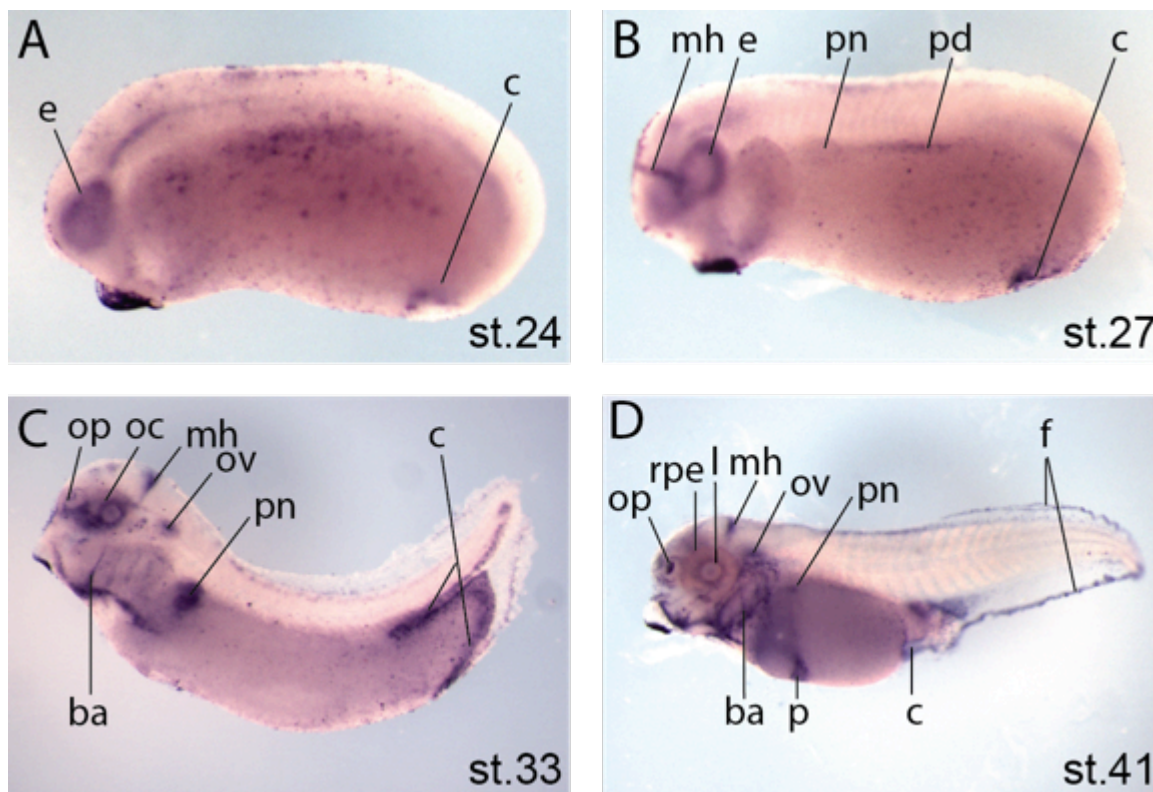


Figure 4-4 The expression pattern of ADAMTS9 in *Xenopus tropicalis* embryos. Developmental stages are according to (Nieuwkoop and Faber, 1994). Lateral views of embryos with anterior on the left and posterior on the right. (A) At stage 24 the expression is in the eye (e) and in the cloaca (c). (B) At stage 27 the expression is in the eye, in the midbrain hindbrain boundary (mh), in the pronephros (pn) and in the pronephric duct and in the cloaca (pd). (C) At stage 33 the expression is in the olfactory placode (op), in the optic cup (oc), in the midbrain hindbrain boundary, in the otic vesicle (ov), in the pronephros (pn), in the branchial arches (ba) and in the cloaca. (D) At stage 41 the expression is also in the lens (l), in the retinal pigment epithelium (rpe) in the pancreas (p) and in the fin (f).

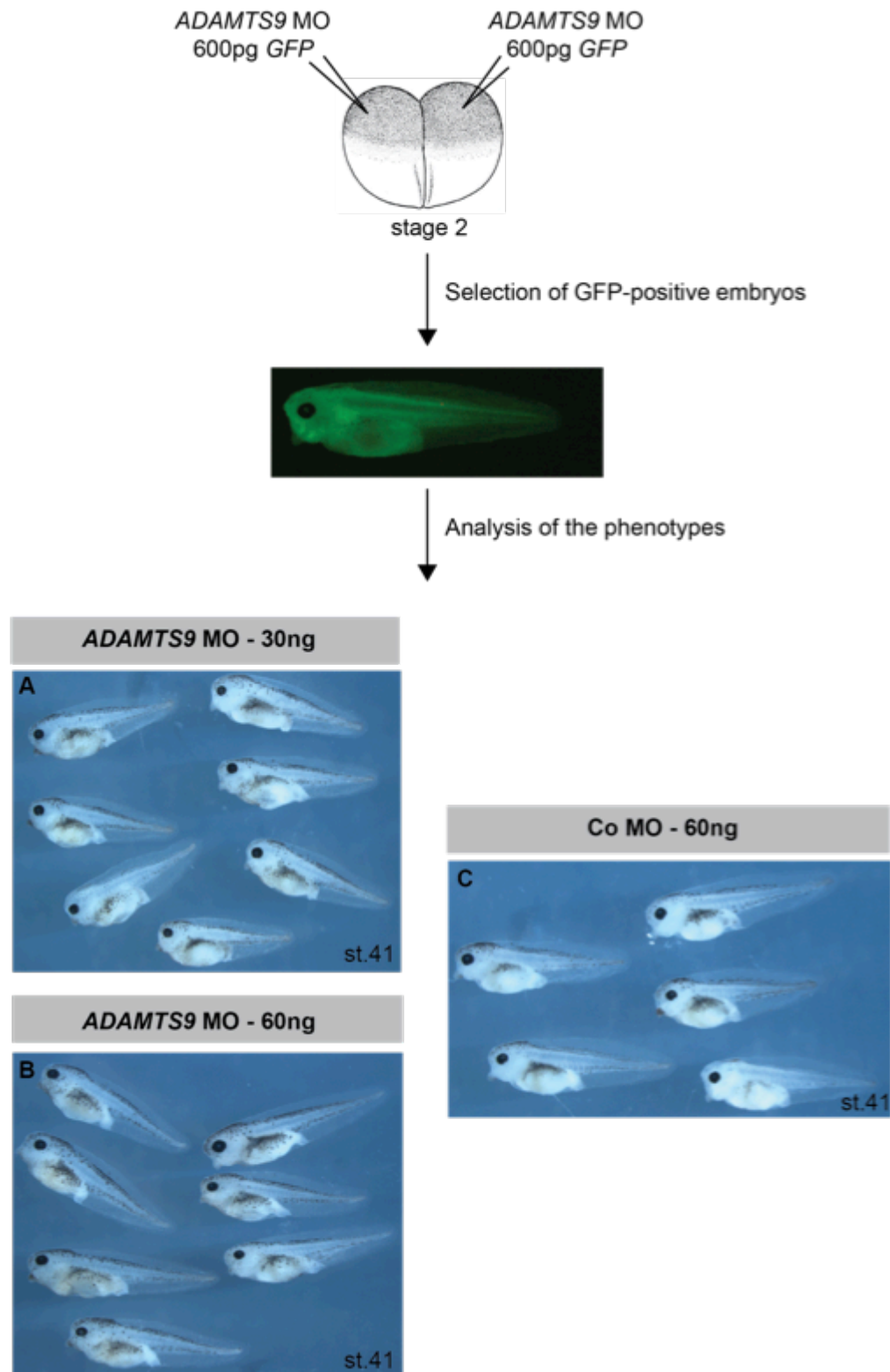


Figure 4-5: The phenotype obtained after *ADAMTS9* knockdown in *Xenopus tropicalis*. At the top is represented a 2 cell stage embryo injected with *ADAMTS9* morpholino and *GFP* mRNA (600pg). In the middle is shown the *GFP* signal in injected embryos. At the bottom are the group pictures of stage 41 injected embryos with (A) 30ng of *ADAMTS9* morpholino (n=33), (B) 60ng of *ADAMTS9* morpholino (n=36) and (C) 60ng of control morpholino (n=42). Co: control and MO: morpholino. Developmental stages are according to (Nieuwkoop and Faber, 1994).

4.2.2 ADAMTSs expression and function in *Xenopus laevis*

4.2.2.1 Expression profile of the hyalactanases family in *Xenopus laevis*

Xenopus laevis was chosen as model organism rather than *Xenopus tropicalis* for the rest of the study due to the larger size of the embryos to realise targeted injections and to observe phenotypes.

The focus for the rest of this study will be on the hyalactanases family composed of *ADAMTS1*, *ADAMTS4*, *ADAMTS5*, *ADAMTS8*, *ADAMTS9*, *ADAMTS15* and *ADAMTS20*, during *Xenopus* development. Hyalactans, subfamily of proteoglycans, have been shown to be essential for development (Brunet et al., 2012) and the different members of this family, aggrecan, versican, neurocan and brevican, can be cleaved by the hyalactanases family of ADAMTSs (Stanton et al., 2011).

As RT-PCR is only a semi quantitative method, quantitative RT-PCR (qRT-PCR) was used in order to look at the hyalactanases quantitative expression profiles during *Xenopus laevis* development. RNA from key developmental stages such as blastula (stage 6), gastrula (stage 11), neurula (stage 16), organogenesis at early tailbud (stage 24), late tailbud (stage 33) and tadpole (stage 42) was extracted. cDNAs synthesised from the RNA of these samples were used for qRT-PCR (figure 4-4) for the hyalactanases gene family and for versican (*VCAN*) one of their substrates. Ct data from qRT-PCR were collected using 7500 Software v2.3 (Applied Biosystems) and analysed using Excel (Microsoft). ΔCt (gene Ct—*odc* Ct) were obtained from Ct values of each gene for normalization and then ΔCt values were converted to relative gene expression using the $2^{-\Delta\text{Ct}}$ method.

The ΔCt values were used to create a heat-map showing the level of expression of the hyalactanases family compare to each other at the different stages of development (figure 4-6A). The analysis of the heat map suggested that all *ADAMTSs* and *VCAN* were expressed higher at organogenesis stages (stages 33 and 42) than at early developmental stages (stages 6, 11 and 16) and that *ADAMTS20* was the least expressed and *VCAN* the most expressed. Only *ADAMTS8* showed a high expression at stage 6 (figure 4-6A).

The $2^{-\Delta\text{Ct}}$ method was used to determine the individuals expression profiles using Graph Pad Prism 6 software (figure 4-6B). The expression was

low at early stages and high at late organogenesis stages (stage 42) for nearly all hyalectanases family members with the exception of *ADAMTS1* that showed a peak of higher expression at stage 11 (gastrula) and *ADAMTS8* that showed a peak of expression at stage 6 (blastula) suggesting a maternal expression (figure 4-6B). *ADAMTS9* and its substrate, *VCAN*, showed the same expression profile with an expression increase at neurula (stage 16) to late organogenesis (stage 42) (figure 4-6B). The gene expression results for the hyalectanases gene family obtained by RT-PCR in *Xenopus tropicalis* (figure 4-3) showed similar higher expression at late stages of development compared to early stages as observed by qRT-PCR in *Xenopus laevis* (figure 4-6).

PCR only gives temporal expression. Wholemount *in situ* hybridisation (WISH) provides spatial as well as temporal information. *In situ* probes were generated for a number of ADAMTSs.

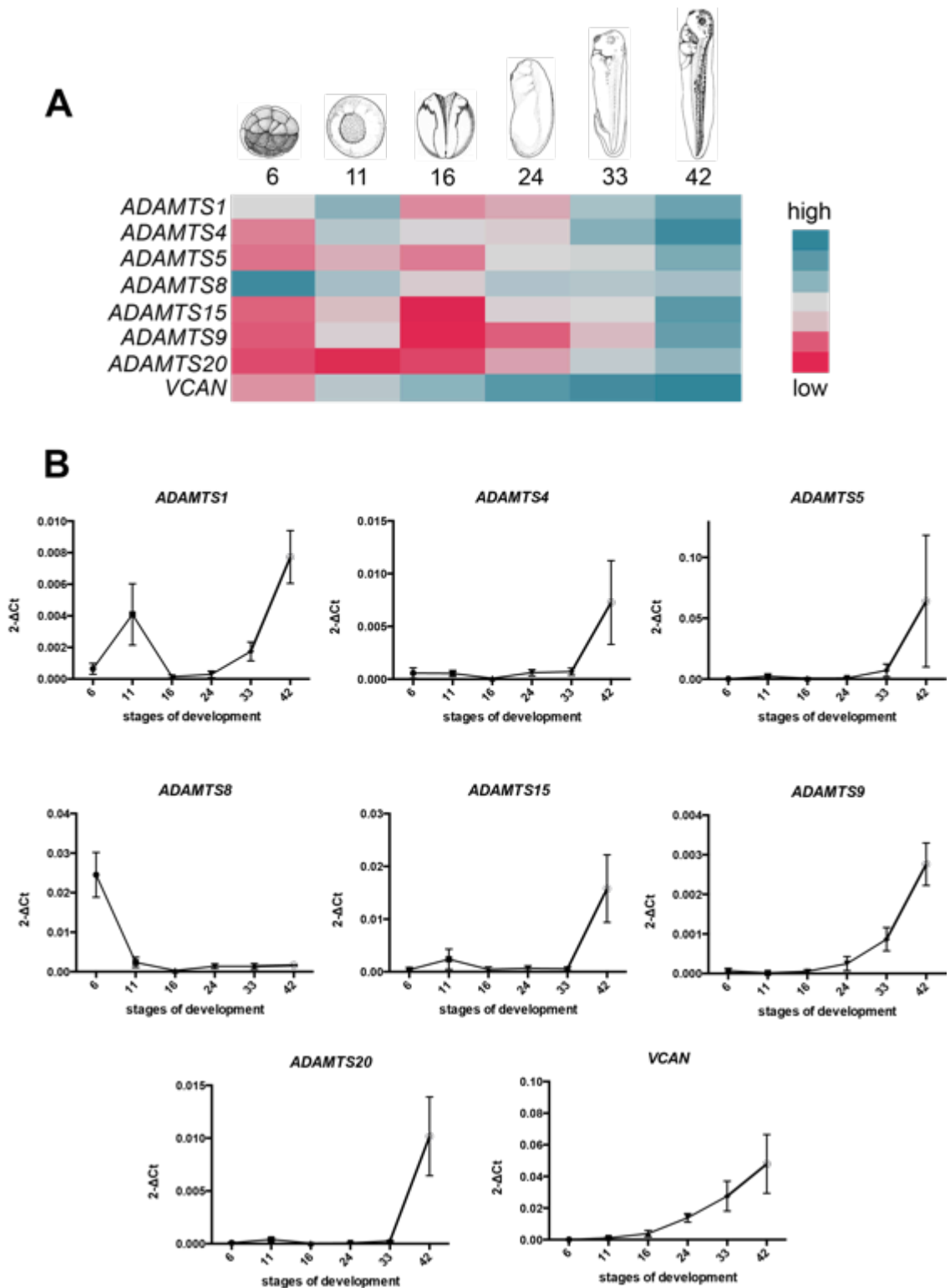


Figure 4-6: Expression profiles of the hyalactanases family and VCAN during *Xenopus laevis* development. Analysis by qRT-PCR of mRNA from stage 6 to stage 42 embryos normalized to *odc* as a loading control. The experiment was done three independent times. Expression profiles are represented as, (A) a heatmap where genes names are on the vertical axis and developmental stages on the horizontal axis according to (Nieuwkoop and Faber, 1994) (NF). (B) Each graph represents the expression profile of a single gene; the numbers on the vertical axis represents the normalized expression value and on the horizontal axis represents stages of development (mean with SEM), n=3.

4.2.2.2 Expression pattern of *ADAMTS9* in *Xenopus laevis*

WISH were carried out, with probes generated from PCR products, for the hyaluronanases family in *Xenopus laevis* but with the exception of *ADAMTS9* (figure 4-8), they did not show any specific signals. An *ADAMTS1* probe was generated from a plasmid containing an image clone sequence of *ADAMTS1* gene in *Xenopus laevis*. The expression of *ADAMTS1* obtained by WISH in *Xenopus laevis* using this probe was found in the posterior part of the embryo at neurula stage (stage 15) and in the branchial arches, the somites and the heart anlage at tailbud stage (stage 26) (figure 4-7). These results were similar to the one previously observed for *ADAMTS1* in *Xenopus laevis* (Suga et al., 2006).

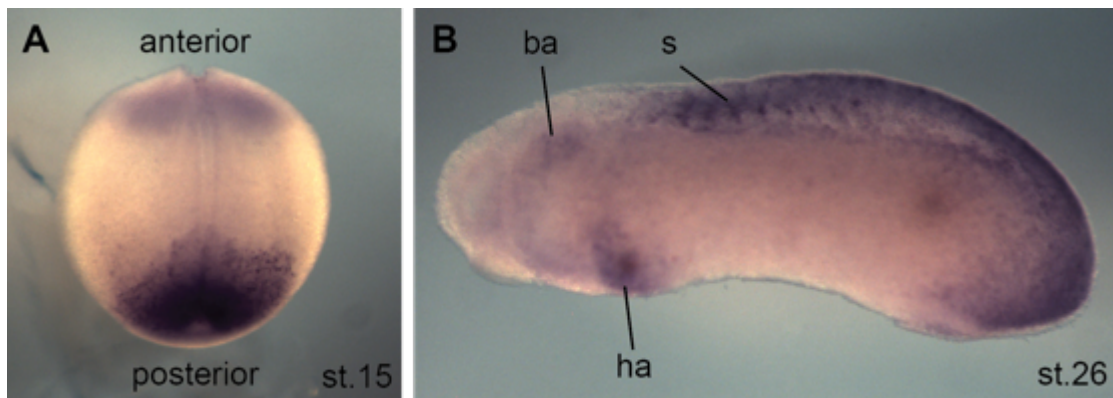


Figure 4-7: The expression pattern of *ADAMTS1* in *Xenopus laevis*. Developmental stages are according to (Nieuwkoop and Faber, 1994). (A) At stage 15 the expression is in the posterior part of the embryo. (B) Lateral view of an embryo at stage 26 with anterior on the left and posterior on the right, the expression is in the branchial arches (ba), in the somites (s) and in the heart anlage (ha).

WISH for *ADAMTS9* did not show any specific signal in early stages before tailbud stages, which confirm qRT-PCR results in *X.laevis* showing that *ADAMTS9* was not expressed before neurula and early tailbud stages (figure 4-6). At early tailbud stages (stages 22) *ADAMTS9* expression was mostly found in the developing eye, in migrating cells localised on the anterior side of the embryo and in the pronephric anlage (figure 4-8A). At tailbud stages (stages 25 and 26), the expression was observed in the eye, in the midbrain hindbrain boundary, in migrating cells localised on the anterior side of the embryo (figure 4-8B and C). At stage 35 the *ADAMTS9* expression was found in numbers of developing organs and structures such as the pronephros, the pronephric duct, the olfactory placode, the optic cup, the otic vesicle, the branchial arches, the

fin and the cloaca (figure 4-8D). At tadpole stages (stages 38) the eye structure was more defined and the *ADAMTS9* expression was specific to the lens and the retinal pigment epithelium, the expression was also found in the pancreas, in the fin and in the cloaca (figure 4-8E).

ADAMTS9 expression was found in the developing pancreas. The expression was observed in the dorsal pancreatic anlage on the dorsal surface of the endoderm at the level of the pronephros (red arrows figure 4-9A' and A'') and in the ventral pancreas formed of two symmetrical (left and right) anlagen at stage 37/38 (black arrows figure 4-9A' and A''). At stage 40 *ADAMTS9* expression was seen in the dorsal and ventral pancreatic anlagen that have fused. The fusion occurs at the junction of the right side of the dorsal pancreatic bud with the dorsal aspect of the fused ventral buds (black and red arrows figure 4-9B' and B'') (Kelly and Melton, 2000).

To look in more detail at the *ADAMTS9* expression profiles the head and the trunk of late tailbud and tadpole stages (stages 35 and 38) embryos were sectioned (figure 4-10A and B). In the head the expression was found in the optic cup, midbrain hindbrain boundary, in the otic vesicle at stage 35 (figure 4-10 1, 2, 3 and 4), in the lens and the retinal pigment epithelium at stage 38 (figure 4-10 6). In the trunk the expression was mostly found in the pronephric anlage at stage 35 and in the pronephros (figure 4-10 5 and 7) (Lienkamp et al., 2012).

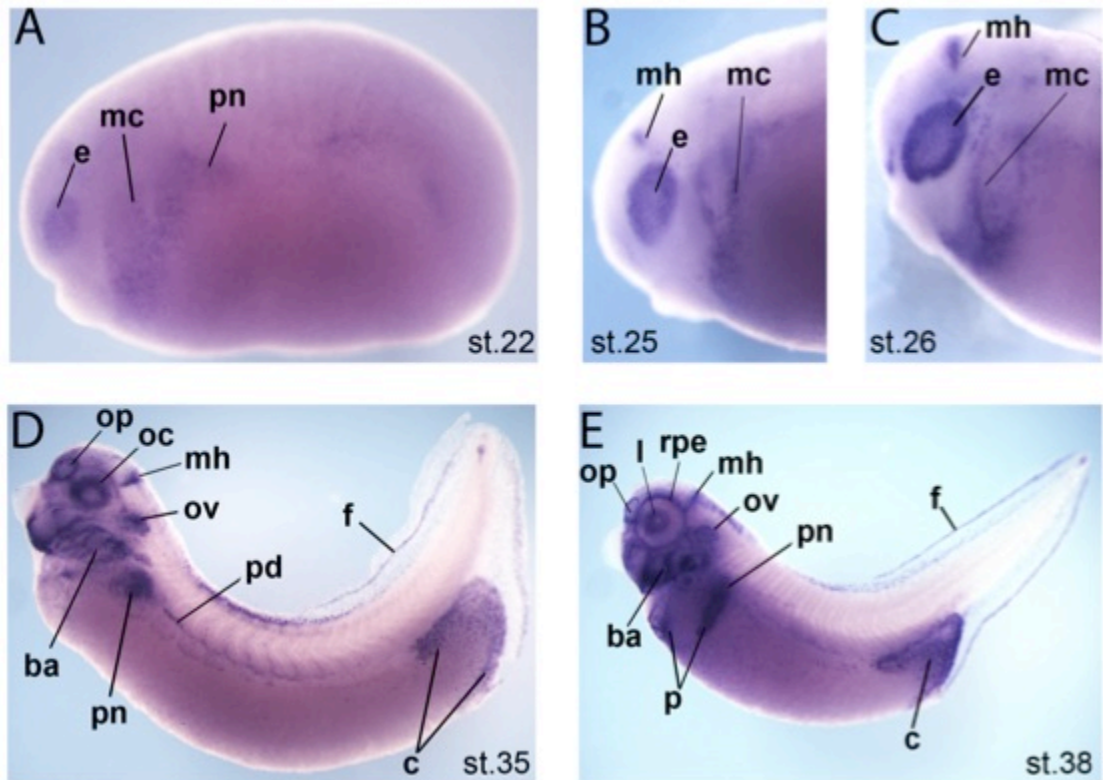


Figure 4-8: The expression pattern of *ADAMTS9* in *Xenopus laevis* embryos. Developmental stages are according to (Nieuwkoop and Faber, 1994). Lateral views of embryos with anterior on the left and posterior on the right. (A) At stage 22 the expression is in the eye (e), in migrating cells (mc) and in the pronephric anlage (pn). (B, C) At stage 25 and 26 the expression is in the eye, in migrating cells (mc) and in the midbrain hindbrain boundary (mh). (D,E) At stage 35 and 38 the expression is in the olfactory placode (op), in the optic cup (oc), in the midbrain hindbrain boundary, in the otic vesicle (ov), in the pronephros (pn), in the pronephric duct (pd), in the branchial arches (ba), in the fin (f) and cloaca (c). (E) At stage 38 the expression is also in the lens (l), in the retinal pigment epithelium (rpe) and in the pancreas (p).

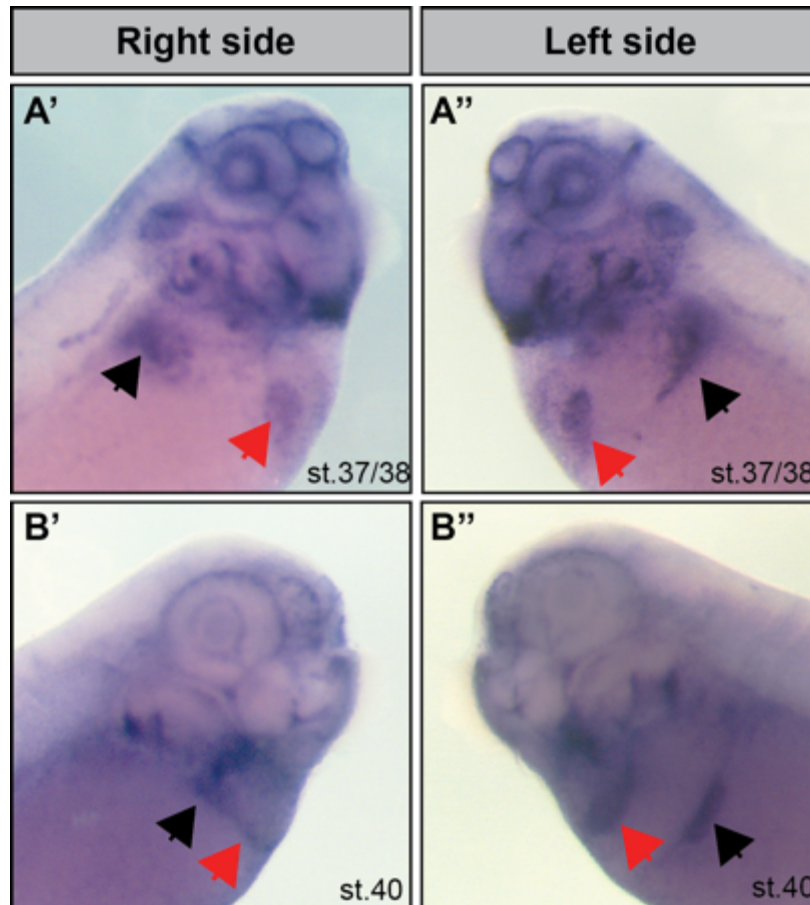


Figure 4-9: The expression pattern of ADAMTS9 in the pancreas of *Xenopus laevis* tadpoles. Lateral view of right and left sides of (A' and A'') stage 37/38 and (B' and B'') stage 40 embryos, developmental stages are according to (Nieuwkoop and Faber, 1994). Red and black arrows indicate ventral and dorsal pancreas respectively (A', A'', B' and B'').

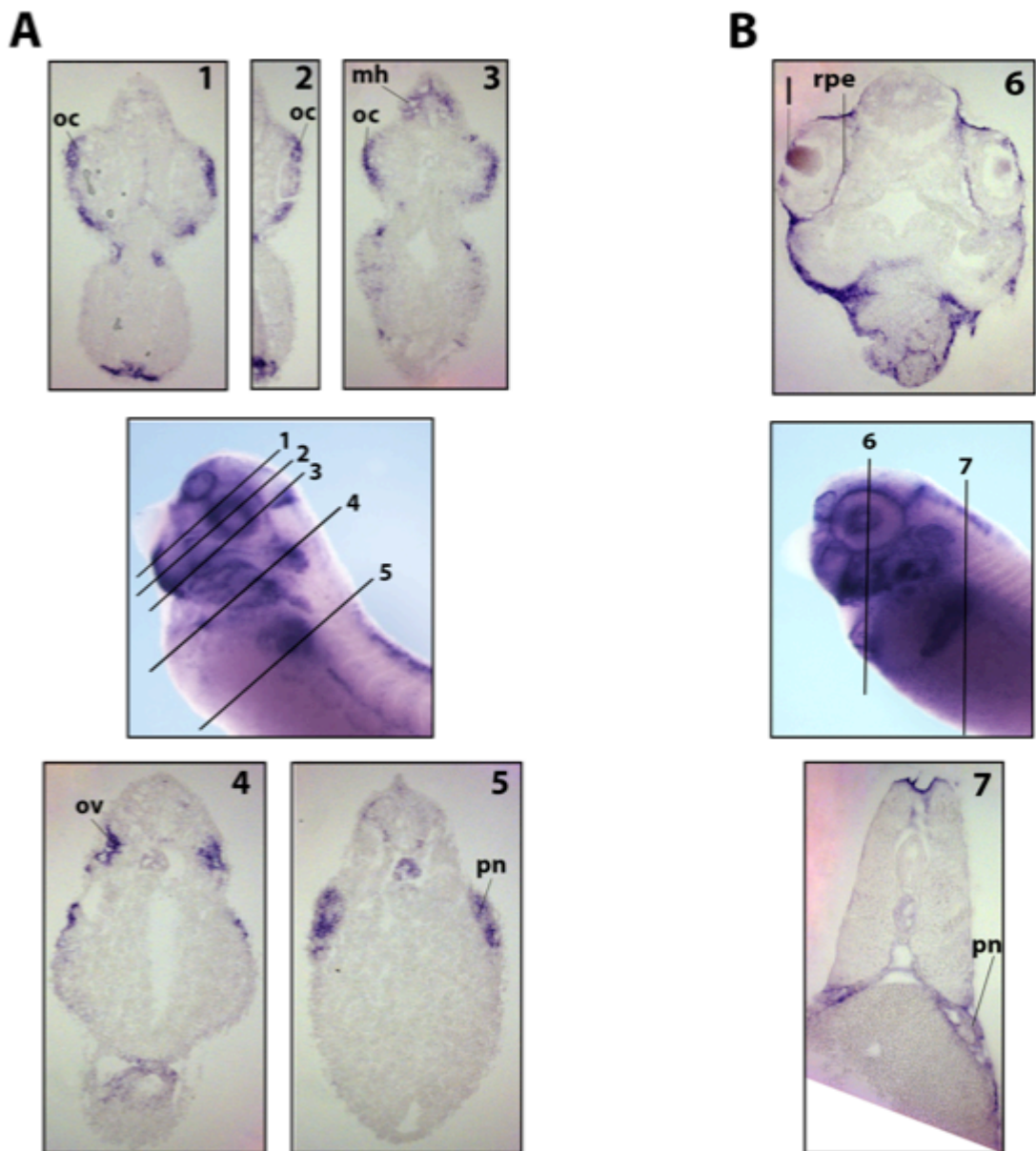


Figure 4-10: Sectioned *Xenopus laevis* embryos after WISH for ADAMTS9. Developmental stages are according to (Nieuwkoop and Faber, 1994). In each panel lines and numbers indicate the level of the sections. Embryos are shown with anterior on the right and sections with dorsal at the top. (A) At stage 35, (1, 2, 3) in the head the expression is in the optic cup (oc), in the midbrain hindbrain boundary (mh) and (4) in the otic vesicle (ov); in the trunk (5) the expression is in the pronephros (pn). (B) At stage 38, (6) in the head the expression is in the lens (l) and in the retinal pigment epithelium (rpe); in the trunk (7) the expression is in the pronephros (pn).

4.2.2.3 ADAMTS9 knockdown in *Xenopus laevis*

The *Xenopus laevis* genome is allotetraploid and is composed of two subgenomes, L and S (see chapter III). The expression profile of the two *ADAMTS9* copies, *ADAMTS9L* and *ADAMTS9S*, was assessed by RT-PCR during *Xenopus laevis* development from unfertilised egg to tadpole (stage 45) (figure 4-11). *ADAMTS9L* expression was not detectable in the unfertilised egg or at stage 6, suggesting no maternal expression. *ADAMTS9L* expression was detectable from neurula (stage 16) whereas *ADAMTS9S* expression was found from stage 6 although the expression appeared low. Both *ADAMTS9L* and *ADAMTS9S* were found at the tailbud and tadpole stages corresponding to neural crest cells migration and organogenesis (figure 4-11).

To study the function of *ADAMTS9* in *Xenopus laevis* development, two morpholinos were designed to block the translation of *ADAMTS9L* and *ADAMTS9S* proteins. Morpholinos were injected into both cells of a two-cell stage embryo at varying concentrations (40 and 60ng) to determine a concentration, which would give a consistent phenotype. At the same time a control morpholino was injected in the same way at the highest concentration of *ADAMTS9* morpholinos (60ng) (figure 4-12).

This experiment showed that the injection of 40ng and 60ng of *ADAMTS9L* or *ADAMTS9S* morpholinos did not appear to have an effect on *Xenopus laevis* development. In comparison with the injected embryos with the control morpholino (group picture figure 4-12E), injected embryos with 40ng and 60ng of *ADAMTS9L* morpholino appeared wild type (two group images figure 4-12A and B) as well as injected embryos with 40ng and 60ng of *ADAMTS9S* morpholino (two group images figure 4-12C and D).

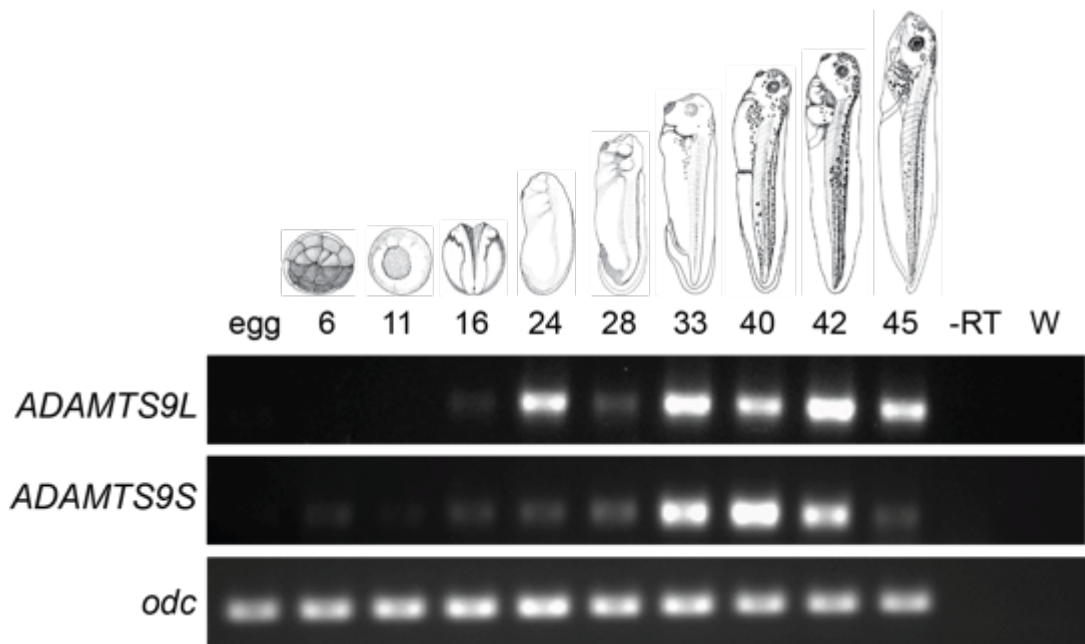


Figure 4-11: Expression of *ADAMTS9L* and *ADAMTS9S* during *Xenopus laevis* development. Analysis by RT-PCR of mRNA from egg to stage 45. *Xenopus laevis* stages are indicated at the top according to (Nieuwkoop and Faber, 1994) (NF) and gene names are indicated on the left. *odc* is a loading control. -RT is a negative control of cDNA synthesis reaction made without adding the Reverse Transcriptase enzyme and W: water (H₂O), is a negative control of the PCR reaction without cDNA template.

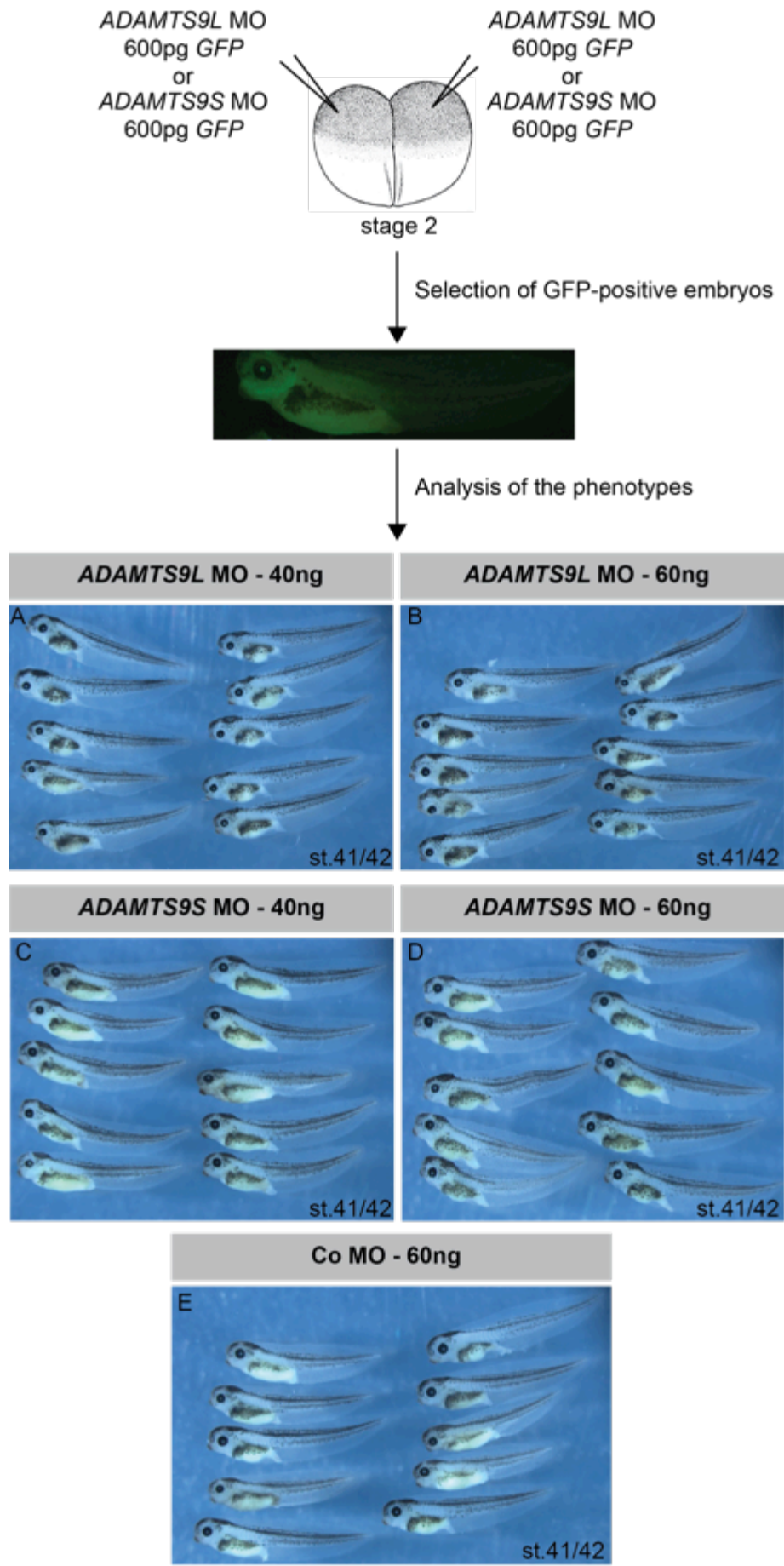


Figure 4-12: The phenotype obtained after *ADAMTS9* knockdown in *Xenopus laevis*. At the top is represented a 2 cell stage embryo injected with *ADAMTS9L* or *ADAMTS9S* morpholino and *GFP* mRNA (600pg). In the middle is shown the GFP signal in injected embryos. At the bottom are the group pictures of stage 41/42 injected embryos with (A) 40ng of *ADAMTS9L* morpholino (n=46), (B) 60ng of *ADAMTS9L* morpholino (n=44), (C) 40ng of *ADAMTS9S* morpholino (n=53), (D) 60ng of *ADAMTS9S* morpholino (46) and (E) 60ng of control morpholino (n=43). Co: control and MO: morpholino. Developmental stages are according to **(Nieuwkoop and Faber, 1994)**.

ADAMTS9 knockdown in *Xenopus tropicalis* and *Xenopus laevis* embryos experiments did not show phenotypes. The qRT-PCR in *Xenopus laevis* showed that *ADAMTS9* and *VCAN* were expressed at the same developmental stages from neurula (stage 16) to organogenesis (stage 42) and it has been shown that *VCAN* was expressed in the same embryonic locations than *ADAMTS9* such as in the branchial arches, structures where NC migrate, and in the pronephros (figure 4-13) (Casini et al., 2008). The co expression of *VCAN* and *ADAMTS9* in these structures suggests a role of ADAMTS9 in the remodeling of the ECM during development by cleavage of versican. In order to assess this hypothesis targeted injections into specific blastomere giving rise to neural crest and pronephros were carried out.

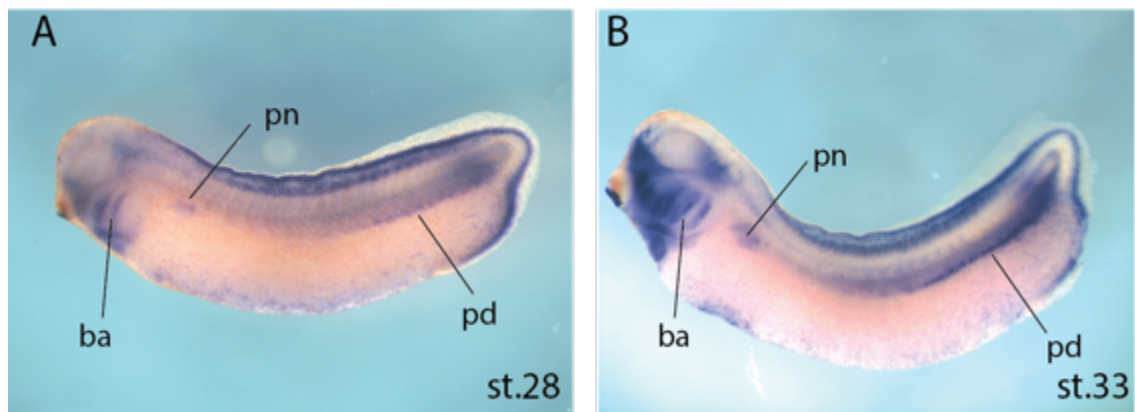


Figure 4-13: The expression pattern of *VCAN* in *Xenopus laevis* embryos. Lateral view of embryos with anterior on the left and posterior on the right. Developmental stages are according to (Nieuwkoop and Faber, 1994). (A) (B) At stage 28 and 33 the expression is in the branchial arches (ba), in the pronephros (pn) and in the pronephric duct (pd).

4.2.2.4 ADAMTS9 knockdown in neural crest of *Xenopus laevis*

To specifically knockdown *ADAMTS9* in the neural crest the injections were targeted into one dorsal blastomere at the 4-cell stage. *GFP* mRNA was co-injected in order to trace the injection, to ensure that it was injected at the right location and to identify which side of the embryos had been injected. Just one side (one blastomere out of two dorsal blastomere) of the embryo was injected and the other side was used as a control to evaluate a phenotype due to the *ADAMTS9* knockdown. *Xenopus laevis* embryos injected at two-cell stage with 60ng of morpholinos did not present toxicity phenotype due to the amount of morpholinos (figure 4-12B, D and E). Targeted co-injection of *ADAMTS9L* and *ADAMTS9S* morpholinos into one blastomere at 4-cell stage *Xenopus laevis* embryos will be carried out at 40ng of each morpholino due to the smaller size of a blastomere at 4-cell stage compared to a two-cell stage. *ADAMTS9L* and *ADAMTS9S*, as well as 600pg of *GFP* mRNA were injected (figure 4-14). After selection of the embryos injected at the right location, the analysis of the effect of the *ADAMTS9* knockdown on neural crest development was carried out using *sox10* as a marker for NC migration at tailbud stages (figure 4-14A). *Sox10* is a transcription factor essential for neural crest cells development (Honoré et al., 2003). The experiment demonstrated that the embryos displayed a wild type phenotype similar to the non-injected side with no perturbation of the NC migration in the anterior part of the embryo (cephalic, enteric and heart NC) or in the trunk of the embryo (trunk neural NC) (figure 4-14A). NC give rise to melanocytes and craniofacial cartilage (Theveneau and Mayor, 2013). Injection of the *ADAMTS9* morpholinos appeared to have no effect on these structures as observed at tadpole stages (stage 41) (figure 4-14B).

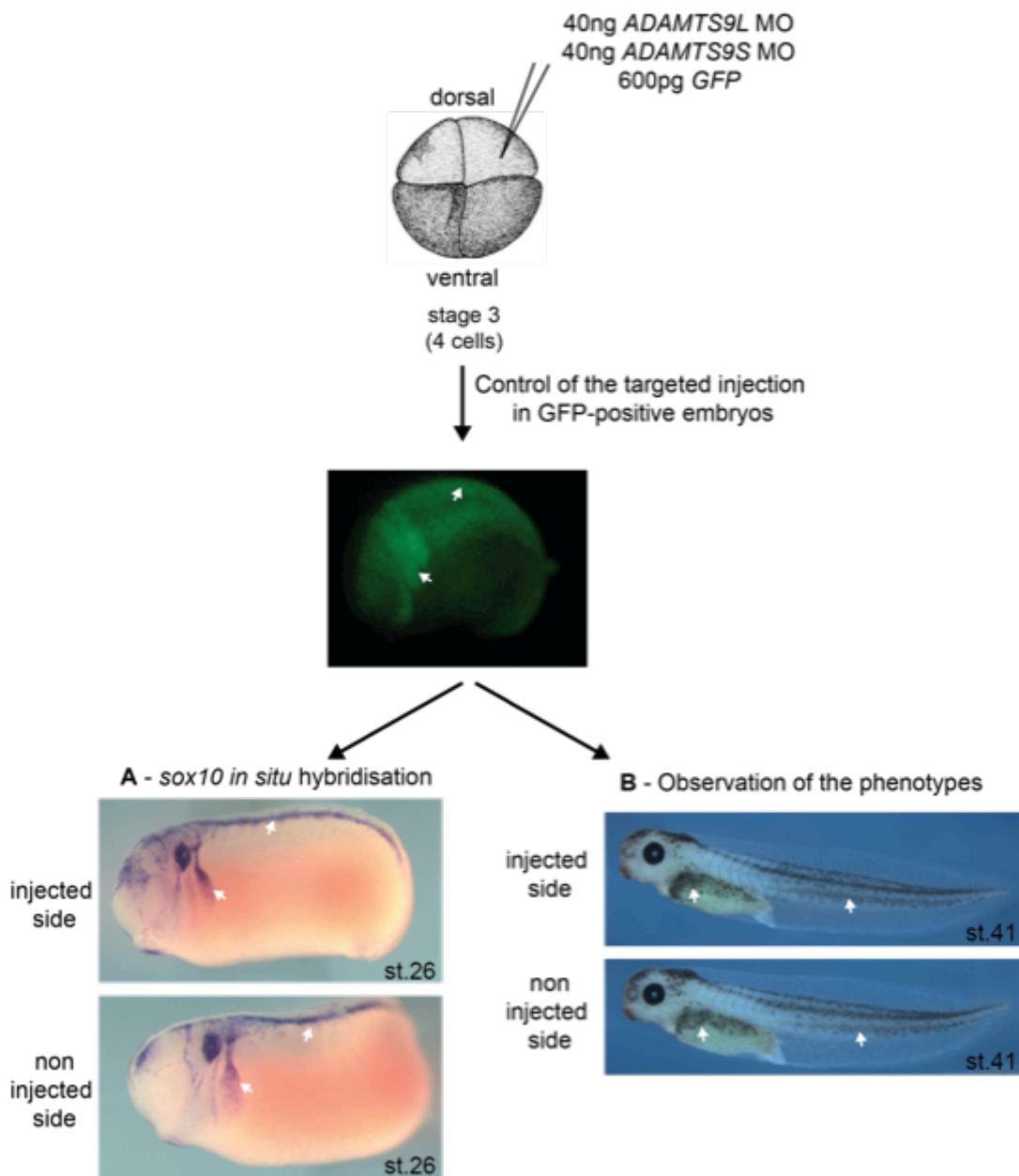


Figure 4-14: Knockdown of ADAMTS9 in neural crest of *Xenopus laevis*. On the left is represented the schematic of an embryo stage 3 and the injection of *ADAMTS9L* and *ADAMTS9S* morpholinos (40ng) and *GFP* mRNA (600pg) into one dorsal blastomere to target NC. In the middle is shown the GFP signal of an injected embryo localised in the migrating NC (white arrows), the correct localisation. At the bottom (A) is a *sox10* in situ realised on injected embryo at stage 26 to look at the phenotype of migrating NC (white arrows) on the injected side compare to the non-injected side (n=15) and (B) is stage 41 injected embryos to look at the pigment cell phenotype (white arrows) (n=10). Developmental stages are according to (Nieuwkoop and Faber, 1994).

4.2.2.5 ADAMTS9 knockdown in the pronephros of *Xenopus laevis*

4.2.2.5.1 Protocol of injection and analysis

ADAMTS9L and *ADAMTS9S* morpholinos with *GFP* mRNA were injected into the ventral V2 blastomere of an 8-cell stage embryo to target the pronephros (figure 4-15). The injection at the correct location, in the pronephros, was assessed using *GFP* signal and embryos with the right localisation of the signal were selected to carry out phenotypic analysis using several markers of pronephros development (figure 4-15).

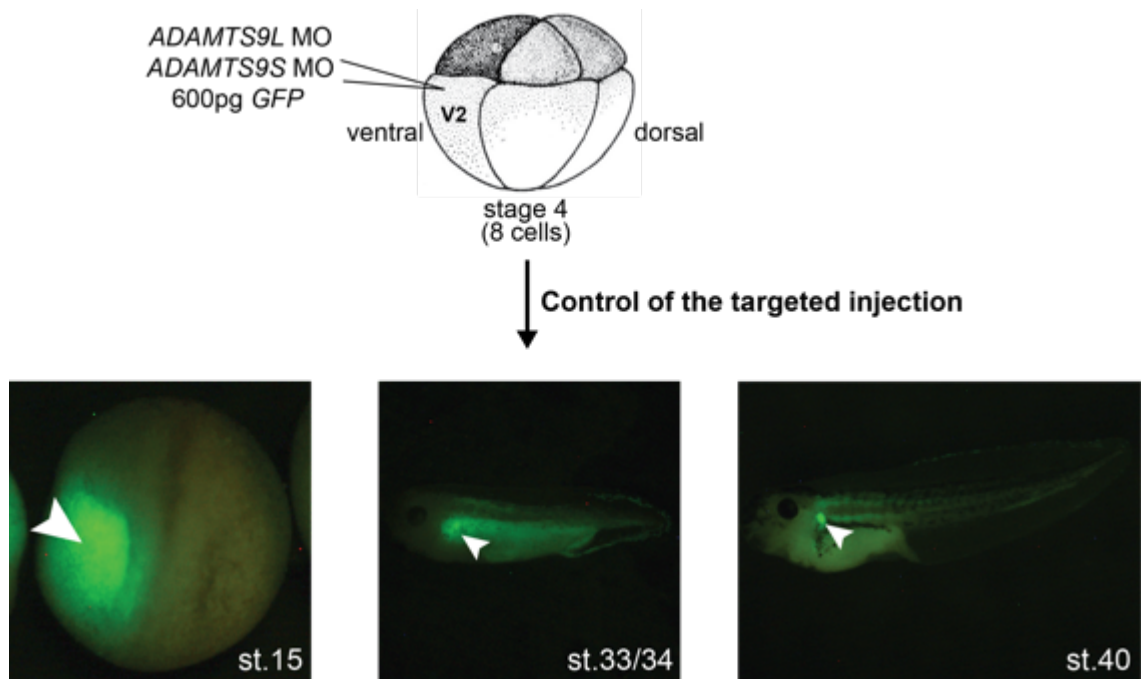


Figure 4-15: Loss of function experiment for *ADAMTS9* during pronephros development in *Xenopus laevis*. At the top is represented an 8 cells embryo injected in the V2 blastomere with *ADAMTS9L* and *ADAMTS9S* morpholinos and *GFP* mRNA (600pg). At the bottom is shown the *GFP* signal in injected embryos at different stages of development located at the right localisation corresponding to the pronephros (white arrow). The developmental stage representations are from (Nieuwkoop and Faber, 1994).

4.2.2.5.2 Early markers, *wt1* and *pax8*

ADAMTS9 has previously been shown to be expressed in the pronephros from early tailbud stages (figure 4-7) suggesting a role of *ADAMTS9* in the pronephros development of *Xenopus laevis*. To investigate this hypothesis, after selection of injected *Xenopus laevis* embryos with 40ng of both *ADAMTS9S* and *ADAMTS9L* morpholinos (and 600pg of *GFP* mRNA) on one side in the pronephros wholemount *in situ* hybridisation were carried out for the zinc finger transcription factor *Wilms' tumor suppressor (wt1)*, a marker for the pronephric anlage and the glomus (Lienkamp et al., 2012), in order to look at the effect of the loss of function of *ADAMTS9* on the glomus development (figure 4-16). No major effects due to *ADAMTS9* knockdown were observed on the glomus development on the injected side of the embryo (figure 4-16 left) compare to the non injected control side (figure 4-16 right).

Next the effect of the loss of function of *ADAMTS9* on the pronephric tubules and duct development were investigated using the transcription factor *paired box gene 8 (pax8)*, a marker for the pronephric anlage, the pronephric tubules and pronephric duct (Heller and Brandli, 1999). *WISH* was carried out on injected embryos on one side in the blastomere giving rise to the pronephros (figure 4-17). A delay was observed in the development of the tubules (figure 4-17, black arrows) and the duct (figure 4-17, white arrows) on the injected side with 40ng of both *ADAMTS9S* and *ADAMTS9L* morpholinos (and 600pg of *GFP* mRNA) when compared to the non injected side from stage 22 to stage 27 embryos (figure 4-17). The duct structure was not formed at early tailbud stage (stage 22) on the injected side (white arrow, figure 4-17A and B). At stage 25 the tubules and the duct structures were less defined on the injected side (white and black arrows, figure 4-17C and D). The same phenotype was seen at stage 27 where the tubules and duct structures were more similar to that at stage 25 on the non injected side when compared to a non injected side of the stage 27 embryo (white and black arrows, figure 4-17C and F).

The phenotypes observed after knock-down of *ADAMTS9* using morpholinos were delay of pronephric tubules and duct development at tailbud stages, showed by *pax8* *in situ* hybridisation, but no phenotypes in the glomus, showed by *wt1* *in situ* hybridisation.

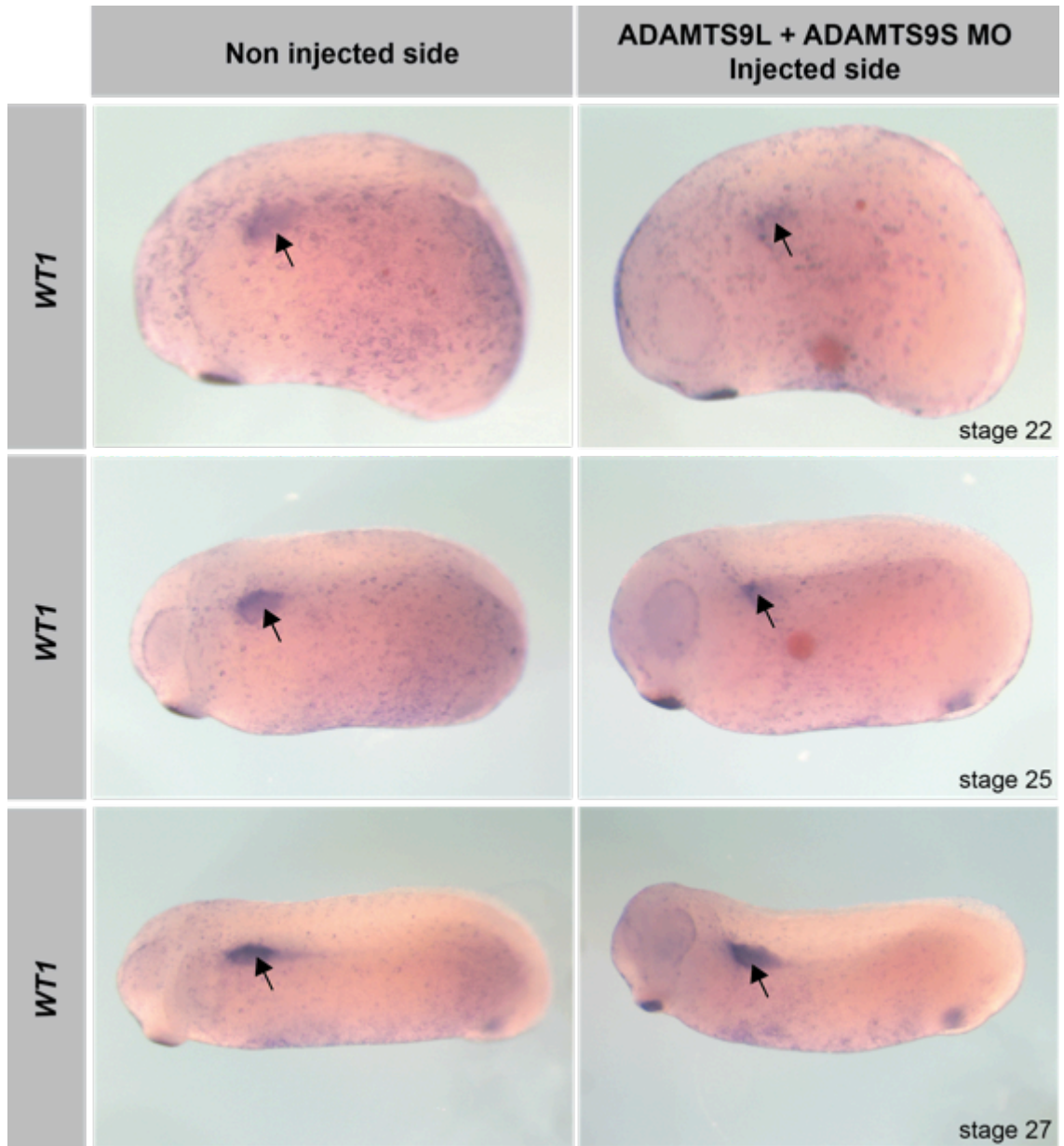


Figure 4-16: Wholemount *in situ* hybridisation for *wt1* in *Xenopus laevis* injected embryos with both *ADAMTS9L* and *ADAMTS9S* morpholinos. On the left side are non injected embryos and on the right side are injected embryos. Developmental stages, according to (Nieuwkoop and Faber, 1994), are indicated at the bottom right of the right picture. The black arrow indicates the specific signal in the glomus (n=5 for stage 22, n=3 for stage 25 and n=12 for stage 27).

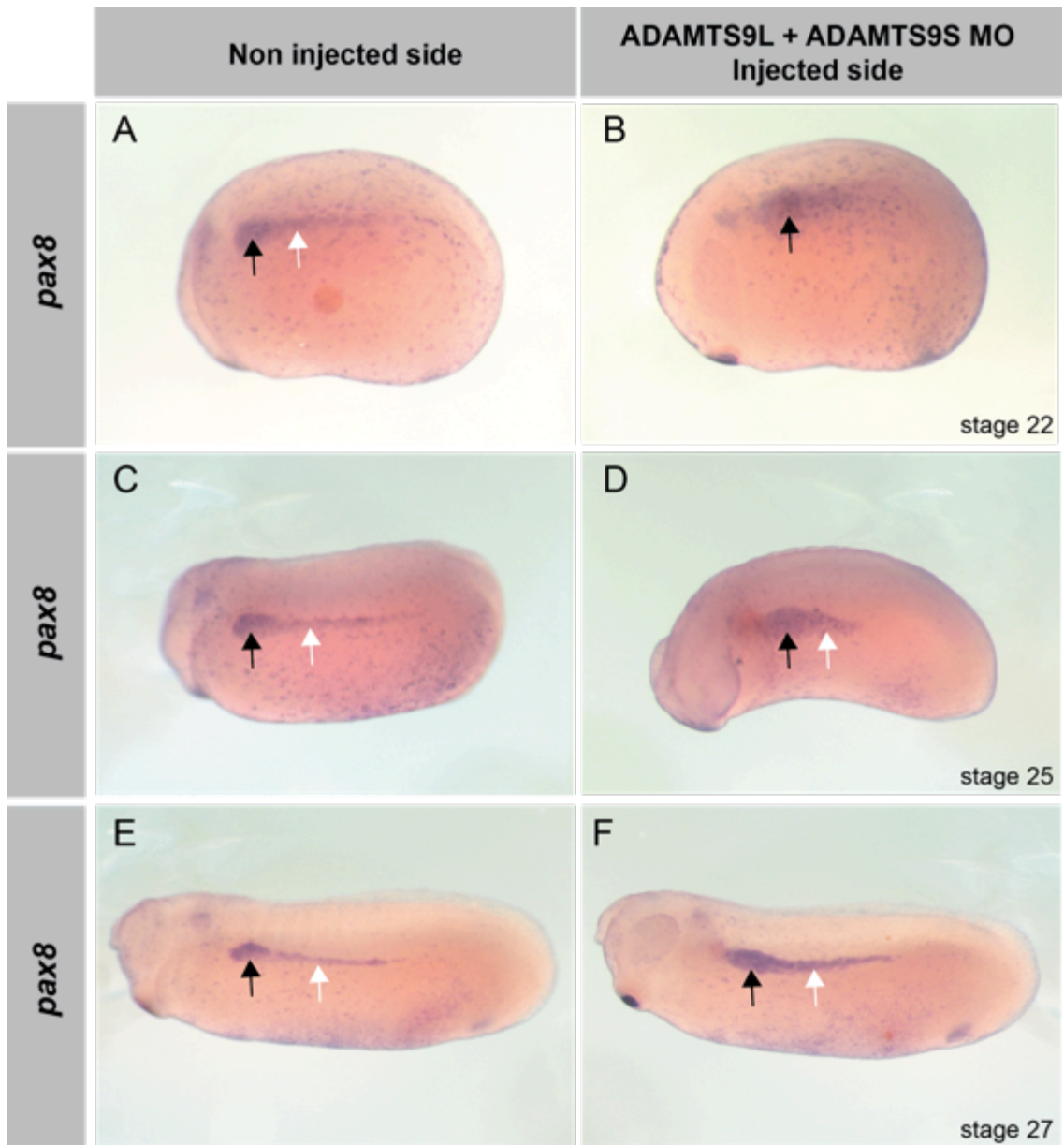


Figure 4-17: Wholemount *in situ* hybridisation for *pax8* in *Xenopus laevis* injected embryos with both *ADAMTS9L* and *ADAMTS9S* morpholinos. On the left side are non injected embryos (A,C and E) and on the right side are injected embryos (B, D and F). Developmental stages, according to (Nieuwkoop and Faber, 1994), are indicated at the bottom right on the right pictures, (A, B) stage 22 (n=6), (C, D) stage 25 (n=4) and (E, F) stage 27 (n=11). The black arrow indicates the specific signal in the tubules and the white arrow indicates the specific signal in the duct.

4.2.2.5.3 Late tailbud markers, *atp1b1*, *Xlim1* and *pax2*

To describe in more details the delay of development observed in the pronephric tubules and duct at late tailbud stages when *ADAMTS9* was knocked-down, terminal differentiation markers of these structures such as the transcription factors *paired box gene 2* (*pax2*) and LIM homeodomain transcription factor Lhx1 (known as *Xlim1* in *Xenopus laevis*) known to be necessary for kidney development were used to visualise the nephrostomes and the tubules and duct and the ion transporter *atp1b1* (ATPase_{Nap/Kp} transporting beta1) was used to visualise tubules and duct (Agrawal et al., 2009) (Buisson et al., 2015). Injected embryos with 40ng of both *ADAMTS9S* and *ADAMTS9L* morpholinos (and 600pg of *GFP* mRNA) on one side in the pronephros were selected to carry out *WISH*.

On the injected sides of the embryos compare to the non injected sides a lack of proximal and intermediate tubules organisation was observed for all three markers indicating a delay of development (pink arrows figure 4-18 A). The expression of *atp1b1* and *Xlim1* in the distal tubules and duct were wilder and less defined on the injected sides that on the non injected side showing a delay in morphogenesis of these structures (black arrows figure 4-18 A). The expression profile of *pax2* on the injected side revealed a pronephros structure more similar to the one observed at stage 27, using *pax8* as a marker (figure 4-17 E), rather than the structure observed on the non injected side of the same embryo (figure 4-18 A). A lack of signal was observed in the nephrostomes on the injected sides compared to the non injected side, using *Xlim1* and *pax2* as markers (grey arrows figure 4-18 A), showing a delay of development of the pronephros. The delay of pronephros development on the injected sides of the embryos was quantified for each markers (figure 4-18 B) and was observed for more than 80% of the embryos for *pax2* and *Xlim1* and for more than 50% for *atp1b1*. Partial and complete loss of *atp1b1* signal was observed for 15% of the embryos indicating a delay more important of development of these injected embryos.

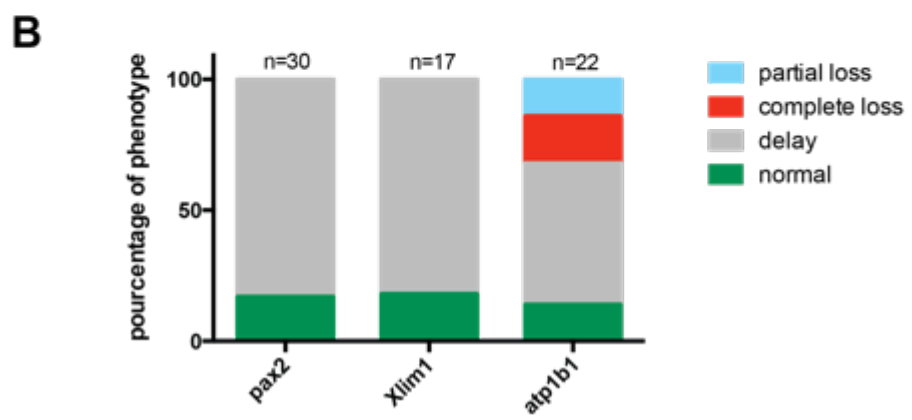
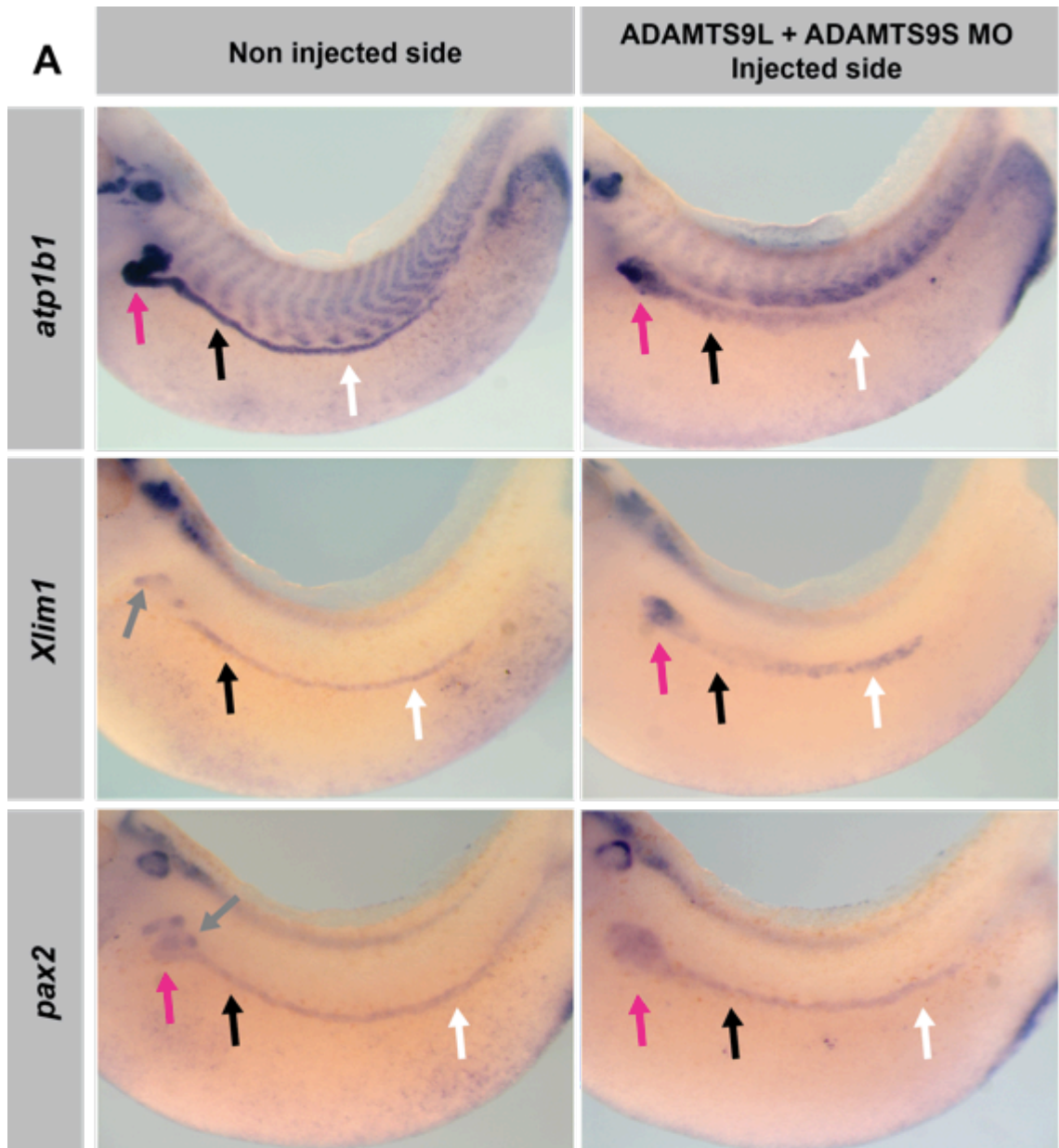


Figure 4-18: Wholemout in situ for *atp1b1*, *Xlim1* and *pax2* in *Xenopus laevis* injected embryos with both ADAMTS9L and ADAMTS9S morpholinos. (A) On the left side are non injected embryos and on the right side are injected embryos. All embryos are at stage 33/34 according to (Nieuwkoop and Faber, 1994). The pink arrows indicate the specific signal in the proximal and intermediate tubules, the black arrows indicate the distal tubule, the white arrows the duct and the grey arrows the signal in the nephrostomes. (B) Percentage of the observed phenotypes on the injected sides of the embryos with *atp1b1*, *Xlim1* and *pax2* staining which are normal (green), delay of development (grey), complete (red) and partial (blue) loss of signal.

4.2.2.5.4 Late markers, 4a6

In order to investigate if the delay of development of the pronephric tubules and duct, observed at tailbud stages persists at tadpole stages, the 4a6 antibody was used to visualise the distal tubules and the pronephric duct in *Xenopus laevis* tadpoles (Vize et al., 1995).

Xenopus laevis embryos were injected into the V2 blastomere on one side with 40ng of *ADAMTS9S* morpholino, 40ng of *ADAMTS9L* morpholino, 40ng of both *ADAMTS9S* and *ADAMTS9L* morpholinos and 40ng and 80ng of control morpholino as a negative control to assess the specificity of the observed phenotypes to *ADAMTS9* morpholinos. All were co injected with 600pg of *GFP* mRNA. Wholemount immuno staining with 4a6 antibody was carried out on injected tadpoles (stage 40) to visualise the distal tubules and the pronephric duct. Observed phenotypes were classified into two categories, partial loss and complete loss, based on their degree of loss of 4a6 signal (figure 4-19A). The percentage of distribution of these different phenotypes in injected embryos was quantified, with normal phenotype defined on being when the injected side looked identical to the non-injected side (figure 4-18B). Partial and complete loss of 4a6 signal in injected embryos with *ADAMTS9L* morpholino and *ADAMTS9S* morpholino with more complete loss with *ADAMTS9S* morpholino was observed (figure 4-19B first two columns on the graph). A very low percentage of normal phenotype (no loss of the 4a6 signal) was observed in tadpoles injected with both *ADAMTS9L* and *ADAMTS9S* morpholinos, most of the observed phenotypes were partial and complete loss of the 4a6 signal (figure 4-19B third column on the graph). When embryos were injected with the control morpholino at 40ng or 80ng no effect was observed (figure 4-19B last two columns on the graph).

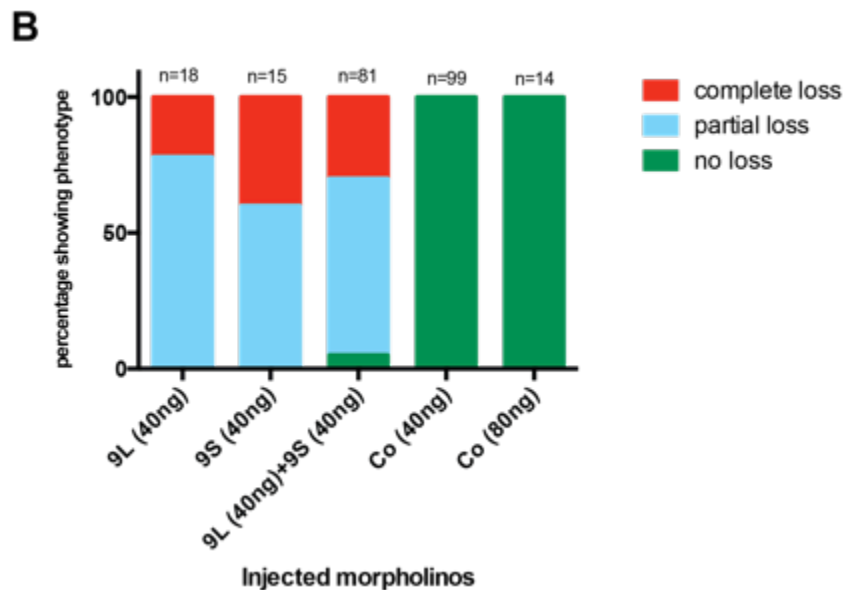
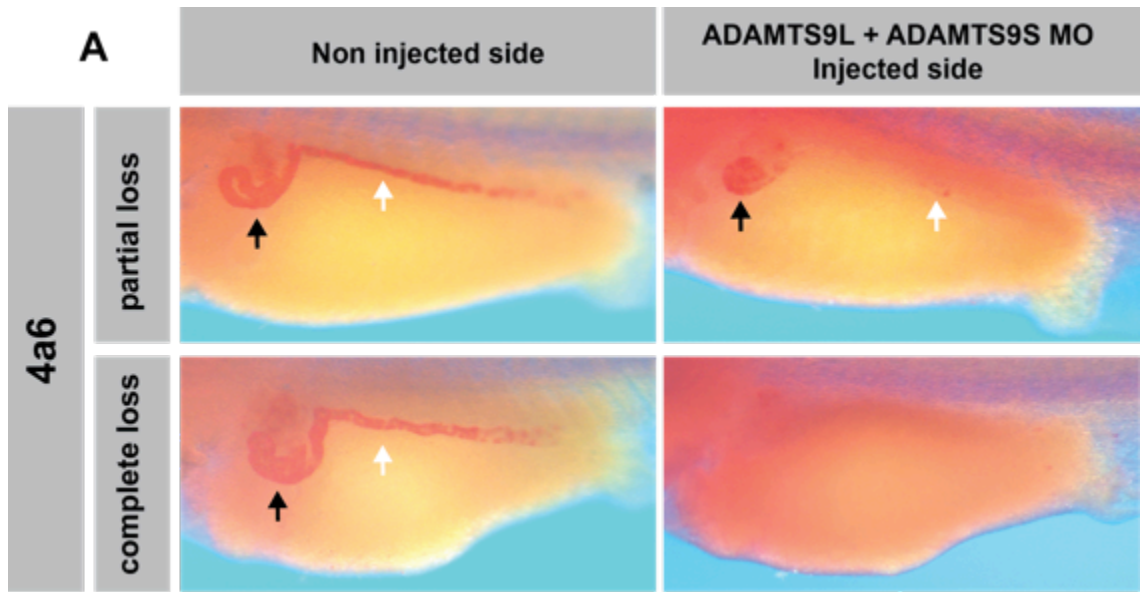


Figure 4-19: Wholemount immuno staining with 4a6 antibody on injected *Xenopus laevis* embryos with ADAMTS9S, ADAMTS9L and control morpholinos. (A) Phenotypes observed in stage 40 embryos with 4a6 staining, partial loss of the signal (top pictures) or complete loss of the signal (bottom pictures) on the injected side (right pictures) compare to the injected side (left pictures). The signal in the tubules is indicated by the black arrows and the signal in the duct is indicated by the white arrows. (B) Percentage of the observed phenotypes with 4a6 staining, which are complete (red), partial (blue) loss and no loss (green) of 4a6 signal on the injected side compared to the non injected side. The number of injected embryos is indicated on the top of the columns. On the horizontal axis is indicated the morpholino and the quantity injected (ng) into the V2 blastomere. 9L for ADAMTS9L, 9S for ADAMTS9S and Co for control morpholinos.

4.2.2.6 Morpholinos efficiency

In order to show the specificity of the translational blocking morpholinos on their *ADAMTS9* target genes (*ADAMTS9L* and *ADAMTS9S*) the level of *ADAMTS9* translated protein in injected embryos has to be assessed. There were no specific *ADAMTS9* antibodies against the *Xenopus* protein and the *ADAMTS9* genes are large (around 6kb) so only the 5'-UTR containing the binding site of the morpholinos, the signal peptide and the pro-domain followed by a C-terminal Human influenza hemagglutinin (HA) tag was cloned allowing the detection by an anti-HA antibody to assess the translation inhibition of *ADAMTS9* by the morpholinos. The function of *ADAMTS9* was not investigated in this experiment so a truncated protein could be used. Embryos were injected with 1ng and 5ng of mRNA of the different constructs, *ADAMTS9S-HA* and *ADAMTS9I-HA*, obtained by in vitro transcription and with *GFP* mRNA (600pg) in order to select injected embryos only. Ten injected embryos were selected at stage 9 for protein extraction in order to assess the amount of translated protein by western blot. 20 μ g of protein was loaded, to check if the truncated proteins were translated and not degraded during the maturation process. A α -actin antibody was used as a loading control. Non-injected embryos were used as a negative control and cmyc-HA protein as a positive control for the HA antibody (figure 4-20E and F). A dose response of *ADAMTS9S-HA* protein related to the amount of mRNA injected was observed (figure 4-20A and B). No signal was detected for the *ADAMTS9I-HA* protein (figure 4-20C and D).

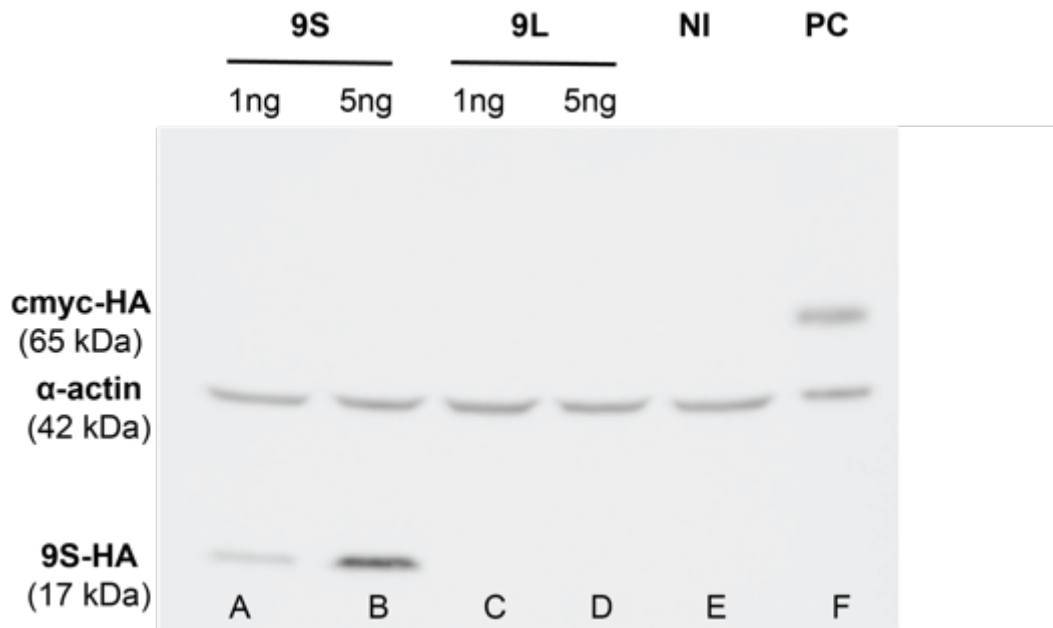


Figure 4-20: Western blot for ADAMTS9S-HA and ADAMTS9L-HA. Lanes A and B show ADAMTS9S-HA protein signal from ten injected embryos with 1ng and 5ng of *ADAMTS9S-HA* mRNA, lanes C and D show ADAMTS9L-HA protein signal from ten injected embryos with 1ng and 5ng of *ADAMTS9L-HA* mRNA, lane E shows the negative control from ten non injected (NI) embryos and lane F shows the positive control (PC) cmyc-HA rotein signal from ten injected embryos with *cmyc-HA* mRNA. 20µg of protein was loaded on the gel.

4.3 Discussion

4.3.1 ADAMTSs expression in *Xenopus*

In this chapter the expression profile of the *ADAMTS* family in *Xenopus* embryonic development was assessed. A phylogenetic study previously showed that the *ADAMTS* family is conserved between *Xenopus*, human and mouse suggesting possible conservation of their functions (chapter III). They were all expressed in *Xenopus tropicalis*, visualised by RT-PCR, and had dynamic profiles showing variation in time and intensity of expression from egg to tadpole stages (stage 45) (figure 4-3). The hyalactanases family of *ADAMTS*s were the focus for the rest of the study as their substrate, the hyalactan/lectican family of chondroitin sulfate proteoglycans, are known to be widely expressed in the extracellular matrices during development (Brunet et al., 2012). To have a more precise view of the expression profiles of *ADAMTS1*, *ADAMTS4*, *ADAMTS5*, *ADAMTS8*, *ADAMTS9*, *ADAMTS15*, *ADAMTS20* and *VCAN* during *Xenopus laevis* development qRT-PCR were carried out from blastula (stage 6) to tadpole (stage 42) stages (figure 4-6). High-resolution RNA-seq time course, showing transcripts per embryo, during *Xenopus tropicalis* embryonic development was published in open access in 2016 (Owens et al., 2016) allowing the comparison of published profiles of the hyalactanases family with the data obtained by qRT-PCR (figure 4-21). The expression profiles were conserved for all of them (*ADAMTS4*, *ADAMTS5*, *ADAMTS15*, *ADAMTS9* and *ADAMTS20*) except for *ADAMTS8* that showed a high expression at stage 6 (maternal expression) in *Xenopus laevis* but not in *Xenopus tropicalis* and *ADAMTS1* that showed a peak of expression during gastrulation (stage 11) (figure 4-21). It has been shown that *ADAMTS1* plays a role in *Xenopus laevis* development at blastula to gastrula stage as a negative regulator of FGF by its C-terminal region, independent to its protease activity (Suga et al., 2006).

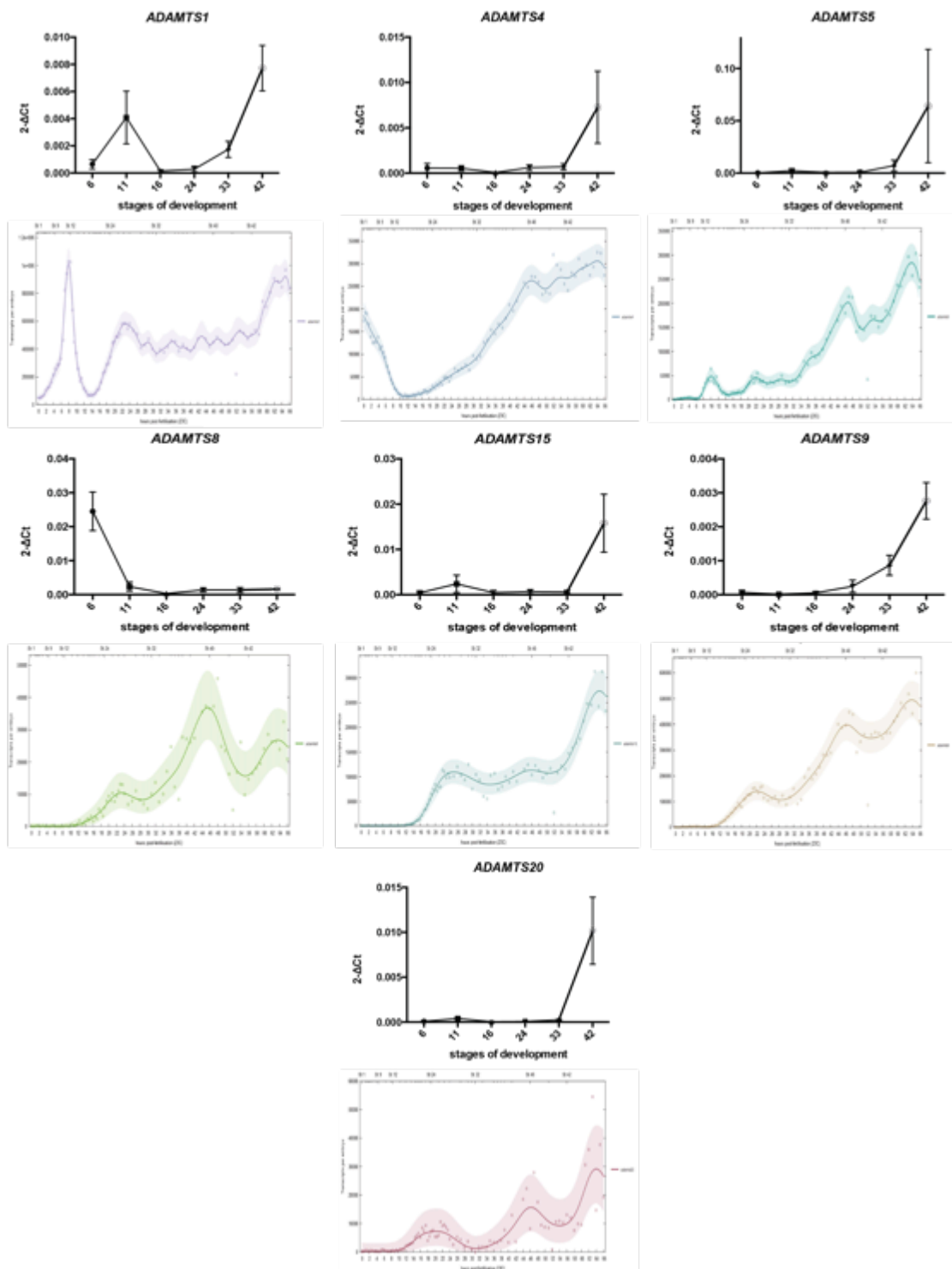


Figure 4-21: Hyaluronanases family expression profile by RT-qPCR in *Xenopus laevis* and by RNA-seq in *Xenopus tropicalis*. RT-qPCR graphs show the expression using the $2^{-\Delta C_t}$ method (black and white graphs) and RNA-seq graphs show the expression by the quantification of the number of transcripts per embryo (colour graphs) from (Owens et al., 2016).

Wholemout *in situ* hybridisation (WISH) for all ADAMTSs in *Xenopus tropicalis* embryos and for the hyaluronanase family in *Xenopus laevis* embryos did not show specific signal, with the exception of *ADAMTS1* in *Xenopus laevis* (figure 4-7) and *ADAMTS9* in both *Xenopus tropicalis* and *Xenopus laevis* (figure 4-4, 4-8). The weak expression level and the high similarities of the *ADAMTS* genes in *Xenopus* could explain the lack of specific signal. New probes could be generated in different areas of the genes and locked nucleic acid (LNA) probes could be used. They are composed of modified RNA nucleotides, which have an additional bridge that bonds the 2' oxygen and the 4' carbon of the pentose, and are highly sensitive and specific and have been used to do WISH in *Xenopus* for miRNA (You et al., 2006) (Ahmed et al., 2015).

ADAMTS9 spatio-temporal expression profiles, assessed by RT-PCR (figure 4-3), RT-qPCR (figure 4-6) and WISH (figure 4-4 and 4-8), were found similar in *Xenopus tropicalis* and *Xenopus laevis* from unfertilised egg to tadpole stages. *ADAMTS9* was highly expressed from early tailbud in the eye, the midbrain hindbrain boundary, and the migrating cells along the branchial arches (possibly neural crest cells) (figure 4-4 and 4-8). At tadpole stages *ADAMTS9* expression was seen in the retinal pigment epithelium, in the branchial arches, in the pronephros, in the pronephric duct and in the pancreas (figure 4-4, 4-8, 4-9 and 4-10). *ADAMTS9* expression in the brain, the craniofacial structures, the kidney and the pancreas are similar for mouse and *Xenopus* (Jungers et al., 2005). These similarities reinforce the hypothesis of a conserved function in these two species.

ADAMTS9 expression was found in the midbrain hindbrain boundary (MHB) from tailbud stages (figure 4-4 and 4-8) whereas its substrate *VCAN* was not expressed in this area (figure 4-13) (Casini et al., 2008). FGF8 is known to be expressed in the MHB and to be essential for MHB development (Fletcher et al., 2006). *ADAMTS1* has been shown to negatively regulate FGF independently to its catalytic activity (Suga et al., 2006). *ADAMTS9* could play a role in the regulation of FGF signaling in the MHB development independently to its protease activity.

It has been shown that *VCAN*, a substrate of *ADAMTS9*, was expressed in *Xenopus laevis* at early stages during gastrulation and neurulation, and at tailbud and tadpole stages the expression was found in the migrating neural

crest, in the branchial arches, heart and pronephros (figure 4-13) (Casini et al., 2008). The co expression of *ADAMTS9* and its substrate *VCAN* in the pronephros, pronephric duct, migrating neural crest and their derivative structures, such as the branchial arches, suggest a role of *ADAMTS9* in the extracellular matrix remodeling during the development of these structures. In order to investigate this hypothesis, loss of function experiments for *ADAMTS9* were carried out in *Xenopus tropicalis* and in *Xenopus laevis*.

4.3.2 Functional study of *ADAMTS9* in *Xenopus tropicalis* and in *Xenopus laevis*

In order to carry out loss of function experiments for *ADAMTS9* in *Xenopus*, translational blocking morpholinos were used.

4.3.2.1 *ADAMTS9* knockdown in *Xenopus tropicalis* and in *Xenopus laevis* embryos

Mice homozygous for a mutation in *ADAMTS9* gene, leading to a knockout, do not survive past gastrulation (E7.5). However conditional and heterozygous mice for *ADAMTS9* mutation survive and show soft tissue syndactyly (STS), when two or more digits are fused together, and cardiac defect, respectively (Dubail et al., 2014) (Kern et al., 2010). Knockdown experiments for *ADAMTS9* in *Xenopus tropicalis* and in *Xenopus laevis*, for each copy, using morpholinos did not show a phenotype (figure 4-5 and 4-12). The lack of phenotype could be due to lack of efficiency of the morpholinos, which has to be assessed in order to establish the optimal concentration of morpholino to inject in order to obtain an efficient knockdown of *ADAMTS9*, and/or to the redundancy of the *ADAMTS* family..

4.3.2.2 *ADAMTS9* knockdown in neural crest of *Xenopus laevis*

It has been shown by *in vivo* and *in vitro* study that versican is a nonpermissive matrix for NC migration leading them to the correct migratory direction by creating restrictive boundaries. The correct confinement is essential for collective NC migration during *Xenopus* development (Szabo et al., 2016). V0 and V1 are the most abundant versican isoforms found in neural crest cells (Dutt et al., 2006). These studies suggest a role of the hyaluronanases family of *ADAMTSs* in NC migration by remodeling of the ECM by degradation of versican. Versican can be cleaved by *ADAMTS9* (Somerville et al., 2003). After

loss of function experiments of ADAMTS9 specifically in NC population using morpholinos against both copies, the phenotype of NC migration was analysed at tailbud stage by wholemount *in situ* hybridisation for *sox10*, a marker of NC, and at tadpole stage by observation of NC derivatives population, such as melanocytes and craniofacial cartilage. No disruptions of the different NC migration pathways, in the anterior part of the embryo and in the trunk, were seen at tailbud stage and no pigmentation and craniofacial phenotypes were observed at tadpole stage (figure 4-14). These results suggest that ADAMTS9 could not be the main ADAMTS necessary for the correct ECM remodeling promoting NC migration in *Xenopus* or that it could be compensated by an other member of the hyaluronanases family.

ADAMTS1 has been shown to have a similar expression profile to *ADAMTS9* in *Xenopus laevis*, such as in the branchial arches, and to have a possible role in NC formation (figure 4-7) (Suga et al., 2006). These data suggest cooperation between these two ADAMTSs in NC and compensation after knockdown of ADAMTS9 in NC explaining the lack of phenotype. *ADAMTS5* has been shown to be expressed in neural crest derivative tissues in mouse such as in Schwann cells and cartilage (McCulloch et al., 2009a). ADAMTS9 and ADAMTS20 have been shown to cooperate in the colonisation of skin by neural crest derived melanoblasts in mouse (Silver et al., 2008). These data suggest cooperation of several ADAMTSs in NC development, which could explain why no phenotype was observed after a knockdown of ADAMTS9 alone.

The next experiments will be to knockdown several ADAMTSs from the hyaluronanases family in NC, in *Xenopus laevis*, by injection of multiple morpholinos against different ADAMTSs and standard control morpholino in order to assess that the obtained phenotype is specific to the knockdown of the targeted genes. Multiple knockdowns by injection of morpholinos has previously been used in *Xenopus* in order to assess cooperation of genes and by inhibition of compensation between them, seen when only a single gene was knocked down, a phenotype could be observed (Tomlinson et al., 2008). The effects on NC migration of ADAMTS9 knockdown and the multiple knockdowns of several hyaluronanases could be investigated in more detail by using other NC markers, such as *twist* and *sox9* (Lander et al., 2013).

4.3.2.3 ADAMTS9 knockdown in the pronephros of *Xenopus laevis*

ADAMTS9 expression was found in the pronephros and the pronephric duct from early tailbud stages (figure 4-8 and 4-10), which overlap with the expression of its substrate *VCAN* (figure 4-13) (Casini et al., 2008) suggesting a role of *ADAMTS9* in the ECM remodeling during pronephros development in *Xenopus*. Morpholinos were used to knockdown both *ADAMTS9* copies (L and S) in *Xenopus laevis*.

Using *wt1* as an early marker for glomus development by *in situ* hybridisation, no disruption of development was observed when *ADAMTS9* was knocked down (figure 4-16) whereas a phenotype was observed using *pax8*, as a marker of pronephric tubules and duct in the early tailbud (figure 4-17) and *atp1b1* in late tailbud (figure 4-18), *Xlim1* and *pax2* as markers for nephrostomes, tubules and duct in late tailbud (figure 4-18) and 4a6 antibody, as a late marker of intermediate and distal tubules and pronephric duct (figure 4-19). At tailbud stages a default of nephrostomes, tubules and duct formation on the injected side of embryos where *ADAMTS9* was knocked-down was observed suggesting a delay of development (figure 4-17 and 4-18). At tadpole stages severe phenotypes characterised by the partial or complete loss of 4a6 signal were observed in the distal tubules and in the pronephric duct suggesting that these structure might be present although not in a final differentiated state allowing the detection by the 4a6 antibody (figure 4-19). This supports the hypothesis of a delay of development when *ADAMTS9* was knocked down (figure 4-17 and 4-18). Injection of standard control morpholino should be carried out on order to assess the specificity of the delay phenotype observed at tailbud stages. The 4a6 immuno staining could be carried out on later stages of development (stage 42) in order to verify this hypothesis and check if the 4a6 signal would be present in injected embryos. These results suggest an important role of *ADAMTS9* in pronephros development, specifically in the formation of the pronephric tubules and duct possibly by the degradation of versican, which is necessary for the correct ECM remodeling during pronephros development.

VCAN is expressed in the pronephros and in the pronephric duct from tailbud stages but is not expressed in tadpoles (figure 4-22) (Casini et al., 2008)

suggesting a transient role in the pronephros development, supporting the hypothesis that degradation by the hyalactanases family of ADAMTSs is crucial.

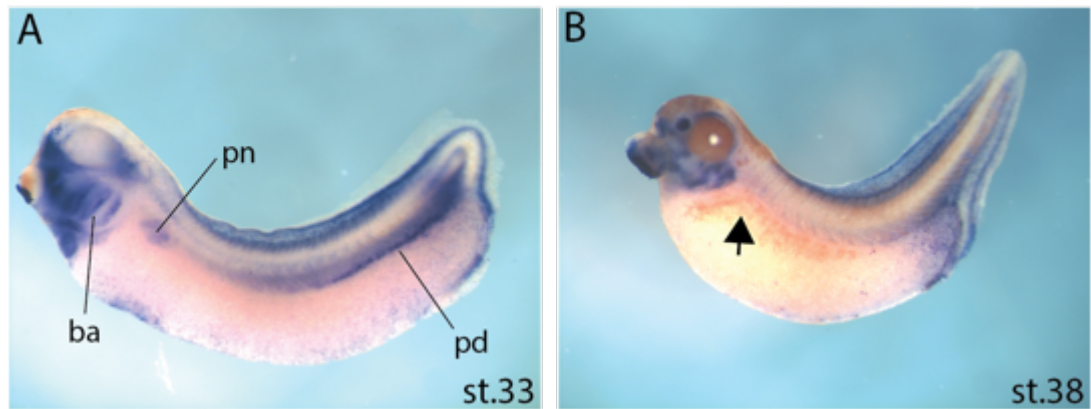


Figure 4-22: The expression pattern of VCAN in *Xenopus laevis* embryos. Lateral views of embryos with anterior on the left and posterior on the right. (A) At stage 33, the expression is present in the pronephros (pn) and in the pronephric duct (pd). (B) At stage 38 the expression is not present in the pronephros (indicated by the black arrow).

The same profile of expression of VCAN has been shown in mice kidney development but the amount of cleaved versican, at the specific ADAMTSs cleavage site, was not affected by the knockout of *ADAMTS1* and *ADAMTS4* (Boerboom et al., 2011), suggesting the role of other members of the hyalactanases family, which could possibly be ADAMTS9. To verify this hypothesis future experiments should investigate the expression profile of VCAN in injected embryos to check if the expression would be found in the pronephros at tadpole stages suggesting a delay of development due to ADAMTS9 knockdown and the amount of cleaved versican in *Xenopus laevis* pronephros. However the ADAMTSs cleavage site is not conserved in the *Xenopus* VCAN so the antibody specific to the new epitope generated after cleavage at this site cannot be used.

Aggrecan is another ADAMTS9 substrate and has been shown to be weakly expressed in the kidney during development in mouse (Boerboom et al., 2011) whereas it was not expressed in the *Xenopus* pronephros (Suzuki et al., 2012).

ADAMTS1 and *ADAMTS4* knockout mice died soon after birth and showed a kidney phenotype characterised by a marked renal medulla thinning (Boerboom et al., 2011) suggesting a role of these two ADAMTSs independent

of their proteases activity on versican. *ADAMTS1* is expressed in the kidney in mouse and knockout mice for *ADAMTS1* show a dysgenic malformation affecting the renal medulla from birth associated with the beginning of its function (Mittaz et al., 2004) (Mittaz et al., 2005). *ADAMTS1* has a similar expression profile to *ADAMTS9* in *Xenopus laevis* in the pronephros (Suga et al., 2006).

In addition, *ADAMTS13* has been shown to be expressed in human podocytes, specialised epithelial cells that line the urinary side of the glomerular basement membrane (GBM) in the Bowman's capsule (glomus in *Xenopus*) with a complex cellular morphology that are responsible for the size exclusion barrier and for preventing large molecules from exiting the blood stream in addition to the synthesis of the GBM. *ADAMTS13* function, as well as von Willebrand factor cleavage could be responsible for the GBM remodeling. *ADAMTS13* mutation is associated with congenital thrombotic thrombocytopenic purpura characterised by the presence of ultra-large von Willebrand factor (ULVWF) multimers in the blood circulation due to deficiency of *ADAMTS13* responsible of their cleavage. In TTP patients *ADAMTS13* was expressed in podocytes but was not secreted suggesting reduced extracellular *ADAMTS13* activity leading to the accumulation of ULVWF multimers and causing the formation of platelet plugs in the glomeruli (Manea et al., 2007).

These data, supported by the findings of the present study, suggest that the *ADAMTS* family plays a crucial role in pronephros development possibly by a different mode of action at specific pronephric localisation and time of development. Injection of multiple morpholinos targeting several *ADAMTS*s in *Xenopus laevis* could be carried out in order to assess cooperation in pronephros development. . In order to characterise in more detail the function of *ADAMTS9* in *Xenopus laevis* pronephros development, other markers should be used such as transcription factors pronephric terminal differentiation markers such as 3g8 antibody (Agrawal et al., 2009) (Buisson et al., 2015).

Surprisingly no compensation by an *ADAMTS9* copy when the other copy was knocked down by the *ADAMTS9* morpholino occurred, which was characterised by the lack of rescue of the phenotype observed in the tubules and pronephric duct (figure 4-13). These results suggest that both copies must be expressed, which support gene dosage hypothesis resulting in the

conservation of both copies of a gene in the two *Xenopus laevis* subgenomes (see chapter III) (Watanabe et al., 2016). An RT-PCR for *ADAMTS9L* of injected *Xenopus laevis* embryos with *ADAMTS9S* morpholino would show if the level of *ADAMTS9L* mRNA increases or not when the other copy, *ADAMTS9S* is knocked down, and the same experiment would be carried out for *ADAMTS9S* expression in embryos when injected with *ADAMTS9L* morpholino.

4.3.2.4 Morpholinos efficiency

In order to test the efficiency of the morpholinos used in this study against *ADAMTS9* in *Xenopus laevis* *ADAMTS9S* and *ADAMTS9L* 5'-UTR containing the binding site of the morpholino, the signal peptide and the pro domain with an HA tag at the C-terminal position to detect the presence of the protein by western blot were successfully cloned. The truncated *ADAMTS9S* protein with an HA tag at the C-terminal position in *Xenopus laevis* embryos was expressed and visualised by western blot using an anti-HA antibody (figure 4-20). This construct will allow to test the efficiency of the *ADAMTS9S* morpholino by injecting it and *ADAMTS9S-HA* mRNA into *Xenopus laevis* embryos and visualise by western blot a decrease of the *ADAMTS9S-HA* signal when co-injected with the translational blocking *ADAMTS9S* morpholino compared to the *ADAMTS9S-HA* signal when co-injected with control morpholino that is not specific to *ADAMTS9S*. However *ADAMTS9L-HA* signal was not seen by western blot suggesting that the protein did not get translated, although the sequencing of the construct showed no mutations, or was degraded. Increasing the number of protein domains to create a longer truncated protein could possibly lead to *ADAMTS9S-HA* translation.

To confirm the specificity of the *ADAMTS9* morpholinos phenotype in *Xenopus laevis* a rescue experiment could be carried out by injecting *ADAMTS9* mRNA with a mutation at the binding site of the morpholino, to avoid its translational blocking action. The compensation of the *ADAMTS9* protein should rescue the observed phenotypes, in the kidney for this study. As *ADAMTS9* is a large gene it has proven to be difficult to avoid cloning mutations, resulting in a non-functional protein. The Suneel Apte team cloned the human *ADAMTS9* and a non-functional *ADAMTS9* with a C-terminal myc-HIS6 tag (Somerville et al., 2003). The presence of this tag will enable

visualising by western blot of the human ADAMTS9 protein if it is translated in *Xenopus laevis*. Using pronephric markers from this study the ability of the human ADAMTS9 to rescue the phenotype caused by *Xenopus ADAMTS9* knockdown by morpholinos will be assessed. *ADAMTS9S* and *ADAMTS9L* morpholinos used in this study will not bind to the human *ADAMTS9* sequence.

In order to performe loss of function experiments, another technique called CRISPR/Cas9 has been developed and used in *Xenopus* (Guo et al., 2014). Guide RNA have been designed to target *ADAMTS9* in *Xenopus tropicalis* and *Xenopus laevis* but none of them showed the efficiency of binding to the target gene in order to allow the cleavage of the DNA sequence by the Cas9 in the embryos.

In this chapter the investigation on the *ADAMTS* family in *Xenopus* development was carried out up to tadpole stages. This project will progress to investigate the *ADAMTS* family in later stage of development in *Xenopus laevis*, specifically during metamorphosis, in collaboration with the Pr. Barbara Demeneix laboratory at the Museum d'Histoire Naturelle in Paris.

**Chapter V: Characterisation of the ADAMTS family,
metalloproteinases and extracellular components in
Xenopus laevis during metamorphosis and heart
regeneration**

5.1 Introduction

As part of the European Marie Curie Initial Training Network called DevCom, for Developmental and Computational Biology, there was an opportunity to do a secondment in a partner laboratory of this network. This secondment was realised in collaboration with the Prof. Barbara Demeneix laboratory at the Museum d'Histoire Naturelle in Paris under the supervision of Dr. Laurent Coen and Dr. Fabrice Girardot. They look at the regulation of *Xenopus laevis* metamorphosis by thyroid hormone, the capacity of *Xenopus laevis* tadpole to regenerate their heart and the loss of this capacity past metamorphosis. At that time they were not looking at the extracellular matrix (ECM) or at metalloproteinases in these different processes. Both labs agreed that this would be an area in which to collaborate.

It has been shown that the extracellular matrix and matrix metalloproteinases are important for organ remodeling during *Xenopus laevis* metamorphosis. The regulation of cell-ECM interactions is important to control apoptosis of embryonic cells and proliferation of adult cells (Fu et al., 2007) (Hasebe et al., 2007b). However the role of other metalloproteinases, such as ADAMTSs and ADAMs, has not been investigated as well as other matrix components such as versican and aggrecan. Little was known about heart regeneration in *Xenopus* but studies on limb, retina and nerve tissue regeneration have shown that they have the ability to regenerate at tadpole stages but not past metamorphosis (Vivien et al., 2016). It would therefore be interesting to know if it is true for heart regeneration as well and analyse the difference in gene expression that leads to this loss of cardiac regeneration after metamorphosis.

ECM components, metalloproteinases, tissue inhibitor of metalloproteinases genes expression were investigated in the brain, the skin and the heart undergoing remodeling during *Xenopus laevis* metamorphosis and in the heart after ventricular resection to determine regeneration during *Xenopus laevis* metamorphosis. Expression profiles were analysed using quantitative PCR and by microfluidic so that a large number of genes with a small amount of tissue could be analysed.

5.1.1 Brain remodeling during *Xenopus laevis* metamorphosis

Before metamorphosis the central nervous system in *Xenopus* is composed of the spinal cord and the brain. The brain can be divided into three sections from the spinal cord that is caudal to rostral position: the rhombencephalon (hindbrain) comprising the medulla oblongata and the cerebellum, the mesencephalon (midbrain) comprising the optic tectum and the tegmentum and the prosencephalon (forebrain) comprising the diencephalon where the hypothalamus is located, the telencephalon and the olfactory bulb. The brainstem that provides the main motor and sensory innervation is composed of the mesencephalon and the rhombencephalon. Similar to all non-mammalian vertebrates, *Xenopus* does not possess corticospinal tracts, which connect the prosencephalon with the spinal cord which control voluntary motor control of the limbs and the trunk. All motor control is integrated in the brainstem. The sensory and motor tracts between the brainstem and the spinal cord are called supraspinal nerve tracts and are conserved in vertebrates. In *Xenopus* neurogenesis of these neurons is mostly complete at pro-metamorphosis stage (Lee-Liu et al., 2016) (Pratt and Khakhalin, 2013).

The composition of the ECM changes during brain development. Embryonic ECM is mostly composed of proteoglycans such as neurocan and versican V1 and glycoproteins such as tenascin-C whereas the ECM in the adult brain is mostly composed of tenascin-R and chondroitin sulfate proteoglycans (CSPG) such as brevican, versican V2 and aggrecan. Hyaluronan (HA) is the backbone of the ECM in the brain by binding to proteoglycans that are linked to glycoproteins such as tenascins; this ECM is called HA-based CM. The ECM functions in the brain during embryonic development are to regulate the formation of glia and neurons, cell migration, directing of axon growth and their myelination and formation of synapses. The functions of the adult ECM are regulation of synapses formation and their plasticity, protection of the neurons and their interactions with glia cells and homeostasis regulation. ECM interacts with cells via cell surface receptors such as integrins. The changes from an immature brain ECM to a more rigid adult brain ECM mediate the transition from a juvenile to an adult plasticity by restricting the neuronal organisation (Happel and Frischknecht, 2016).

The adult brain is composed of three ECM, which differ in their composition and functions. The basement membrane or basal lamina (BL) surrounds blood vessels and pial surface (most inner layer of the meninges that are the membranes that envelops the brain and the spinal cord) and is mostly composed of collagen, fibronectin, laminin and proteoglycan such as perlecan. It maintains the blood–brain barrier (BBB) between blood vessels and the brain parenchyma (composed of neurons, glia cells and interstitial ECM) and regulates the maturation of endothelial cells. The perineuronal nets (PNNs) are mostly composed of proteoglycans such as aggrecan, HA and tenascin-R. It enwraps synapses, which protect and maintain their plasticity. The neural interstitial matrix is the ECM in the parenchyma and is mostly composed of proteoglycans, HA and tenascins with a minority of collagen, fibronectin and laminin that forms a dense three-dimensional network (Vecino and Kwok, 2016). In addition to these main components the brain ECM is composed of reelin, thrombospondins and guidance molecules. ECM components regulate the axon growth. Laminin and fibronectin promote the axon growth whereas chondroitin sulphate proteoglycans (CSPGs) create barriers where axons cannot grow creating paths for the axons to grow at the correct location to the precise target. CSPGs inhibit axonal regeneration and neurogenesis after brain injury such as spinal cord injury or Alzheimer’s disease and mutations in CSPGs can cause neuropsychiatric disorders such as bipolar disorder and schizophrenia (Barros et al., 2011) (Avram et al., 2014). ECM remodeling by metalloproteinases is crucial for brain development and the dysregulation of this process can cause neuropsychiatric diseases (Gottschall and Howell, 2015).

5.1.2 Skin remodeling during *Xenopus laevis* metamorphosis

At pro-metamorphosis the embryonic epidermis is composed of three cell layers; apical, skein and basal cells, which is separated from the dermis (a single layer of fibroblasts and melanophores) by a thin acellular collagen lamella composed of type I collagen secreted by basal embryonic cells. All the layers of epidermal cells proliferate. At climax, when the concentration of thyroid hormone increases, only the basal epidermal cells differentiate into adult stem cells and proliferate to give rise to adult skin whereas the two other layers, skein and apical cells, undergo apoptosis in a cell-autonomous manner (Schreiber

and Brown, 2003). The dermis and the collagen lamella are thicker and presumptive secretory glands (PSGs) form. Fibroblasts migrate from the connective tissue into the collagen lamella (Suzuki et al., 2009). The adult skin is formed post-metamorphosis with a multi layer epidermis where only the basal cells replicate, similar to the 'germinative' adult epithelium in all vertebrates. Mature glands are present in the dermis, composed of the collagen lamella and connective tissue (Schreiber and Brown, 2003). In tail remodeling, embryonic basal cells of the epidermis do not give rise to adult cells and only apoptosis occurs which leads to the tail resorption (Schreiber and Brown, 2003). Proteoglycans are important components of the ECM in the skin; they provide hydration, viscoelasticity, scaffold for a good ECM structure by interacting with other components such as collagen and fibrillin, growth factors to regulate cell signaling, ECM components, migration and proliferation (Smith and Melrose, 2015).

5.1.3 Heart remodeling during *Xenopus laevis* metamorphosis

Xenopus cardiogenesis starts at gastrulation (stage 10) when cardiac progenitors cells, from precardiac mesoderm migrate anteriorly to the ventral midline where they fuse posteriorly to the cement gland in a crescent-like structure by stage 13. The precardiac mesoderm is located on either side of the Spemann's organiser on the dorsal side of the embryo. The resultant cell population of cardiac progenitors splits into two different cell lineages called the first heart field (FHF) and the second heart field (SHF). The SHF forms the outflow tract (OFT) and the FHF forms the single ventricle and the two atria. These two differentiating patches of cells fuse into a single cardiogenic plate, which then rolls to create a lumen and gives rise to the primary heart tube at stage 32. Morphogenetic movements lead the heart tube to loop and it contains differentiated cardiomyocytes which are able to contract at stage 35. Then remodeling defines the different chambers and the ventricular myocardium undergoes trabeculation, the creation of a supporting tissue in the form of small beams, giving rise to a functional embryonic heart by stage 40 (Hempel and Kühl, 2016).

ECM remodeling is an important process for heart development. During heart formation, a mature ECM composed of hyaluronan, proteoglycans,

collagens, elastin, fibrilin, tenascin, fibronectins, and laminins replaces the initially immature versican-rich ECM. Degradation of the ECM by metalloproteinases during cardiac development is an essential process (Lockhart et al., 2011).

5.1.4 Heart regeneration during *Xenopus laevis* metamorphosis

The adult *Xenopus laevis* heart does not regenerate after ventricle resection but shows a deposition of fibrotic tissue and hypertrophy of the amputated ventricle, this is characteristic of a non regenerated heart seen in adult mammals (Marshall et al., 2017). *Xenopus laevis* tadpoles at pro metamorphosis stage can regenerate their hearts after amputation (unpublished data, Coen L.). However the reasons of the loss of the cardiac regenerative capacity past metamorphosis in *Xenopus laevis* are unknown. Studies on heart regeneration in the newt, another amphibian, shows that ECM remodeling is a key process. (Mercer et al., 2013) proposed a model where after an amputation of the distal ventricular tip (around 20%) a regeneration-specific matrix containing tenascin-C, HA and fibronectin regulates the proliferation of progenitor cells in the myocardium that migrate with the help and support of the regenerative ECM. This regenerative ECM is rich in HA, creating a highly hydrated matrix, which promotes cell migration toward the wound site, where they dedifferentiate to regenerate the amputated part. In addition, this regeneration-specific ECM is a reservoir of signaling factors that can be released by metalloproteinases regulating cell behaviour of progenitor cells such as migration, proliferation and differentiation state. Cells participating in the regeneration of the missing heart tissue can be dedifferentiated cardiomyocytes or activated stem cells. This ECM remodeling model seems to be conserved between vertebrates capable of heart regeneration (Mercer et al., 2013). In axolotl, both cardiomyocytes and epicardial cells proliferate after amputation, which suggests that several cell types are involved in this process (Vivien et al., 2016).

ECM components, metalloproteinases, tissue inhibitor of metalloproteinases genes expression and regulation were assessed in the brain, the skin and the heart undergoing remodeling during *Xenopus laevis* metamorphosis and in the heart after ventricular resection. Their expression profiles were measured by

quantitative PCR and by microfluidic to be able to look at a large number of genes with a small amount of tissue.

5.2 Results

5.2.1 ADAMTSs, versican, aggrecan and TIMPs expression in the skin and the brain during *Xenopus laevis* metamorphosis

To look at gene expression during metamorphosis, body skin (head and trunk) and brain samples were dissected from stage 57 and 61 *Xenopus laevis* tadpoles and from stage 66 juvenile frog (froglet) (figure 5-1A). cDNAs synthesised from the RNA of these samples were used to carry out RT-qPCR (figure 5-1B and C) for the *ADAMTS* gene family, versican (*VCAN*), aggrecan (*ACAN*) and the *TIMP* family (*TIMP1*, *TIMP2* and *TIMP3*). *TIMP4* is not present in the *X.laevis* and *X.tropicalis* genome. Primers for *VCAN* recognise the N-terminal G1 domain common to all five isoforms.

Ct data from RT-qPCR were collected using ExpressionSuite Software (Applied Biosystems) and analysed using Excel (Microsoft). Δ Ct were first obtained using Ct values of each gene of interest normalised against *pten*, the housekeeping gene (gene Ct - *pten* Ct). Then Δ Ct values were converted to relative gene expression using the $2^{-\Delta Ct}$ method. This method was used rather than the fold change method in order to look at gene expression level in each stage rather than gene regulation compared to one condition. The results showed that in general the level of gene expression of the *ADAMTS* gene family and the *TIMP* family was higher in the body skin than in the brain whereas the gene expression level for *VCAN* was similar (figure 5-1B and C). *ADAMTS6* was the most expressed gene of the *ADAMTS* family in the brain with an up-regulation at and after metamorphosis compared to before metamorphosis. The hyalactanases family members were expressed in the brain with *ADAMTS5*, *ADAMTS8* and *ADAMTS4* being the most expressed, *ADAMTS1*, *ADAMTS9* and *ADAMTS15* less expressed whereas *ADAMTS20* was not expressed at all. With the exception of *ADAMTS8* and *ADAMTS15* that were downregulated at the metamorphic climax, all members of the hyalactanases family were up regulated at and after metamorphosis compared to before. *ADAMTS2* and *ADAMTS17* were also detected and showed the same expression profile (figure 5-1B'). *ACAN* and *VCAN* showed opposite

profiles of expression, *ACAN* was upregulated at and after metamorphosis compared to before, whereas *ACAN* was downregulated although their expression levels were similar at and after metamorphosis (figure 5-1B''). Of the *TIMPs*, *TIMP2* was the most expressed with no difference of expression in function of the metamorphosis periods. *TIMP3* was upregulated at and after metamorphosis compared to before, whereas *TIMP1* was expressed at a low level for all metamorphosis periods (figure 1B'''). All *ADAMTSs* (except the lesser expressed *ADAMTS12*, *ADAMTS17* and *ADAMTS19*) were upregulated in the skin at metamorphosis and even more so after, compared to before. Members of the hyalactanases family were all expressed with *ADAMTS8*, *ADAMTS15* and *ADAMTS1* being the most expressed and *ADAMTS9* and *ADAMTS20* the least expressed. *ADAMTS2* was highly expressed as well as *ADAMTS6* (figure 5-1C'). *ACAN* was not detected but *VCAN* was expressed at similar levels in the skin during metamorphosis (figure 5-1C''). *TIMP1* was the most expressed member of the *TIMP* family in the skin and had a peak of expression at the metamorphic climax. *TIMP1* was more expressed after metamorphosis than before. *TIMP2* showed the same profile of expression and *TIMP3* was up regulated in the skin at and after metamorphosis compared to before (figure 5-1C''').

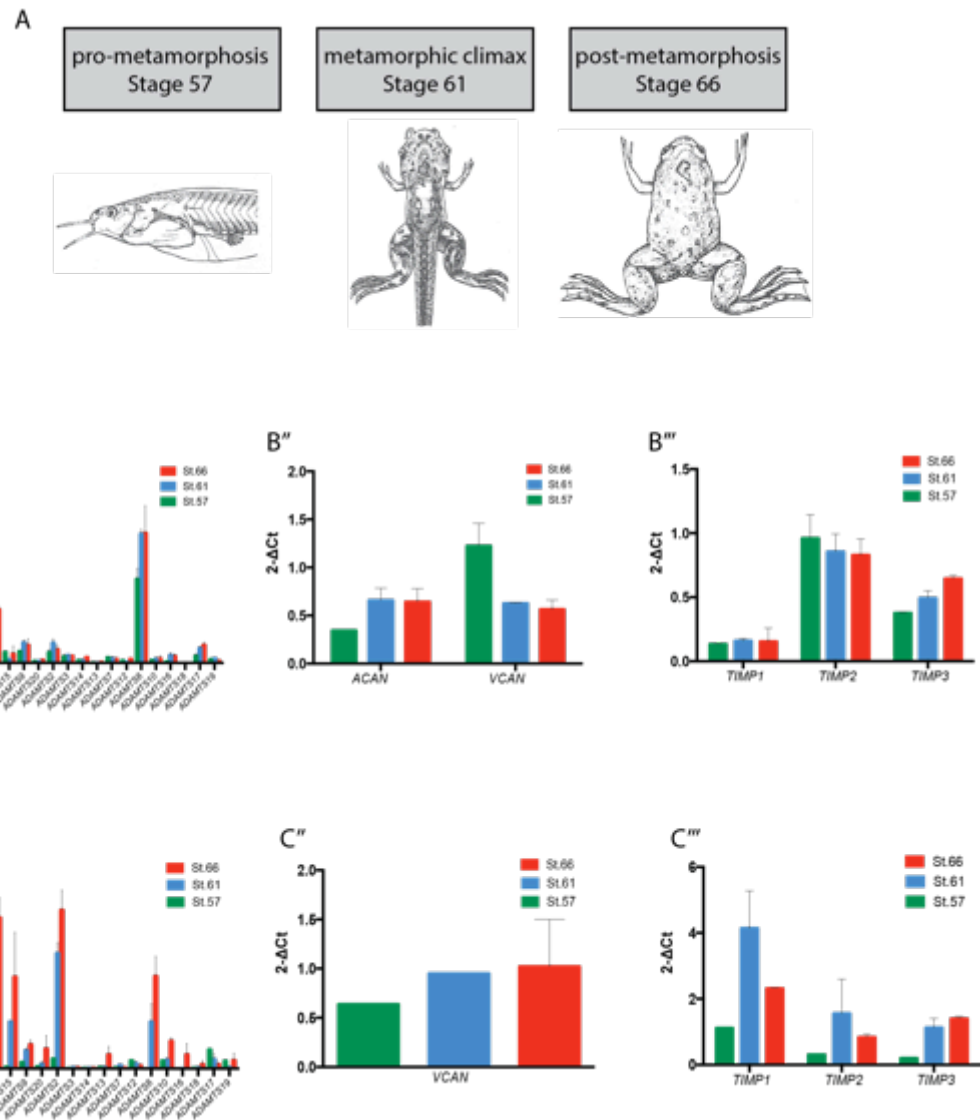


Figure 5-1: Gene expression of the ADAMTS family, versican (VCAN), aggrecan (ACAN) and TIMP1, TIMP2 and TIMP3 evaluated by RT-qPCR on brain and skin tissues from *Xenopus laevis* tadpole and juvenile during metamorphosis. (A) *Xenopus* stages used in this study to dissect out the body skin and the brain. Graphs show gene expression fold differences before (St.57), at (St.61) and after (St.66) metamorphosis. The results show the mean with standard error of the mean (SEM) for one (results without error bars) or two independent (results show with error bars) experiments. (B) Gene expression in the brain during metamorphosis of (B') the ADAMTS family, (B'') ACAN and VCAN, (B''') TIMP1, TIMP2 and TIMP3. (C) Gene expression in the skin during metamorphosis of (C') the ADAMTS family, (C'') VCAN, (C''') TIMP1, TIMP2 and TIMP3. The developmental stages representations are from (Nieuwkoop and Faber, 1994).

5.2.2 Gene expression in the heart undergoing remodeling and in the heart after ventricular resection during *Xenopus laevis* metamorphosis

In order to look at the expression of a large number of genes in the small amount of tissue that is the *Xenopus laevis* heart, the microfluidic technique was used, which allows for fast and efficient quantitative PCR reactions in nanoliter volumes. Ten hearts from *Xenopus laevis* tadpoles at pro-metamorphosis (stage 57), at metamorphic climax (stage 61) and post-metamorphosis stages from juvenile and adult frogs were collected at 1, 3 and 7 days post amputation (dpa) for each experimental condition (control, SHAM and amputated) (figure 5-2). The genes selected for this study included ECM components, metalloproteinases, tissue inhibitor of metalloproteinases genes expression gene expression in the heart during metamorphosis (table 5-1). The control hearts were used to look at normal heart remodeling during metamorphosis. SHAM were used as placebo control where just the pericardial sac was opened but the heart was not amputated. The amputated hearts were cut using a ventricular resection procedure removing around 4% of the ventricle (Marshall et al., 2017).

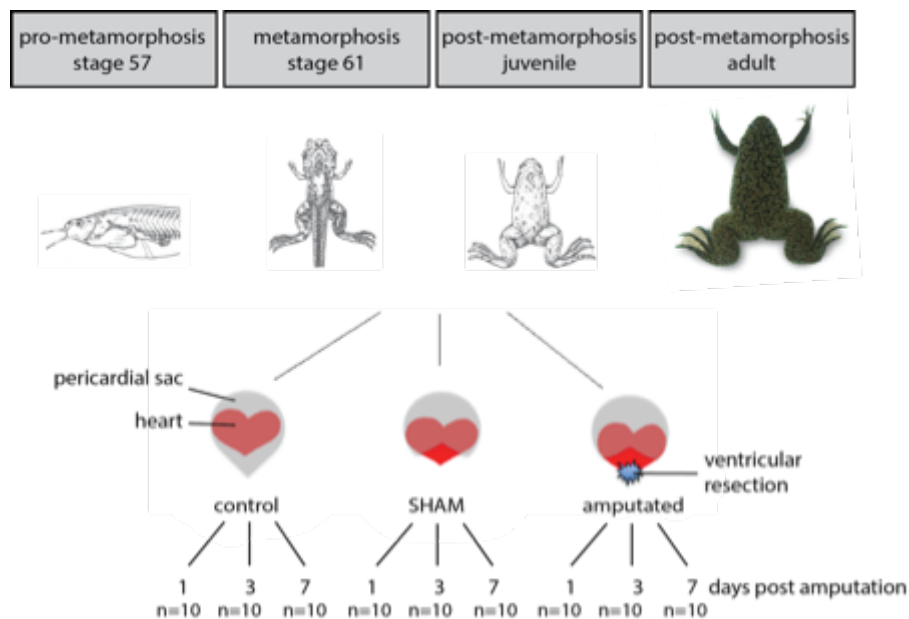


Figure 5-2: Schematic of the different experimental conditions used to look at gene expression in the heart during *Xenopus laevis* metamorphosis. The control hearts were used to look at normal heart remodeling during metamorphosis. SHAM hearts were used as placebo control where just the pericardial sac was opened but the heart was not amputated. The amputated hearts were cut using a ventricular resection procedure (removing around 4% of the ventricle). Samples were collected at 1, 3 and 7 days post amputation (dpa). Ten hearts were used for each experimental procedure (n=10).

Table 5-1: List of genes analysed in heart development and regeneration during *Xenopus laevis* metamorphosis. The different gene categories are indicated in the first two rows and the specific gene name is indicated below. For *ADAMTS*, *ADAM*, *MMP*, *TIMP* and *syndecan* only the gene number is indicated in the column meaning *ADAMTS1*, *ADAM7*, *MMP2*, *TIMP1* and *syndecan1* are for all different genes. *tPA*: tissue plasminogen activator; *PAI1*: plasminogen activator inhibitor-1; *uPAR*: urokinase plasminogen activator receptor.

metalloproteinases				ECM	plasminogen	<i>syndecan</i>
<i>ADAMTS</i>	<i>ADAM</i>	<i>MMP</i>	<i>TIMP</i>			
1	9	2	1	<i>VCAN</i>	<i>tPA</i>	1
2	10	9	2	<i>ACAN</i>	<i>PAI1</i>	2
3	11	7	3	<i>tenascin-C</i>	<i>uPAR</i>	3
4	12	1		<i>fibronectin 1</i>		4
5	15	14		<i>collagen 1a1</i>		
6	17					
7	19					
8	22					
9	23					
10	28					
12	33					
13						
14						
15						
16						
17						
18						
19						
20						

5.2.2.1 Gene expression in the heart undergoing remodeling during *Xenopus laevis* metamorphosis

The quantitative PCR was carried out using primers listed in table 1 and primers for fibronectin 1 (*fn1*) and collagen, type I, alpha 1 (*col1a1*) from Dr. Laurent Coen with the microfluidic method. The results were grouped into four groups, according to (Nieuwkoop and Faber, 1994) (NF) *Xenopus laevis* stages, NF57 (pro-metamorphosis), NF61 (metamorphic climax), juvenile and adult (post-metamorphosis). The first analysis was carried out using the Real-Time PCR Analysis v4.1.3 software (Fluidigm) to look at the quality of the results and discard any data without any or non-specific gene amplification (Ct values). In order to normalise the data five housekeeping genes (*baf60*, *hand2*, *pten*, *akt1* and *smn2*), previously established by Dr. Laurent Coen's team to be stable in the experimental conditions, were used in this study to obtain the delta Ct (Δ Ct) values. In the controls hearts the data from the three different time points (1, 3 and 7 days post the amputation, figure 5-2) for each stage of development were combined to carry out the analysis of gene expression during *Xenopus laevis* metamorphosis (n=30). The Δ Ct values were used to create a heat-map showing the level of expression at the different stages of development (figure 5-3). The analysis of the heat-map showed three distinct groups of genes in function of their level of expression in the heart during metamorphosis. One group showed a high level of expression (indicated in blue on the heat-map) such as *syndecan2*, *VCAN*, *ADAMTS1*, *ADAM9*, *MMP14* and *TIMP3* (figure 5-3). Genes such as *ADAMTS8*, *ADAM17*, *MMP9*, *tPa* and *TIMP1* showed a moderate level of expression whereas genes such as *ADAM22*, *ADAMTS16*, *ACAN* and *MMP1* were lowly expressed (figure 5-3).

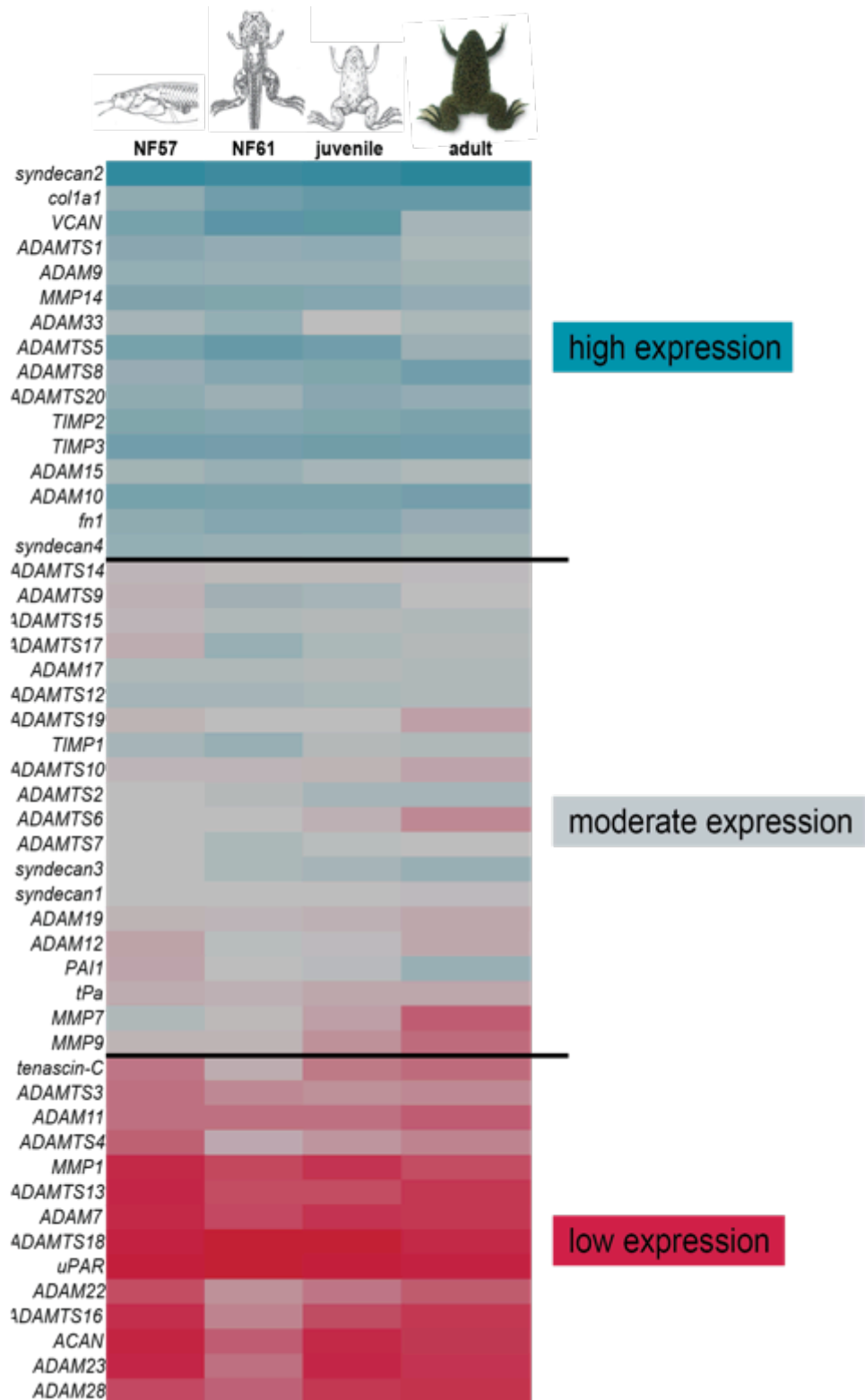
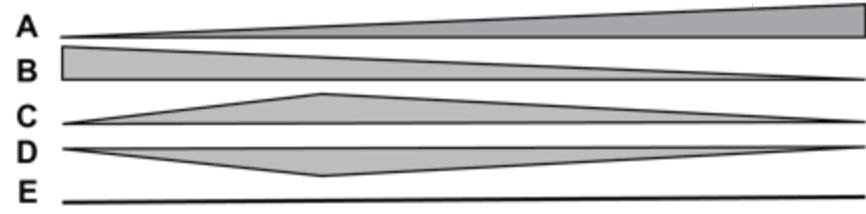


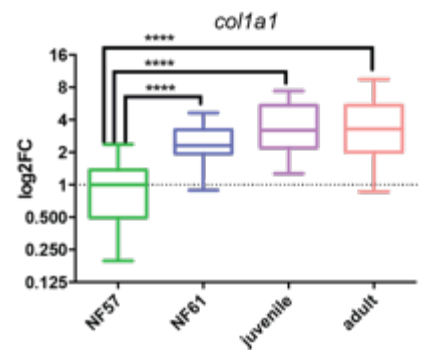
Figure 5-3: Heat-map of gene expression in the heart during *Xenopus laevis* metamorphosis. *Xenopus* stages are indicated at the top according to (Nieuwkoop and Faber, 1994) (NF) and gene names are indicated on the left of the heat-map. The level of gene expression is indicated in blue for a high level, in grey for a moderate level and in red for a low level of expression. fn1: fibronectin 1; col1a1: collagen, type I, alpha 1.

To look at the variation of gene expression between the four different *Xenopus laevis* stages, NF57 was established as the group control and the other three stages were normalised with it to obtain the delta delta Ct ($\Delta \Delta Ct$) values and then the fold change (FC) values were obtained using the formula $2^{\Delta \Delta Ct}$. Graph Pad Prism 6 software was used to create graphs and look at statistical differences. The ROUT method was used to identify outliers that were far enough from the mean of the data set to be called outliers based on the ΔCt values. Statistics were carried out on ΔCt values using the D'Agostino-Pearson omnibus normality test ($\alpha=0.05$) to assess if the data had a normal distribution (data were distributed in a 'bell shape', clustered around the mean) or not (data points were distributed far and/or unequally from the mean). This test was necessary to know which statistical test to use. The samples (four different stages) were all compared to each other so if the data passed the normality test the parametric Ordinary one-way ANOVA test (P value < 0.05) was applied and if they did not the non-parametric Kruskal Wallis test (P value < 0.05) was applied. In order to create graphs to look at the variation of expression the \log_2FC was used for the y axis in function of the stages of development on the x axis. The analysis revealed different gene expression profiles in the heart in function of the stages of development during metamorphosis (figure 5-4, appendix 3). Some genes showed an upregulation of expression such as *col1a1* (figure 5-4A and A'), or a downregulation of expression such as *MMP14* (figure 5-4B and B') during metamorphosis from stage 57 to the adult stage. Some genes showed specific regulation at the metamorphic climax (stage 61), some were upregulated such as *ADAMTS5* (figure 5-4C and C') and some were downregulated such as *ADAMTS20* (figure 5-4D and D'). Some expression profiles did not show a difference of expression in the heart during metamorphosis such as *TIMP3* (figure 5-4E and E').

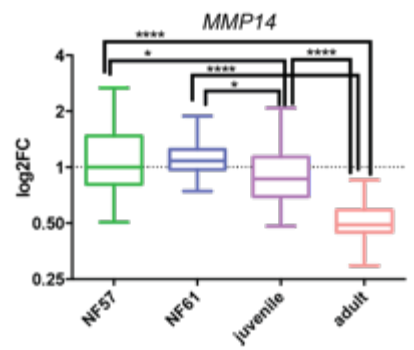
The analysis of the results from the quantitative PCR, realised using the microfluidic method, on *Xenopus laevis* heart sample at stage 57 (pre-metamorphosis), stage 61 (metamorphic climax), juvenile and adult (post-metamorphosis) showed different level and regulation of ECM components, metalloproteinases and TIMPs gene expression (table 5-2).



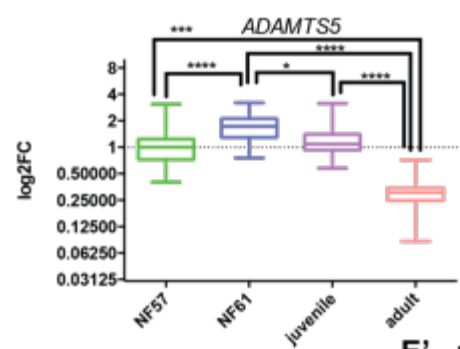
A' - up regulated during metamorphosis



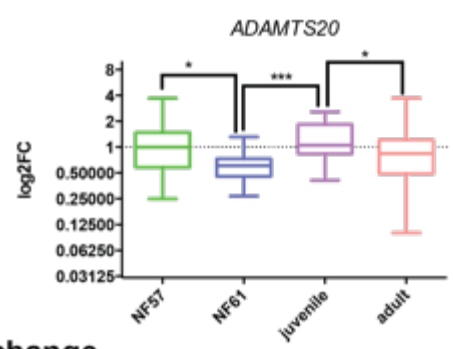
B' - down regulated during metamorphosis



C' - up regulated at metamorphic climax



D' - down regulated at metamorphic climax



E' - no change

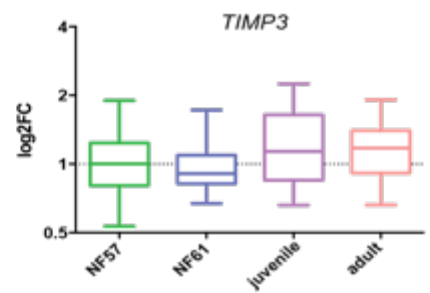


Figure 5-4: Different profile of gene expression in the heart during *Xenopus laevis* metamorphosis. Control hearts from stage 57 (NF57), stage 61 (NF61), juvenile and adult *Xenopus laevis*, corresponding at pro-metamorphosis, metamorphic climax and post-metamorphosis period, were used to look at gene expression. (A) Some genes were upregulated during metamorphosis such as *col1a1* (A') whereas (B) some genes were downregulated during metamorphosis such as *MMP14* (B'). (C) Some genes were upregulated at metamorphic climax such as *ADAMTS5* (C') whereas (D) some genes were downregulated at metamorphic climax such as *ADAMTS20* (D'). (E) Some genes did not show a change in their expression in the heart during metamorphosis such as *TIMP3* (E'). Stages were according to (Nieuwkoop and Faber, 1994) (NF). The height of the box shows the interquartile range (IQR), the line in the box shows the median and the whiskers show the minimum and the maximum values. Stars on the graphs show statistical differences with *, $p < 0.05$, **, $p < 0.01$, ***, $p < 0.001$, ****, $p < 0.0001$.

Table 5-2: Summary table of the different gene expression profiles in the heart during *Xenopus laevis* metamorphosis. Some genes were highly expressed (written in blue), some had a moderate expression level (written in grey) and some were lowly expressed (written in red) in the *Xenopus laevis* heart undergoing metamorphosis. During metamorphosis from stage 57 to the adult frog some gene expression showed no change such as *TIMP3* (first column), some genes were upregulated such as *col1a1* (second column) or downregulated such as *ADAMTS1* (third column). Some genes were specifically upregulated such as *VCAN* (fourth column) or downregulated such as *syndecan2* (fifth column) at the metamorphic climax.

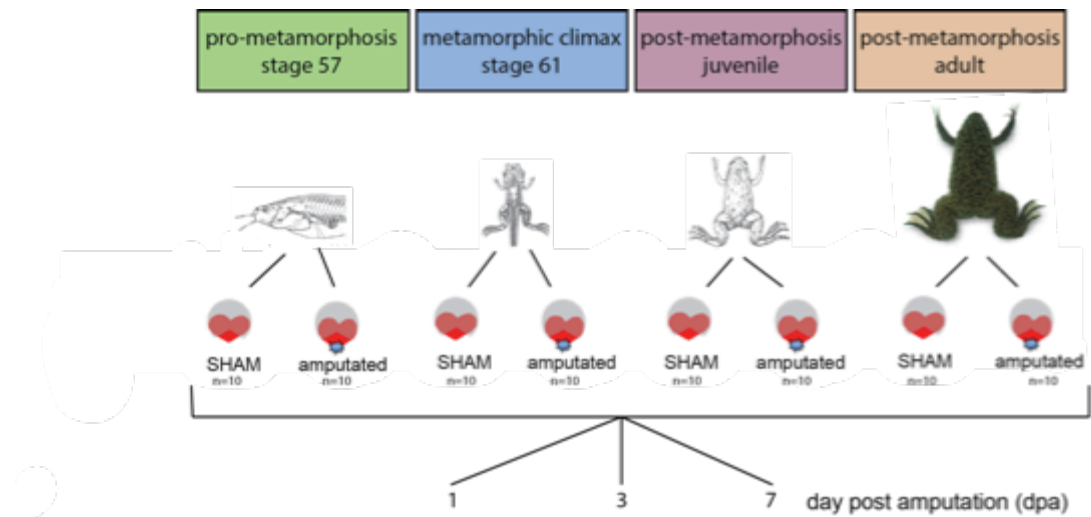
metamorphosis			metamorphic climax	
no change	up regulated	down regulated	up regulated	down regulated
<i>TIMP3</i>	<i>col1a1</i>	<i>ADAMTS1</i>	<i>VCAN</i>	<i>syndecan2</i>
<i>ADAMTS14</i>	<i>ADAMTS8</i>	<i>ADAM9</i>	<i>ADAMTS5</i>	<i>ADAMTS20</i>
<i>ADAM17</i>	<i>TIMP2</i>	<i>MMP14</i>	<i>fn1</i>	<i>ADAM10</i>
<i>ADAMTS12</i>	<i>ADAMTS15</i>	<i>ADAM33</i>	<i>ADAMTS9</i>	<i>ADAMTS18</i>
<i>syndecan1</i>	<i>ADAMTS2</i>	<i>ADAM15</i>	<i>ADAMTS17</i>	<i>uPAR</i>
<i>tPa</i>	<i>syndecan3</i>	<i>syndecan4</i>	<i>ADAMTS19</i>	
<i>ADAM11</i>	<i>PAI1</i>	<i>ADAMTS10</i>	<i>TIMP1</i>	
<i>ADAMTS13</i>	<i>ADAMTS3</i>	<i>ADAMTS6</i>	<i>ADAMTS7</i>	
<i>ACAN</i>	<i>ADAMTS4</i>	<i>ADAM19</i>	<i>ADAM12</i>	
	<i>MMP1</i>	<i>MMP7</i>	<i>tenascin-C</i>	
		<i>MMP9</i>	<i>ADAM22</i>	
			<i>ADAMTS16</i>	
			<i>ADAM23</i>	
			<i>ADAM28</i>	

5.2.2.2 Gene expression in the heart after ventricular resection during *Xenopus laevis* metamorphosis

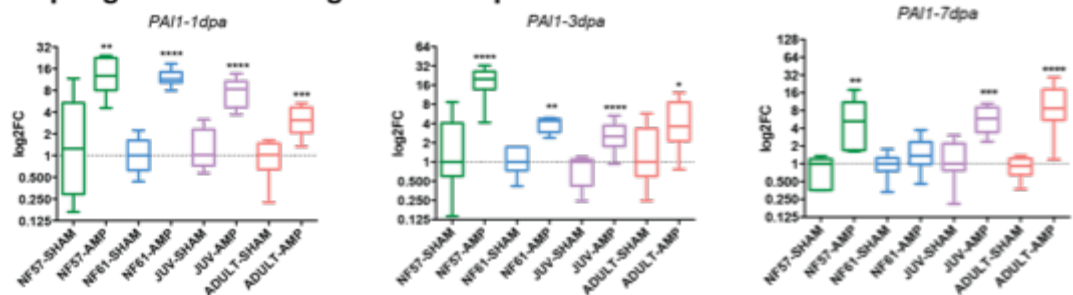
As described in section 5.2.2.1 for the control hearts gene expression analysis the quality of the results was analysed using the Real-Time PCR Analysis v4.1.3 software (Fluidigm) and any data without any or non-specific gene amplification (Ct values) were discarded. Data were normalised using the same five housekeeping genes that were *baf60*, *hand2*, *pten*, *akt1* and *smn2* to obtain the delta Ct (Δ Ct) values. The results were grouped into four groups, according to (Nieuwkoop and Faber, 1994) (NF) *Xenopus laevis* stages, NF57 (pro-metamorphosis), NF61 (metamorphic climax), juvenile and adult (post-metamorphosis). Ten hearts were collected at 1, 3 and 7 days post the amputation procedure for all the experimental conditions (figure 5-2). SHAM samples were used as the placebo control for the ventricular resection surgery. Embryos were treated the same way for both procedures but for the SHAM embryos, the pericardial sac was opened but the ventricle was not amputated (figure 5-2). In order to look at the variation of gene expression between the four different developmental stages and the three different time points for each one, the data from the amputated hearts (Δ Ct values) were normalised using the data from the SHAM hearts (Δ Ct values) in order to obtain the delta delta Ct ($\Delta\Delta$ Ct) values and then subsequently the fold change (FC) values were obtained using the formula $2^{\Delta\Delta Ct}$. Graph Pad Prism 6 software was used to create the graphs and look at statistical differences. The ROUT method was used to identify outliers that were far enough from the mean of the data set to be called outliers based on the ddCt values. Statistics were carried out on $\Delta\Delta$ Ct values using the D' Agostino-Pearson omnibus normality test ($\alpha=0.05$) to assess if the data had a normal distribution (data were distributed in a 'bell shape', clustered around the mean) or not (data points were distributed far and/or unequally from the mean). This test was necessary to know which statistical test to use. Each amputated sample for each stage and each time point was compared to the corresponding SHAM sample. If the data passed the normality test, the parametric unpaired Welch's *t*-test (P value < 0.05) was applied (this test compared two independent groups, SHAM and amputated, that could be of unequal variance and sample size but with a normal

distribution). If they did not pass the normality test, the non-parametric Mann–Whitney *U* test (*P* value < 0.05) was applied. In order to create graphs to look at the variation of expression, the log₂FC was used for the y axis in function of the stages of development and the experimental conditions on the x axis. The analyses revealed different interesting gene expression profiles in the heart in function of the stages of development during metamorphosis and in function of the day post amputation (figure 5-5, appendix 4). Some genes were upregulated in all stages after amputation during metamorphosis such as *PAI1* at 1, 3 and 7 dpa (figure 5-5A). Some genes were only upregulated after amputation at stages NF57 and NF61 such as *ADAMTS14* at 1 and 3 dpa (figure 5-5B). Some genes were upregulated after amputation at metamorphic climax such as *col1a1* at 1,3 and 7 dpa (figure 5-5C) and some genes were downregulated after amputation such as *ADAMTS5* in stage 57, stage 61 and juvenile at 1dpa (figure 5-5D).

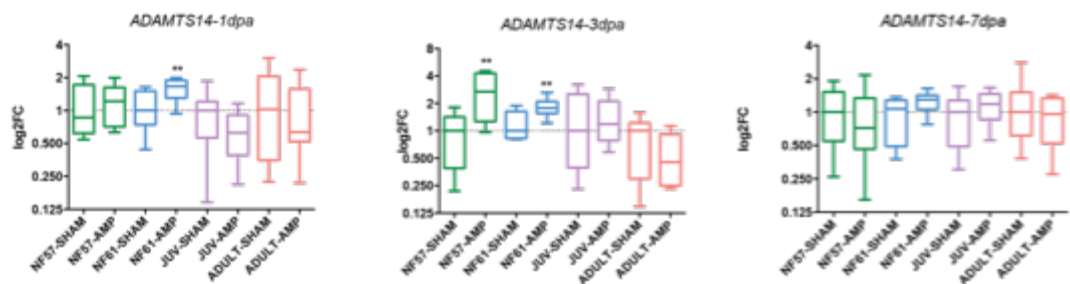
The analysis of the results from the quantitative PCR, investigated using the microfluidic method, on *Xenopus laevis* SHAM and amputated heart samples of stage 57 (pro-metamorphosis), stage 61 (metamorphic climax), juvenile and adult (post-metamorphosis) frogs at 1, 3 or 7 day post amputation showed a different regulation of ECM components, metalloproteinases and TIMPs expression (table 5-3).



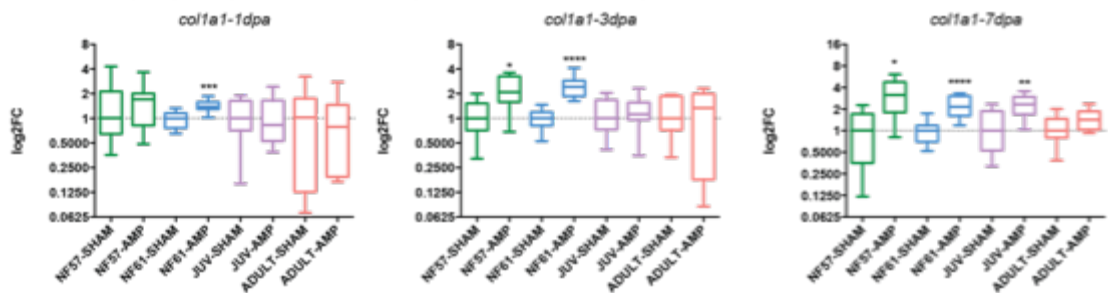
A - Up regulated in all stages after amputation



B - Up regulated only in stages NF57 and NF61 after amputation



C - Mostly up regulated in stage NF61 after amputation



D - Down regulated after amputation

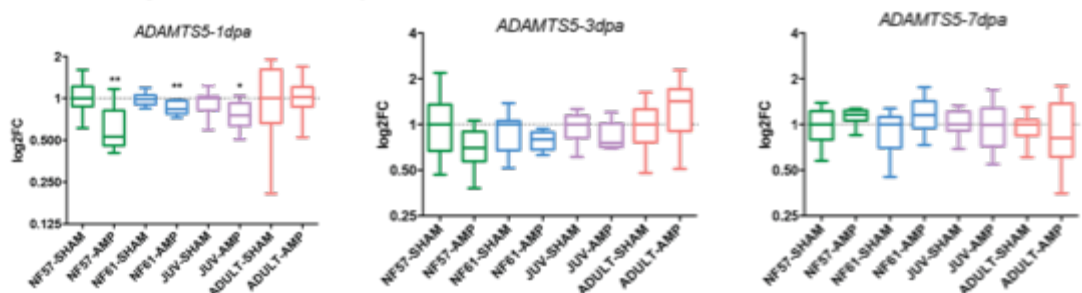


Figure 5-5: Different gene expression profiles in the heart after ventricular resection during *Xenopus laevis* metamorphosis. SHAM and amputated hearts from stage 57 (NF57), stage 61 (NF61), juvenile (JUV) and adult *Xenopus laevis*, representative of the pro-metamorphosis, metamorphic climax and post-metamorphosis periods respectively, were used to look at gene expression at 1, 3 and 7 days post amputation (dpa). SHAM hearts were used as placebo controls for the surgery and were used for the gene regulation analysis to normalise the data from the amputated hearts. (A) Some genes were upregulated in all stages after amputation during metamorphosis such as *PAI1*. (B) Some genes were only upregulated after amputation at stages NF57 and NF61 such as *ADAMTS14*. (C) Some genes were upregulated after amputation at metamorphic climax such as *col1a1* and (D) some genes were downregulated after amputation such as *ADAMTS5*. Stages were determined according to (Nieuwkoop and Faber, 1994) (NF). The height of the box shows the interquartile range (IQR), the line in the box shows the median and the whiskers show the minimum and the maximum values. Stars on the graphs show statistical differences with *, $p < 0.05$, **, $p < 0.01$, ***, $p < 0.001$, ****, $p < 0.0001$.

Table 5-3: Summary table of the different gene expression profiles in the heart after ventricular resection during *Xenopus laevis* metamorphosis. During metamorphosis from stage 57 to adult frog some genes were upregulated in all stages such as *tPa* (first column) whereas some genes were only upregulated in stage NF57 and NF61 such as *MMP14* (second column). Some genes were mostly upregulated in stage NF61 such as *col1a1* and some genes were downregulated such as *ADAMTS5* (fourth column). Some genes were highly expressed (written in blue), some had a moderate expression level (written in grey) and some were lowly expressed (written in red) in the *Xenopus laevis* control hearts undergoing metamorphosis.

After ventricular resection some genes were:			
up regulated in all stages	up regulated only in stage NF57 and NF61	mostly up regulated in stage NF61	down regulated
<i>PAI1</i>	<i>ADAM33</i>	<i>tenascin-C</i>	<i>ADAMTS5</i>
<i>fn1</i>	<i>ADAMTS6</i>	<i>ADAM33</i>	<i>ADAMTS18</i>
<i>tPa</i>	<i>ADAMTS10</i>	<i>ADAMTS13</i>	<i>uPAR</i>
<i>TIMP1</i>	<i>syndecan3</i>	<i>TIMP3</i>	<i>ADAMTS12</i>
<i>MMP1</i>	<i>ADAMTS14</i>	<i>ADAMTS15</i>	
<i>syndecan4</i>	<i>ADAMTS20</i>	<i>ADAMTS4</i>	
<i>MMP9</i>	<i>ADAMTS9</i>	<i>col1a1</i>	
<i>MMP7</i>	<i>MMP14</i>	<i>ADAM9</i>	
<i>ADAM28</i>	<i>ADAMTS2</i>	<i>ADAMTS6</i>	
<i>ACAN</i>	<i>ADAMTS17</i>	<i>ADAMTS8</i>	
<i>ADAM23</i>		<i>ADAM12</i>	
<i>VCAN</i>		<i>ADAM15</i>	
<i>ADAM17</i>		<i>ADAMTS10</i>	
		<i>ADAM19</i>	

5.3 Discussion

5.3.1 ADAMTSs, versican, aggrecan and TIMPs expression in the skin and the brain during *Xenopus laevis* metamorphosis

5.3.1.1 Brain remodeling during *Xenopus laevis* metamorphosis

In the *Xenopus laevis* brain from stage 57 to the adult stage, ACAN and VCAN were expressed and the hyaluronanases family members were the most expressed ADAMTSs (figure 5-1 B' and B''). It is known that lecticans/hyaluronans (aggrecan, versican, neurocan and brevican) are the most abundant CSPGs in the brain and the hyaluronanases family of ADAMTSs comprising ADAMTS1, 4, 5, 8, 9, 15 and 20, can cleave them. Aggrecan can be cleaved by all of them except by ADAMTS20, versican by all of them except by ADAMTS8, brevican by ADAMTS4 and 5 and neurocan by ADAMTS4 (Kelwick et al., 2015a) (Tauchi et al., 2012). ADAMTS1 (Krampert et al., 2005), ADAMTS5 (McCulloch et al., 2009b), ADAMTS9 (Jungers et al., 2005), ADAMTS20 (Llamazares et al., 2003), ADAMTS8 (Dunn et al., 2006), ADAMTS4 and ADAMTS15 (Levy et al., 2015) are expressed in the brain in physiological conditions. The conservation of expression of these ADAMTSs in the brain suggests *Xenopus laevis* is a good model to study brain remodeling during development.

PCSG and ADAMTSs have been shown to have a region dependent expression profile in the brain mostly in perineuronal nets such as aggrecan and brevican (Dauth et al., 2016) and ADAMTS15 and ADAMTS8 (Rossier et al., 2015) (Levy et al., 2015). It will be interesting to look in more detail at the specific location of the ADAMTSs in the *Xenopus laevis* brain by *in situ* hybridisation. ADAMTS4 has been shown to promote neurite growth by degrading CSPGs, independent of its proteolytic activity, by activating MAP/ERK (mitogen activated protein/extracellular signal-regulated kinase) signaling pathway (Hamel et al., 2008). ADAMTS4 and 5 play a role in brain development by cleaving reelin, an extracellular signaling protein essential for neuronal migration, synapse development and function (Krstic et al., 2012). ADAMTS4, ADAMTS8 and ADAMTS5 were the most expressed hyaluronanases in the *Xenopus laevis* brain suggesting that their function might be conserved and that they may play a role in brain development (figure 5-1 B').

Interestingly *ADAMTS6* was the most expressed gene of the *ADAMTS* family in the *Xenopus laevis* brain (figure 5-1 B'). However nothing is known about its function in brain development. It has been shown that *ADAMTS6* disrupts the deposition of microfibrils at heparan sulphate-rich cellular interfaces (such as focal adhesions and epithelial cell-cell junctions) by its metalloproteinase activity *in vitro* in retinal epithelial cells whereas *ADAMTS10* downregulates *ADAMTS6* and is required for the integrity of these structures. The depletion of *ADAMTS10* can be rescued by syndecan4 that can be cleaved by *ADAMTS6* (Cain et al., 2016). Syndecan4 is expressed in the brain and has been shown to play a role in neural cell proliferation and axon formation in zebrafish (Luo et al., 2016). The high level of remodeling in the *Xenopus laevis* brain during metamorphosis could explain the high expression of *ADAMTS6* needed to disorganize focal adhesions by cleavage of syndecan4 promoting cell migration and the low level of *ADAMTS10* expression that modulates this action.

The ECM remodeling by metalloproteinases is crucial during brain development and has to be highly regulated. *TIMP2* and *TIMP3* were more expressed than *TIMP1* in the *Xenopus laevis* brain during metamorphosis (figure 5-1 B'''), which has been shown in mouse (Pagenstecher et al., 1998). *TIMP2* plays a role in the development of the central nervous system (Brew and Nagase, 2010) and *TIMP3* can inhibit several *ADAMTSs* such as *ADAMTS4* and *ADAMTS5* important during brain development (Lim et al., 2010).

After brain injury CSPGs inhibit axonal regeneration (Barros et al., 2011) (Avram et al., 2014). Some *ADAMTSs* such as *ADAMTS1*, *ADAMTS5* and *ADAMTS9*, are induced after spinal cord injury (Demircan et al., 2013). Local delivery of *ADAMTS4* has been shown to promote spinal cord recovery such as motor recovery and axonal regeneration (Tauchi et al., 2012). These findings suggest that the *ADAMTSs* can play different roles after brain injury, and could be an attractive therapeutic option. *Xenopus laevis* is a good model to study the regeneration of the central nervous system after injury and neurodevelopmental disorders (Lee-Liu et al., 2016) (Pratt and Khakhalin, 2013).

5.3.1.2 Skin remodeling during *Xenopus laevis* metamorphosis

In the skin at metamorphosis and even more so after metamorphosis compared to before, members of the hyalactanases family were all expressed and upregulated with *ADAMTS8*, *ADAMTS15* and *ADAMTS1* being the most expressed and *ADAMTS9* and *ADAMTS20* the least expressed (figure 5-1 C'). *ACAN* was not detected but *VCAN* was expressed at similar levels in the skin during metamorphosis (figure 5-1C''). Different phenotypes were seen using different strains of *ADAMTS5* knockout mice. In one study it has been shown that the accumulation of non-degraded versican in the PCM of fibroblasts leads to their transition to myofibroblasts, which is necessary for wound healing (Hattori et al., 2011). In the other study, the accumulation of non-degraded aggrecan blocked the transition of fibroblast immature cells to mature contractile fibroblasts necessary for wound healing (Velasco et al., 2011). The process of transition between fibroblasts and myofibroblasts has been shown to be regulated by TGF β and the PCM composition in aggrecan and versican associated with hyaluronan (HA) that could bind to the cell receptor CD44 could regulate this signaling pathway (Hattori et al., 2011) (Velasco et al., 2011).

ADAMTS20 mutant mice (called belted) show a phenotype in melanoblast colonisation of the skin causing white belts in their lumbar region, possibly caused by the dysregulation of the ECM composition such as the accumulation of versican and the dysregulation of Kit signaling by inhibition of the response to soluble Kit ligand (sKitl), which is necessary for melanoblast development by direct action or due to abnormal ECM composition (Silver et al., 2008). The high expression of the hyalactanases family in the *Xenopus laevis* skin suggests that they may play a role in the versican turnover necessary for skin remodeling.

ADAMTS2 was highly expressed in the *Xenopus laevis* skin (figure 5-1 C') and it has been shown that it is crucial for fibrillar collagen organization. Mutant mice for *ADAMTS2* show skin fragility. The aminoprocollagen (a chain of collagen with a propeptide at the N-terminal position due to the lack of cleavage by *ADAMTS2*) accumulates and does not assemble correctly, creating a structure with poor mechanical properties leading to skin fragility (Bekhouche

and Colige, 2015). The high expression of *ADAMTS2* in *Xenopus laevis* skin suggests that it plays a role in skin remodeling.

TIMP1 was the most expressed member of the *TIMP* family in the *Xenopus laevis* skin (figure 5-1 C'') and has been shown to play a role in skin homeostasis (Hornebeck, 2003).

5.3.2 Gene expression in the heart undergoing remodeling and in the heart after ventricular resection during *Xenopus laevis* metamorphosis

5.3.2.1 Heart remodeling during *Xenopus laevis* metamorphosis

ECM components, metalloproteinases and TIMPs had different expression (figure 5-3) and regulation profiles (figure 5-4) in the *Xenopus laevis* heart during metamorphosis (table 5-2).

ECM components were upregulated in heart undergoing remodeling during metamorphosis. *Col1a1* were up regulated during metamorphosis (figure 5-4A and A'). This suggests that it is an important ECM component for cardiac ECM remodeling from tadpole stage to adult stage. Similar results have previously been reported in mouse (Peacock et al., 2008). *fn1* and *VCAN* were upregulated at metamorphic climax (appendix 8-12) suggesting their role in the heart remodeling from tadpole to froglet stage. Studies on mutant mice for versican (called *hdf* (heart defect) mice) have a homozygous lethal chromosomal 13 insertion that was mapped to the *Cspg2* (*VCAN*) gene, showed that homozygous mutant mice died before birth between ED10.5 and 11.0 with severe heart development defects (Yamamura et al., 1997). These phenotypes were also seen in mutant mice for hyaluronan (HA) that can bind to versican (Camenisch et al., 2000). Mutant mice for fibronectin died before birth at ED10 due to cardiovascular and vascular defects and *fn1* played a role in heart development by regulating Notch signaling (Lockhart et al., 2011) (Wang et al., 2013). These results confirm previous studies on the important role of ECM components during heart development.

ECM remodeling by metalloproteinases is an important process during heart development. Most of the metalloproteinases were upregulated in *Xenopus laevis* hearts during metamorphosis. The pro-collagen N-propeptidases *ADAMTS2* and *ADAMTS3* (appendix 8-10) showed the same upregulation of expression as *col1a1* during metamorphosis suggesting their

role in the collagen maturation during cardiac ECM remodeling from tadpole stage to adult stage. Several ADAMTSs have been identified to be expressed in the developing heart and play a role in heart formation, especially members of the hyaluronanase family that cleave the early versican-rich cardiac ECM. *ADAMTS5* and *ADAMTS9* were upregulated at the metamorphic climax in *Xenopus laevis* heart, suggesting their role in the remodeling of the early versican-rich ECM, which is replaced by the mature cardiac ECM (figure 5-4C', appendix 8-12). *ADAMTS9* expression has been shown in the developing mouse heart at the same location as the neo-epitope DPEAAE, which is exposed after cleavage of versican by this protease. Hemizygous mutated mice for *ADAMTS9* showed a decrease of detection of this neo-epitope, an accumulation of non-cleaved versican and heart defects suggesting an important role of *ADAMTS9* for ECM remodeling of the early versican-rich matrix (Kern et al., 2010). Heart phenotype was also seen in knockout mice for *ADAMTS5* due to the reduction of versican cleavage. This phenotype was rescued by intercrossing the mutant mice for *ADAMTS5* with heterozygous mutant mice for versican suggesting that *ADAMTS5* is also an important protease to clear the initial versican-rich cardiac ECM (Dupuis et al., 2011). *ADAMTS20* is downregulated at the metamorphic climax suggesting that the regulation of hyaluronanases is necessary for cardiac ECM remodeling.

Several metalloproteinases such as *ADAMTS1*, *ADAMTS6*, *ADAMTS10*, *MMP14*, *MMP9* and *ADAM9* (figure 5-4A and A', appendix 8-11) were downregulated during metamorphosis suggesting that they play a role in early cardiac remodeling during metamorphosis but not in the adult heart. *MMP9* and *MMP14* have been identified in heart development and can cleave fibrillar collagen that is present in the cardiac ECM (Fan et al., 2012). Knockout mice for *ADAM17* and *ADAM19* and knockout mice for *ADAM9* and *ADAM18* show heart defects when mutated for both genes suggesting function redundancy of these proteases during cardiac development (Horiuchi et al., 2005). It has been shown that *ADAMTS1* cleaves versican at early stages and during trabeculation; knockout mice show a heart phenotype and hypertrabeculation due to accumulation of intact versican (Stankunas et al., 2008).

The expression of the ECM components and the metalloproteinases was conserved in mammals and the morphological organisation of the mammalian

heart is conserved, which makes the *Xenopus laevis* heart a good model to study heart development and suggests the involvement of ECM in heart congenital diseases (Hempel and Kühl, 2016).

5.3.2.2 Heart regeneration during *Xenopus laevis* metamorphosis

After cardiac injury three major processes are necessary for heart regeneration: (1) the removal of damaged cardiac structures associated with an inflammatory response site, (2) the reparative process and (3) the repopulation of the wound site with cardiomyocytes for regeneration (Uygur and Lee, 2016). The infiltration of the damaged tissue by neutrophils and macrophages is associated with an increase of MMP9 expression and activity to allow the migration of the inflammatory response cells through the damaged site (Tao et al., 2004). The reparative process starts with the rebuilding of a new highly hydrated cardiac ECM composed of collagen, fibronectin, tenascin-C and HA to maintain robustness of the damaged ventricular wall and to allow cardiomyocytes proliferation and migration toward the wound site (Mercer et al., 2013) (Wang et al., 2013). Adult *Xenopus laevis* hearts do not regenerate after ventricle resection but show a deposition of fibrotic tissue (excess of collagen and fibronectin) and a hypertrophy of the amputated ventricle characteristic of a non regenerate heart as seen in adult mammals (Marshall et al., 2017). Past metamorphosis juvenile and adult *Xenopus laevis* frogs cannot regenerate the heart after ventricle resection (unpublished data, Coen L.) suggesting a difference in gene expression, regulation and function before and after metamorphosis

The present study was focused on the early response (1, 3 and 7 days post amputation (dpa)) of the ECM components, metalloproteinases and their inhibitors to heart injury. A heart injury model was established by carrying out ventricular resection in the *Xenopus laevis* tadpole at pro-metamorphosis (stage 57), at metamorphic climax (stage 61) and post-metamorphosis (juvenile and adult frog). Gene regulation in response to ventricle injury was stage- and time-dependent (figure 5-5, appendix 4).

The most regulated genes observed after ventricle amputation were genes involved in the urokinase-type/tissue-type plasminogen activator (uPa/tPa), plasmin, MMPs pathway and the inhibitor of uPA/tPa, plasminogen

activator inhibitor 1 (PAI1). tPa is a serine protease that converts the zymogen plasminogen to the active serine protease plasmin that activates the zymogen pro-MMP9 to active MMP9. tPa is inhibited by PAI1 (Ghosh and Vaughan, 2012) (figure 5-6). Under physiological conditions, PAI1 regulates uPA/tPa/plasmin/MMP proteolytic activities to maintain tissue homeostasis but under pathological conditions (such as fibrosis after cardiac injury caused by myocardial infarction) PAI1 is highly regulated and contributes to the accumulation of non-degraded ECM such as ECM rich in collagen leading to fibrotic tissue (Takeshita et al., 2004). However it has been shown that a transient collagen-rich scar is necessary for heart regeneration in zebrafish and this process is regulated by TGF β that recruits fibroblast-like cells, which synthesize collagen, at the wound site (Chablais and Jazwinska, 2012). PAI1 has been shown to be regulated by TGF β and latent TGF β is activated by plasmin, which is activated by tPa, and by MMP9, which is activated by plasmin (Ghosh and Vaughan, 2012) (Lyons et al., 1990) (Yu and Stamenkovic, 2000) (figure 5-6). In the present study *tPa*, *PAI1* and *MMP9* were upregulated in all stages after amputation (figure 5A, appendix 4) confirming the important regulation of this signaling pathways in response to heart injury and for cardiac regeneration (figure 5-6).

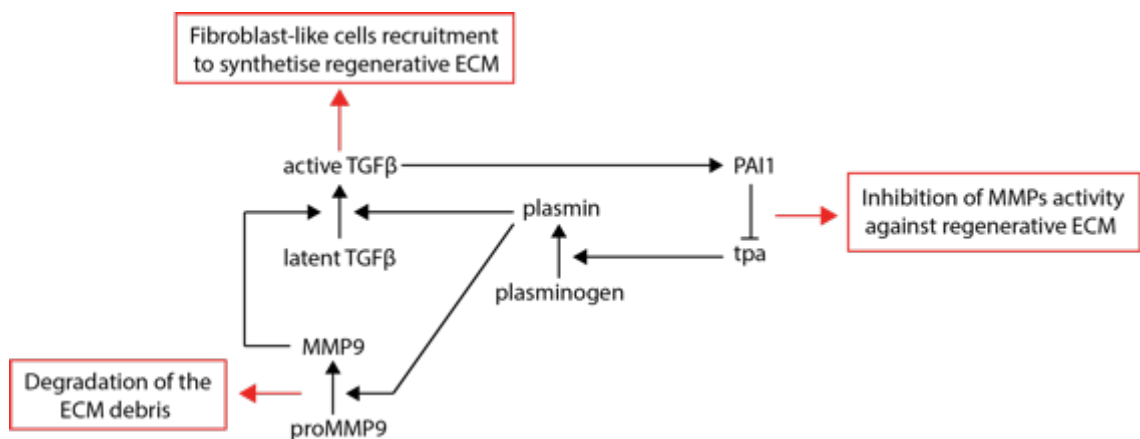


Figure 5-6: Model of regulation of the cardiac regeneration process by the uPA/tPa/plasmin pathways and the inhibitor PAI1. Activation of zymogen pro-MMP9 by plasmin, activated by tPa is necessary to clear the wound site of ECM debris. Active TGF β , activated by the pathway tPa/plasmin, recruits fibroblast-like cells to synthesise the collagen rich regenerative ECM at the wound site. Regulation of the tPa/plasmin pathway by the inhibitor PAI1, positively regulated by TGF β , is necessary to inhibit the action of MMP9 against the transient regenerative ECM.

ECM components of the transient regenerative cardiac ECM, such as collagen (*col1a1*), fibronectin (*fn1*) and *tenascin-C*, were upregulated after ventricle amputation at 1, 3 and 7 dpa in stages before and past metamorphosis (figure 5-5C, appendix 4). This suggests that the early creation of a transient ECM scar deposition is common at all stages and is not the cause of the loss of regeneration observed in adult *Xenopus laevis*. Upregulation of CSPGs such as *VCAN* and *ACAN* was also observed after heart amputation, mostly at 3 dpa in pro and past metamorphosis stages (appendix 4). A study in rats shows that in response to aortic banding, proteins are upregulated as well as *VCAN* and *ACAM* mRNA levels (Vistnes et al., 2014). CSPGs can interact with HA to create a highly hydrated ECM, such as the regenerative cardiac ECM, and are expressed in the immature cardiac ECM (Mercer et al., 2013) (Lockhart et al., 2011). The data presented in this study suggests that versican and aggrecan could be components of the transient ECM scar, creating a highly hydrated matrix promoting cell migration. Although the deposition of a collagen-rich scar has been shown to be essential for heart regeneration, its degradation by proteases is crucial to allow its replacement by new cardiomyocytes (Chablais and Jazwinska, 2012).

ADAMTS5 has been shown to clear the initial versican-rich cardiac ECM (Dupuis et al., 2011). *ADAMTS5* was downregulated at 1 dpa in all stages except the adult stage (figure 5-5D). These data suggest that the early inhibition of *ADAMTS5* is necessary for the formation of the transient scar ECM composed of CSPGs. Some genes were only upregulated at stage 57 and stage 61, corresponding at before and at metamorphic climax, such as *ADAMTS14* and *ADAMTS2* (figure 5-5B, appendix 4). These two *ADAMTS*s are pro-collagen N-propeptidases and *ADAMTS2* and *ADAMTS14* have been shown to be necessary for the maturation of the collagen by cleaving the propeptide of the α chains (Bekhouche and Colige, 2015). Mature α chains assemble to form collagen fibrils. These data suggest that *ADAMTS2* and *ADAMTS14* could be necessary for the correct organisation of the collagen-rich scar after cardiac amputation. *ADAMTS9* has been shown to play a role in the remodeling of the initial versican-rich cardiac ECM (Kern et al., 2010). *ADAMTS9* is upregulated in stage 61 only at 7dpa (appendix 4) suggesting it has a role in the degradation of the transient regenerative ECM necessary for

its replacement by new cardiomyocytes. A study in rats shows that in response to aortic banding, *ADAMTS4* and *ADAMTS1* mRNA and proteins were upregulated (Vistnes et al., 2014). In the present study an upregulation of *ADAMTS4* after 1 and 7 dpa in pro and past metamorphosis stages and a low upregulation of *ADAMTS1* in adult heart at 1 and 3 dpa were observed (appendix 4). This could be explained by the difference in the heart injury procedure.

Syndecan4 was upregulated in all stages at 1, 3 and 7 dpa (appendix 4). Full-length syndecan4 has been shown to be pro-fibrotic in heart fibrosis whereas syndecan4 shedding fragments have been shown to have an anti-fibrotic effect (Lunde et al., 2016). Several *MMPs*, *ADAMs* and *ADAMTSs* were upregulated after ventricle resection in *Xenopus laevis*, suggesting a regulation of syndecan4 activity by the proteases leading to pro-fibrotic effects in the post metamorphosis heart, which cannot regenerate, or anti-fibrotic effects before metamorphosis when the *Xenopus laevis* heart has the capacity to regenerate.

TIMP1 has been shown to be up regulated after cardiac injury and *TIMP3* plays a role in remodeling following myocardial infarction (Fan et al., 2012). *TIMP1* was upregulated in all stages at 1, 3 and 7 dpa whereas *TIMP3* was mostly upregulated at 1 and 3 dpa (appendix 4) suggesting they have a function in the inhibition of the metalloproteinases activities against the early ECM scar deposition at the wound site.

To summarize, ECM components, proteases and their regulators were differently regulated after ventricle resection in *Xenopus laevis* depending on the stage of development and the time after the amputation. This suggests they have an important role in cardiac regeneration. Some expression and regulation profiles were similar to previous studies in other model organisms demonstrating that *Xenopus laevis* could be a good model to study cardiac regeneration. The loss of this ability past metamorphosis is similar to the embryonic and adult transition in mammals.

The present study looked at 1, 3 and 7 days post amputation showing short-term transcriptional responses of ECM components, proteases and their regulators before, at and after metamorphosis and in the future it would be interesting to look at these long-term gene responses, in months, after ventricle resection to show their role in the regeneration process or fibrosis processes

depending on the regenerative capacity of the *Xenopus laevis* stages of development.

All the data of this chapter were gene expression data, which does not show protease activity, as it is known that most of the metalloproteinases studied here require proteolytic activation to be active and might be inhibited by their inhibitors. In order to assess the activity of the metalloproteinases antibodies against neo-epitope generated after cleavage of their specific substrate can be used (Genovese et al., 2014).

Interestingly it has been shown that thyroid hormone (T3) can regulate the gene expression of MMPs, such as MMP9 and MMP14 in *Xenopus laevis*, by binding to its nuclear receptor that acts as a transcriptor factor by forming a complex with RXR that bind to TRE motifs on the gene promoter (Fujimoto et al., 2007) suggesting a role of the TH in the regulation of ECM remodeling by modulating metalloproteinase expression.

The presented results showed that some ECM components and metalloproteinases were specifically up- or down- regulated at the metamorphic climax when there is a peak of TH, suggesting a regulation of their expression by the TH pathway. To follow this study, in collaboration with Dr. Laurent Coen's team, genes that showed an interesting profile in the heart during metamorphosis (table 5-4) were selected in order to look at their modulation of expression in tadpoles treated with T3 hormones during metamorphosis. The analysis of the results is on going but preliminary analysis showed an interesting profile for some genes such as MMP9, previously showed to be regulated by TH in other organs by its TRE motif. Genomic analysis of the most interesting genes, which would appear to be regulated by TH could show if a TRE motif is present in their promoters.

Table 5-4: List of genes analysed in heart development during *Xenopus laevis* metamorphosis in embryos treated with T3. The different gene categories are indicated in the first two rows and specific gene name is indicated below. For *ADAMTS*, *ADAM*, *MMP*, *TIMP* and *syndecan* only the gene number is indicated in the column meaning *ADAMTS1*, *ADAM7*, *MMP2*, *TIMP1* and *syndecan1* for all different genes. *PAI1*: plasminogen activator inhibitor-1.

metalloproteinases						
<i>ADAMTS</i>	<i>ADAM</i>	<i>MMP</i>	<i>TIMP</i>	ECM	plasminogen	<i>syndecan</i>
1	9	9	3	<i>VCAN</i>	<i>PAI1</i>	1
2	10	7		<i>ACAN</i>		2
4	12	14		<i>tenascin-C</i>		3
5	15					4
6	22					
8	23					
9						
10						
13						
14						
15						
16						
17						
19						
20						

Chapter VI: Discussion

6.1 The ADAMTS family in *Xenopus* genome

In this study *Xenopus* was used as a model organism to begin to study the extracellular matrix (ECM) remodeling during development and specially the role of the metalloproteinases family, the A Disintegrin and Metalloproteinase with Thrombospondin type-1 motifs (ADAMTS) family. The 19 members of the ADAMTS family were identified in *Xenopus* and their evolutionary history was conserved with mouse and human suggesting a conservation of their functions between these species. *Xenopus tropicalis* and *Xenopus laevis* were used in this study. *Xenopus tropicalis* has the advantage of being diploid, which can facilitate genetic manipulation to carry out functional experiments such as loss of function using morpholinos and CRISPR/Cas9 (Guo et al., 2014), however the embryos are small making targeted injection into specific blastomere more difficult (Harland and Grainger, 2011). *Xenopus laevis* has the disadvantage of being allotetraploid (genome composed of subgenome L and subgenome S) meaning that both copies of a gene have to be targeted in order to accomplish genetic manipulation to carry out functional experiments. A recent version of the *Xenopus laevis* genome has been published (Session et al., 2016) with better sequencing and gene annotation, moreover the embryos are bigger than the *Xenopus tropicalis* embryos facilitating manipulation such as targeted injection and visualisation of phenotypes (Harland and Grainger, 2011). These two *Xenopus* species diverged from each other around 48 million years ago (Ma) before the divergence of the two diploid species (that are still unknown) that gave rise to the *X. laevis* subgenomes L and S, which occurred around 34 Ma (Session et al., 2016). The conservation of the chromosomal gene organisation (synteny) and the phylogeny of the ADAMTS family between *X. tropicalis* and *X. laevis* were established to help understand the evolutionary history of the *Xenopus laevis* genome and assess which subgenome was more conserved to the *Xenopus tropicalis* genome representing the ancestral genome. The 19 ADAMTS genes were found in the *Xenopus laevis* subgenome L and in *Xenopus tropicalis*, the same as in mammals, whereas only 12 were present in the subgenome S due to a loss of copies for seven ADAMTSs (*ADAMTS7*, *ADAMTS8*, *ADAMTS12*, *ADAMTS13*, *ADAMTS16*, *ADAMTS19* and *ADAMTS20*). These proportions follow the ones found for the general

conservation of the protein coding genes between the *Xenopus laevis* subgenomes and the *Xenopus tropicalis* genome (Session et al., 2016) and contribute to the understanding of the evolutionary history of *Xenopus laevis* and *Xenopus tropicalis*. The chromosomal organisation on the *X. laevis* subgenome L was more similar to the one on *X. tropicalis* genome than the *X. laevis* subgenome S supporting the hypothesis that the ancestral chromosomal organisation is the one found in *Xenopus tropicalis* and in the subgenome L of *Xenopus laevis*. In addition identified ADAMTSs genes in this study were not annotated and were located on scaffolds (part of genomic DNA not allocated to a chromosome during genome assembly). By analyses of the synteny of these genes compared to their homoeologous in *Xenopus laevis* subgenomes and their orthologous in *Xenopus tropicalis*, they were assigned to their corresponding chromosome contributing to the improvement of *Xenopus* genomes assembly and annotation.

6.2 ADAMTS9 in the pronephros

Xenopus diverged from mammals some 360 million years ago and has been shown to be a good animal model relative to human as they are both tetrapod, their genomes show conserved synteny and their organ development and function are highly similar (Wheeler and Brandli, 2009).

In this study, in addition to showing that the evolutionary history of the ADAMTS family was conserved between *Xenopus* and human, their expression in different tissues such as kidney, brain, skin and heart were shown to be similar to that found in human (see chapters IV and V). The ECM remodeling during development was investigated; *Xenopus* is a good model to study these events during embryonic development because it can be seen externally unlike in mammals where embryonic development is *in utero*. This advantage allows a good visualisation of the phenotypes due to the disruption of a gene, by gain or loss of function experiments, and can help to define the timing of the apparition of these phenotypes.

ADAMTS9 knockdown caused a defect of pronephros development in *Xenopus laevis* embryos. It has been shown that segmentation and molecular markers are conserved between the *Xenopus* pronephros and the mammalian metanephric nephron (Lienkamp et al., 2012). Different markers expressed at

different times of development were used and their analysis lead to the conclusion that the loss of function of *ADAMTS9* in the pronephros in *Xenopus laevis* disrupt the development of the pronephric tubules and duct from early tailbud stages (using *pax8* as a marker), to tadpole stages (using 4a6 antibody as a marker), but not the development of the glomus, using *wt1* as a marker (see chapter IV). In *Xenopus* the kidney tubulogenesis can be visualised through the surface ectoderm, by injecting mRNA encoding membrane-bound green fluorescent protein (GFP) to allow single cell definition. This advantage helped to understand in an *in vivo* context where cells differentiate, migrate and interact to assemble the pronephros whereas fixed tissues or organ culture was used to study mammalian kidney development (Lienkamp et al., 2012) (Lienkamp et al., 2010). It would be interesting to use these visualisation techniques to characterise in more detail the phenotypes obtained during tubulogenesis when *ADAMTS9* was knocked down.

Chronic kidney disease (CKD) is a common pathological condition, 14.8% of the adult population in the USA had CKD in 2011-2014 as estimated by the US Renal Data System 2016 Annual Data Report, which can lead to an end-stage renal disease (ESRD) with kidney transplant as only treatment. Renal fibrosis is associated with CKD. Recent studies looked at the ECM components and metalloproteinases as potential biomarkers to improve the prognosis and as the potential treatment in a non-invasive manner avoiding the renal biopsy often used (Genovese et al., 2014). Several studies show that some MMPs, such as MMP-2, -7 and -9, have increased expression in kidney diseases (Genovese et al., 2014). *ADAMTS7* expression was increased in elderly mouse kidney, compared to adult mouse kidney, from renal inflammation caused by angiotensin II administration, which is known to play a role in the progression of chronic kidney damage, contributing to renal inflammation and fibrosis. This suggests *ADAMTS7* plays a role in early inflammatory kidney damage associated with aging (Gao et al., 2013). *ADAM19* and *ADAM17* expression are up regulated in kidney diseases (Melenhorst et al., 2006) (Mulder et al., 2012). In this study *ADAMTS9* was shown to play a role during kidney development possibly by the degradation of its substrate versican expressed in the developing kidney. It has been shown that the expression of V0 and V1 isoforms of versican were increased in patients with CKD suggesting versican

as a potential biomarker (Rudnicki et al., 2012). However they did not look at the neo epitope of versican generated by its specific cleavage by ADAMTSs. The increase of V0 and V1 could be due to an increase of intact versican suggesting a lack of action of ADAMTSs or could be due to an increase of cleaved versican suggesting an increase of ADAMTSs activities, possibly of ADAMTS9. Looking at the neo-epitope generated after specific cleavage of ECM components by metalloproteinases such as ADAMTSs, ADAMs and MMPs is called protein fingerprint technology. A comparison of the amount of the cleaved forms compare to the amount of their intact forms could be used as a biomarker for diseases such as CKD by indicating renal fibrosis for example (Genovese et al., 2014). This technology is more reliable than looking at the level of expression of metalloproteinases, as most of them require post translational modifications to be active in order to assess their roles in CKD and potentially their used as biomarkers.

The only treatment for ESRD is kidney transplant causing a high demand for transplantable organs higher than the amount of available organs leading to the development of organ bioengineering and regeneration as potential inexhaustible sources of organs (Orlando et al., 2013). It has been shown that ECM is essential to a correct kidney development *in vitro*, by addition of ECM components in organ culture (Sebinger et al., 2013) or by using whole-kidney ECM scaffolds used after their decellularization (Orlando et al., 2013). *Xenopus* is a robust model to study kidney development *in vitro* by isolating animal caps dissected from embryos at blastula stage and treated with activin and retinoic acid in order to differentiate and form pronephric organoids. These organoids can be transplanted into a host embryo, previously removed of its pronephric anlage tissue, and be functional as proven by the lack of oedema formation that is characteristic of kidney failure. However the success of these transplantations was only of 21% (Krneta-Stankic et al., 2017). These data suggest the essential influence of ECM on correct kidney development *in vitro* and the data in this study, showing the role of ADAMTS9 in pronephros development in *Xenopus laevis*, support the importance of ECM and the secreted proteins present in the ECM. It would be interesting to carry out the transplant experiment in *Xenopus laevis* with animal cap explants from injected embryos with ADAMTS9 morpholinos and analyse their capacity to form pronephric organoids compared

to control embryos as well as adding ECM components, such as versican, to explants in culture to look at the improvement of their development. These explants could be then transplanted and could potentially obtained a higher success rate than previous studies.

6.3 ECM and metalloproteinases in post embryonic development

In this study, the ECM and metalloproteinases gene expression in *Xenopus laevis* during metamorphosis, which is similar to the postembryonic development in mammals, were investigated. This process is regulated by a peak of thyroid hormone (TH) concentration and is comparable to the one during birth in humans, which suggests *Xenopus* is a good model to study ECM remodeling during this important time of development (Brown and Cai, 2007). In *Xenopus* the thyroid hormone signalling pathway regulates main events that occur during metamorphic climax such as the creation of adult organs, organ remodeling, regression of embryonic organs and apoptosis of embryonic cells replaced by adult cells (Buchholz, 2015). Organ remodeling includes pancreas, liver, blood, immune system, skeleton, intestine, brain, olfactory organ and skin (Brown and Cai, 2007).

ECM has been shown to play an important role in organ remodeling during metamorphosis as it is a structural scaffold and can regulate cell-cell and cell-ECM interactions. ECM can interact directly with cells by cell surface receptors, such as integrin, and can indirectly affect these interactions by regulating the availability of various factors, such as growth factors. Cell-cell and cell-ECM interactions determine cell-fate such as programmed death or proliferation. These two processes are highly regulated by TH in time and space during metamorphosis (Fu et al., 2007). The remodeling of the ECM is mainly due to metalloproteinases. Organ remodeling under the control of TH during *Xenopus* metamorphosis is a good model to identify these proteins. By remodeling the extracellular matrix they alter the cell-ECM interactions and regulate cell death and proliferation in specific organs during metamorphosis. The resorption of the tail has been established as a model system since 1962 using an *in vitro* tail culture called tail fins (Gross and Lapiere, 1962). The remodeling of the intestine is another good model as it can be cultured *in vitro* (Su et al., 1997) as well as the resorption of gills (Derby et al., 1979). These

model systems helped to identify proteases, due to the abundance of matrix degradation, cell death and cell proliferation. Most studies looked at MMPs regulation by TH during metamorphosis. MMP14, MMP11 and MMP9TH have a high affinity between their TRE on their promoter and the TR/RXR heterodimer forming a stable complex, which leads to a rapid response to the increase of plasmatic TH (Fujimoto et al., 2007).

In this study the *ADAMTSs* expression in physiological condition have been shown to be conserved in *Xenopus laevis* brain and skin and have previously been shown to be conserved with human and mouse by phylogenetic study (see chapter III). This suggests that their function would be conserved. Functional studies would confirm these hypotheses for *ADAMTSs* genes with known function in the brain, such as *ADAMTS4* and *ADAMTS5* (Krstic et al., 2012), and in the skin, such as *ADAMTS2* (Bekhouche and Colige, 2015). However these studies could generate new findings in regard to *ADAMTSs* genes function in these processes, such as *ADAMTS6*, which showed a high expression level in these organs during metamorphosis. The juvenile and adult *Xenopus laevis* brain and skin organisation is conserved in mammals. ECM components and metalloproteinases gene expression and regulation profiles, such as *VCAN*, *ADAMTS5* and *ADAMTS9*, in the *Xenopus laevis* heart development were similar to the ones found in mammalian heart studies suggesting their conserved function in *Xenopus laevis* (Yamamura et al., 1997) (Kern et al., 2010) (Dupuis et al., 2011). Functional experiments, such as loss of functions, using morpholinos and CRISPR/cas9, for genes of interest could be carried out to look at their function in *Xenopus laevis* and their role in organ remodeling during development from juvenile to adult organisation. Genes of interest would include ECM components and metalloproteinases known to be expressed and have a function in the mammalian brain, skin and heart development or genes which showed interesting expression and regulation profiles but are not known to play a role in these organs. In order to look at their regulation by TH during metamorphosis tadpoles could be treated with TH and TH disruptor and genes expression would be compared to the one obtained in this study in normal conditions.

A transgenic *Xenopus laevis* line has been created by Pr. Barbara Demeneix in order to look at the effect of chemicals on thyroid hormone

signaling during development. This line, called *Tg(thibz:eGFP)*, expresses GFP under the control of a regulatory region of the TH/bZIP, a leucine zipper transcription factor highly sensitive to thyroid hormone regulation that contains a consensus thyroid hormone element (TRE), known to be an optimal TH response gene (Fini et al., 2007). By using this transgenic line they were able to identify chemicals disrupting thyroid hormone signaling affecting brain development (Fini et al., 2017).

It would be interesting to look at the expression of ECM genes that have been identified as potential genes regulated by thyroid hormones, following the experiment with embryos treated with T3 during metamorphosis, in the presence of chemicals disrupting thyroid hormones and their impact on brain, skin and heart development in *Xenopus laevis*. This could suggest the same impact in humans as thyroid hormone signaling and the structures of these organs are highly conserved. It is known that TH signaling is important for human heart fetal and postnatal development (Li et al., 2014) so it would be interesting to know the impact of chemicals on ECM during this process as ECM has been shown to be important for heart development (Lockhart et al., 2011). The results of gene expression showed in the present study could be used as a control for gene expression analysis of these genes in disease conditions as *Xenopus* has been shown to be a good model for neurodevelopmental disorders (Pratt and Khakhalin, 2013) and for congenital heart defects (Hempel and Kühl, 2016). Functional studies of genes of interest could allow the identification of new ECM genes involved in these different diseases and their potential therapeutic application.

6.4 ECM and metalloproteinases in heart regeneration

This study showed ECM components, metalloproteinases and tissue inhibitor of metalloproteinases genes expression in *Xenopus laevis* following heart injury by ventricular resection. It is known that ECM and MMPs are regulated by the inflammatory response following injury. The inflammatory response is divided in three phases: acute (hours after injury), granulation (days after injury) and maturation (weeks after injury). After myocardial infarction, cardiac fibroblasts secrete proinflammatory cytokines and chemokines such as tumour necrosis factor α (TNF α) and interleukin-1 (IL-1) and MMPs such as

MMP-1, -2, -3, -9 and -14 to degrade the ECM in the acute phase. In the granulation phase they migrate, proliferate and differentiate into myofibroblasts in the damaged zone and secrete MMPs and pro-angiogenic molecules such as vascular endothelial growth factor (VEGF) to promote revascularisation. In the maturation phase, the inflammation response is inhibited by anti-inflammatory cytokines and myofibroblasts secrete new ECM components to form a scar in response to profibrotic signals for example, transforming growth factor- β (TGF β), angiotensin II and basic fibroblast growth factor (bFGF). Cardiac fibroblasts regulate MMP activity after myocardial injury by secreting their inhibitors, TIMPs such as TIMP-1 (van Nieuwenhoven and Turner, 2013) (Turner et al., 2010).

In this study gene expression was analysed at 1,3 and 7 days post amputation corresponding to the acute and granulation phases of inflammation characterised by metalloproteinases secretion and angiogenesis. It has been previously shown in adult human cardiac myofibroblasts that have been treated with IL-1 for 6 hours, thus reproducing an acute inflammatory response after myocardial infarction, that *MMP-1*, *MMP-9* and *MMP-14* are up regulated as well as ECM components such as *col1a1*, *fibronectin 1*, *versican*, and *TIMP1* whereas *ADAMTS1* was downregulated (Turner et al., 2010). *ADAMTS1* inhibits neovascularization through the inhibition of VEGF signaling (Luque et al., 2003) and by the release of anti-angiogenic peptides from thrombospondins-1 and -2 (Lee et al., 2006). This study suggests that IL-1, by inhibiting *ADAMTS1*, promotes angiogenesis after myocardial infarction (Turner et al., 2010). An upregulation of *col1a1*, *fibronectin 1*, *VCAN*, *MMP-1*, *MMP-9* and *MMP-14* as well as *TIMP1* after ventricle resection in *Xenopus laevis* during metamorphosis was showed in this study, which supports previously *in vitro* published data (Turner et al., 2010). Downregulation of *ADAMTS1* was not observed; suggesting that *ADAMTS1* regulation by IL-1 is a fast response (hours) to inflammation signals. However *ADAMTS1* was upregulated in the adult frogs suggesting a role in the inhibition of the angiogenesis leading to the lack of regeneration. It has been shown that *ADAMTS1* is positively regulated by the mitogen-activated protein kinase (MAPK) p38 (Turner et al., 2010), which is up regulated in heart failure associated with a diminution of the vasoreactivity such as endothelial dysfunction (Arabacilar and Marber, 2015). Little is known

about the downstream mechanisms of MAPK p38 in heart failure but ADAMTS1 could be a potential factor. The ADAMTS family has been the main focus of the present study. Several ADAMTSs have been shown to be expressed in atherosclerosis, an inflammatory coronary artery disease characterised by endothelial dysfunction and the accumulation of lipid and cholesterol in the intima (inner layer) eventually resulting in the formation of a cholesterol-rich plaque. *ADAMTS4*, *ADAMTS8* and *ADAMTS9* were upregulated after stimulation with $TNF\alpha$, *ADAMTS4* and *ADAMTS8* were expressed in macrophage-rich areas known to secrete metalloproteinases during inflammation response (Wagsater et al., 2008). Several studies showed that *ADAMTS7*, by cleavage of its substrate COMP, can promote vascular smooth muscle cell (VSMC) migration in the arterial intima and vascular calcification leading to the development of an atherosclerotic plaque. This suggests *ADAMTS7* is a potential therapeutic target for atherosclerosis (Patel and Ye, 2013). An upregulation of *ADAMTS4*, *ADAMTS8* and *ADAMTS9* was observed suggesting these proteases have been stimulated in response to the inflammatory signal after ventricle resection. However no upregulation of *ADAMTS7* was observed, which could be due to its timing of regulation being before 1 day post amputation or after 7 days post amputation or that *ADAMTS7* could not be regulated during inflammation following ventricle resection. Little is known about the mode of actions of these ADAMTSs in inflammation but they could be good candidates for a therapeutic application in order to manage the inflammatory response following heart injury to improve the recovery. Angiogenesis is an important process for cardiac regeneration after injury (Marin-Juez et al., 2016).

The ADAMTS family have been shown to have pro- and anti- angiogenic properties. *ADAMTS1* (Luque et al., 2003) (Lee et al., 2006), *ADAMTS4*, *ADAMTS8* (Vazquez et al., 1999), *ADAMTS2* (Dubail et al., 2010), *ADAMTS12* (Llamazares et al., 2007) and *ADAMTS5* (Sharghi-Namini et al., 2008) have been shown to have anti-angiogenic activities independent of their protease activity whereas the *ADAMTS9* (Koo et al., 2010) anti-angiogenic action is dependent on its protease activity but the mode of action is unknown. *ADAMTS13* has been shown to promote angiogenesis by its C-terminal TSP1 motif, which upregulates VEGF and the phosphorylation of VEGFR2 (Lee et al.,

2015). An upregulation of these ADAMTSs after ventricle resection at 1, 3 and 7 dpa was observed. Angiogenesis is needed for heart regeneration and is a fast response after injury (hours) (Marin-Juez et al., 2016). ADAMTSs shown to have anti-angiogenic properties could be downregulated early after cardiac injury. This was not observed in this study however in heart remodeling after injury the ADAMTS family could play a different role promoting ECM remodeling and regulating angiogenesis.

To complete the mRNA data, antibody staining on the *Xenopus laevis* amputated hearts for the ADAMTS family could show their localisation in the ECM or in the endothelial cells, giving an indication on their possible role in the process of heart regeneration. It would be interesting to see if their profile of expression differ from *Xenopus laevis* tadpoles that have the capacity to regenerate their heart compared to juvenile and adult frogs that loose this capacity. This would indicate their potential as a therapeutic target to improve treatment after heart injury promoting regeneration.

References

Agrawal, R., Tran, U., Wessely, O., 2009. The miR-30 miRNA family regulates *Xenopus* pronephros development and targets the transcription factor *Xlim1/Lhx1*. *Development* 136, 3927-3936.

Ahmed, A., Ward, N.J., Moxon, S., Lopez-Gomollon, S., Viaut, C., Tomlinson, M.L., Patrushev, I., Gilchrist, M.J., Dalmay, T., Dotlic, D., Munsterberg, A.E., Wheeler, G.N., 2015. A Database of microRNA Expression Patterns in *Xenopus laevis*. *PLoS One* 10, e0138313.

Aldea, D., Hanna, P., Munoz, D., Espinoza, J., Torrejon, M., Sachs, L., Buisine, N., Oulion, S., Escriva, H., Marcellini, S., 2013. Evolution of the vertebrate bone matrix: an expression analysis of the network forming collagen paralogues in amphibian osteoblasts. *J Exp Zool B Mol Dev Evol* 320, 375-384.

Alfandari, D., Cousin, H., Gaultier, A., Smith, K., White, J.M., Darribere, T., Desimone, D.W., 2001. *Xenopus* ADAM 13 is a metalloprotease required for cranial neural crest-cell migration. *Current Biology* 11, 918-930.

Arabacilar, P., Marber, M., 2015. The case for inhibiting p38 mitogen-activated protein kinase in heart failure. *Front Pharmacol* 6, 102.

Ataca, D., Caikovski, M., Piersigilli, A., Moulin, A., Benarafa, C., Earp, S.E., Guri, Y., Kostic, C., Arsenijevic, Y., Soininen, R., Apte, S.S., Brisken, C., 2016. *Adams18* deletion results in distinct developmental defects and provides a model for congenital disorders of lens, lung, and female reproductive tract development. *Biol Open* 5, 1585-1594.

Avram, S., Shaposhnikov, S., Buiu, C., Mernea, M., 2014. Chondroitin sulfate proteoglycans: structure-function relationship with implication in neural development and brain disorders. *Biomed Res Int* 2014, 642798.

Bandtlow, C.E., Zimmermann, D.R., 2000. Proteoglycans in the Developing Brain: New Conceptual Insights for Old Proteins. *Physiological Reviews* 80, 1267-1282.

Barros, C.S., Franco, S.J., Muller, U., 2011. Extracellular matrix: functions in the nervous system. *Cold Spring Harb Perspect Biol* 3, a005108.

Beare, A.H., O'Kane, S., Krane, S.M., Ferguson, M.W., 2003. Severely impaired wound healing in the collagenase-resistant mouse. *J Invest Dermatol* 120, 153-163.

Beck, C.W., Izpisua Belmonte, J.C., Christen, B., 2009. Beyond early development: *Xenopus* as an emerging model for the study of regenerative mechanisms. *Dev Dyn* 238, 1226-1248.

Bekhouche, M., Colige, A., 2015. The procollagen N-proteinases ADAMTS2, 3 and 14 in pathophysiology. *Matrix Biol* 44-46, 46-53.

Blitz, I.L., Andelfinger, G., Horb, M.E., 2006. Germ layers to organs: using *Xenopus* to study "later" development. *Semin Cell Dev Biol* 17, 133-145.

Boerboom, D., Lafond, J.F., Zheng, X., Lapointe, E., Mittaz, L., Boyer, A., Pritchard, M.A., DeMayo, F.J., Mort, J.S., Drolet, R., Richards, J.S., 2011. Partially redundant functions of Adamts1 and Adamts4 in the perinatal development of the renal medulla. *Dev Dyn* 240, 1806-1814.

Brew, K., Nagase, H., 2010. The tissue inhibitors of metalloproteinases (TIMPs): an ancient family with structural and functional diversity. *Biochim Biophys Acta* 1803, 55-71.

Brocker, C.N., Vasiliou, V., Nebert, D.W., 2009. Evolutionary divergence and functions of the ADAM and ADAMTS gene families. *HUMAN GENOMICS* 4, 43-55.

Brown, D.D., Cai, L., 2007. Amphibian metamorphosis. *Dev Biol* 306, 20-33.

Brown, H.M., Dunning, K.R., Robker, R.L., Boerboom, D., Pritchard, M., Lane, M., Russell, D.L., 2010. ADAMTS1 cleavage of versican mediates essential structural remodeling of the ovarian follicle and cumulus-oocyte matrix during ovulation in mice. *Biol Reprod* 83, 549-557.

Brunet, F., Kintakas, C., Smith, A.D., McCulloch, D.R., 2012. The Function of the Hyalectan Class of Proteoglycans and Their Binding Partners during Vertebrate Development. *Advances in Medicine and Biology* 52.

Buchholz, D.R., 2015. More similar than you think: Frog metamorphosis as a model of human perinatal endocrinology. *Dev Biol* 408, 188-195.

Buisson, I., Le Bouffant, R., Futel, M., Riou, J.F., Umbhauer, M., 2015. Pax8 and Pax2 are specifically required at different steps of *Xenopus* pronephros development. *Dev Biol* 397, 175-190.

Cain, S.A., Mularczyk, E.J., Singh, M., Massam-Wu, T., Kielty, C.M., 2016. ADAMTS-10 and -6 differentially regulate cell-cell junctions and focal adhesions. *Sci Rep* 6, 35956.

Cal, S., Lopez-Otin, C., 2015. ADAMTS proteases and cancer. *Matrix Biol* 44-46, 77-85.

Camenisch, T.D., Spicer, A.P., Brehm-Gibson, T., Biesterfeldt, J., Augustine, M.L., Calabro, A., Jr., Kubalak, S., Klewer, S.E., McDonald, J.A., 2000.

Disruption of hyaluronan synthase-2 abrogates normal cardiac morphogenesis and hyaluronan-mediated transformation of epithelium to mesenchyme. *J Clin Invest* 106, 349-360.

Casini, P., Ori, M., Avenoso, A., D'Ascola, A., Traina, P., Mattina, W., Perris, R., Campo, G.M., Calatroni, A., Nardi, I., Campo, S., 2008. Identification and gene expression of versican during early development of *Xenopus*. *Int J Dev Biol* 52, 993-998.

Chablais, F., Jazwinska, A., 2012. The regenerative capacity of the zebrafish heart is dependent on TGFbeta signaling. *Development* 139, 1921-1930.

Cousin, H., Abbruzzese, G., Kerdavid, E., Gaultier, A., Alfandari, D., 2011. Translocation of the cytoplasmic domain of ADAM13 to the nucleus is essential for Calpain8-a expression and cranial neural crest cell migration. *Dev Cell* 20, 256-263.

Crane, J.F., Trainor, P.A., 2006. Neural Crest Stem and Progenitors Cells. *Annu. Rev. Cell Dev. Biol.* 22, 267-286.

Dale, L., Slack, J.M., 1987. Fate map for the 32-cell stage of *Xenopus laevis*. *Development* 99, 527-551.

Dancevic, C.M., Fraser, F.W., Smith, A.D., Stupka, N., Ward, A.C., McCulloch, D.R., 2013. Biosynthesis and Expression of a Disintegrin-like and Metalloproteinase Domain with Thrombospondin-1 Repeats-15. *THE JOURNAL OF BIOLOGICAL CHEMISTRY* 288, 37267-37276.

Dauth, S., Grevesse, T., Pantazopoulos, H., Campbell, P.H., Maoz, B.M., Berretta, S., Parker, K.K., 2016. Extracellular matrix protein expression is brain region dependent. *J Comp Neurol* 524, 1309-1336.

Demircan, K., Yonezawa, T., Takigawa, T., Topcu, V., Erdogan, S., Ucar, F., Armutcu, F., Yigitoglu, M.R., Ninomiya, Y., Hirohata, S., 2013. ADAMTS1, ADAMTS5, ADAMTS9 and aggrecanase-generated proteoglycan fragments are induced following spinal cord injury in mouse. *Neurosci Lett* 544, 25-30.

Derby, A., Jeffrey, J.J., Eisen, A.Z., 1979. The Induction of Collagenase and Acid Phosphatase by Thyroxine in Resorbing Tadpole Gills In Vitro. *J. EXP. ZOOL.* 207, 391-398.

Dubail, J., Apte, S.S., 2015. Insights on ADAMTS proteases and ADAMTS-like proteins from mammalian genetics. *Matrix Biol* 44-46, 24-37.

Dubail, J., Aramaki-Hattori, N., Bader, H.L., Nelson, C.M., Katebi, N., Matuska, B., Olsen, B.R., Apte, S.S., 2014. A new Adamts9 conditional mouse allele

identifies its non-redundant role in interdigital web regression. *Genesis* 52, 702-712.

Dubail, J., Kesteloot, F., Deroanne, C., Motte, P., Lambert, V., Rakic, J.M., Lapiere, C., Nusgens, B., Colige, A., 2010. ADAMTS-2 functions as anti-angiogenic and anti-tumoral molecule independently of its catalytic activity. *Cell . Mol. Life Sci.* 67, 4213-4232.

Dun, M.D., Anderson, A.L., Bromfield, E.G., Asquith, K.L., Emmett, B., McLaughlin, E.A., Aitken, R.J., Nixon, B., 2012. Investigation of the expression and functional significance of the novel mouse sperm protein, a disintegrin and metalloprotease with thrombospondin type 1 motifs number 10 (ADAMTS10). *Int J Androl* 35, 572-589.

Dunn, J.R., Reed, J.E., du Plessis, D.G., Shaw, E.J., Reeves, P., Gee, A.L., Warnke, P., Walker, C., 2006. Expression of ADAMTS-8, a secreted protease with antiangiogenic properties, is downregulated in brain tumours. *Br J Cancer* 94, 1186-1193.

Dupuis, L.E., McCulloch, D.R., McGarity, J.D., Bahan, A., Wessels, A., Weber, D., Diminich, A.M., Nelson, C.M., Apte, S.S., Kern, C.B., 2011. Altered versican cleavage in ADAMTS5 deficient mice; a novel etiology of myxomatous valve disease. *Dev Biol* 357, 152-164.

Dutt, S., Kleber, M., Matasci, M., Sommer, L., Zimmermann, D.R., 2006. Versican V0 and V1 guide migratory neural crest cells. *J Biol Chem* 281, 12123-12131.

Edwards, D.R., Handsley, M.M., Pennington, C.J., 2008. The ADAM metalloproteinases. *Mol Aspects Med* 29, 258-289.

Enomoto, H., Nelson, C.M., Somerville, R.P., Mielke, K., Dixon, L.J., Powell, K., Apte, S.S., 2010. Cooperation of two ADAMTS metalloproteases in closure of the mouse palate identifies a requirement for versican proteolysis in regulating palatal mesenchyme proliferation. *Development* 137, 4029-4038.

Fan, D., Takawale, A., Lee, J., Kassiri, Z., 2012. Cardiac fibroblasts, fibrosis and extracellular matrix remodeling in heart disease. *Fibrogenesis & Tissue Repair* 5.

Fini, J.B., Le Mevel, S., Turque, N., Palmier, K., Zalko, D., P., C.J., Demeneix, B.A., 2007. An In Vivo Multiwell-Based Fluorescent Screen for Monitoring Vertebrate Thyroid Hormone Disruption. *Environ. Sci. Technol.* 41, 5908-5914.

Fini, J.B., Mughal, B.B., Le Mevel, S., Leemans, M., Lettmann, M., Spirhanzlova, P., Affaticati, P., Jenett, A., Demeneix, B.A., 2017. Human

amniotic fluid contaminants alter thyroid hormone signalling and early brain development in *Xenopus* embryos. *Sci Rep* 7, 43786.

Fletcher, R.B., Baker, J.C., Harland, R.M., 2006. FGF8 spliceforms mediate early mesoderm and posterior neural tissue formation in *Xenopus*. *Development* 133, 1703-1714.

Foulcer, S.J., Nelson, C.M., Quintero, M.V., Kuberan, B., Larkin, J., Dours-Zimmermann, M.T., Zimmermann, D.R., Apte, S.S., 2014. Determinants of versican-V1 proteoglycan processing by the metalloproteinase ADAMTS5. *J Biol Chem* 289, 27859-27873.

Fu, L., Hasebe, T., Ishizuya-Oka, A., Shi, Y.B., 2007. Roles of Matrix Metalloproteinases and ECM Remodeling during Thyroid Hormone-Dependent Intestinal Metamorphosis in *Xenopus laevis*. *Organogenesis* 3.

Fujimoto, K., Nakajima, K., Yaoita, Y., 2007. Expression of matrix metalloproteinase genes in regressing or remodeling organs during amphibian metamorphosis. *Dev Growth Differ* 49, 131-143.

Gao, Y.X., Yu, C.A., Lu, J.H., Gao, H.M., Li, G., Kong, W., Zheng, J., 2013. ADAMTS-7 expression increases in the early stage of angiotensin II-induced renal injury in elderly mice. *Kidney Blood Press Res* 38, 121-131.

Garcion, E., Halilagic, A., Faissner, A., French-Constant, C., 2004. Generation of an environmental niche for neural stem cell development by the extracellular matrix molecule tenascin C. *Development* 131, 3423-3432.

Genovese, F., Manresa, A.A., Leeming, D.J., Karsdal, M.A., Boor, P., 2014. The extracellular matrix in the kidney: a source of novel non-invasive biomarkers of kidney fibrosis? *Fibrogenesis & Tissue Repair* 7, 1-14.

George, E.L., Georges-Lebouesse, E.N., Patel-King, R.S., Rayburn, H., Hynes, R.O., 1993. Defects in mesoderm, neural tube and vascular development in mouse embryos lacking fibronectin. *Development* 119, 1079-1091.

Gerhardt, S., Hassall, G., Hawtin, P., McCall, E., Flavell, L., Minshull, C., Hargreaves, D., Ting, A., Pauptit, R.A., Parker, A.E., Abbott, W.M., 2007. Crystal structures of human ADAMTS-1 reveal a conserved catalytic domain and a disintegrin-like domain with a fold homologous to cysteine-rich domains. *J Mol Biol* 373, 891-902.

Ghosh, A.K., Vaughan, D.E., 2012. PAI-1 in tissue fibrosis. *J Cell Physiol* 227, 493-507.

Gomis-Ruth, F.X., 2009. Catalytic domain architecture of metzincin metalloproteases. *J Biol Chem* 284, 15353-15357.

Gottschall, P.E., Howell, M.D., 2015. ADAMTS expression and function in central nervous system injury and disorders. *Matrix Biol* 44-46, 70-76.

Gross, J., Lapiere, C.M., 1962. Collagenolytic activity in amphibian tissues: a tissue culture assay. *PNAS* 48, 1014–1022.

Guo, X., Zhang, T., Hu, Z., Zhang, Y., Shi, Z., Wang, Q., Cui, Y., Wang, F., Zhao, H., Chen, Y., 2014. Efficient RNA/Cas9-mediated genome editing in *Xenopus tropicalis*. *Development* 141, 707-714.

Hamel, M.G., Ajmo, J.M., Leonardo, C.C., Zuo, F., Sandy, J.D., Gottschall, P.E., 2008. Multimodal signaling by the ADAMTSs (a disintegrin and metalloproteinase with thrombospondin motifs) promotes neurite extension. *Exp Neurol* 210, 428-440.

Hamodi, A.S., Pratt, K.G., 2015. The horizontal brain slice preparation: a novel approach for visualizing and recording from all layers of the tadpole tectum. *J Neurophysiol* 113, 400-407.

Happel, M., F., Frischknecht, R., 2016. Neuronal Plasticity in the Juvenile and Adult Brain Regulated by the Extracellular Matrix. *Composition and Function of the Extracellular Matrix in the Human Body*.

Harland, R.M., Grainger, R.M., 2011. *Xenopus* research: metamorphosed by genetics and genomics. *Trends Genet* 27, 507-515.

Harrison, M., Abu-Elmagd, M., Grocott, T., Yates, C., Gavrilovic, J., Wheeler, G.N., 2004. Matrix metalloproteinase genes in *Xenopus* development. *Dev Dyn* 231, 214-220.

Hartmann, D., de Strooper, B., Serneels, L., Craessaerts, K., Herreman, A., Annaert, W., Umans, L., Lubke, T., Illert, A.L., von Figura, K., Saftig, P., 2002. The disintegrin/metalloprotease ADAM 10 is essential for Notch signalling but not for a-secretase activity in fibroblasts. *Human Molecular Genetics* 11.

Hasebe, T., Hartman, R., Fu, L., Amano, T., Shi, Y.B., 2007a. Evidence for a cooperative role of gelatinase A and membrane type-1 matrix metalloproteinase during *Xenopus laevis* development. *Mech Dev* 124, 11-22.

Hasebe, T., Kajita, M., Fujimoto, K., Yaoita, Y., Ishizuya-Oka, A., 2007b. Expression profiles of the duplicated matrix metalloproteinase-9 genes suggest their different roles in apoptosis of larval intestinal epithelial cells during *Xenopus laevis* metamorphosis. *Dev Dyn* 236, 2338-2345.

Hattori, N., Carrino, D.A., Lauer, M.E., Vasanji, A., Wylie, J.D., Nelson, C.M., Apte, S.S., 2011. Pericellular versican regulates the fibroblast-myofibroblast

transition: a role for ADAMTS5 protease-mediated proteolysis. *J Biol Chem* 286, 34298-34310.

Heasman, J., 2006. Patterning the early *Xenopus* embryo. *Development* 133, 1205-1217.

Hehr, C.L., Hocking, J.C., McFarlane, S., 2005. Matrix metalloproteinases are required for retinal ganglion cell axon guidance at select decision points. *Development* 132, 3371-3379.

Heller, N., Brandli, A.W., 1999. *Xenopus* Pax-2/5/8 Orthologues: Novel Insights Into Pax Gene Evolution and Identification of Pax-8 as the Earliest Marker for Otic and Pronephric Cell Lineages. *DEVELOPMENTAL GENETICS* 24, 208-219.

Hempel, A., Kühl, M., 2016. A Matter of the Heart: The African Clawed Frog *Xenopus* as a Model for Studying Vertebrate Cardiogenesis and Congenital Heart Defects. *J. Cardiovasc. Dev. Dis.* 3, 1-13.

Hisanaga, A., Morishita, S., Suzuki, K., Sasaki, K., Koie, M., Kohno, T., Hattori, M., 2012. A disintegrin and metalloproteinase with thrombospondin motifs 4 (ADAMTS-4) cleaves Reelin in an isoform-dependent manner. *FEBS Lett* 586, 3349-3353.

Honoré, S.M., Aybar, M.J., Mayor, R., 2003. Sox10 is required for the early development of the prospective neural crest in *Xenopus* embryos. *Developmental Biology* 260, 79-96.

Horiuchi, K., Zhou, H.M., Kelly, K., Manova, K., Blobel, C.P., 2005. Evaluation of the contributions of ADAMs 9, 12, 15, 17, and 19 to heart development and ectodomain shedding of neuregulins beta1 and beta2. *Dev Biol* 283, 459-471.

Hornebeck, W., 2003. Down-regulation of tissue inhibitor of matrix metalloprotease-1 (TIMP-1) in aged human skin contributes to matrix degradation and impaired cell growth and survival. *Pathologie Biologie* 51, 569-573.

Huxley-Jones, J., Apte, S.S., Robertson, D.L., Boot-Handford, R.P., 2005. The characterisation of six ADAMTS proteases in the basal chordate *Ciona intestinalis* provides new insights into the vertebrate ADAMTS family. *Int J Biochem Cell Biol* 37, 1838-1845.

Huxley-Jones, J., Clarke, T.K., Beck, C., Toubaris, G., Robertson, D.L., Boot-Handford, R.P., 2007. The evolution of the vertebrate metzincins; insights from *Ciona intestinalis* and *Danio rerio*. *BMC Evol Biol* 7, 63.

Ishizuya-Oka, A., 2011. Amphibian organ remodeling during metamorphosis: insight into thyroid hormone-induced apoptosis. *Dev Growth Differ* 53, 202-212.

Ismat, A., Cheshire, A.M., Andrew, D.J., 2013. The secreted AdamTS-A metalloprotease is required for collective cell migration. *Development* 140, 1981-1993.

Jablonska-Trypuc, A., Matejczyk, M., Rosochacki, S., 2016. Matrix metalloproteinases (MMPs), the main extracellular matrix (ECM) enzymes in collagen degradation, as a target for anticancer drugs. *J Enzyme Inhib Med Chem* 31, 177-183.

Jackson, H.W., Defamie, V., Waterhouse, P., Khokha, R., 2017. TIMPs: versatile extracellular regulators in cancer. *Nat Rev Cancer* 17, 38-53.

Jungers, K.A., Le Goff, C., Somerville, R.P., Apte, S.S., 2005. Adamts9 is widely expressed during mouse embryo development. *Gene Expr Patterns* 5, 609-617.

Kashiwagi, M., Enghild, J.J., Gendron, C., Hughes, C., Caterson, B., Itoh, Y., Nagase, H., 2004. Altered proteolytic activities of ADAMTS-4 expressed by C-terminal processing. *J Biol Chem* 279, 10109-10119.

Kelly, O.G., Melton, D.A., 2000. Development of the pancreas in *Xenopus laevis*. *Dev Dyn* 218, 615-627.

Kelwick, R., Desanlis, I., Wheeler, G.N., Edwards, D.R., 2015a. The ADAMTS (A Disintegrin and Metalloproteinase with Thrombospondin motifs) family. *Genome Biol* 16, 113.

Kelwick, R., Wagstaff, L., Decock, J., Roghi, C., Cooley, L.S., Robinson, S.D., Arnold, H., Gavrilovic, J., Jaworski, D.M., Yamamoto, K., Nagase, H., Seubert, B., Kruger, A., Edwards, D.R., 2015b. Metalloproteinase-dependent and -independent processes contribute to inhibition of breast cancer cell migration, angiogenesis and liver metastasis by a disintegrin and metalloproteinase with thrombospondin motifs-15. *International Journal of Cancer* 136, 14-26.

Kern, C.B., Wessels, A., McGarity, J., Dixon, L.J., Alston, E., Argraves, W.S., Geeting, D., Nelson, C.M., Menick, D.R., Apte, S.S., 2010. Reduced versican cleavage due to Adamts9 haploinsufficiency is associated with cardiac and aortic anomalies. *Matrix Biol* 29, 304-316.

Kochegarov, A., Lemanski, L.F., 2016. New Trends in Heart Regeneration: A Review. *J Stem Cells Regen Med* 12.

Koo, B.H., Apte, S.S., 2010. Cell-surface processing of the metalloprotease pro-ADAMTS9 is influenced by the chaperone GRP94/gp96. *J Biol Chem* 285, 197-205.

Koo, B.H., Coe, D.M., Dixon, L.J., Somerville, R.P., Nelson, C.M., Wang, L.W., Young, M.E., Lindner, D.J., Apte, S.S., 2010. ADAMTS9 is a cell-autonomously acting, anti-angiogenic metalloprotease expressed by microvascular endothelial cells. *Am J Pathol* 176, 1494-1504.

Koo, B.H., Longpre, J.M., Somerville, R.P., Alexander, J.P., Leduc, R., Apte, S.S., 2007. Regulation of ADAMTS9 secretion and enzymatic activity by its propeptide. *J Biol Chem* 282, 16146-16154.

Krampert, M., Kuenzle, S., Thai, S.N., Lee, N., Iruela-Arispe, M.L., Werner, S., 2005. ADAMTS1 proteinase is up-regulated in wounded skin and regulates migration of fibroblasts and endothelial cells. *J Biol Chem* 280, 23844-23852.

Krneta-Stankic, V., DeLay, B.D., Miller, R.K., 2017. *Xenopus*: leaping forward in kidney organogenesis. *Pediatr Nephrol* 32, 547-555.

Krstic, D., Rodriguez, M., Knuesel, I., 2012. Regulated proteolytic processing of Reelin through interplay of tissue plasminogen activator (tPA), ADAMTS-4, ADAMTS-5, and their modulators. *PLoS One* 7, e47793.

Kuno, K., Kanada, N., Nakashima, E., Fujiki, F., Ichimura, F., Matsushima, K., 1997. Molecular Cloning of a Gene Encoding a New Type of Metalloproteinase-disintegrin Family Protein with Thrombospondin Motifs as an Inflammation Associated Gene. *THE JOURNAL OF BIOLOGICAL CHEMISTRY* 272, 556-562.

Kurohara, K., Komatsu, K., Kurisaki, T., Masuda, A., Irie, N., Asano, M., Sudo, K., Nabeshima, Y., Iwakura, Y., Sehara-Fujisawa, A., 2004. Essential roles of Meltrin beta (ADAM19) in heart development. *Dev Biol* 267, 14-28.

Lander, R., Nasr, T., Ochoa, S.D., Nordin, K., Prasad, M.S., LaBonne, C., 2013. Interactions between Twist and other core epithelial–mesenchymal transition factors are controlled by GSK3-mediated phosphorylation. *Nat Commun* 4.

Le Douarin, N.M., Dupin, E., 2003. Multipotentiality of the neural crest. *Curr Opin Genet Dev* 13, 529-536.

Lee, M., Keener, J., Xiao, J., Long Zheng, X., Rodgers, G.M., 2015. ADAMTS13 and its variants promote angiogenesis via upregulation of VEGF and VEGFR2. *Cell Mol Life Sci* 72, 349-356.

Lee, N.V., Sato, M., Annis, D.S., Loo, J.A., Wu, L., Mosher, D.F., Iruela-Arispe, M.L., 2006. ADAMTS1 mediates the release of antiangiogenic polypeptides from TSP1 and 2. *the EMBO journal* 25, 5270-5283.

Lee-Liu, D., Mendez-Olivos, E.E., Munoz, R., Larrain, J., 2016. The African clawed frog *Xenopus laevis*: a model organism to study regeneration of the Central Nervous System. *Neurosci Lett*.

Levy, C., Brooks, J.M., Chen, J., Su, J., Fox, M.A., 2015. Cell-specific and developmental expression of lectican-cleaving proteases in mouse hippocampus and neocortex. *J Comp Neurol* 523, 629-648.

Li, M., Iismaa, S.E., Naqvi, N., Nicks, A., Husain, A., Graham, R.M., 2014. Thyroid hormone action in postnatal heart development. *Stem Cell Res* 13, 582-591.

Lienkamp, S., Ganner, A., Boehlke, C., Schmidt, T., Arnold, S.J., Schafer, T., Romaker, D., Schuler, J., Hoff, S., Powelske, C., Eifler, A., Kronig, C., Bullerkotte, A., Nitschke, R., Kuehn, W.E., Kim, E., Burkhardt, H., Brox, T., Ronneberger, O., Gloy, J., Walz, G., 2010. Inversin relays Frizzled-8 signals to promote proximal pronephros development. *PNAS* 107, 20388–20393.

Lienkamp, S.S., 2016. Using *Xenopus* to study genetic kidney diseases. *Semin Cell Dev Biol* 51, 117-124.

Lienkamp, S.S., Liu, K., Karner, C.M., Carroll, T.J., Ronneberger, O., Wallingford, J.B., Walz, G., 2012. Vertebrate kidney tubules elongate using a planar cell polarity-dependent, rosette-based mechanism of convergent extension. *Nat Genet* 44, 1382-1387.

Lim, N.H., Kashiwagi, M., Visse, R., Jones, J., Enghild, J.J., Brew, K., Nagase, H., 2010. Reactive-site mutants of N-TIMP-3 that selectively inhibit ADAMTS-4 and ADAMTS-5: biological and structural implications. *Biochem J* 431, 113-122.

Llamazares, M., Cal, S., Quesada, V., Lopez-Otin, C., 2003. Identification and characterization of ADAMTS-20 defines a novel subfamily of metalloproteinases-disintegrins with multiple thrombospondin-1 repeats and a unique GON domain. *J Biol Chem* 278, 13382-13389.

Llamazares, M., Obaya, A.J., Moncada-Pazos, A., Heljasvaara, R., Espada, J., Lopez-Otin, C., Cal, S., 2007. The ADAMTS12 metalloproteinase exhibits anti-tumorigenic properties through modulation of the Ras-dependent ERK signalling pathway. *J Cell Sci* 120, 3544-3552.

Lockhart, M., Wirrig, E., Phelps, A., Wessels, A., 2011. Extracellular matrix and heart development. *Birth Defects Res A Clin Mol Teratol* 91, 535-550.

Loffek, S., Schilling, O., Franzke, C.W., 2011. Series "matrix metalloproteinases in lung health and disease": Biological role of matrix metalloproteinases: a critical balance. *Eur Respir J* 38, 191-208.

Lohler, J., Timpl, R., Jaenisch, R., 1984. Embryonic Lethal Mutation in Mouse Collagen I Gene Causes Rupture of Blood Vessels and Is Associated with Erythropoietic and Mesenchymal Cell Death. *Cell* 38, 597-607.

Longpre, J.M., McCulloch, D.R., Koo, B.H., Alexander, J.P., Apte, S.S., Leduc, R., 2009. Characterization of proADAMTS5 processing by proprotein convertases. *Int J Biochem Cell Biol* 41, 1116-1126.

Lunde, I.G., Herum, K.M., Carlson, C.C., Christensen, G., 2016. Syndecans in heart fibrosis. *Cell Tissue Res* 365, 539-552.

Luo, N., Li, H., Xiang, B., Qiao, L., He, J., Ji, Y., Liu, Y., Li, S., Lu, R., Li, Y., Meng, W., Wu, Y., Xu, H., Mo, X., 2016. Syndecan-4 modulates the proliferation of neural cells and the formation of CaP axons during zebrafish embryonic neurogenesis. *Sci Rep* 6, 25300.

Luque, A., Carpizo, D.R., Iruela-Arispe, M.L., 2003. ADAMTS1/METH1 inhibits endothelial cell proliferation by direct binding and sequestration of VEGF165. *J Biol Chem* 278, 23656-23665.

Lyons, R.M., Gentry, L.E., Purchio, A.F., Moses, H.L., 1990. Mechanism of Activation of Latent Recombinant Transforming Growth Factor beta1 by Plasmin . *The Journal of Cell Biology* 110, 1361-1367.

Majerus, E.M., Zheng, X., Tuley, E.A., Sadler, J.E., 2003. Cleavage of the ADAMTS13 propeptide is not required for protease activity. *J Biol Chem* 278, 46643-46648.

Manea, M., Kristoffersson, A., Schneppenheim, R., Saleem, M.A., Mathieson, P.W., Morgelin, M., Bjork, P., Holmberg, L., Karpman, D., 2007. Podocytes express ADAMTS13 in normal renal cortex and in patients with thrombotic thrombocytopenic purpura. *Br J Haematol* 138, 651-662.

Marin-Juez, R., Marass, M., Gauvrit, S., Rossi, A., Lai, S.L., Materna, S.C., Black, B.L., Stainier, D.Y., 2016. Fast revascularization of the injured area is essential to support zebrafish heart regeneration. *113*, 11237-11242.

Marshall, L., Vivien, C., Girardot, F., Pericard, L., Demeneix, B.A., Coen, L., Chai, N., 2017. Persistent fibrosis, hypertrophy and sarcomere disorganisation after endoscopy-guided heart resection in adult *Xenopus*. *PLoS One* 12, e0173418.

Matsui, Y., Ikesue, M., Danzaki, K., Morimoto, J., Sato, M., Tanaka, S., Kojima, T., Tsutsui, H., Uede, T., 2011. Syndecan-4 prevents cardiac rupture and dysfunction after myocardial infarction. *Circ Res* 108, 1328-1339.

Mauch, C., Zamek, J., Abety, A.N., Grimberg, G., Fox, J.W., Zigrino, P., 2010. Accelerated wound repair in ADAM-9 knockout animals. *J Invest Dermatol* 130, 2120-2130.

McCulloch, D.R., Le Goff, C., Bhatt, S., Dixon, L.J., Sandy, J.D., Apte, S.S., 2009a. Adamts5, the gene encoding a proteoglycan-degrading metalloprotease, is expressed by specific cell lineages during mouse embryonic development and in adult tissues. *Gene Expr Patterns* 9, 314-323.

McCulloch, D.R., Nelson, C.M., Dixon, L.J., Silver, D.L., Wylie, J.D., Lindner, V., Sasaki, T., Cooley, M.A., Argraves, W.S., Apte, S.S., 2009b. ADAMTS metalloproteases generate active versican fragments that regulate interdigital web regression. *Dev Cell* 17, 687-698.

McCusker, C., Cousin, H., Neuner, R., Alfandari, D., 2009. Extracellular Cleavage of Cadherin-11 by ADAM Metalloproteases Is Essential for Xenopus Cranial Neural Crest Cell Migration. *Molecular Biology of the Cell* 20, 78-89.

Melenhorst, W.B., van den Heuvel, M.C., Timmer, A., Huitema, S., Bulthuis, M., Timens, W., van Goor, H., 2006. ADAM19 expression in human nephrogenesis and renal disease: associations with clinical and structural deterioration. *Kidney Int* 70, 1269-1278.

Mercer, S.E., Odelberg, S.J., Simon, H.G., 2013. A dynamic spatiotemporal extracellular matrix facilitates epicardial-mediated vertebrate heart regeneration. *Dev Biol* 382, 457-469.

Mittaz, L., Ricardo, S., Martinez, G., Kola, I., Kelly, D.J., Little, M.H., Hertzog, P.J., Pritchard, M.A., 2005. Neonatal calyceal dilation and renal fibrosis resulting from loss of Adamts-1 in mouse kidney is due to a developmental dysgenesis. *Nephrol Dial Transplant* 20, 419-423.

Mittaz, L., Russell, D.L., Wilson, T., Brasted, M., Tkalcevic, J., Salamonsen, L.A., Hertzog, P.J., Pritchard, M.A., 2004. Adamts-1 is essential for the development and function of the urogenital system. *Biol Reprod* 70, 1096-1105.

Mohan, R., Chintala, S.K., Jung, J.C., Villar, W.V., McCabe, F., Russo, L.A., Lee, Y., McCarthy, B.E., Wollenberg, K.R., Jester, J.V., Wang, M., Welgus, H.G., Shipley, J.M., Senior, R.M., Fini, M.E., 2002. Matrix metalloproteinase gelatinase B (MMP-9) coordinates and effects epithelial regeneration. *J Biol Chem* 277, 2065-2072.

Morales, J., Al-Sharif, L., Khalil, D.S., Shinwari, J.M., Bavi, P., Al-Mahrouqi, R.A., Al-Rajhi, A., Alkuraya, F.S., Meyer, B.F., Al Tassan, N., 2009. Homozygous mutations in ADAMTS10 and ADAMTS17 cause lenticular myopia, ectopia lentis, glaucoma, spherophakia, and short stature. *Am J Hum Genet* 85, 558-568.

Mosyak, L., Georgiadis, K., Shane, T., Svenson, K., Hebert, T., McDonagh, T., Mackie, S., Olland, S., Lin, L., Zhong, X., Kriz, R., Reifenberg, E.L., Collins-Racie, L.A., Corcoran, C., Freeman, B., Zollner, R., Marvell, T., Vera, M., Sum, P.E., Lavallie, E.R., Stahl, M., Somers, W., 2008. Crystal structures of the two major aggrecan degrading enzymes, ADAMTS4 and ADAMTS5. *Protein Sci* 17, 16-21.

Mulder, G.M., Melenhorst, W.B., Celie, J.W., Kloosterhuis, N.J., Hillebrands, J.L., Ploeg, R.J., Seelen, M.A., Visser, L., van Dijk, M.C., van Goor, H., 2012. ADAM17 up-regulation in renal transplant dysfunction and non-transplant-related renal fibrosis. *Nephrol Dial Transplant* 27, 2114-2122.

Munoz, R., Moreno, M., Oliva, C., Orbenes, C., Larrain, J., 2006. Syndecan-4 regulates non-canonical Wnt signalling and is essential for convergent and extension movements in *Xenopus* embryos. *Nat Cell Biol* 8, 492-500.

Nandadasa, S., Foulcer, S., Apte, S.S., 2014. The multiple, complex roles of versican and its proteolytic turnover by ADAMTS proteases during embryogenesis. *Matrix Biol* 35, 34-41.

Neuner, R., Cousin, H., McCusker, C., Coyne, M., Alfandari, D., 2009. *Xenopus* ADAM19 is involved in neural, neural crest and muscle development. *Mech Dev* 126, 240-255.

Nicholson, A.C., Malik, S.B., Logsdon, J.M., Jr., Van Meir, E.G., 2005. Functional evolution of ADAMTS genes: evidence from analyses of phylogeny and gene organization. *BMC Evol Biol* 5, 11.

Nieuwkoop, P.D., Faber, J., 1994. *Normal Table of Xenopus laevis (Daudin)*. Garland Publishing Inc, New-York.

Oh, J., Takahashi, R., Adachi, E., Kondo, S., Kuratomi, S., Noma, A., Alexander, D.B., Motoda, H., Okada, A., Seiki, M., Itoh, T., Itohara, S., Takahashi, C., Noda, M., 2004. Mutations in two matrix metalloproteinase genes, MMP-2 and MT1-MMP, are synthetic lethal in mice. *Oncogene* 23, 5041-5048.

Orlando, G., Booth, C., Wang, Z., Totonelli, G., Ross, C.L., Moran, E., Salvatori, M., Maghsoudlou, P., Turmaine, M., Delario, G., Al-Shraideh, Y., Farooq, U., Farney, A.C., Rogers, J., Iskandar, S.S., Burns, A., Marini, F.C., De Coppi, P.,

Stratta, R.J., Soker, S., 2013. Discarded human kidneys as a source of ECM scaffold for kidney regeneration technologies. *Biomaterials* 34, 5915-5925.

Otto, S.P., 2007. The evolutionary consequences of polyploidy. *Cell* 131, 452-462.

Owens, N.D., Blitz, I.L., Lane, M.A., Patrushev, I., Overton, J.D., Gilchrist, M.J., Cho, K.W., Khokha, M.K., 2016. Measuring Absolute RNA Copy Numbers at High Temporal Resolution Reveals Transcriptome Kinetics in Development. *Cell Rep* 14, 632-647.

Pagenstecher, A., Stalder, A.K., Kincaid, C.L., Shapiro, S.D., Campbell, I.L., 1998. Differential Expression of Matrix Metalloproteinase and Tissue Inhibitor of Matrix Metalloproteinase Genes in the Mouse Central Nervous System in Normal and Inflammatory States. *American Journal of Pathology*, 729-741.

Patel, R.S., Ye, S., 2013. ADAMTS7: a promising new therapeutic target in coronary heart disease. *Expert Opin Ther Targets* 17, 863-867.

Peacock, J.D., Lu, Y., Koch, M., Kadler, K.E., Lincoln, J., 2008. Temporal and spatial expression of collagens during murine atrioventricular heart valve development and maintenance. *Dev Dyn* 237, 3051-3058.

Pegoraro, C., Monsoro-Burq, A.H., 2013. Signaling and transcriptional regulation in neural crest specification and migration: lessons from xenopus embryos. *Wiley Interdiscip Rev Dev Biol* 2, 247-259.

Pilcher, B.K., Dumin, J.A., Sudbeck, B.D., Krane, S.M., Welgus, H.G., Parks, W.C., 1997. The Activity of Collagenase-1 Is Required for Keratinocyte Migration on a Type I Collagen Matrix. *The Journal of Cell Biology* 137, 1445-1457.

Pratt, K.G., Khakhalin, A.S., 2013. Modeling human neurodevelopmental disorders in the *Xenopus* tadpole: from mechanisms to therapeutic targets. *Dis Model Mech* 6, 1057-1065.

Quesada, V., Ordonez, G.R., Sanchez, L.M., Puente, X.S., Lopez-Otin, C., 2009. The Degradome database: mammalian proteases and diseases of proteolysis. *Nucleic Acids Res* 37, D239-243.

Rao, C., Foernzler, D., Loftus, S.K., Liu, S., McPherson, J.D., Jungers, K.A., Apte, S.S., Pavan, W.J., Beier, D.R., 2003. A defect in a novel ADAMTS family member is the cause of the belted white-spotting mutation. *Development* 130, 4665-4672.

Rawlings, N.D., Morton, F.R., Kok, C.Y., Kong, J., Barrett, A.J., 2008. MEROPS: the peptidase database. *Nucleic Acids Res* 36, D320-325.

Rodriguez-Manzaneque, J.C., Fernandez-Rodriguez, R., Rodriguez-Baena, F.J., Iruela-Arispe, M.L., 2015. ADAMTS proteases in vascular biology. *Matrix Biol* 44-46, 38-45.

Rodriguez-Manzaneque, J.C., Milchanowski, A.B., Dufour, E.K., Leduc, R., Iruela-Arispe, M.L., 2000. Characterization of METH-1/ADAMTS1 processing reveals two distinct active forms. *J Biol Chem* 275, 33471-33479.

Rossier, J., Bernard, A., Cabungcal, J.H., Perrenoud, Q., Savoye, A., Gallopin, T., Hawrylycz, M., Cuenod, M., Do, K., Urban, A., Lein, E.S., 2015. Cortical fast-spiking parvalbumin interneurons enwrapped in the perineuronal net express the metalloproteinases Adamts8, Adamts15 and Neprilysin. *Mol Psychiatry* 20, 154-161.

Roughley, P.J., Mort, J.S., 2014. The role of aggrecan in normal and osteoarthritic cartilage. *Journal of Experimental Orthopaedics* 1, 1-11.

Rudnicki, M., Perco, P., Neuwirt, H., Noppert, S.J., Leierer, J., Sunzenauer, J., Eder, S., Zoja, C., Eller, K., Rosenkranz, A.R., Muller, G.A., Mayer, B., Mayer, G., 2012. Increased renal versican expression is associated with progression of chronic kidney disease. *PLoS One* 7, e44891.

Schreiber, A.M., Brown, D.D., 2003. Tadpole skin dies autonomously in response to thyroid hormone at metamorphosis. *Proc Natl Acad Sci U S A* 100, 1769-1774.

Sebinger, D.D., Ofenbauer, A., Gruber, P., Malik, S., Werner, C., 2013. ECM modulated early kidney development in embryonic organ culture. *Biomaterials* 34, 6670-6682.

Session, A.M., Uno, Y., Kwon, T., Chapman, J.A., Toyoda, A., Takahashi, S., Fukui, A., Hikosaka, A., Suzuki, A., Kondo, M., van Heeringen, S.J., Quigley, I., Heinz, S., Ogino, H., Ochi, H., Hellsten, U., Lyons, J.B., Simakov, O., Putnam, N., Stites, J., Kuroki, Y., Tanaka, T., Michiue, T., Watanabe, M., Bogdanovic, O., Lister, R., Georgiou, G., Paranjpe, S.S., van Kruijsbergen, I., Shu, S., Carlson, J., Kinoshita, T., Ohta, Y., Mawaribuchi, S., Jenkins, J., Grimwood, J., Schmutz, J., Mitros, T., Mozaffari, S.V., Suzuki, Y., Haramoto, Y., Yamamoto, T.S., Takagi, C., Heald, R., Miller, K., Haudenschild, C., Kitzman, J., Nakayama, T., Izutsu, Y., Robert, J., Fortriede, J., Burns, K., Lotay, V., Karimi, K., Yasuoka, Y., Dichmann, D.S., Flajnik, M.F., Houston, D.W., Shendure, J., DuPasquier, L., Vize, P.D., Zorn, A.M., Ito, M., Marcotte, E.M., Wallingford, J.B., Ito, Y., Asashima, M., Ueno, N., Matsuda, Y., Veenstra, G.J., Fujiyama, A., Harland, R.M., Taira, M., Rokhsar, D.S., 2016. Genome evolution in the allotetraploid frog *Xenopus laevis*. *Nature* 538, 336-343.

Sharghi-Namini, S., Fan, H., Sulochana, K.N., Potturi, P., Xiang, W., Chong, Y.S., Wang, Z., Yang, H., Ge, R., 2008. The first but not the second

thrombospondin type 1 repeat of ADAMTS5 functions as an angiogenesis inhibitor. *Biochem Biophys Res Commun* 371, 215-219.

Silver, D.L., Hou, L., Somerville, R., Young, M.E., Apte, S.S., Pavan, W.J., 2008. The secreted metalloprotease ADAMTS20 is required for melanoblast survival. *PLoS Genet* 4, e1000003.

Smith, M.M., Melrose, J., 2015. Proteoglycans in Normal and Healing Skin. *Adv Wound Care (New Rochelle)* 4, 152-173.

Somerville, R.P., Longpre, J.M., Apel, E.D., Lewis, R.M., Wang, L.W., Sanes, J.R., Leduc, R., Apte, S.S., 2004. ADAMTS7B, the full-length product of the ADAMTS7 gene, is a chondroitin sulfate proteoglycan containing a mucin domain. *J Biol Chem* 279, 35159-35175.

Somerville, R.P., Longpre, J.M., Jungers, K.A., Engle, J.M., Ross, M., Evanko, S., Wight, T.N., Leduc, R., Apte, S.S., 2003. Characterization of ADAMTS-9 and ADAMTS-20 as a distinct ADAMTS subfamily related to *Caenorhabditis elegans* GON-1. *J Biol Chem* 278, 9503-9513.

Stankunas, K., Hang, C.T., Tsun, Z.Y., Chen, H., Lee, N.V., Wu, J.I., Shang, C., Bayle, J.H., Shou, W., Iruela-Arispe, M.L., Chang, C.P., 2008. Endocardial Brg1 represses ADAMTS1 to maintain the microenvironment for myocardial morphogenesis. *Dev Cell* 14, 298-311.

Stanton, H., Melrose, J., Little, C.B., Fosang, A.J., 2011. Proteoglycan degradation by the ADAMTS family of proteinases. *Biochim Biophys Acta* 1812, 1616-1629.

Su, Y., Shi, Y., Stolow, M.A., Shi, Y.B., 1997. Thyroid Hormone Induces Apoptosis in Primary Cell Cultures of Tadpole Intestine: Cell Type Specificity and Effects of Extracellular Matrix. *The Journal of Cell Biology* 139, 1533-1543.

Suga, A., Hikasa, H., Taira, M., 2006. *Xenopus* ADAMTS1 negatively modulates FGF signaling independent of its metalloprotease activity. *Dev Biol* 295, 26-39.

Suzuki, K., Machiyama, F., Nishino, S., Watanabe, Y., Kashiwagi, K., Kashiwagi, A., Yoshizato, K., 2009. Molecular features of thyroid hormone-regulated skin remodeling in *Xenopus laevis* during metamorphosis. *Dev Growth Differ* 51, 411-427.

Suzuki, K.T., Suzuki, M., Shigeta, M., Fortriede, J.D., Takahashi, S., Mawaribuchi, S., Yamamoto, T., Taira, M., Fukui, A., 2016. Clustered *Xenopus* keratin genes: A genomic, transcriptomic, and proteomic analysis. *Dev Biol*.

Suzuki, T., Kusakabe, M., Nakayama, K., Nishida, E., 2012. The protein kinase MLTK regulates chondrogenesis by inducing the transcription factor Sox6. *Development* 139, 2988-2998.

Szabo, A., Melchionda, M., Nastasi, G., Woods, M.L., Campo, S., Perris, R., Mayor, R., 2016. In vivo confinement promotes collective migration of neural crest cells. *J Cell Biol* 213, 543-555.

Takeshita, K., Hayashi, M., Iino, S., Kondo, T., Inden, Y., Iwase, M., Kojima, T., Hirai, M., Ito, M., Loskutoff, D.J., Saito, H., Murohara, T., Yamamoto, K., 2004. Increased Expression of Plasminogen Activator Inhibitor-1 in Cardiomyocytes Contributes to Cardiac Fibrosis after Myocardial Infarction. *American Journal of Pathology* 164.

Tamura, K., Stecher, G., Peterson, D., Filipinski, A., Kumar, S., 2013. MEGA6: Molecular Evolutionary Genetics Analysis version 6.0. *Mol Biol Evol* 30, 2725-2729.

Tao, Z.-Y., Cavaasin, M.A., Yang, F., Liu, Y.-H., Yang, X.-P., 2004. Temporal changes in matrix metalloproteinase expression and inflammatory response associated with cardiac rupture after myocardial infarction in mice. *Life Sciences* 74, 1561-1572.

Tauchi, R., Imagama, S., Natori, T., Ohgomori, T., Muramoto, A., Shinjo, R., Matsuyama, Y., Ishiguro, N., Kadomatsu, K., 2012. The endogenous proteoglycan-degrading enzyme ADAMTS-4 promotes functional recovery after spinal cord injury. *Journal of Neuroinflammation* 9.

Theocharis, A.D., Skandalis, S.S., Gialeli, C., Karamanos, N.K., 2016. Extracellular matrix structure. *Adv Drug Deliv Rev* 97, 4-27.

Theveneau, E., Mayor, R., 2012. Neural crest delamination and migration: from epithelium-to-mesenchyme transition to collective cell migration. *Dev Biol* 366, 34-54.

Theveneau, E., Mayor, R., 2013. Collective cell migration of epithelial and mesenchymal cells. *Cell Mol Life Sci* 70, 3481-3492.

Thiery, J.P., Acloque, H., Huang, R.Y., Nieto, M.A., 2009. Epithelial-mesenchymal transitions in development and disease. *Cell* 139, 871-890.

Tomlinson, M.L., Garcia-Morales, C., Abu-Elmagd, M., Wheeler, G.N., 2008. Three matrix metalloproteinases are required in vivo for macrophage migration during embryonic development. *Mech Dev* 125, 1059-1070.

Tomlinson, M.L., Guan, P., Morris, R.J., Fidock, M.D., Rejzek, M., Garcia-Morales, C., Field, R.A., Wheeler, G.N., 2009. A chemical genomic approach identifies matrix metalloproteinases as playing an essential and specific role in *Xenopus* melanophore migration. *Chem Biol* 16, 93-104.

Turner, N.A., Warburton, P., O'Regan, D.J., Ball, S.G., Porter, K.E., 2010. Modulatory effect of interleukin-1alpha on expression of structural matrix proteins, MMPs and TIMPs in human cardiac myofibroblasts: role of p38 MAP kinase. *Matrix Biol* 29, 613-620.

Uygun, A., Lee, R.T., 2016. Mechanisms of Cardiac Regeneration. *Dev Cell* 36, 362-374.

van Nieuwenhoven, F.A., Turner, N.A., 2013. The role of cardiac fibroblasts in the transition from inflammation to fibrosis following myocardial infarction. *Vascul Pharmacol* 58, 182-188.

van Tetering, G., van Diest, P., Verlaan, I., van der Wall, E., Kopan, R., Vooijs, M., 2009. Metalloprotease ADAM10 is required for Notch1 site 2 cleavage. *J Biol Chem* 284, 31018-31027.

Vazquez, F., Hastings, G., Ortega, M.A., Lane, T.F., Oikemus, S., Lombardo, M., Iruela-Arispe, M.L., 1999. METH-1, a Human Ortholog of ADAMTS-1, and METH-2 Are Members of a New Family of Proteins with Angio-inhibitory Activity. *THE JOURNAL OF BIOLOGICAL CHEMISTRY* 274, 23349-23357.

Vecino, E., Kwok, C.F., 2016. The Extracellular Matrix in the Nervous System: The Good and the Bad Aspects. *Composition and Function of the Extracellular Matrix in the Human Body*.

Velasco, J., Li, J., DiPietro, L., Stepp, M.A., Sandy, J.D., Plaas, A., 2011. Adamts5 deletion blocks murine dermal repair through CD44-mediated aggrecan accumulation and modulation of transforming growth factor beta1 (TGFbeta1) signaling. *J Biol Chem* 286, 26016-26027.

Vistnes, M., Aronsen, J.M., Lunde, I.G., Sjaastad, I., Carlson, C.R., Christensen, G., 2014. Pentosan Polysulfate Decreases Myocardial Expression of the Extracellular Matrix Enzyme ADAMTS4 and Improves Cardiac Function In Vivo in Rats Subjected to Pressure Overload by Aortic Banding. *PLoS One* 9.

Vivien, C.J., Hudson, J.E., Porello, E.R., 2016. Evolution, comparative biology and ontogeny of vertebrate heart regeneration. *npj Regenerative Medicine* 1.

Vize, P.D., Jones, E.A., Pfister, R., 1995. Development of the *Xenopus* pronephric system. *Dev Biol* 171, 531-540.

Wagsater, D., Bjork, H., Zhu, C., Bjorkegren, J., Valen, G., Hamsten, A., Eriksson, P., 2008. ADAMTS-4 and -8 are inflammatory regulated enzymes expressed in macrophage-rich areas of human atherosclerotic plaques. *Atherosclerosis* 196, 514-522.

Wang, J., Karra, R., Dickson, A.L., Poss, K.D., 2013. Fibronectin is deposited by injury-activated epicardial cells and is necessary for zebrafish heart regeneration. *Dev Biol* 382, 427-435.

Wang, P., Tortorella, M., England, K., Malfait, A.M., Thomas, G., Arner, E.C., Pei, D., 2004. Proprotein convertase furin interacts with and cleaves pro-ADAMTS4 (Aggrecanase-1) in the trans-Golgi network. *J Biol Chem* 279, 15434-15440.

Watanabe, M., Yasuoka, Y., Mawaribuchi, S., Kuretani, A., Ito, M., Kondo, M., Ochi, H., Ogino, H., Fukui, A., Taira, M., Kinoshita, T., 2016. Conservatism and variability of gene expression profiles among homeologous transcription factors in *Xenopus laevis*. *Dev Biol*.

Weber, S., Saftig, P., 2012. Ectodomain shedding and ADAMs in development. *Development* 139, 3693-3709.

Wei, S., Whittaker, C.A., Xu, G., Bridges, L.C., Shah, A., White, J.M., Desimone, D.W., 2010. Conservation and divergence of ADAM family proteins in the *Xenopus* genome. *BMC Evol Biol* 10, 211.

Wheeler, G.N., Brandli, A.W., 2009. Simple vertebrate models for chemical genetics and drug discovery screens: lessons from zebrafish and *Xenopus*. *Dev Dyn* 238, 1287-1308.

Wu, Y.J., La Pierre, D.P., Wu, J., Yee, A.J., Yang, B.B., 2005. The interaction of versican with its binding partners. *Cell Research* 15, 483-494.

Yamamura, H., Zhang, M., Markwald, R.R., Mjaatvedt, C.H., 1997. A Heart Segmental Defect in the Anterior-Posterior Axis of a Transgenic Mutant Mouse. *Dev Biol* 186, 58-72.

You, Y., Moreira, B.G., Behlke, M.A., Owczarzy, R., 2006. Design of LNA probes that improve mismatch discrimination. *Nucleic Acids Res* 34, e60.

Yu, Q., Stamenkovic, I., 2000. *GENES & DEVELOPMENT* 14, 163-176.

Zheng, X., Chung, D., Takayama, T.K., Majerus, E.M., Sadler, J.E., Fujikawa, K., 2001. Structure of von Willebrand factor-cleaving protease (ADAMTS13), a metalloprotease involved in thrombotic thrombocytopenic purpura. *J Biol Chem* 276, 41059-41063.

Appendices

8.1 Appendix 1: Primers used in this study

Appendix 8-1: Sequences and terms of use of each primer set for RT-qPCR and microfluidic in *Xenopus laevis*.

<i>Xenopus laevis</i> gene name	Product length (bp)	T _m (°C)	Sense primer	Anti-sense primer	Reference
<i>ADAMTS1</i>	124	57	CAGGAGGCACGAGG AAGAA	ATGAGGGTGAGG AGATAATGTTTC	Primerdesign
<i>ADAMTS4</i>	99	56.6	CTATCGCCGCTATCA ACTACAA	TGAGTCCTCCAC CTTCCAAG	Primerdesign
<i>ADAMTS5</i>	90	57	GGGCAAGGTGGGCT ACAT	CTGAAGTGGGGA GACAACAAC	Primerdesign
<i>ADAMTS8</i>	129	56.4	TTTAGTTCCTGATGA TGCTTTTCTT	GCTGCCAGTGGT TCCATAC	Primerdesign
<i>ADAMTS15</i>	91	56.7	AATCCAATCAACATT GTCGTTGTG	TCAGTGTGATGG CGGCATT	Primerdesign
<i>ADAMTS9</i>	98	56.4	GCCCGACTGGAATA CAATGAT	ATGTTTTGCGTTT TACTGAAGAGA	Primerdesign
<i>ADAMTS20</i>	88	56.8	TTAGAACCACTGATG AAACCTGAT	AATGTTTGACTTT GTGCTTGTAGA	Primerdesign
<i>ADAMTS2</i>	123	57	TCCGAACAGTTAAGT GTATTCAGC	GAGCAGGACAAG GTTGACGA	Primerdesign
<i>ADAMTS3</i>	129	56.6	CGAACATTTGCGAAT TGTAACAA	GTGACCCTTGTA GCACCACT	Primerdesign
<i>ADAMTS14</i>	130	56.7	CAGAACAGTCTTACA GTCAGGATG	CCTCCGTATGAT GGCTCTGG	Primerdesign
<i>ADAMTS13</i>	110	56.8	CGAGCAGTTGGAAG TGTAAG	ATGTTGAGGTTG GTTAGGATGTAT C	Primerdesign
<i>ADAMTS7</i>	91	56.7	AGCCTCTGTGACCAT GAACC	GAGTGCAGGAGA CATTGTTCTG	Primerdesign
<i>ADAMTS12</i>	127	56.9	GCCTTACAAGAATGA ACTGTACCA	CGTACCATCAAT CACCGCATC	Primerdesign
<i>ADAMTS6</i>	128	56.7	GCAAGCACTTTCACT TAAACCTG	TCCTGTATAGTG GCAGTTGTCTAT A	Primerdesign
<i>ADAMTS10</i>	95	56.4	GGTAATAGATGACAA GCCTTGGA	CTTGCTGTGTCT GGTTGGATC	Primerdesign
<i>ADAMTS16</i>	109	56.8	ATTCTGTGAAGTTTC CTCACGA	CGGCTTGCTGTT ATACTCTGC	Primerdesign
<i>ADAMTS18</i>	105	57	CAGTGTGTTGAGAAA TCTACAATGC	GCAGTCCTGAAT GTTACAAGCC	Primerdesign
<i>ADAMTS17</i>	117	56.7	CAGAGTAACTGCCAT GTTGTATCA	CTCCACGCTGTG CTCTTCA	Primerdesign
<i>ADAMTS19</i>	86	56.9	CGCATCGTGTTTACA GGAGAAA	TGTAACCTCCACA GTATGGCTGAT	Primerdesign
<i>ADAM7</i>	129	56.6	GGCTCATCCAGACG GAAGG	TATATGTTGTGTT GTCCACTCCAC	Primerdesign
<i>ADAM9</i>	129	56.9	TACAGTGGCGTGAG ACTAACC	CGGCATGACTTC TGGAACATAC	Primerdesign
<i>ADAM10</i>	106	56.6	TTTAAATTGGAGGTT GGAGGAGAAA	CAACAACAGATC CGTGACTION	Primerdesign
<i>ADAM15</i>	124	56.8	AGTTGGTGTGGTG GCAGATA	CGGACATTGAGA GGTCGGTAA	Primerdesign

<i>ADAM19</i>	126	56.9	GGACATTCCATCCA GTTAGAGGA	GTCAGCCACCAG GTACAGTT	Primerdesign
<i>ADAM17</i>	118	56.8	TAGTTGTGGCTGAC CATCGG	CACGAGGTGTTT TTGTAGATGTC	Primerdesign
<i>ADAM28</i>	114	56.8	TGTTATCCAGGATCA CAGCCAA	GATGAGCAAGTA CAGTGAGGTTT	Primerdesign
<i>ADAM22</i>	118	56.9	CCTCAGCACCTCGG CATG	CTCGCATGAGCC AGATGGAT	Primerdesign
<i>ADAM33</i>	127	57	CAAGAGGCTGTATC ATGGCT	TTGGCATGTTGA ATAGGCACATT	Primerdesign
<i>ADAM23</i>	111	56.8	CTCCTGCTGCTGCT GTCC	GTCTTCTTCTGC CAATCTACCAG	Primerdesign
<i>ADAM12</i>	130	56.8	ATTGTAGCGGATAAT CGTGAGTATC	CAACCAGAGCCA CTCGTATATTC	Primerdesign
<i>ADAM11</i>	116	56.6	AGGCAGAACTGGAT TCAGTGTA	CTCATACTGGTG ATGTCTCCATTC	Primerdesign
<i>MMP14</i>	110	56.7	GAGACGGAAGAGAT ACGCCAT	TCGCCTCATAGG TAGAATACTCG	Primerdesign
<i>MMP1</i>	89	56.6	ATCCTCCAATCCAGT CCAACC	CTCTCATGGTGG TGACAGCA	Primerdesign
<i>MMP7</i>	130	57	TCGCCAAGTGGTAG ATGACG	TCCATGCGTGCC TGCTC	Primerdesign
<i>MMP9</i>	108	56.8	CACTTACCCTATTCT GAACTACTCC	GTGAAGGACAGA GGTGTGACA	Primerdesign
<i>MMP2</i>	85	57.2	TCAAGGCAACACATA CAACAGC	CTTGTTCATAGTCT TCTGTGGTAGC	Primerdesign
<i>TIMP1</i>	90	57	GGCTTCGAGGAGGT GTATCG	GCACTGGCTGTC CGACTC	Primerdesign
<i>TIMP3</i>	72	56.7	TACTACCTTCCCTGT TTCATCACT	GTAGCCGAAGTT GGAGAGCA	Primerdesign
<i>TIMP2</i>	107	56.7	CACATTGACATTCCA ACACCAAC	CATATCAACACA AGCATAGCAAGA G	Primerdesign
<i>uPAR</i>	97	56.7	GTGACCTATTGCTCT ACCCTTAC	TTTGTGTGAAATT GTTACAGTTGCT	Primerdesign
<i>tPA</i>	79	57	CTGTGCGGAGGAAC ACTCAT	GTGGTGCTGTTG AGATATCATTGA	Primerdesign
<i>PAI1</i>	130	56.9	CAAGCCAAGGACAT CATTAAATCAAT	TGCCACTGAAGT GTATAGCACT	Primerdesign
<i>SYNDECAN4B</i>	119	56.9	CATTCAACGAGAACA ACGAGATTG	TCTCTGGAAGAA TCCTGAAGACC	Primerdesign
<i>SYNDECAN2B</i>	95	56.9	ATGATTACTCTTCTG GATCTGGCT	GCTGCTTATAAG TGTCTGGACAG	Primerdesign
<i>SYNDECAN1</i>	73	56.9	GCACACTGATACGAT GGACAAG	CGTTACAGCCAG CGAGCA	Primerdesign
<i>SYNDECAN3</i>	78	56.6	GGCTGCTCTTCATCA TCACAC	GATCAACAGGTC GCTCATCTTC	Primerdesign
<i>ACAN</i>	111	56.8	CTCCTGCTGCTGCT GTCC	GTCTTCTTCTGC CAATCTACCAG	Primerdesign
<i>TENASCIN-C</i>	118	56.7	TCTGGTACAAGAACT GTCACAGA	TCGGCAAAGTGA ATGGAGTATTC	Primerdesign
<i>VCAN</i>	124	56.8	TCATTATCTGGAAGA GTGAATCTGC	CATCTCTGCTCT GGACAATCTTG	Primerdesign

Appendix 8-2: Sequences and terms of use of each primer set for RT-PCR in *Xenopus tropicalis*. ADAMTS9 and ADAMTS20 primers highlighted in orange are used to make probes as well.

<i>Xenopus tropicalis</i> gene name	Product length (bp)	T _m (°C)	Sense primer	Anti-sense primer	Reference
ADAMTS1	180	59.2	CTTTTCTTGCCCCGG ACTTC	CTCGGTAGAAGAAG GCTCCC	PRIMER3/S IGMA
ADAMTS4	173	59.2	GACCCCAGTTTTCTC TCCGA	TGCAGAACCCCAACA AGAGA	PRIMER3/S IGMA
ADAMTS5	218	59.1	TACGCGGATGGGAA GAAGTT	TAATGGGCATGCTTG ACTGC	PRIMER3/S IGMA
ADAMTS8	200	58.9	GACCTTGCGATTTAC TGCAC	CACCCCTGAACACCTT TGCA	PRIMER3/S IGMA
ADAMTS15	151	59.2	CTATGCACTTCCCTG GCTCT	TATTCCTCCCCTTG TAGCC	PRIMER3/S IGMA
ADAMTS9	693	62	TTAGCAGTGGTCCAT GATGAA	TTCCCGGCTCACATT CG	PRIMER3/S IGMA
ADAMTS20	522	59	GGGCTTGTCTGTCAT CTCT	AGGTGTGGTTTGTG TGCTC	PRIMER3/S IGMA
ADAMTS2	151	58.9	AGTTCCGGACAGTGA AGTGT	TGAGACCAAGGCC AATTCT	PRIMER3/S IGMA
ADAMTS3	174	59.1	AAAGCTGTGGAAGTT CTGGC	CAGACCATGCCCT GTTTT	PRIMER3/S IGMA
ADAMTS14	224	59.1	AGCCAAAACCAATAC GCAGA	TGGTGTCCGATTACA GGGTC	PRIMER3/S IGMA
ADAMTS13	208	59	CAATGGGGTGGTACT GGAGT	GGGTTCCAGGTCCAT GTACA	PRIMER3/S IGMA
ADAMTS7	232	59	GGAGATGGTGGACA AGGGAA	GTGCCTCTGACTGG GTACTT	PRIMER3/S IGMA
ADAMTS12	164	58.8	ATGAGCCGTGTGATT CCTCT	TGGTAAGAAGATGCG CCTCT	PRIMER3/S IGMA
ADAMTS6	178	58.9	CCTTGTTCATGGCTTC ATCGG	ACTCCTCCTCCTCCT CAAGT	PRIMER3/S IGMA
ADAMTS10	242	59	GAGGTCTGGACTGG AAGCAT	CTCCAAGTGTGACG TTGCA	PRIMER3/S IGMA
ADAMTS16	134	58.3	ACCAAGGAAGATTCA AACGATCA	TGTCAACACGTAGGT AGTAATGT	PRIMER3/S IGMA
ADAMTS18	245	58.6	GAGATCAGCGCGAA GTTCAA	GGAAACCTGACATGC CATCA	PRIMER3/S IGMA
ADAMTS17	184	58.9	ACAGAGGAGAGGGA CCAAAC	TCCCTGGTTTTCTCC TCCAC	PRIMER3/S IGMA
ADAMTS19	217	59.2	CAACCAACGCATCAT CTCCC	GAAGATCCTCTCCAC TCCCG	PRIMER3/S IGMA

Appendix 8-3: Sequences and terms of use of M13 primer set for PCR on plasmids.

Primers name	Product length (bp)	T _m (°C)	Sense primer	Anti-sense primer	Reference
M13	depending on the plasmid used	55	CGCCAGGGTTTTCCCA GTCACGAC	TCACACAGGAAACAG CTATGAC	PRIMER3/SI GMA

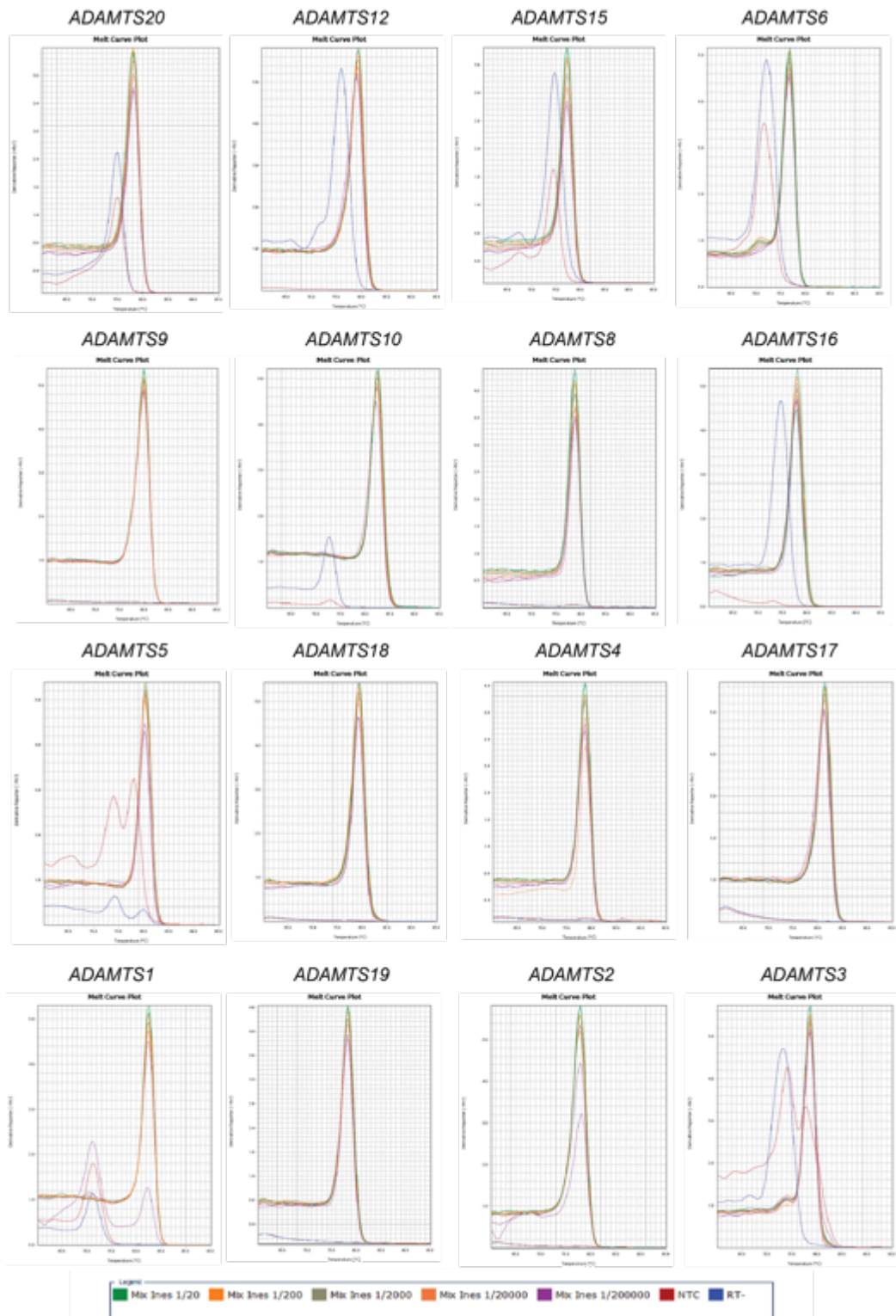
Appendix 8-4: Sequences and terms of use of each primer set to make *Xenopus laevis* probes.

<i>Xenopus laevis</i> gene name	Product length (bp)	T _m (°C)	Sense primer	Anti-sense primer	Reference
ADAMTS4	577	62	GACCCCAGTTTTCTCT CCGA	CCGCCTTCCAATCA CAACA	PRIMER3/ SIGMA
ADAMTS5	590	60	ACATGCCCACTACACC ATCA	CGTGCTCATCATCC AGTTGG	PRIMER3/ SIGMA
ADAMTS8	556	58	ATGTGGAGTATGCGG AGGAG	TCCACCCTCCACAT CTTGAC	PRIMER3/ SIGMA
ADAMTS15	579	58	TGCGATCCAAAACGTA GCTG	AGTCCGGGAACATT GACCAT	PRIMER3/ SIGMA
ADAMTS9	717	58	TTAGCAGTGGTCCAC GATGAA	AGGAACACATACTC CATATCTG	PRIMER3/ SIGMA
ADAMTS20	699	59	GTGTGCTGTAACATGT GGAA	GAATGTACTIONTGTGTA CTGGCAC	PRIMER3/ SIGMA
VCAN	562	59	GTTTCAGCGGAGATC AATGTGA	GCATTTTCTACCAAA GGAGGCT	PRIMER3/ SIGMA

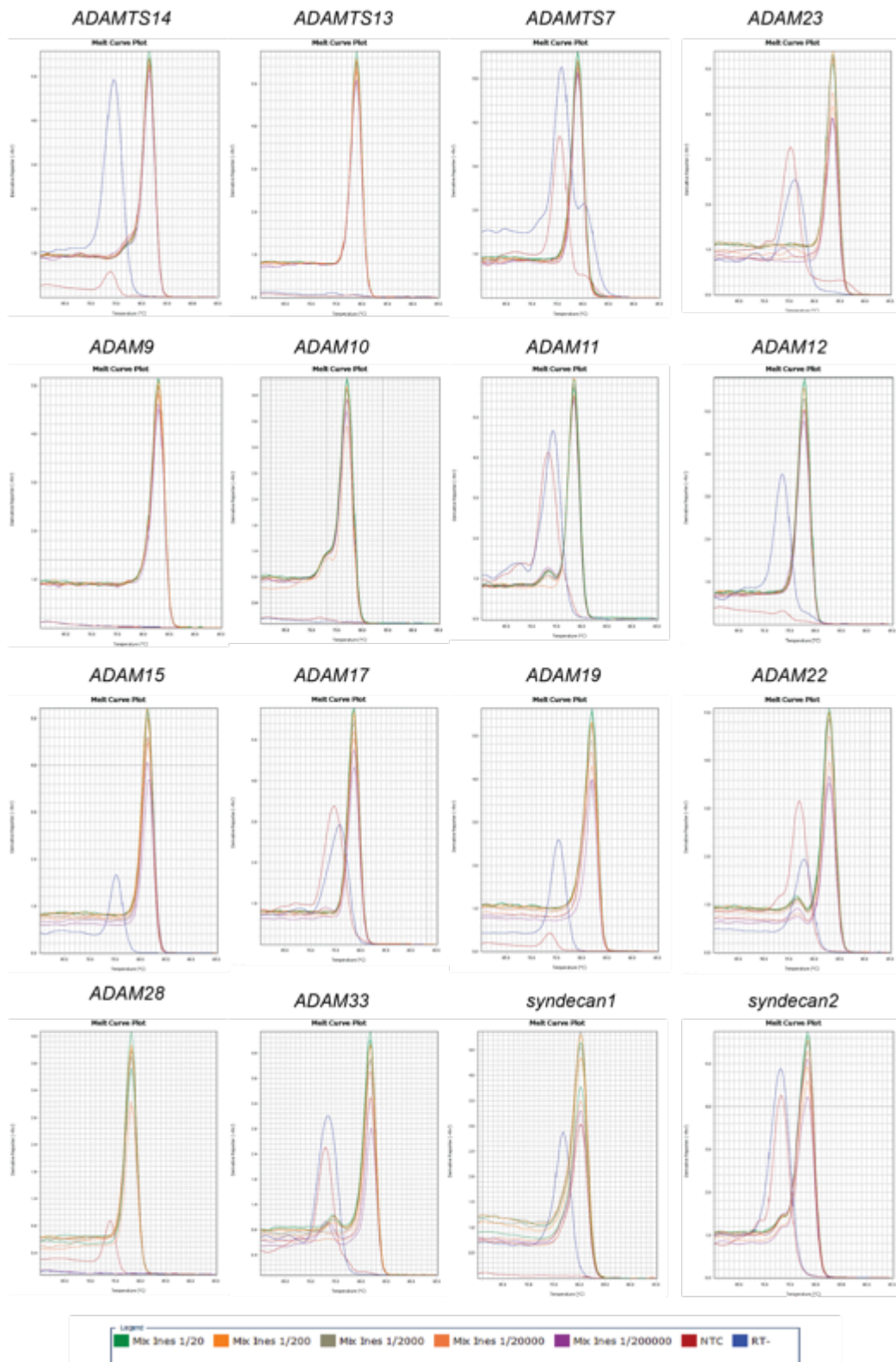
Appendix 8-5: Sequences and terms of use of each primer set to make *Xenopus tropicalis* probes

<i>Xenopus tropicalis</i> gene name	Product length (bp)	T _m (°C)	Sense primer	Anti-sense primer	Reference
ADAMTS1	528	59.1	GTAAAGGCAGGCTGT GATCG	TTCGATGACCCATTC CGACA	PRIMER3/ SIGMA
ADAMTS4	649	59	GACCCCAGTTTTCTCT CCGA	CGCAGAAGTTCCTC AGCATC	PRIMER3/ SIGMA
ADAMTS5	599	59.1	TACGCGGATGGGAAG AAGTT	TTCCCGTACTTCTTG GCCAT	PRIMER3/ SIGMA
ADAMTS8	587	59	ATCAGTGCAGGATGT GACCA	CATTCTACTGCCCGT CGTTG	PRIMER3/ SIGMA
ADAMTS15	647	59.1	CTATGCACTTCCCTGG CTCT	CCATTTCTTCTGCCA CCCAC	PRIMER3/ SIGMA
ADAMTS2	681	58.9	AGTCCGGACAGTGA AGTGT	GTTGTGGCACTTCG TTCTGT	PRIMER3/ SIGMA
ADAMTS3	539	59	TCGGTGTAGTGGTCA GGAAC	GTTGACACTGTTGG GCTCTG	PRIMER3/ SIGMA
ADAMTS14	638	58.6	AGCCAAAACCAATACG CAGA	TGGAGTCAAACCTGG TAGGGG	PRIMER3/ SIGMA
ADAMTS13	581	59	CGGTATCCAAAGCCG TCAAG	ACTCCAGTACCACC CCATTG	PRIMER3/ SIGMA
ADAMTS7	575	59	TGGACATTGGCCTGAT TCCT	TGTTCTCTTTGCAG GCCAC	PRIMER3/ SIGMA
ADAMTS12	577	59.1	ATTCCTTGACGCGGT GATTG	AGTCGCACTACAGT CTGTCC	PRIMER3/ SIGMA
ADAMTS6	510	59	CCTTGTCATGGCTTCA TCGG	TCATGGCTGTAGTG CTTGGA	PRIMER3/ SIGMA
ADAMTS10	668	59	GAGGTCTGGACTGGA AGCAT	GCCACTCTCCGAAA TTGCAT	PRIMER3/ SIGMA
ADAMTS16	516	59.1	ACCAAGGAAGATTCAA ACGATCA	CATCGTGGACCATG CCAAAA	PRIMER3/ SIGMA
ADAMTS18	657	58.9	GAGATCAGCGCAAG TTCAA	ACGCTGTCTTTGCC ATGTTT	PRIMER3/ SIGMA
ADAMTS17	593	58.9	ACAGAGGAGAGGGAC CAAAC	CTGCACCATGTCCG AATCAG	PRIMER3/ SIGMA
ADAMTS19	618	59.1	CAACCAACGCATCATC TCCC	TTCTAGTGGCTTCTG GTCCG	PRIMER3/ SIGMA

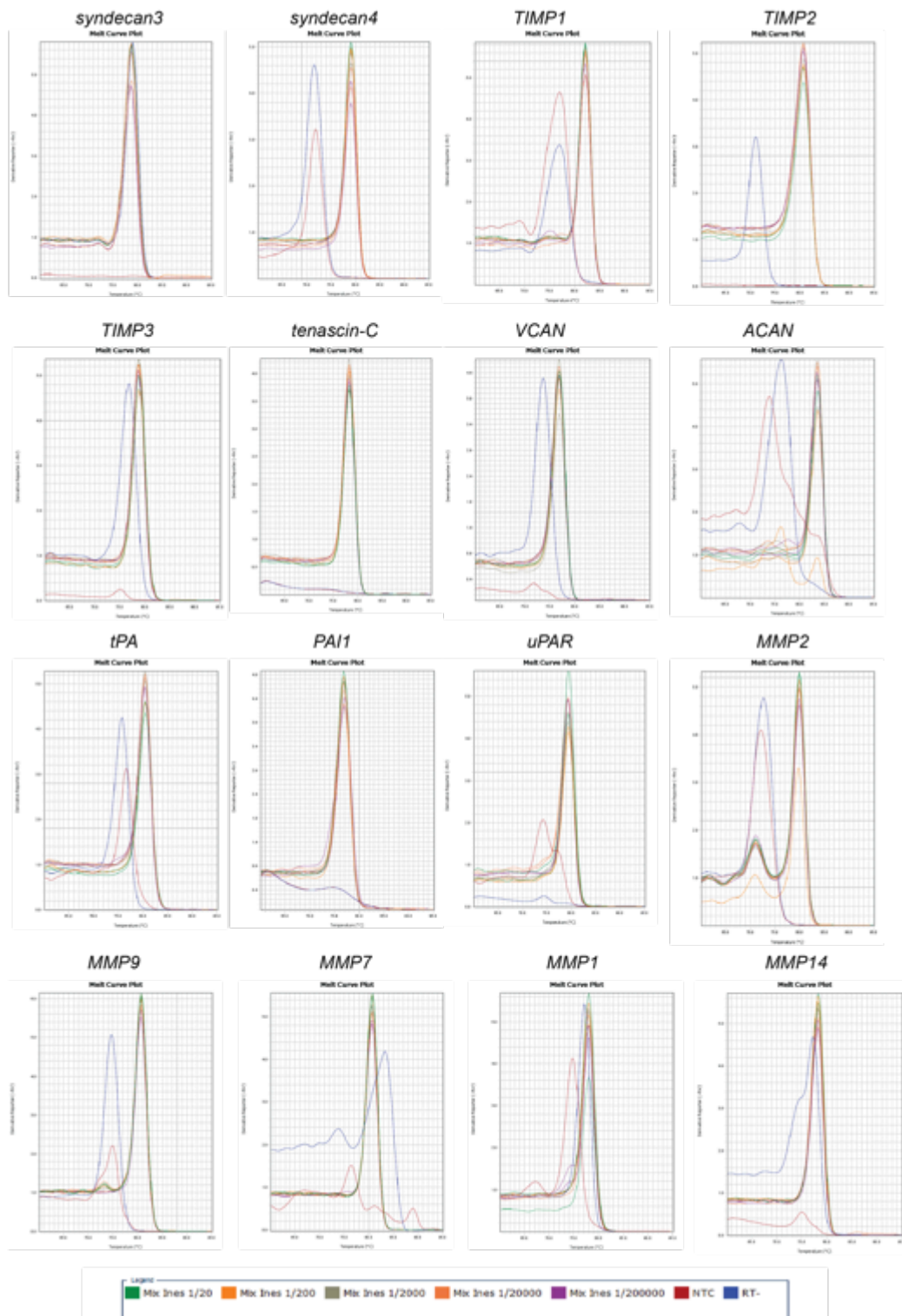
8.2 Appendix 2: Melt curve of primers used for the microfluidic



Appendix 8-6: Melt curve of primers used for RT-qPCR and microfluidic experiments in *Xenopus laevis*. Five different dilutions of cDNA (1/20, 1/200, 1/2000, 1/20000 and 1/200000) was used to test the efficiency and the specificity of cDNA amplification of the primers and negatives controls were water (NTC) and a negative control of cDNA synthesis reaction made without adding the Reverse Transcriptase enzyme to look at any genomic DNA contamination (RT-).



Appendix 8-7: Melt curve of primers used for RT-qPCR and microfluidic experiments in *Xenopus laevis*. Five different dilutions of cDNA (1/20, 1/200, 1/2000, 1/20000 and 1/200000) was used to test the efficiency and the specificity of cDNA amplification of the primers and negatives controls were water (NTC) and a negative control of cDNA synthesis reaction made without adding the Reverse Transcriptase enzyme to look at any genomic DNA contamination (RT-).

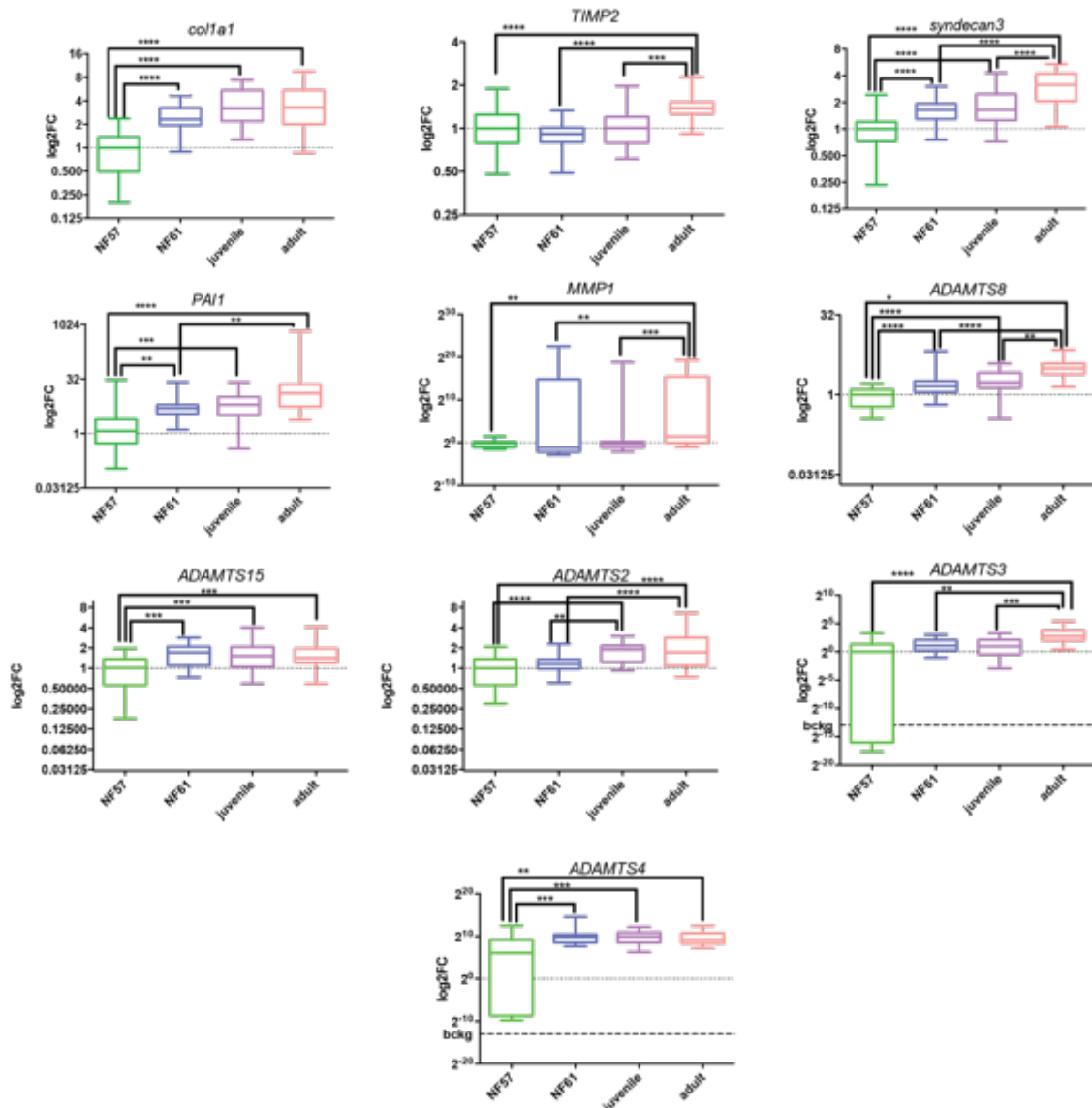


Appendix 8-8: Melt curve of primers used for RT-qPCR and microfluidic experiments in *Xenopus laevis*. Five different dilutions of cDNA (1/20, 1/200, 1/2000, 1/20000 and 1/200000) was used to test the efficiency and the specificity of cDNA amplification of the primers and negatives controls were water (NTC) and a negative control of cDNA synthesis reaction made without adding the Reverse Transcriptase enzyme to look at any genomic DNA contamination (RT-).

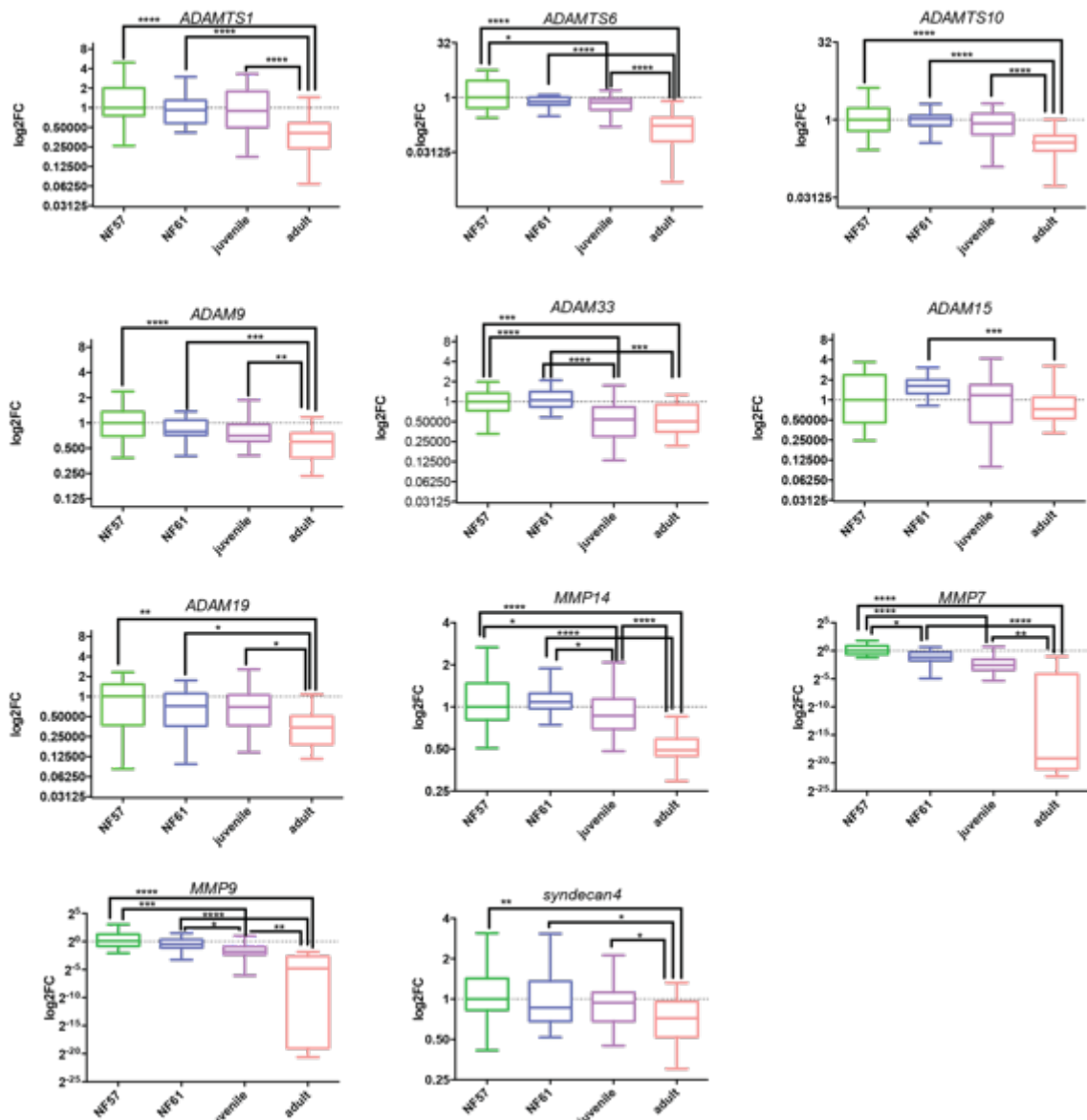
Appendix 8-9: Efficiency of the genes analysed in heart development and regeneration during *Xenopus laevis* metamorphosis. The different genes categories are indicated in the first two rows and specific gene name is indicated below. For *ADAMTS*, *ADAM*, *MMP*, *TIMP* and syndecan only the gene number is indicated in the column meaning *ADAMTS1*, *ADAM7*, *MMP2*, *TIMP1* and syndecan1 for all different genes. The percentage of efficiency is written in bold under the corresponding gene name. *ADAM*, a disintegrin and metalloproteinase; *tPA*, tissue plasminogen activator; *PAI1*, plasminogen activator inhibitor-1; *uPAR*, urokinase plasminogen activator receptor.

metalloproteinases							
<i>ADAMTS</i>		<i>ADAM</i>	<i>MMP</i>	<i>TIMP</i>	ECM	plasminogen	<i>syndecan</i>
1	13	9	2	1	<i>VCAN</i>	<i>tPA</i>	1
112.67	111.17	116.05	115.63	108.39	109.84	112.33	100.27
2	14	10	9	2	<i>ACAN</i>	<i>PAI1</i>	2
103.34	113.77	116.79	111.6	112.85	165.17	115.96	106.67
3	15	11	7	3	<i>tenascin-C</i>	<i>uPAR</i>	3
113.98	109.53	115.39	110.92	111.22	115.6	116.69	107.03
4	16	12	1				4
108.86	109.88	113.22	111.31				104.18
5	17	15	14				
112.98	114.18	106.74	110.44				
6	18	17					
109.02	99.46	107.81					
7	19	19					
111.95	106.54	101.08					
8	20	22					
113.13	116.19	104.05					
9		23					
113.88		100.1					
10		28					
114.7		90.36					
12		33					
111.6		94.86					

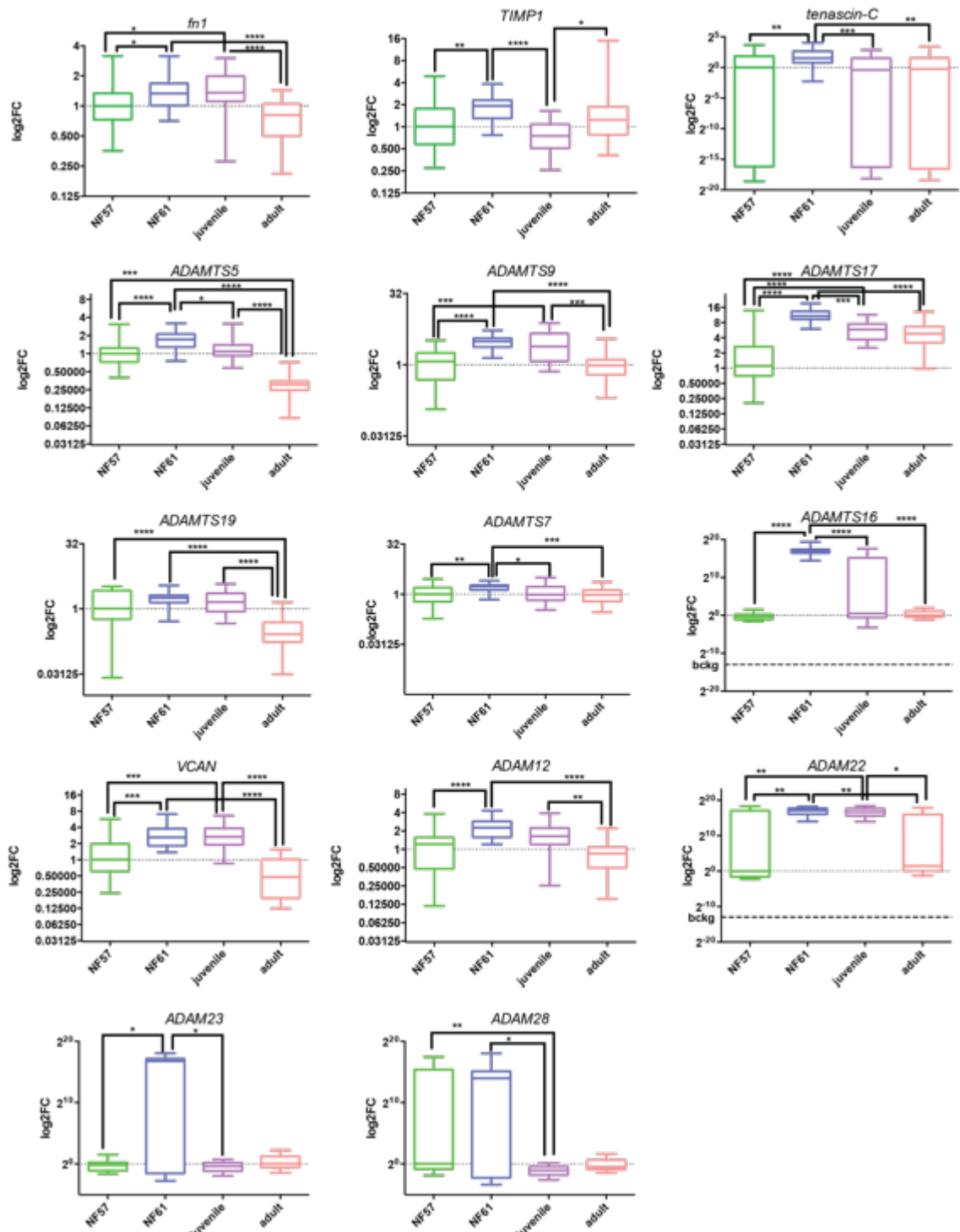
8.3 Appendix 3: Graphs of gene expression and regulation in the heart during *Xenopus laevis* metamorphosis



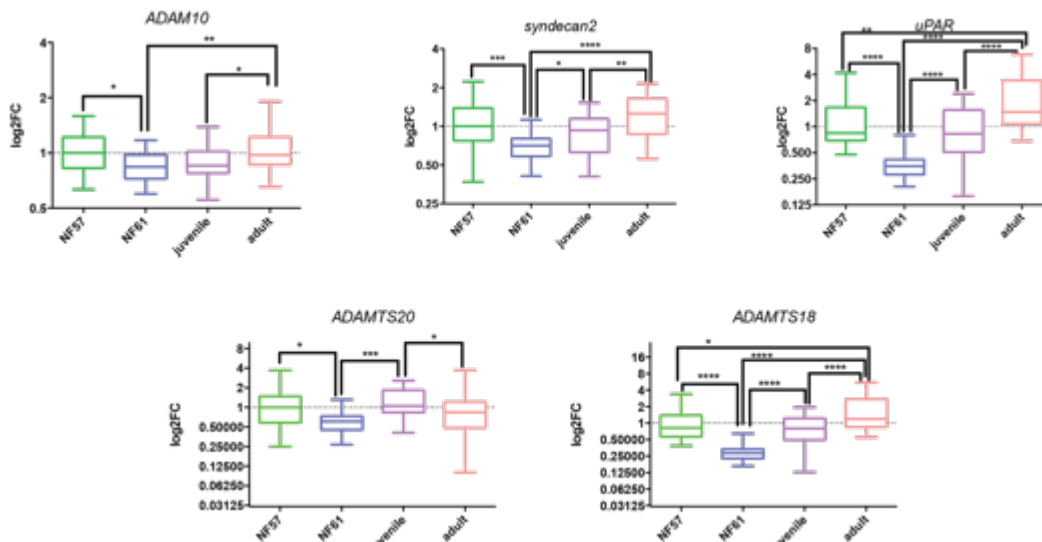
Appendix 8-10: Genes up regulated in the heart during *Xenopus laevis* metamorphosis. Graphs show gene expression in the heart at stage 57 (NF57), stage 61 (NF61), juvenile and adult *Xenopus laevis* in log₂FC (y axis) in function of the stages of development according to (Nieuwkoop and Faber, 1994) (NF) (x axis). The width of the box shows the interquartile range (IQR), the line in the box shows the median and the whiskers show the minimum and the maximum values. Stars on the graphs show statistical differences with P < 0.05.



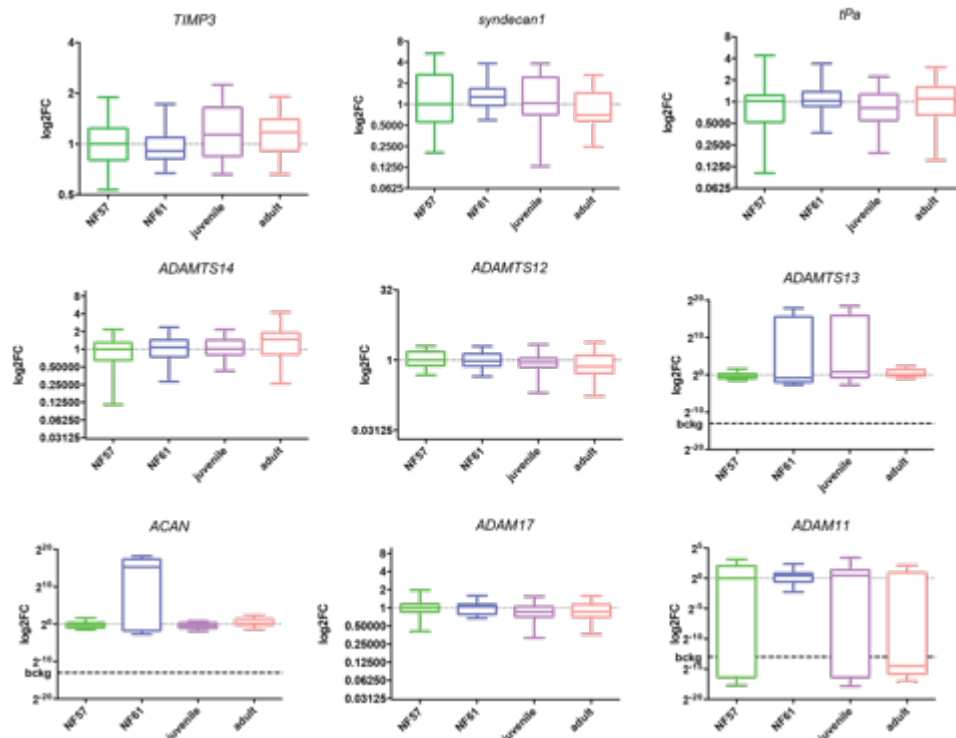
Appendix 8-11: Genes down regulated in the heart during *Xenopus laevis* metamorphosis. Graphs show gene expression in the heart at stage 57 (NF57), stage 61 (NF61), juvenile and adult *Xenopus laevis* in log₂FC (y axis) in function of the stages of development according to (Nieuwkoop and Faber, 1994) (NF) (x axis). The width of the box shows the interquartile range (IQR), the line in the box shows the median and the whiskers show the minimum and the maximum values. Stars on the graphs show statistical differences with P < 0.05.



Appendix 8-12: Genes up regulated in the *Xenopus laevis* heart at metamorphic climax. Graphs show gene expression in the heart at stage 57 (NF57), stage 61 (NF61), juvenile and adult *Xenopus laevis* in log₂FC (y axis) in function of the stages of development according to (Nieuwkoop and Faber, 1994) (NF) (x axis). The width of the box shows the interquartile range (IQR), the line in the box shows the median and the whiskers show the minimum and the maximum values. Stars on the graphs show statistical differences with $P < 0.05$.



Appendix 8-13: Genes down regulated in the *Xenopus laevis* heart at metamorphic climax. Graphs show gene expression in the heart at stage 57 (NF57), stage 61 (NF61), juvenile and adult *Xenopus laevis* in log₂FC (y axis) in function of the stages of development according to (Nieuwkoop and Faber, 1994) (NF) (x axis). The width of the box shows the interquartile range (IQR), the line in the box shows the median and the whiskers show the minimum and the maximum values. Stars on the graphs show statistical differences with P < 0.05.



Appendix 8-14: Genes showing no change of expression in the heart during *Xenopus laevis* metamorphosis. Graphs show gene expression in the heart at stage 57 (NF57), stage 61 (NF61), juvenile and adult *Xenopus laevis* in log₂FC (y axis) in function of the stages of development according to (Nieuwkoop and Faber, 1994) (NF) (x axis). The width of the box shows the interquartile range (IQR), the line in the box shows the median and the whiskers show the minimum and the maximum values. Stars on the graphs show statistical differences with P < 0.05.

8.4 Appendix 4: Graphs of gene expression and regulation in the heart after ventricular resection during *Xenopus laevis* metamorphosis.

Appendix 8-15: Different profile of gene expression in the heart after ventricular resection during *Xenopus laevis* metamorphosis. SHAM and amputated hearts from stage 57 (NF57), stage 61 (NF61), juvenile and adult *Xenopus laevis*, corresponding at pro-metamorphosis, metamorphic climax and post-metamorphosis period, were used to look at gene expression at 1, 3 and 7 days post amputation (dpa). SHAM hearts were used as placebo controls for the surgery and were used for the gene regulation analysis to normalise the data from the amputated hearts. Stages were according to (Nieuwkoop and Faber, 1994) (NF). The width of the box shows the interquartile range (IQR), the line in the box shows the median and the whiskers show the minimum and the maximum values. Stars on the graphs show statistical differences with $P < 0.05$.

